

January 2015

Thiol-Disulfide Exchange in Human Growth Hormone

Saradha Chandrasekhar
Purdue University

Follow this and additional works at: https://docs.lib.purdue.edu/open_access_dissertations

Recommended Citation

Chandrasekhar, Saradha, "Thiol-Disulfide Exchange in Human Growth Hormone" (2015). *Open Access Dissertations*. 1449.
https://docs.lib.purdue.edu/open_access_dissertations/1449

This document has been made available through Purdue e-Pubs, a service of the Purdue University Libraries. Please contact epubs@purdue.edu for additional information.

**PURDUE UNIVERSITY
GRADUATE SCHOOL
Thesis/Dissertation Acceptance**

This is to certify that the thesis/dissertation prepared

By Saradha Chandrasekhar

Entitled

Thiol-Disulfide Exchange in Human Growth Hormone

For the degree of Doctor of Philosophy

Is approved by the final examining committee:

Elizabeth M. Topp

Chair

Stephen R. Byrn

Gregory T. Knipp

Weiguo A. Tao

To the best of my knowledge and as understood by the student in the Thesis/Dissertation Agreement, Publication Delay, and Certification Disclaimer (Graduate School Form 32), this thesis/dissertation adheres to the provisions of Purdue University's "Policy of Integrity in Research" and the use of copyright material.

Approved by Major Professor(s): Elizabeth M. Topp

Approved by: Lynne S. Taylor

Head of the Departmental Graduate Program

7/20/2015

Date

THIOL-DISULFIDE EXCHANGE IN HUMAN GROWTH HORMONE

A Dissertation

Submitted to the Faculty

of

Purdue University

by

Saradha Chandrasekhar

In Partial Fulfillment of the

Requirements for the Degree

of

Doctor of Philosophy

August 2015

Purdue University

West Lafayette, Indiana

To my parents Chandrasekhar and Visalakshi

&

To my fiancé Niranjana

ACKNOWLEDGEMENTS

I would like to thank Dr. Elizabeth M. Topp for her tremendous support, guidance and valuable suggestions throughout. The successful completion of my PhD program would not have been possible without her constant encouragement and enthusiasm. Through the last five years, I've learned so much as a graduate student in her lab. My thesis committee members: Dr. Stephen R. Byrn, Dr. Gregory T. Knipp and Dr. Weiguo A. Tao, thank you for your time and for all your valuable comments during my oral preliminary exam. I would also like to thank Dr. Fred Regnier for his suggestions with the work on human growth hormone.

I am grateful to all my lab members and friends for their assistance and support. I would like to especially thank Dr. Andreas S. Sophocleous, Dr. Jun Zhang and Dr. Shenbaga Moorthy Balakrishnan for helpful discussions, answering questions and for training on me on different instruments in the lab. Special thanks and gratitude go to Daniel E. Epling for his help with the temperature studies, Ruichao Xie for performing peptide studies and to John O. Grady for training me on the Perfinity Flash digest protocol.

I am very grateful to my parents, who have encouraged and believed in me from the beginning. Thank you for being so patient and for giving me the opportunity to pursue my dreams. I am also thankful to my fiancé, Niranjana, for supporting me through the good and bad times of my graduate student life. I will be forever indebted to you all.

TABLE OF CONTENTS

	Page
LIST OF TABLES	ix
LIST OF FIGURES	xi
LIST OF ABBREVIATIONS.....	xix
ABSTRACT	xxi
CHAPTER 1. OVERVIEW OF THERAPEUTIC PROTEINS.....	1
1.1 Introduction.....	1
1.2 Recombinant DNA technology.....	3
1.3 Stability of protein drugs	4
1.3.1 Physical degradation	5
1.3.2 Chemical degradation	7
1.4 Thiols and disulfide bonds.....	9
1.5 Disulfide bond formation in proteins.....	10
1.5.1 Disulfide bond disruption and rearrangement.....	14
1.6 Factors that influence disulfide bond reactivity.....	18
1.6.1 Intrinsic factors	18
1.6.2 Extrinsic factors	20
1.7 Impact on protein physical stability and biological activity	23
1.8 Formulation strategies for Cys-containing proteins	25
1.8.1 Formulating proteins with a reducing agent	25
1.8.2 Chemical modification of thiol groups	25
1.8.3 Protein engineering	27
1.9 Lyophilization of peptide and protein drugs.....	29
1.9.1 Thiol-disulfide exchange in the solid-state	30

	Page
1.10	Disulfide bond mapping32
1.11	Research objectives and specific aims.....36
1.12	Research Significance.....38
CHAPTER 2. ELUCIDATING THE MECHANISM AND KINETICS OF THIOL- DISULFIDE EXCHANGE IN PEPTIDES DERIVED FROM HUMAN GROWTH HORMONE IN AQUEOUS SOLUTION 41	
2.1	Abstract.....41
2.2	Keywords.....42
2.3	Introduction.....42
2.4	Materials46
2.5	Methods47
2.5.1	Preparation of peptide stock solutions and disulfide linked peptides for kinetic studies..... 47
2.5.2	Homodimer formation 47
2.5.3	Buffer preparation..... 48
2.5.4	Quantification of reactants and products by HPLC 49
2.5.5	Determination of reaction order..... 52
2.5.6	Thiol-disulfide exchange reactions 52
2.5.7	Determining activation parameters for the reaction of T20 with T20-T21 53
2.6	Data analysis54
2.7	Results.....57
2.7.1	Addition of oxidation suppressants to favor the thiol-disulfide exchange reaction 57
2.7.2	Apparent order of reaction; reaction of T20 and T20-T21 60
2.7.3	Effect of oxidation suppressants on thiol-disulfide exchange 62
2.7.4	Effect of pH on the reaction of T20 with T20-T21..... 64
2.7.5	Activation parameters for the reaction of T20 with T20-T21..... 71
2.7.6	Effect of peptide cyclization on thiol-disulfide exchange 74

	Page
2.8 Discussion.....	77
2.9 Conclusion.....	81
CHAPTER 3. INVESTIGATING THE EFFECT OF LYOPHILIZATION AND SUBSEQUENT STORAGE IN THE SOLID STATE ON THIOL-DISULFIDE EXCHANGE IN PEPTIDES DERIVED FROM HUMAN GROWTH HORMONE	
	83
3.1 Abstract.....	83
3.2 Keywords.....	84
3.3 Introduction.....	84
3.4 Materials	88
3.4.1 Quantification of reactants and products by HPLC	89
3.4.2 Thiol-disulfide exchange reactions	90
3.4.3 Lyophilization of peptide samples	93
3.4.4 Peptide adsorption to ice.....	94
3.4.5 Method for detecting reaction intermediates	95
3.4.6 Data analysis	96
3.5 Results.....	98
3.5.1 Effect of lyophilization on thiol-disulfide exchange	98
3.5.2 Disulfide bond stability during lyophilization	103
3.5.3 Thiol-disulfide exchange in lyophilized powders during storage.....	106
3.6 Discussion.....	116
3.7 Conclusion.....	124
CHAPTER 4. THIOL-DISULFIDE EXCHANGE IN HUMAN GROWTH HORMONE	
	125
4.1 Abstract.....	125
4.2 Keywords.....	126
4.3 Introduction.....	126
4.4 Materials	130
4.5 Method.....	131
4.5.1 hGH expression and purification	131

	Page
4.5.2	Thiol-disulfide exchange in model peptides..... 134
4.5.3	Enzymatic digestion using the Perfinity flash digest protocol..... 136
4.5.4	Removal of unreacted peptides using a desalting column..... 136
4.5.5	LC-MS analysis and disulfide bond identification using MassHunter software 137
4.5.6	Thiol-disulfide exchange in hGH..... 138
4.5.7	Near-UV CD measurement..... 141
4.5.8	Amide hydrogen-deuterium exchange mass spectrometry (HDX-MS) 142
4.6	Results..... 143
4.6.1	Thiol-disulfide exchange in hGH: product identification 143
4.6.2	Thiol-disulfide exchange in hGH: product quantitation 146
4.6.3	Effect of higher order structure on thiol-disulfide exchange 150
4.6.4	Effect of hGH structure on regeneration of native disulfide..... 154
4.7	Discussion..... 159
4.8	Conclusion 164
CHAPTER 5.	CONCLUSIONS AND SUGGESTIONS FOR FUTURE WORK.. 166
5.1	Thiol-disulfide exchange in aqueous solution (Chapter 2)..... 166
5.2	Thiol-disulfide exchange during lyophilization and storage in the solid state (Chapter 3) 167
5.3	Thiol-disulfide exchange in human growth hormone (Chapter 4) 168
5.4	Recommendations for future work 169
5.5	Implications for protein formulation 171
REFERENCES 175
APPENDICES	
	Appendix A: Data modeling with SCIENTIST® 192
	Appendix B: SGA and DSC measurements for lyophilized samples..... 193
	Appendix C: purification and digestion optimization of hgh 194
VITA 197

LIST OF TABLES

Table	Page
Table 1.1: Chemical cleavage reagents and proteases commonly used for disulfide mapping in proteins [104].	36
Table 2.1: Abbreviations and amino acid sequences of hGH-derived peptides used in studies of thiol-disulfide exchange.	46
Table 2.2: Measured rate constants for all buffer concentrations for the reaction of T20 with T20-T21, 0.08 M ionic strength (with EDTA and N ₂ sparged) at 22 °C.	70
Table 2.3: Activation parameters for thiol-disulfide exchange reactions and oxidation reaction (k_s). Values for ΔH^\ddagger , ΔS^\ddagger and ΔG^\ddagger were obtained from the Eyring plot shown in Figure 2.15.	75
Table 2.4: The change in cT20-T21 and T20-T21 concentrations obtained after 6 hours for thiol-disulfide exchange reactions with T20 at different pH and temperature at thiol: disulfide of 10:1.	75
Table 3.1: Abbreviations and amino acid sequences of peptides detected in solid-state studies with hGH-derived peptides.	92
Table 3.2: Lyophilization cycle used for solid-state studies with hGH-derived peptides	93
Table 3.3: Microscopic and observed rate constants for thiol-disulfide exchange between T20 and T20-T21 in lyophilized solids and aqueous solution.	109
Table 3.4: Abbreviations and amino acid sequences of tocinoic acid, glutathione and their mixed disulfides.	123
Table 4.1: Amino acid sequence of disulfide-linked peptides in hGH: native and scrambled disulfides.	140

Table	Page
Table 4.2: Amino acid sequence of model peptides used to investigate thiol-disulfide exchange reactions	141
Table 4.3: Amino acid sequence of mixed disulfide-linked peptides from hGH: for the reaction of hGH with T20a.	145
Table 4.4: Amino acid sequence of mixed disulfide-linked peptides from hGH: for the reaction of hGH with GSH.	145
Table 4.5: Amino acid sequence of mixed disulfide-linked peptides from hGH: for the reaction of hGH with CR, C and RCR.....	146
Table 4.6: The change in native disulfide concentration in peptides and hGH obtained after 1 hour and 1 day for thiol-disulfide exchange reactions with different free thiols at pH 7.0 and 37 °C.....	154
Table 4.7: Oxidation state prediction for thiol-containing peptides using DiANNA	164
Table C.1: Comparing different digestion protocols for hGH.....	195
Table C.2: Amino acid sequence of all possible scrambled intra-and intermolecular disulfide-linked peptides from hGH.	196

LIST OF FIGURES

Figure	Page
Figure 1.1: Categories of biologic drugs in terms of US sales in 2012 taken from reference [1].	1
Figure 1.2: a) Monoclonal antibody structure showing regions that are prone to undergo chemical modifications, resulting in product heterogeneity. b) Schematic showing a typical protein manufacturing process [8].	4
Figure 1.3: A pathway for protein disulfide bond formation in the endoplasmic reticulum (ER). Oxidizing equivalents flow from Ero1p to Pdi1p, and then from Pdi1p to secretory proteins through a series of thiol-disulfide exchange reactions [43].	11
Figure 1.4: Thermodynamic cycle linking disulfide bond stability in the reduced and oxidized folded structure with the stability of the folded and unfolded states [45].	13
Figure 1.5: Energy diagram for thiol-disulfide exchange reactions [53].	15
Figure 1.6: Oxidative pathways for thiols, adapted from [52].	15
Figure 1.7: Different thiol-disulfide exchange reactions: A) intramolecular, B) intermolecular and C) intermolecular disulfide bond disrupted by thiol-disulfide exchange [54].	16
Figure 1.8: Different pathways that lead to disulfide bond disruption. A) Thiol-disulfide exchange (nuc: nucleophile, c: central sulfur and lvg: leaving group). B) Direct attack of hydroxyl ion on disulfide bond generates sulfenic acid and thiolate anion. C) Acid-base assisted hydrolysis of disulfide bond. D) Disulfide bond disruption under acidic conditions.	18
Figure 1.9: Scheme showing assumed effects of the appearance of steric and electrostatic hindrances after the formation of a mixed disulfide on thiol-disulfide exchange in Hsp25. The two subunits that form the subunit are shown in black [67].	21

Figure	Page
Figure 1.10: Dependence of fraction of subunits forming the inter-subunit disulfide bond (PSSP) on urea concentration (left) and on temperature (right) [67].	22
Figure 1.11: Thiol derivatizing agents that are commonly used to derivatize thiols in proteins to prevent reaction with other groups [3].	27
Figure 1.12: Thiol-disulfide exchange in interleukin-2 [90].	28
Figure 1.13: FTIR spectra of human growth hormone. 1- hGH in solution, 2- hGH lyophilized with sucrose, 3- hGH lyophilized with trehalose and 4- hGH lyophilized alone [101].	32
Figure 2.1: hGH-trypsin digestion map, tryptic fragments are labeled T1 to T21 starting from the N-terminus. Disulfide bonds are represented by the two solid lines between T6-T16 and T20-T21. Adapted from [139].	45
Figure 2.2: HPLC chromatograms showing T20-T20 formation over time at pH 6.0 in 50 mM phosphate buffer with H ₂ O ₂ as the oxidizing agent.	48
Figure 2.3: HPLC chromatograms (215nm) at various times during the reaction of T20 with T20-T21 at pH 7.0, 10 mM phosphate buffer with 0.5 mM EDTA. A) 0 mins. B) 180 mins and C) 1440 mins.	51
Figure 2.4: The concentration of reactants and products for a kinetic study with T20 and T20-T21 at pH 7.0, 10 mM PB and 0.08 M ionic strength (without EDTA or N ₂ sparging). Initial concentrations of peptides were: [T20] = 350 μM; [T20-T21] = 250 μM. The symbols represent actual data points obtained from samples at different times (n=3, +/-SD). Solid lines are model predictions for the reactions in Scheme 2.1.	59
Figure 2.5: Concentrations of cT20-T21 (▲) and rT20-T21 (●) for the reaction of cT20-T21 with T20 in 10 mM carbonate buffer, pH 9.0, and 0.08 M ionic strength (with EDTA and N ₂ sparged) at 22 °C.	59
Figure 2.6: Thiol-disulfide exchange initial rate studies in which the concentration of one reactant (either T20 or T20-T21) was fixed while the concentration of the second reactant (either T20 or T20-T21) was varied (see text). Reaction kinetics was monitored at pH 7.0, 10mM PB, 0.08M ionic strength with EDTA and N ₂ sparging at 22 °C. Log-log plots of rate of loss of T20 versus T20 concentration (■) and rate of loss of T20-T21 versus T20-T21 concentration (◆).	62

Figure	Page
Figure 2.7: The concentration of reactants and products for a kinetic study with T20 and T20-T21 at pH 7.0, 10mM phosphate buffer with 0.5 mM EDTA and N ₂ sparging. Initial concentrations of peptides were: [T20] = 350 μM; [T20-T21] = 250 μM. The symbols represent actual data points obtained from samples at different times (n=3, +/- SD). Solid lines are model predictions for the reactions in Scheme 2.1.....	63
Figure 2.8: Comparison of rate constants for reactions with and without oxidation suppressants (0.5 mM EDTA and N ₂ sparging) at pH 7.0, 10 mM PB and 0.08 M ionic strength at 22 °C. Initial concentrations of peptides were: [T20] = 350 μM and [T20-T21] = 250 μM (n=3, +/- SD). Unit for k ₅ is M ⁻³ s ⁻¹	64
Figure 2.9: Rate constants vs. buffer concentration. Rate constants were obtained from model fits to reaction scheme 2.1 (n=3, +/-SD): A) pH 6.0, B) pH 7.0, C) pH 8.0, D) pH 9.0, and E) pH 10.0 at 0.08 M ionic strength, different buffer concentrations of 10, 20 and 40 mM (with EDTA and N ₂ sparging) and at 22 °C. Initial concentrations of peptides were: [T20] = 350 μM; [T20-T21] = 250 μM. Dotted lines are trendlines.	67
Figure 2.10: Kinetic plots at different pH for the reaction of T20 with T20-T21 at 22 °C. Symbols represent actual data points (n=3, +/- SD) and solid lines represent model fits.[T20] = 350 μM; [T20-T21] = 250 μM. Buffer conditions: pH 6.0-8.0 is with 10 mM phosphate buffer and pH 9.0-10.0 is with 10 mM carbonate buffer. Ionic strength (0.08 M) and EDTA (0.5 mM) were the same at all pH values. A) pH 6.0, B) pH 8.0, C) pH 9.0, and D) pH 10.0.....	69
Figure 2.11: pH-rate profile for second order microscopic rate constants (see Scheme 2.1 and text for details) obtained for kinetic studies with T20 and T20-T21 at 22 °C. All rate constants are values extrapolated to zero buffer concentration (n=3, +/- SD).	70
Figure 2.12: Pseudo-first order rate constant for the loss of T20-T21 (◆) at different pH (10 mM buffer, 0.08 M ionic strength with oxidation suppressants) and at 22 °C. Rate constants were determined by non-linear regression. Uncertainties are within the size of the symbol (n=3, +/-SD).	71
Figure 2.13: Arrhenius plots for microscopic rate constants for the reaction of T20 and T20-T21 (Scheme 2.1) at pH 7.0, 10 mM phosphate buffer and 0.08 M ionic strength with 0.5 M EDTA and N ₂ sparging (n=3, +/- SD). Solid lines represent trendlines.....	72
Figure 2.14: Arrhenius plot for microscopic rate constant k ₅ (●) for the reaction of T20 and T20-T21 (see 2.1). The reaction was monitored at pH 7.0, 10 mM buffer and 0.08 M ionic strength (with EDTA and N ₂ sparging) (n=3, +/- SD). Solid lines represent trendlines.....	73

Figure	Page
Figure 2.15: Eyring plot for microscopic rate constants for the reaction of T20 with T20-T21 at pH 7.0, 10 mM buffer and 0.08 M ionic strength (with EDTA and N ₂ sparging) (n=3, +/- SD). Solid lines represent trendlines.	73
Figure 2.16: Far-UV CD spectra for A) T20-T21 and B) cT20-T21. The far-UV CD spectrum for T20-T21 is representative of peptides T20, T21, T20-T20 and T20-T21. ...	76
Figure 2.17: Observed pseudo-first order rate constants for the loss of cT20-T21 and T20-T21 at different concentration ratios and temperatures. Ratios in figure legend represents thiol:disulfide ratio (T20:T20-T21/cT20-T21). Initial concentrations of peptides were: [T20] = 450 μM; [T20-T21] = 45 μM for 10:1 studies and [T20] = 350 μM; [T20-T21] = 250 μM for the 1.4:1 study. Uncertainties are within the size of the symbol (n=3).	77
Figure 3.1: Picture of an ice surface formed on the cold finger after 10 mins (left). Picture of cold finger after adsorption of the peptide solution to the ice surface for one hour (right).	95
Figure 3.2: Change in native disulfide content during lyophilization (n=3, +/- SD) at pH 7.0 (10 mM PB, 0.08 M ionic strength, 0.5 mM EDTA and N ₂ sparged); I-freezing, II-primary drying and III-secondary drying. Reaction of T20 with a) T20-T21 (thiol: disulfide = 1.4:1), b) T20-T21 (◆) and cT20-T21 (■) at thiol: disulfide = 10:1. Black dashed lines indicate the end of each stage during lyophilization and the black dotted lines represent predicted values from solution Arrhenius parameters (see text).	101
Figure 3.3: Change in concentrations of reactants and products during lyophilization (n=3, +/- SD) for the reaction of T20 with T20-T21 (thiol: disulfide = 10:1, pH 7.0, 10 mM PB, 0.08 M ionic strength, 0.5 mM EDTA and N ₂ sparged); I-freezing, II-primary drying and III-secondary drying. Symbols represent actual data points: T20 (■), T21 (●), T20-T20 (□), T21-T21 (○) and T20-T21 (◆). Initial concentrations of reactants in solution (before lyophilization): [T20] = 450 μM; [T20-T21] = 45 μM. On the plot, t=0 (min) represents solution concentrations before lyophilization.	102
Figure 3.4: Change in concentrations of reactants and products during lyophilization (n=3, +/- SD) for the reaction of T20 with cT20-T21 (thiol: disulfide = 10:1, pH 7.0, 10 mM PB, 0.08 M ionic strength, 0.5 mM EDTA and N ₂ sparged); I-freezing, II-primary drying and III-secondary drying. Symbols represent actual data points: T20 (■), T20-T20 (□), cT20-T21 (◆) and rT20-T21 (◇). Initial concentrations of reactants in solution (before lyophilization): [T20] = 450 μM; [T20-T21] = 45 μM. On the plot, t=0 (min) represents solution concentrations before lyophilization.	102

Figure 3.5: Effect of buffer type and buffer concentration on thiol-disulfide exchange during lyophilization; freezing (I), primary drying (II) and secondary drying (III). Plot shows change in T20-T21 concentration (n=3, +/- SD), co-lyophilized with T20. All buffers contain 0.5 mM EDTA and were sparged with N₂, pH of reaction mixture was adjusted to 7.0 before lyophilization. Initial concentrations of reactants in solution (before lyophilization): [T20] = 450 μM; [T20-T21] = 45 μM. On the plot, t=0 (min) represents solution concentrations before lyophilization. 105

Figure 3.6: Change in concentration of T20-T21 lyophilized with T20 (thiol: disulfide = 6:1, pH 7.0, 10 mM PB, 0.08 M ionic strength, 0.5 mM EDTA and N₂ sparged) during freezing and primary drying (n=3) (◆). Primary drying time was increased from 2 to 6 hours. On the plot, t=0 (min) represents solution concentrations before lyophilization. 106

Figure 3.7: Concentration of scrambled and native disulfides formed via oxidative pathways during storage of lyophilized powders (n=3, +/- SD). Inset zooms in to show change in concentrations of T20-T21 and T21-T21. T20-T21 was co-lyophilized with T20 (thiol: disulfide = 10:1, pH 7.0, 10 mM PB, 0.08 M ionic strength, 0.5 mM EDTA and N₂ sparged) (see text for details). 107

Figure 3.8: Reaction of T20 with T20-T21 in lyophilized powders stored at 22 °C (n=3, +/- SD). Initial concentrations of reactants in solution (before lyophilization): [T20] = 450 μM; [T20-T21] = 45 μM. Buffer conditions: pH 7.0 , 10 mM phosphate buffer, 0.08 M ionic strength, 0.5 mM EDTA and N₂ sparged. 108

Figure 3.9: Reaction of T20 with T20-T21 in lyophilized powders stored at 22 °C (n=3, +/- SD). Initial concentrations of reactants in solution (before lyophilization): [T20] = 450 μM; [T20-T21] = 45 μM. Buffer conditions: pH 7.0 , 10 mM phosphate buffer, 0.08 M ionic strength, 0.5 mM EDTA and N₂ sparged. Plot shows concentrations of T20 (■), T21 (●), T20-T20 (□), T21-T21 (○) and T20-T21 (◆). Solid lines are non-linear regressions based on the model in Scheme 3.1. Initial time point (t = 0 days) corresponds to a sample reconstituted immediately after lyophilization. 109

Figure 3.10: Change in concentration of cT20-T21 lyophilized with T20 (thiol: disulfide = 10:1, pH 7.0, 10 mM PB, 0.08 M ionic strength, 0.5 mM EDTA and N₂ sparged) during storage (n=3, +/- SD) at 22 °C (■), and in solution (◆) (thiol: disulfide = 10:1, pH 7.0, 10 mM PB, 0.08 M ionic strength, 0.5 mM EDTA and N₂ sparged). Both solid and solution samples were stored at 22 °C in lyo vials, n = 3. Open symbols show the initial concentration of cT20-T21 in solution before lyophilization (□) and before storage as solution at 22 °C (◇). Initial data points (t = 0 days, filled symbols) represent solution sample and lyophilized sample reconstituted immediately after lyophilization. 111

Figure	Page
Figure 3.11: HPLC chromatograms (215 nm) obtained at various times during storage of lyophilized T20 and cT20-T21 at 22 °C (pH before lyophilization was 7.0). Solution sample before lyophilization (A), solid sample immediately after lyophilization (B) and solid sample after 3 days (C). Peak labels: 1) T20; 2) T20-T20; 3) DMD; 4) SMD 1&2; 5) cT20-T21 and 6) rT20-T21.....	112
Figure 3.12: The concentration of reactants and products for a kinetic study with T20 and cT20-T21 during storage at 22 °C. Buffer conditions before lyophilization: pH 7.0, 10mM phosphate buffer with 0.5 mM EDTA and N ₂ sparging. Initial concentrations of peptides were: [T20] = 450 μM (Δ); [cT20-T21] = 45 μM (○). The symbols represent actual data points obtained from samples at different times (n=3, +/- SD): T20 (■), cT20-T21 (◆), T20-T20 (□) and rT20-T21 (◇).....	113
Figure 3.13: Change in T20-T21 (pH 8.0, 10 mM PB, 0.08 M ionic strength, 0.5 mM EDTA and N ₂ sparged) concentration during storage (n=3, +/- SD) without T20, as a lyophilized powder (◆) and in solution (■). T = 0 (day) on plot represents solution sample analyzed at the same time as samples reconstituted immediately after lyophilization. Initial concentration of T20-T21 in solution before lyophilization is represented by Δ.	114
Figure 3.14: Change in cT20-T21 (pH 8.0, 10 mM PB, 0.08 M ionic strength, 0.5 mM EDTA and N ₂ sparged) concentration during storage (n=3, +/- SD) without T20, as a lyophilized powder (◆) and in solution (■). T = 0 (day) on plot represents solution sample analyzed at the same time as samples reconstituted immediately after lyophilization. Initial concentration of cT20-T21 in solution before lyophilization is represented by Δ.	115
Figure 3.15: Mass spectrum (extracted ion chromatogram) showing the T20-S-dimedone adduct. Lyophilized T20-T21 (initial concentration = 250 μM, PB pH 8.0, 0.5 mM EDTA, 0.08 M ionic strength and N ₂ sparged) was analyzed on the LC-MS upon reconstitution after storage at 22 °C for 2 weeks.	115
Figure 4.1: Amino acid sequence of hGH expressed and purified in our lab (MW = 25 kDa). Sequence highlighted in blue shows the additional 28 amino acids at the N-terminus. Highlighted in yellow are the four Cys residues and the native disulfide bonds are represented by the red dotted lines.....	132
Figure 4.2: <i>Expression and purification of rhGH:</i> (A) Expression of r-hGH in uninduced (lane 1) and induced (lane 2) culture was checked with 12% SDS-PAGE. (B) Purification of refolded r-hGH in HiPrep 26/60 Sephacryl S-100 high resolution column (Amersham Biosciences, Piscataway, NJ). Gel filtration chromatogram showing the resolved monomeric r-hGH. Inset, 12% SDS-PAGE shows the purified r-hGH (lane 1). (M: Molecular weight marker).....	133

Figure	Page
Figure 4.3: Total ion chromatogram for tryptic digest of r-hGH. The two native disulfide bonds are in peptides T6-T16 and T20-T21 with retention times 26.1 and 12.17 min respectively. The figure insets show the isotope pattern and the charge state of the two disulfide-containing peptides.	133
Figure 4.4: Change in concentration of T20-T21 (◆) for the reaction with A) T20a (10 mM PB, pH 7.0, 0.08 M ionic strength, 0.5 mM EDTA and N ₂ sparged) and with B) T20a (50 mM Tris.HCl and 2% sucrose, pH 7.0) at 22 °C (n=3, +/- SD). Initial concentration of peptides were; [T20a] = 500 μM and [T20-T21] = 50 μM.....	135
Figure 4.5: Calibration plot for T20-T21 (synthetic standard from GenScript); constructed using peak areas (n=3, +/- SD) from XIC at different peptide concentrations.	139
Figure 4.6: Concentrations of T20-T21 (◆), T20 (■), T21 (●) and T20a-T20+T20a-T21 or T20-S-S-G+T21-S-S-G (▲) for the reaction of hGH with T20a (A) and GSH (B) at pH 7.0 (40 mM Tris.HCl and 1.6% sucrose) and 37 °C (n=3, +/- SD). Initial molar ratio of thiol: hGH was 100:1. Concentration of hGH alone before reaction with T20a is represented by ◇. Lines on plot are to improve readability and do not represent regression analysis.....	148
Figure 4.7: Concentrations of T20-T21 (◆), T20 (■), T21 (●) and mixed disulfides (▲) for the reaction of hGH with (A) RCR, (B) CR and (C) C at pH 7.0 (40 mM Tris.HCl and 1.6% sucrose) and 37 °C (n=3, +/- SD). Initial molar ratio of thiol: hGH was 100:1. Control sample represents hGH alone before reaction with CR. Lines on plot are to improve readability and do not represent regression analysis.	149
Figure 4.8: Concentrations of T20-T21 (◆), T20 (■), T21 (●) and T20-S-S-G+T21-S-S-G (▲) for the reaction of Prospec hGH with GSH at pH 7.0 (40 mM Tris.HCl and 1.6% sucrose) and 37 °C (n=3, +/- SD). Initial molar ratio of thiol: hGH was 100:1. T=0 min sample represents hGH alone before reaction with GSH. Lines on plot are to improve readability and do not represent regression analysis.....	150
Figure 4.9: Concentrations of species for the reaction of cT20-T21/T20-T21 _{pep} with GSH at pH 7.0 (10 mM phosphate buffer) and 37 °C (n=3, +/- SD), initial molar ratio of GSH: cT20-T21/T20-T21 _{pep} was 100:1. A) Concentrations of cT20-T21 (◆), rT20-T21 (■) and SMDs + DMD (▲). B) Concentrations of T20-T21 _{pep} (◆), T20 (■), T21 (●) and mixed disulfides (▲). T=0 min represents concentration of native disulfide (cT20-T21/T20-T21 _{pep}) before initiation of reaction by adjusting the pH to 7.0. Lines on plot are to improve readability and do not represent regression analysis.	152

Figure	Page
Figure 4.10: Distribution of cT20-T21 (◆), rT20-T21 (■) and SMDs+DMD (▲) for the reaction of cT20-21 with A) T20a, B) CR, C) RCR, D) QCR and E) C and F) T20 at pH 7.0 and 37 °C in 10 mM PB (0.08 M ionic strength, 0.5 mM EDTA and N ₂ sparged). T=0 min represents sample collected before reaction was initiated by adjusting pH to 7.0, thiol: disulfide ratio was 100: 1 (molar ratio).....	153
Figure 4.11: Near-UV CD spectra for hGH native (solid line) and reduced (dotted line).	155
Figure 4.12: Crystal structure of hGH (PDB ID: 1 HGU) representing the percent deuterium uptake in native (A) and reduced (B) state following 5 min of HDX. Data from 31 overlapping peptic fragments were mapped onto the structure.	156
Figure 4.13: Concentration vs time plot for the loss of cT20-T21 (n=3, +/- SD) during the reaction with GSH (■), CR (▲), RCR (●), QCR (□) and C (Δ) at pH 7.0 and 37 °C in 10 mM PB (0.08 M ionic strength, 0.5 mM EDTA and N ₂ sparged). Initial thiol: disulfide was 100:1 (molar ratio). Lines on plot are to improve readability and do not represent regression analysis.	158
Figure B.1: VTI data for lyo sample (T20 and cT20-T21, pH 7.0, 10 mM PB, 0.08 M ionic strength and 0.5 mM EDTA) collected on SGA-100 (VTI Corporation, Hialeah, FL). Data was measured at 0% RH and at 25 °C at the end of secondary drying.	193
Figure B.2: DSC data for lyo sample (T20 and cT20-T21, pH 7.0, 10 mM PB, 0.08 M ionic strength and 0.5 mM EDTA) collected on DSC Q-2000 (TA instruments, New Castle, DE).	193
Figure C.1: Flow chart showing purification steps for hGH from the cell pellet. Buffers used for each step are shown in boxes and amount of each buffer added are in green next to the boxes.	194

LIST OF ABBREVIATIONS

aa	amino acid
ACN	acetonitrile
Arg	arginine
BSA	bovine serum albumin
Cys	cysteine
DDI	double distilled water
DTT	dithiothreitol
EDTA	ethylenediaminetetraacetic acid
ESI	electrospray ionization
FA	formic acid
FDA	food and drug administration
GSH	reduced glutathione
GSSG	oxidized glutathione
hGH	human growth hormone
RP-HPLC	reverse phase-high-pressure liquid chromatography
rhGH	recombinant human growth hormone
IgG	immunoglobulin G

mAb	monoclonal antibody
Met	methionine
MS	mass spectrometry/ mass spectrometer
MSC	model selection criterion
NBE	new biological entity
PDI	protein disulfide isomerase
PB	phosphate buffer
rDNA	recombinant DNA
rHA	recombinant human albumin
ROS	reactive oxygen species
RS ⁻	thiolate anion
RSH	thiol group
RSOH	sulfenic acid
RSO ₂ H	sulfinic acid
RSO ₃ H	sulfonic acid
SDS-PAGE	sodium dodecyl sulfate-polyacrylamide gel electrophoresis
TB	terrific broth
TFA	trifluoroacetic acid
TIC	total ion chromatogram
XIC/EIC	extracted ion chromatogram

ABSTRACT

Chandrasekhar, Saradha. Ph.D., Purdue University, August 2015. Thiol-Disulfide Exchange in Human Growth Hormone. Major Professor: Elizabeth M. Topp.

The biopharmaceutical industry has been growing at a tremendous rate, with sales of \$63.6 billion 2012 in the US [1]. Nevertheless, the successful development of many protein drugs has been impeded by physical and chemical instabilities arising from their inherent chemical complexity and often leading to protein aggregation. The formation of non-native disulfide bonds is a common route to covalent aggregation of therapeutic proteins and other biologics [2, 3]. Disulfide bonds participate in hydrolytic and oxidative degradation reactions that form non-native disulfide bonds and other reactive species. The mechanisms responsible for protein aggregation are poorly understood and formulations are currently optimized on a trial and error basis. This approach contributes to high development costs and increases the time to market. The main goal of our research is to elucidate the mechanisms of thiol-disulfide exchange and disulfide scrambling in therapeutic proteins. To accomplish this goal, model peptides derived from human growth hormone (hGH) and intact hGH were used to investigate reaction mechanisms and kinetics in solution and solid-state environments. The results will be useful in the rational development of stable, safe and efficacious protein formulations that contain free cysteines and disulfides.

Chapter 1 of this dissertation focuses on background information and explains the role of disulfide bonds in proteins, their advantages and limitations and different degradation pathways. Research objective and specific aims are also outlined in Chapter 1. Model hGH-derived tryptic peptides were used to investigate reaction mechanism and kinetics in aqueous solution (Chapter 2). RP-HPLC was used as a quantitative tool and product identity was further confirmed on the LC-MS. The effects of pH, temperature, oxidation suppressants and peptide secondary structure on thiol-disulfide exchange were also explored.

Protein drugs are also manufactured as lyophilized powders to improve stability and retain potency during storage. In Chapter 3 of this dissertation, thiol-disulfide exchange during lyophilization and storage in the solid state using model peptides are discussed. Comparisons are drawn to the aqueous solution studies in Chapter 2. We also investigated the effect of factors that may contribute to thiol-disulfide exchange during lyophilization and these include; initial peptide concentration, temperature, buffer type and concentration, length of primary drying time and peptide adsorption to ice.

In Chapter 4, thiol-disulfide exchange in intact hGH was investigated to understand the effects of higher-order structure on reaction kinetics. Free thiol containing peptides of different length and sequence and GSH were used to facilitate thiol-disulfide exchange in intact hGH and hGH-derived peptides with a disulfide bond. Finally, concluding remarks, future perspectives and implications for protein formulations are discussed in Chapter 5.

CHAPTER 1. OVERVIEW OF THERAPEUTIC PROTEINS

1.1 Introduction

Many low molecular weight drugs are chemically manufactured and processed into tablets and capsules that are easily ingestible. In contrast, protein drugs are macromolecules that contain many labile groups and have fragile, dynamic three-dimensional structures. Protein pharmaceuticals have been gaining widespread importance as new treatments for serious diseases such as cancer, cardiovascular and autoimmune diseases. The growth of protein therapeutics has been facilitated by the rapid development of recombinant DNA (rDNA) technology since the approval of recombinant insulin. The different categories of biologic drugs and their 2012 U.S. sales are shown in Figure 1.1.

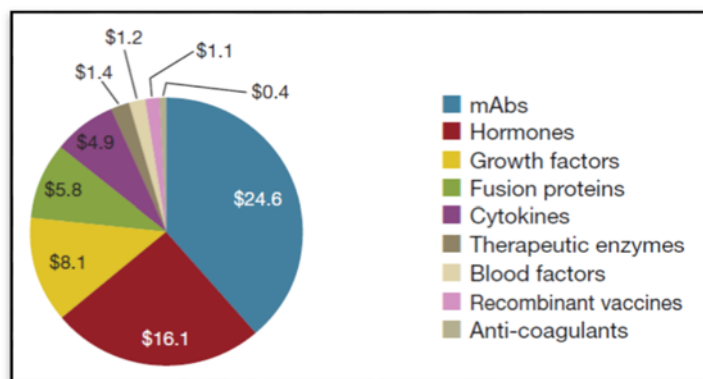


Figure 1.1: Categories of biologic drugs in terms of US sales in 2012. Adapted with permission from [1].

Protein drugs and other biologics are the fastest growing sector of the U.S. pharmaceutical industry, with sales expected to increase to \$144 billion by 2016 [1]. Nine new biopharmaceutical entities (NBE) were approved by the FDA in 2012 [4] and industry pipelines suggest the potential for many more protein drugs in the future. Protein instability presents many challenges to the development of new protein drug products which ultimately increase the time and cost required. Recent data suggest that approximately \$400 million is associated with pre-clinical development of new biopharmaceuticals, a cost ultimately borne by the public [5].

Protein drug development is further complicated by the fact that formulations often contain an ensemble of protein conformations, which include the native state, partially unfolded states and even completely denatured states. This heterogeneity stems from the dynamics and thermodynamics of protein folding, the source of the protein (usually a complex biological mixture of proteins from cells), and the effects of upstream and downstream processing conditions. An ideal protein formulation would contain the pure protein in its native state; however, structural complexity and the presence of numerous reactive centers in proteins make it almost impossible to identify optimum conditions to maintain this ideal. In addition, the mechanisms of most aggregation pathways have not yet been investigated in detail and aggregates of protein drugs are typically classified as covalent and non-covalent [6]. This broad classification of protein aggregates precludes the mechanistic details of aggregation pathways like thiol-disulfide exchange and is a limitation in designing rational approaches to improve protein stability during manufacture, processing and storage.

1.2 Recombinant DNA technology

Therapeutic proteins are now produced using recombinant DNA (rDNA) technology, where a vector containing the gene of interest is transformed into a host cell for protein expression. The protein of interest is then purified from the cell lysate; this process varies depending on the type of protein, the way it is expressed (secreted vs. inclusion bodies) and the host cell in which it is expressed. Insulin was the first recombinant product to be licensed for therapeutic use in 1982. FDA approved recombinant proteins for therapeutic use includes hormones, growth factors, coagulation factors, interferons, interleukins and enzymes [7]. Theoretically any protein can be produced using rDNA technology. However, the protein may undergo changes during manufacture/purification/processing (Figure 1.2) that make it unstable and unsuitable for therapeutic use. During a typical protein manufacturing process, nearly 20-30 unit operations are performed and these steps increase the chances of variability in the final protein product [8]. Protein properties are also affected by post-translational modifications such as glycosylation, amidation, carboxylation, sulfation and hydroxylation [9]. Overall, the process of expressing and purifying proteins is a rate-limiting process in research, demanding expertise and making protein therapeutics very expensive.

Different factors associated with the host cell and manufacturing process can affect protein drug quality [8]. Some of these undesirable modifications are: i) undesirable host cell and process modifications: truncation, glycation, methylation and isomerization, ii) undesirable process modifications: aggregation, oxidation, deamidation and misfolded

forms of protein and impurities from host cell and process related impurities: host cell proteins and endotoxins.

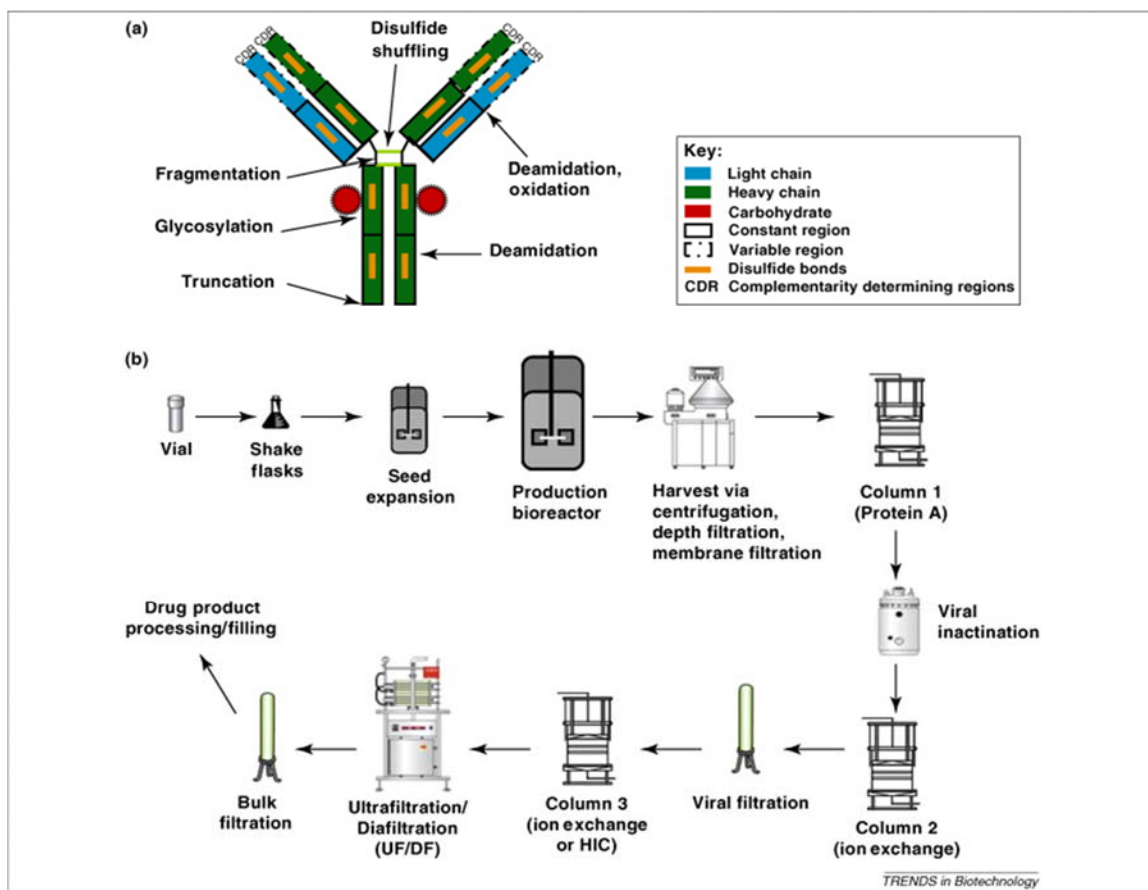


Figure 1.2: a) Monoclonal antibody structure showing regions that are prone to undergo chemical modifications, resulting in product heterogeneity. b) Schematic showing a typical protein manufacturing process. Adapted with permission from [8].

1.3 Stability of protein drugs

Challenges associated with the development of protein pharmaceuticals arise from the unique flexible structure of proteins that enable them to interact with other biological molecules and also adapt to changes in their microenvironment. Structural flexibility

promotes conformational changes, chemical modifications (via exposure to reactive species like ROS), aggregation and precipitation. Such modifications have been associated with loss of biological activity and immunogenicity [10-12]. Aggregation is known to occur both in solution [13] and the solid state [14-16] and can be induced by chemical and/or physical changes. Chemical instabilities that involve bond formation or cleavage include deamidation, thiol-disulfide exchange, proteolysis and oxidation. Physical instabilities result in changes to higher order structure without covalent modification; these include denaturation, aggregation, adsorption to surfaces and precipitation [6]. The onset of aggregation is protein specific and the effect of stabilizers on therapeutic proteins must be studied on a case-by-case basis, which further retards drug development and increases manufacturing costs. Different chemical and physical degradation pathways in proteins and peptides are discussed below.

1.3.1 Physical degradation

Denaturation: protein denaturation is the loss of tertiary or secondary structure or both, which can then lead to any of the other degradation pathways listed below. Protein denaturation is further classified as thermal, cold, chemical or pressure-induced [6]. Thermal denaturation occurs at elevated temperatures and is irreversible, these thermally unfolded proteins have a tendency to associate and form aggregates. There are few reports on cold denaturation of proteins; nevertheless it is an important phenomenon as even at -20 °C and in the presence of stabilizers, they have mobility. Chaotropes like guanidine hydrochloride and urea are used to chemically denature proteins. These reagents are used in studies to determine the free energy associated with unfolding events. For pressure-

induced denaturation to occur, proteins must be exposed to pressures in the range of 2000-4000 bar. A lower pressure range (1000-1500 bar) is typically employed to dissociate aggregates. Pressure-induced denaturation is usually reversible, unlike the other types of protein denaturation described above [17].

Aggregation: involves the formation of non-native bonds following disruption of native bonds. Loss of native protein conformation during purification, formulation, freeze-thawing and freeze-drying often leads to the exposure of hydrophobic residues in unfolded and partially unfolded states that can then promote aggregation [6]. Both non-covalent and covalent interactions can result in protein aggregation, which ultimately affects biological activity and can result in a severe immunogenic response after administration. Proteins do not aggregate via a single pathway and this adds to the challenges associated with investigating the mechanism of aggregation. There are five general mechanisms of protein aggregation: 1) association of native monomers, 2) aggregation of conformationally altered monomers, 3) aggregation of chemically-modified monomers, 4) nucleation-controlled aggregation and 5) surface-induced aggregation [18]. Typically, protein conformational stability is considered to be a significant factor in regulating aggregation; a partially unfolded state is the aggregation initiator (also the rate-limiting factor) [6, 19]. Stabilizing agents like sucrose and Tween have been used to effectively suppress aggregation in human interferon- γ^{13} and human growth hormone respectively [20].

Surface adsorption: proteins are exposed to a multitude of surfaces to which they can adsorb during manufacture, processing and storage. The physical state of a protein can be altered when it adsorbs to a surface or is exposed to interfacial stress [6]. Though both the native and partially unfolded states can adsorb to surfaces, adsorption of a partially

unfolded protein may be energetically favored due to the exposure of more hydrophobic residues when compared to the native state, in which they are buried within the core. A combination of interfacial structure perturbation and desorption of partially unfolded proteins can set off nucleation and result in aggregation [21-24]. The effects of surface adsorption on protein function and conformation have been reported previously [25, 26].

Precipitation: there are two different mechanisms by which proteins can precipitate. First, salting out of proteins in the presence of an excluded solvent can result in precipitation, a process that is usually reversible upon dilution [27]. Further, salted-out proteins retain activity similar to that of the native protein. Second, aggregates can grow so large in size that they are no longer soluble and manifest as haziness or cloudiness. The observed haziness is termed particulate formation and is typically irreversible. Particulate identification and detection is a major concern to the pharmaceutical industry and regulatory agencies as the particles may have immunogenic implications [28]. It is important to distinguish particulates formed from protein aggregates and foreign materials.

1.3.2 Chemical degradation

Oxidation: amino acids His, Trp, Met, Cys and Tyr can undergo oxidation in the presence of a reactive oxygen species (ROS) [29]. Oxidation reactions in proteins are classified as site-specific (metal catalyzed) and non-site specific (photooxidation and free radical cascades). Methionine (Met) is oxidized easily to its sulfoxide and sulfone in the presence of ROS and molecular oxygen. Met oxidation has been reported in mAbs, particularly in the Fc region [30]. Oxidation of Trp generates kynurenine derivatives and

can occur both in the presence and absence of light. Yang et al. determined Trp oxidation in mAbs using RP-HPLC as an analytical tool [31].

Deamidation: is one of the most common pathways for chemical degradation in peptides and proteins. Asn and Gln can undergo deamidation to form Asp and Glu respectively at neutral to alkaline pH. Gln deamidation is less common due to the formation of a less stable six-membered ring intermediate. Primary structure effects on deamidation have been explored, and faster deamidation is observed when smaller amino acids are present after (e.g., N+1) residues due to minimal steric effects [6]. Deamidation is also favored in polypeptide regions that are known to be flexible and when amino acid side chains that can act as hydrogen bond donors are present in the N+1 position. Asn-Gly is frequently the most reactive sequence for deamidation to occur in peptides and proteins. Preceding (e.g., N-1) amino acids typically have little effect on deamidation in solution, however, in the solid-state deamidation is accelerated with a Gln or Glu residue. Deamidation has been observed in therapeutic proteins like rhGH [32], glucagon [33] and mAbs [34]. Asp residues can also participate in isomerization and racemization reactions, which follow mechanisms similar to that for deamidation.

Proteolysis/hydrolysis/clipping: hinge region hydrolysis can occur in mAbs and peptide backbone hydrolysis can occur near Asp residues. Asp hydrolysis in the solid state has been observed for recombinant bovine growth hormone [35]. Hinge region hydrolysis facilitated by hinge region flexibility and Fab region conformational instability has been reported in mAbs.

Dityrosine formation and formaldehyde mediated cross-linking: Formaldehyde can form covalent bonds with a nitrogen atom of Lys or His to produce a hydroxymethyl

derivative, which is then transformed into a Schiff base imine upon condensation. The imine is reactive and facilitates a cross-linking reaction with Tyr [36]. Dityrosine can be formed by photoactivation or enzyme catalysis. Dityrosine formation between two tyrosyl residues has been identified in calmodulin [37].

Thiol-disulfide exchange and disulfide scrambling: Thiols and disulfides in proteins have functional roles and can participate in oxidative and hydrolytic pathways. Disulfide scrambling has been observed in therapeutic proteins like mAbs [38], insulin [39] and hGH [40]. However, very little is known about the effect of higher order structure on the mechanism and kinetics of thiol-disulfide exchange and disulfide scrambling. As the number of antibodies and antibody- or albumin-fusion drug products increases, the need to control thiol/disulfide reactivity becomes more acute. This reaction is the focus of the work presented in this dissertation and is discussed in detail in below.

1.4 Thiols and disulfide bonds

There are three types of Cys: i) free SH groups, ii) ligand SH groups and iii) disulfides (cystines) [41]. Cysteine is similar to Serine but is a poorer hydrogen bond donor. In vivo, free Cys are present only in reducing environments that make them less harmful, for example in bacterial and viral proteins [41]. A common location for free Cys is on a β strand, pointing inward and buried. They are rarely found on the surface of proteins due to their reactive nature. Wolfenden et al. have shown Cys to be neutral or mildly hydrophobic and this could also explain their tendency to be the most buried amino acid [42]. Ligand Cys can bind to different metals and prosthetic groups like Fe, Cu, Zn, Fe-S clusters and

hemes. Typically, ligand Cys are found in coil regions and in helices, they are quite rare in β -sheets. Mettalothonien is an example of a protein that contains ligand Cys with 20 Cys that can bind to seven metals [41]. Disulfide bonds stabilize native protein structures by crosslinking distant regions into a compact three- dimensional structure and reducing conformational entropy of the unfolded state. However, in their reduced forms (as free thiol groups) they may have very little role in the early folding process. The $C\alpha$ - $C\beta$ vectors are either antiparallel or perpendicular in the most common disulfide conformations, the left-handed spiral and right-handed hook respectively. In addition to the vector orientation, the distance between the α -carbons of the cysteines must be 4-7.5 Å.

1.5 Disulfide bond formation in proteins

In eukaryotes, protein disulfide bonds are formed in the endoplasmic reticulum (ER) where the redox state is more favorable when compared to the cytosol. Oxidation of cysteines is initiated when proteins are translocated into the ER lumen. The rate of disulfide bond formation in living cells is faster than the rate of formation in vitro (in air), this has been attributed to the role of enzymes in the catalysis of protein oxidative folding in addition to the role of small-molecule redox buffers (GSH/GSSG) [43]. GSH provides reducing equivalents that are necessary to optimize folding conditions and counterbalance conditions of oxidative stress [43]. Protein disulfide isomerase (PDI) is an enzymatic catalyst that facilitates disulfide bond formation, reduction and isomerization. At the active site of PDI is a Cys-x-x-Cys motif similar to thioredoxin. When the cysteines are oxidized,

PDI transfers disulfide bonds to proteins in the ER (Figure 1.3). Disulfide scrambling is catalyzed when the cysteines in PDI are in the reduced state.

Similarly, in prokaryotes, DsbA (thioredoxin-like oxidoreductase, disulfide bond A enzyme) and DsbB (a membrane protein) initiate disulfide bond formation in periplasmic proteins. DsbA oxidizes cysteines in periplasmic proteins with the reduction of its own disulfide bond, DsbA is then reoxidized by DsbB. Components of the electron transport system help maintain DsbB in its oxidized state. DsbC reduces non-native disulfides in protein substrates, this is followed by re-oxidation of the Cys residues in the substrate by DsbA or DsbC. The role of DsbD is to maintain DsbC in its oxidized state, and cytoplasmic thioredoxin then reduces DsbD.

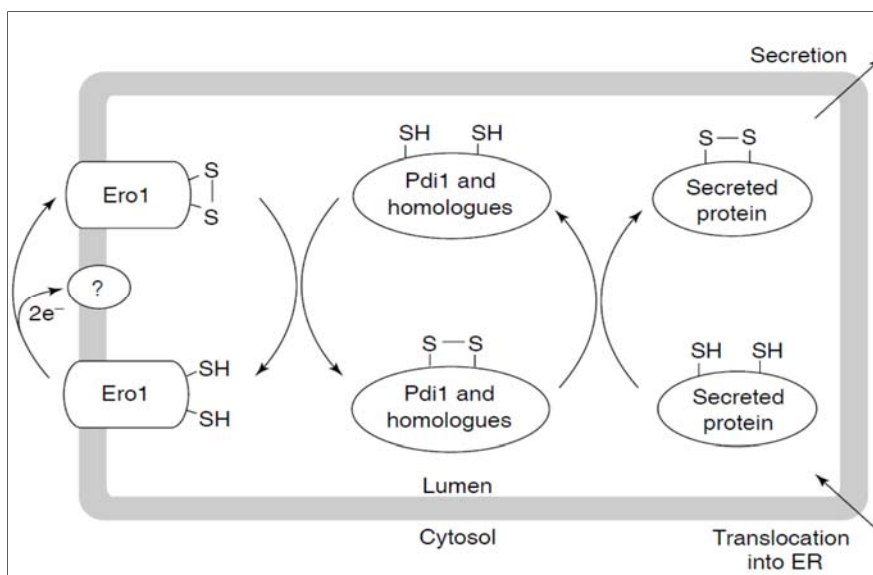


Figure 1.3: A pathway for protein disulfide bond formation in the endoplasmic reticulum (ER). Oxidizing equivalents flow from Ero1p to Pdi1p, and then from Pdi1p to secretory proteins through a series of thiol-disulfide exchange reactions. Adapted with permission from [43].

Disulfide bond formation in proteins is typically favored at neutral to alkaline pH and the rate of oxidative folding is increased in the presence of an oxidizing agent. A common oxidizing agent that is used to facilitate oxidative folding of proteins is oxidized glutathione (GSSG). Denaturing agents like guanidine hydrochloride and urea disrupt the folding process [3]. One exception to this general rule is murine prion protein (mPrP), which has only one intramolecular disulfide bond. At alkaline pH and in the absence of a denaturing agent, disulfide bond formation in mPrP is very slow [44]. However, at pH 8.0 in the presence of both a denaturing agent and glutathione, mPrP folds correctly. The optimum pH for oxidative refolding of mPrP is 4.0-5.0. In the absence of a denaturant, mPrP is in a stable conformation at pH 8.0, where the Cys residues are isolated from one another and cannot form a disulfide bond. In the denaturant-mediated unfolded state, the Cys residues are in close enough proximity to form a stable disulfide bond. This is a good example of both intrinsic and extrinsic factors (discussed below in section 1.6) contributing to disulfide bond formation.

Many therapeutic proteins like antibodies, enzymes and hormones contain disulfide bonds that crosslink distant regions to help maintain the native fold and stabilize the three-dimensional structure of proteins [45, 46]. Other roles of disulfide bonds include enzyme catalysis [47], regulation of biological activity [46], structural stabilization of extracellular proteins [47] and protection against oxidative damage [45]. It is not always easy to predict the effect a disulfide bond can have on a protein. In some cases, engineered disulfide bonds can have destabilizing effects, if the entropy of the folded state is decreased by reduced flexibility [3]. In the same way, mutating Cys to other amino acid residues may not

necessarily impede degradation via other pathways and in addition may be accompanied by a loss of biological activity.

Figure 1.4 shows how disulfide bond stability and stability provided to the folded protein by a disulfide bond are thermodynamically linked; ΔG of this cycle is zero [45]. In one pathway, formation of disulfide bonds occurs first by organizing the unfolded protein in such a way that the entropy loss accompanying protein folding is less than that of the unfolded state [45]. In an alternative pathway, the protein folds first bringing together distant Cys residues that can then be oxidized to form stable disulfide bonds.

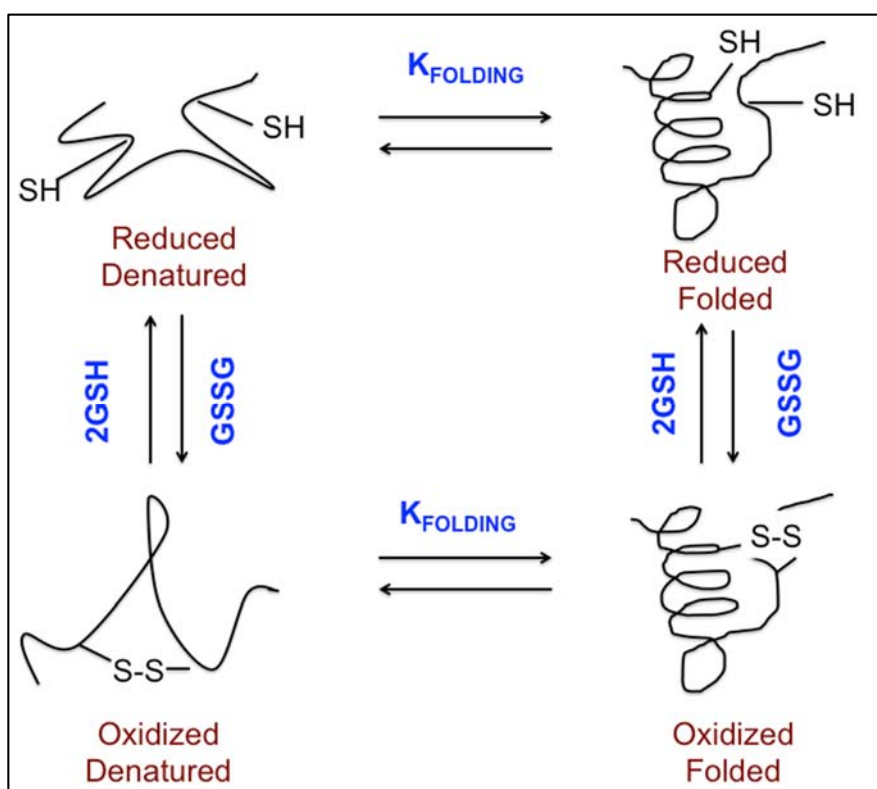


Figure 1.4: Thermodynamic cycle linking disulfide bond stability in the reduced and oxidized folded structure with the stability of the folded and unfolded states [45].

1.5.1 Disulfide bond disruption and rearrangement

Disulfide bonds are prone to undergo cleavage because they have 0.4-fold lower dissociation energy than C-C and C-H bonds [49]. Some of the mechanisms by which disulfide bonds may be disrupted include thiol-disulfide exchange, alkaline hydrolysis, photodegradation, thioether formation and trisulfide variants.

Thiol-disulfide exchange: This reaction typically occurs at alkaline pH [50], as the reactive species is the thiolate anion with pKa 8-9. Reactivity of the thiol group can however be increased by a decrease in pKa, influenced by surrounding amino acid residues. This means that thiol-disulfide exchange reactions cannot be ruled out even under physiological conditions or lower pH. Thiol-disulfide exchange involves the nucleophilic attack (S_N2) of a thiolate anion (RSH^-) on a disulfide bond (S-S) to form a transition state (TS), expelling a thiol group (with lower pKa) and forming a new disulfide bond [45]. In the TS, negative charge is delocalized over the three sulfur atoms, with more negative charge on the terminal sulfurs than the central sulfur atom [51]. The energy barrier between the reactants and TS is the activation energy (E_a) of the reaction and the potential energy difference between reactants and products in ΔE (Figure 1.5). Thiol-disulfide exchange is reversible at room temperature and at physiological pH. In the presence of oxygen, metal and reactive oxygen species (ROS) other products of thiol oxidation like sulfenic, sulfinic, sulfonic acids and thiosulfonate (Figure 1.6) may be generated [52, 53]. Both intra- and intermolecular disulfide bonds can undergo scrambling reactions (Figure 1.7).

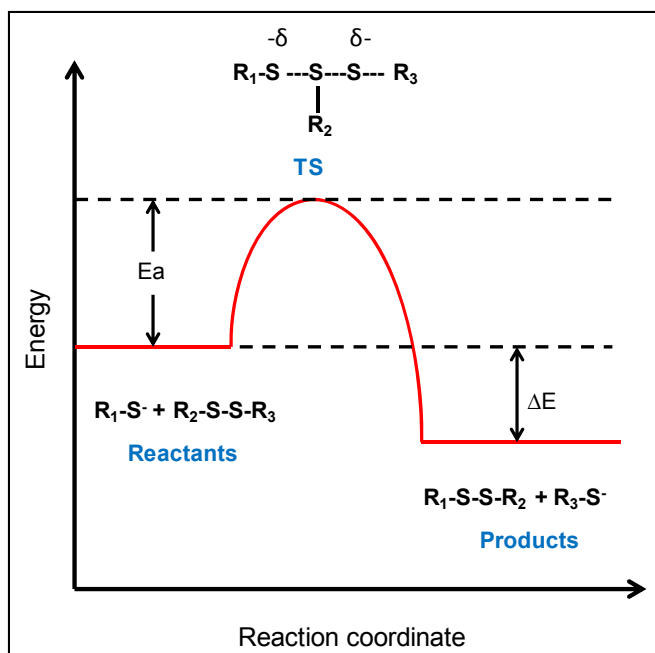


Figure 1.5: Energy diagram for thiol-disulfide exchange reactions.

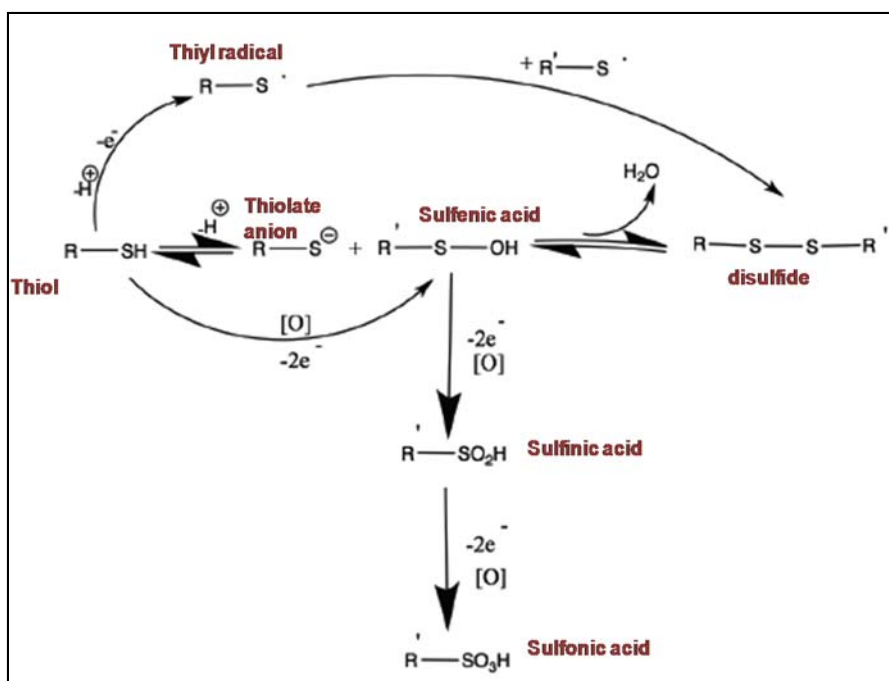


Figure 1.6: Oxidative pathways for thiols, adapted with permission from [52].
Copyright 2003 American Chemical Society.

Direct hydrolysis: The direct attack of a hydroxyl ion on a sulfur atom generates sulfenic acid (RSOH) and thiolate anion (RS⁻). RS⁻ is a reactive nucleophile which can react with another disulfide bond (R'SSR'') to form RSSR'' and release R'S⁻ (Figure 1.8B).

β -elimination: involves proton abstraction from the α -carbon on Cys to form dehydroalanine and thiocysteine. Removal of a sulfur atom from the thiocysteine generates a thiolate anion and hydrosulfide ion. Thiolate anion can then participate in the formation of non-native disulfide bonds via thiol-disulfide exchange or oxidative pathways. The hydrosulfide ion can initiate disulfide scrambling via thiol-catalyzed exchange. Dehydroalanine can react further with lysine to form lysinoalanine cross-links.

α -elimination: involves proton abstraction from the β -carbon of the Cys residue to form thiolate and thioaldehyde. Thioaldehyde can react further to form an aldehyde or imine group. Thiolate anion can also react further with disulfides, reactive oxygen species to form the products shown in Figure 1.6.

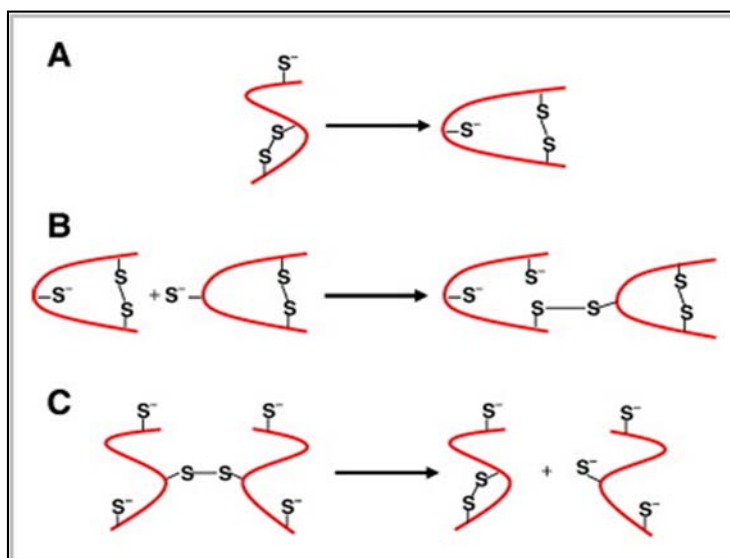


Figure 1.7: Different thiol-disulfide exchange reactions: A) intramolecular, B) intermolecular and C) intermolecular disulfide bond disrupted by thiol-disulfide exchange. Adapted with permission from reference [54].

At low pH: Protons can cleave disulfide bonds to give sulfenium ions (RS^+) under strong acidic conditions (Figure 1.8D). Sulfenium ions can then react with a sulfur atom in another disulfide bond via an electrophilic displacement to form a scrambled disulfide, expelling another sulfenium ion ($R'S^+ + RSSR \leftrightarrow R'SSR + RS^+$).

Photodegradation: Photoionization of tyrosine/tryptophan generates a solvated electron which can then reduce a disulfide bond to thiyl radical ($RS\bullet$) and thiolate anion (RS^-)¹. Thiyl radicals are reactive and can form disulfide bonds ($RSSR$) with other thiyl radicals or a reductive disulfide radical anion ($RSSR\bullet^-$) with a thiolate.

Thioether formation: Tous et al. identified thioether (-C-S-C) linkages (also called lanthionine) that are formed by the removal of a sulfur atom from a disulfide bond (-C-S-S-C-) in monoclonal antibodies (mAbs) during production and storage [55]. Thioether-linked antibodies have been detected even in endogenous antibodies [56]. The effect of thioether formation on the safety and efficacy of mAbs has not been reported; nevertheless it may affect protein conformation and biological activity and should be characterized in recombinant therapeutic proteins.

Trisulfide variants: Formation of trisulfides in proteins is not a common post-translational modification. Proteins that are known to form trisulfide variants include superoxide dismutase [57], mutein of interleukin [58], monoclonal antibodies [59] and hGH. A trisulfide variant (-C-S-S-S-C-) of hGH was identified only in recombinant protein expressed in E.coli and not in hGH preparations from human pituitaries [60]. Although the trisulfide variant did not affect the biological activity of hGH and converted completely into disulfides in IgG1 upon intraperitoneal injection in rats, the identification and characterization of such variants is still critical in determining protein drug quality.

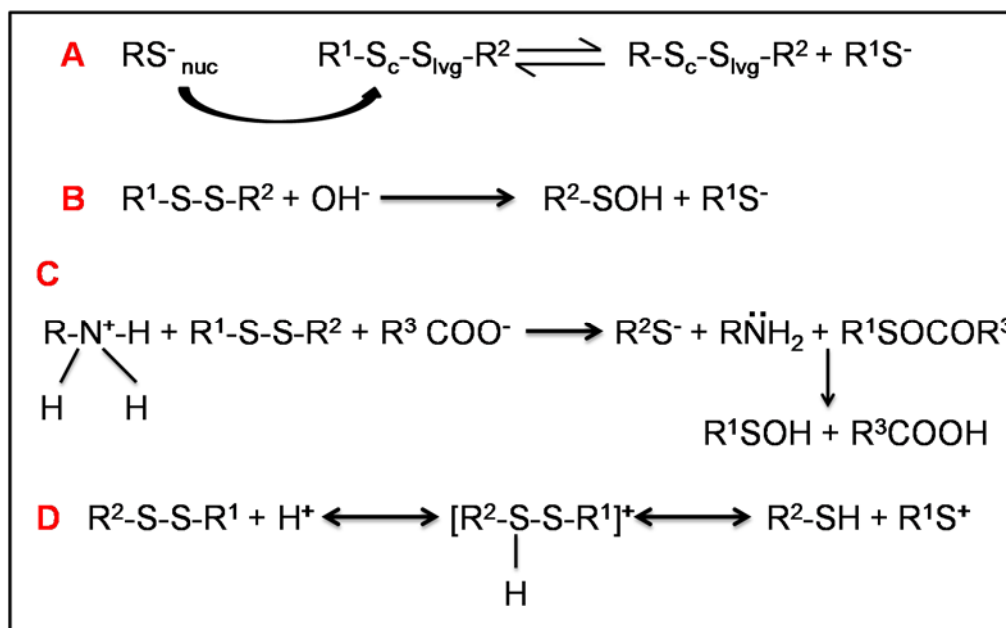


Figure 1.8: Different pathways that lead to disulfide bond disruption. A) Thiol-disulfide exchange (nuc: nucleophile, c: central sulfur and lvg: leaving group). B) Direct attack of hydroxyl ion on disulfide bond generates sulfenic acid and thiolate anion. C) Acid-base assisted hydrolysis of disulfide bond. D) Disulfide bond disruption under acidic conditions.

1.6 Factors that influence disulfide bond reactivity

Both intrinsic (physicochemical properties of the protein) and extrinsic factors (environmental factors like pH, temperature, mechanical force and in the presence of low molecular weight thiols in serum) can affect disulfide bond stability.

1.6.1 Intrinsic factors

These are factors that are innate to the protein itself. Primary sequence and higher order structure have been shown to affect thiol-disulfide exchange [61, 62]. Introduction of a positively charged amino acid neighboring a Cys residue in a model redox-sensitive

yellow fluorescent protein promoted electrostatic interactions with glutathione disulfide (GSSG) and decreased thiol pKa such that the rate of thiol-disulfide exchange increased 13-fold [62]. In another study with cyanogen bromide fragments of hen egg white lysozyme, for a Cys with two positively charged neighbors, the rate of thiol-disulfide exchange increased 6.5-fold in a 20 mM ionic strength medium relative to a lower ionic strength medium [63]. In a high ionic strength medium (≥ 20 mM), the rate of thiol-disulfide exchange was reported to decrease by 700-fold. Ionic influences from distant residues are minimized at a high ionic strength (≥ 20 mM), thus reducing the rate of thiol disulfide exchange.

In a thioredoxin from *E.coli*, disulfide reactivity is 10^2 - 10^3 times greater than that of normal disulfides due to the presence of a lysyl residue nearby with a positively charged group [47]. Similarly, in seminal ribonuclease, the presence of positively charged groups nearby (from Lys) was found to influence reactivity of the Cys31-Cys32 disulfide in addition to contributions from adjacency of the thiols and protein tertiary structure [64]. In peptides with the sequence Cys-X-Cys (where X is any amino acid), Zhang et al. have shown that disulfide bonds can be reduced rather easily. In contrast, in peptides with 4-5 residues between terminal Cys residues, the disulfide bonds were more resistant to reduction and formed stable loops [65]. The equilibrium constant for ring closure in dipeptide (-Cys-Cys-) and tripeptide (-Cys-Val-Cys-) models was not affected by the addition of an Ala residue C-terminal to Cys [65].

Disulfide reactivity can also be influenced by geometric strain that the protein native state imposes on a disulfide bond. For example, α -lactalbumin has four native disulfides of which Cys6-Cys120 was reported to be 140 times more reactive in the fully

unfolded state; observed super reactivity of this disulfide bond was attributed to the geometric strain imposed on it in the native folded state [66]. Zavialov et al. elucidated the relationship between protein structure and the formation of a disulfide bond between small heat shock protein 25 (Hsp25) and GSH [67]. Hsp25 has a free Cys residue at position 41, in a redox environment; Hsp25 in its reduced form (PSH) is in equilibrium with a mixed disulfide (PSSG) and its oxidized dimer (PSSP). Tertiary and/or quaternary structural changes induced by protein denaturation prevent Hsp25 from forming the dimer (PSSP) due to changes in proximity of the 2 subunits. This study shows the importance of the proximity of a disulfide bond to a Cys residue to undergo thiol-disulfide exchange. The authors also demonstrated the effect of steric and electrostatic hindrances on thiol-disulfide exchange. Figure 1.9 below shows the formation of a mixed disulfide between heat shock protein and GSH; steric and electrostatic hindrances appear after the formation of this mixed disulfide, entry of another GSH molecule is inhibited thus resulting in an intersubunit disulfide [67].

1.6.2 Extrinsic factors

Extrinsic factors like pH (neutral to alkaline) will influence the rate of disulfide interchange by affecting the formation of the reactive species. Thiol-disulfide exchange in general is accelerated under neutral to alkaline pH [45], however it can also occur in strong acidic media facilitated by a sulfenium ion (Figure 1.8D). Benesch and Benesch have reported that disulfide exchange is rapid in concentrated HCl and the rate drops below a concentration of 9 N. At lower acid concentrations, the amount of RS^+ generated also decreases thus affecting the overall rate of interchange [68]. Similar observations favoring

sulfenium ion mediated exchange in strong acidic media (7-12 N HCl) were reported by Ryle and Sanger [69]. In moderately acidic solutions disulfide interchange is not observed.

The effects of temperature on thiol-disulfide exchange reactions have been studied in small organic molecules and proteins [70, 71]. Thiol-disulfide exchange follows Arrhenius behavior with activation energies in the range of 30-70kJ/mol [70]. The effects of urea and temperature on the formation of the disulfide-linked dimer of Hsp25 are shown in Figure 1.10; the fraction of subunits forming the dimer decreases with increasing urea concentration and temperature [67]. In addition to pH and temperature, recent studies have shown the effects of an external mechanical force on thiol-disulfide exchange. Using cardiac titin domain as a model protein, Wiita et al. have shown that an applied mechanical force > 100 pN promotes thiol-disulfide exchange [70].

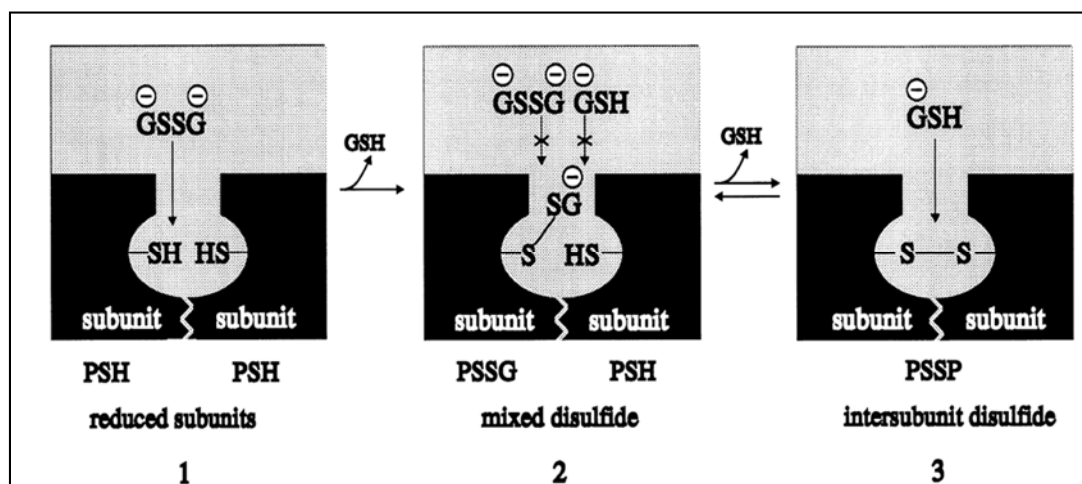


Figure 1.9: Scheme showing assumed effects of the appearance of steric and electrostatic hindrances after the formation of a mixed disulfide on thiol-disulfide exchange in Hsp25. The two subunits that form the subunit are shown in black. Adapted with permission from reference [67].

Disulfide exchange can also occur in the presence of low molecular weight thiols both *in vitro* and *in vivo*. Thiols in serum like GSH, cysteine and cystine are known to

mediate thiol-disulfide exchange [72]. The formation of correct disulfides inside cells is regulated by a redox environment, typically consisting of GSH and GSSG, and where the ratio of GSH/GSSG varies from 30: 1 to 100:1 [39]. Once the protein is secreted from the cell, it is no longer exposed to a reducing environment. Instead, exposure to small amounts of thiols can initiate disulfide interchange that results in altered conformations and thus reduced protein activity [39, 49]. Disulfide-linked dimers have been reported in IgG2 both in cell culture and in human serum [73]. Disulfide isoforms have also been observed in IgG4, a phenomenon known as Fab-arm exchange. Fab-arm exchange occurs in the presence of GSH concentrations as low as 0.5 mM *in vitro* and results in the formation of bispecific antibodies that can bind only monovalently even to repeating antigens [74]. Thus, disulfide exchange may be favored in the reducing environment in cell culture during recombinant protein expression and in blood after administration of protein therapeutics.

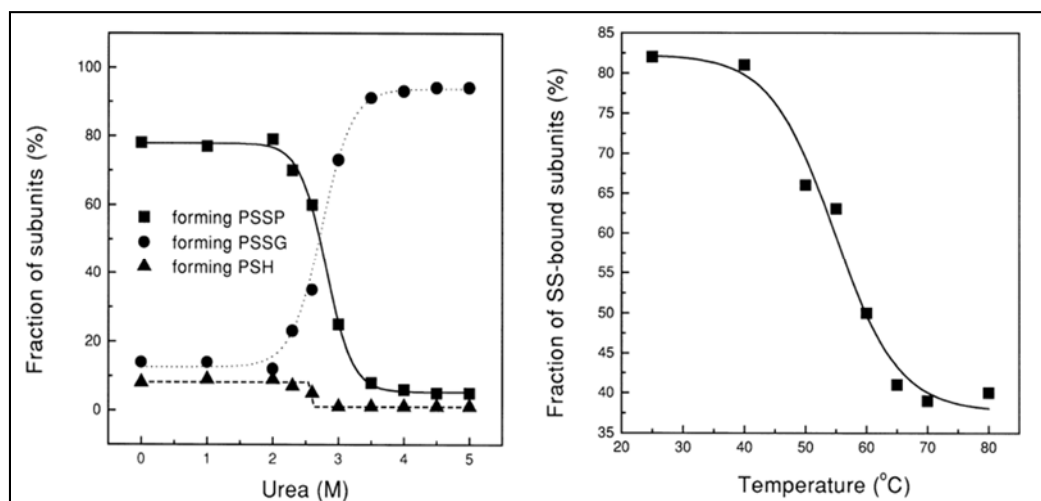


Figure 1.10: Dependence of fraction of subunits forming the inter-subunit disulfide bond (PSSP) on urea concentration (left) and on temperature (right). Adapted with permission from reference [67].

1.7 Impact on protein physical stability and biological activity

The effect of disulfide bonds on protein stability can be advantageous or disadvantageous; some of these effects are discussed in this section. In general, the native state of a protein (N) and its unfolded state (U) are in equilibrium such that $N \leftrightarrow U$. The introduction of a disulfide bond in a protein increases the free energy of U, with the assumption is that there is no difference in the enthalpies of the disulfide-linked protein and the reduced form of the protein. The contribution of an intramolecular disulfide bond to the decrease in entropy of U can be calculated using the equation: $\Delta S = -2.1-(3/2)R \ln n$, where R is the gas constant and n is the number of residues between the two Cys residues that form the intramolecular disulfide bond. An engineered intramolecular disulfide bond (Cys61-S-S-Cys98) in subtilisin E improved protein stability with a 4.5 °C increase in the melting temperature and a longer half time while there was no significant effect on enzymatic activity [75].

There have been numerous reports of how disulfide scrambling can lead to aggregation [76-79]. Aggregates can affect therapeutic efficacy, biological activity and safety of protein drugs. Atypical disulfide bond formation can lead to misfolded forms of proteins that are dysfunctional [55]. Proteins like bovine pancreatic trypsin inhibitor [80], bovine pancreatic ribonuclease A [81] and human proinsulin [82] fold into their native conformations only after most of their native disulfide bonds have been formed. This has provided a useful approach to studying the folding pathways of these proteins in detail by trapping the different disulfide intermediates. In natriuretic peptide receptor-A, an intermolecular disulfide bond functions as an allosteric bond where the formation of a

disulfide-linked dimer (undesirable in protein therapeutics) is essential for its activation [83]. Dillon et al. measured *in vitro* binding ability and biological activity of different IgG2 disulfide isoforms. The authors reported significant differences in biological activity of the isoforms and attributed these differences to changes in conformational angles and flexibility of the Fab region of IgG2 [38]. In another study, Qiao et al. reported that human insulin requires the correct formation of both intra- and interchain disulfide bonds to function properly [82]. Thus non-native disulfide bonding patterns can introduce conformational changes in proteins that may be detrimental to their therapeutic activity.

Disulfide bonds can also have a positive impact on biological activity. For example, recombinant immunotoxins (RITs) are anti-cancer agents that contain the Fv region of an antibody and a protein toxin from bacteria or plants. Liu et al. observed that engineering a disulfide bond into an RIT significantly lowered immunogenicity in mice while retaining cytotoxicity and anti-tumor activity [84]. HA22-LR-DB, formed by anti-CD22 Fv fused to domain III of pseudomonas exotoxin A, with a disulfide bond in domain III improved thermal stability and altered the kinetics of antibody formation in mice. In another study, the aggregation propensity in IgG1 antibodies was found to be significantly lower when compared to IgG2 antibodies, though they share 95% sequence identity [85]. This was attributed to the presence of an interchain disulfide bond in IgG1. Thus it is important to understand the roles of disulfide bonds in therapeutic proteins before suitable formulation strategies can be employed.

1.8 Formulation strategies for Cys-containing proteins

As described in the section above, disulfide bonds can be advantageous or disadvantageous to protein function/activity. Different strategies have been employed to minimize disulfide exchange and disulfide-mediated aggregation in proteins that contain free thiols and/or disulfide bonds [3]. Some of these approaches are discussed below.

1.8.1 Formulating proteins with a reducing agent

There have been reports of covalent dimer formation in E-Cadherin via a disulfide bond which ultimately leads to protein degradation [86]. Dithiothreitol (DTT), a reducing agent, and thiol group derivatizing agents like iodoacetamide and polyethylene-glycol maleimide were used in formulations to improve protein stability [86]. Addition of DTT prevented dimer formation and further inhibited protein precipitation. This strategy may not be suitable for all proteins, especially if the protein also contains a functional disulfide bond. Addition of a reducing agent could reduce the native disulfide bond and change protein conformation, exposing reactive centers to a myriad of degradation pathways.

1.8.2 Chemical modification of thiol groups

Another strategy to formulate proteins that contain unpaired cysteine residues is to derivatize the thiol group in order to prevent thiol mediated aggregation. The thiol group on Cys residues is a reactive species that can participate in oxidation reactions in addition to thiol-disulfide exchange. Some of the derivatizing agents that have been used are iodoacetate, iodoacetamide, 1,3-propane sultone, methyl methanethiosulfonate,

methoxycarbonylmethyl disulfide, maleimide, tetrathionates, and dinitrophenyl alkyl disulfides. Ruegg et al. have used 1,3 propane sultone to derivatize thiol groups on [Lys8] vasopressin, human serum albumin, bovine insulin and bovine pancreatic ribonuclease, increasing their stability to acid hydrolysis [87]. Some commonly used Cys-derivatizing agents are shown in Figure 1.11. Cys residues can also be PEGylated with PEG-maleimide, PEG-iodoacetamide and PEG-epoxide [3]. Proteins generally have fewer Cys than Lys residues thus making Cys-PEGylation more selective. PEGylated proteins have improved physicochemical stability, pharmacokinetic and pharmacodynamic properties.

PEG can also react with disulfide bonds; PEG-monosulfone forms a three carbon bridge with the native disulfide bond-sulfurs. For example, the native disulfide bond in interferon α -2b was conjugated with PEG and retained its biological activity and tertiary structure [88]. Although thiol derivatization is an attractive option, it is not a feasible one for proteins where free Cys and/or the native disulfide bond are important in biological activity and protein stability.

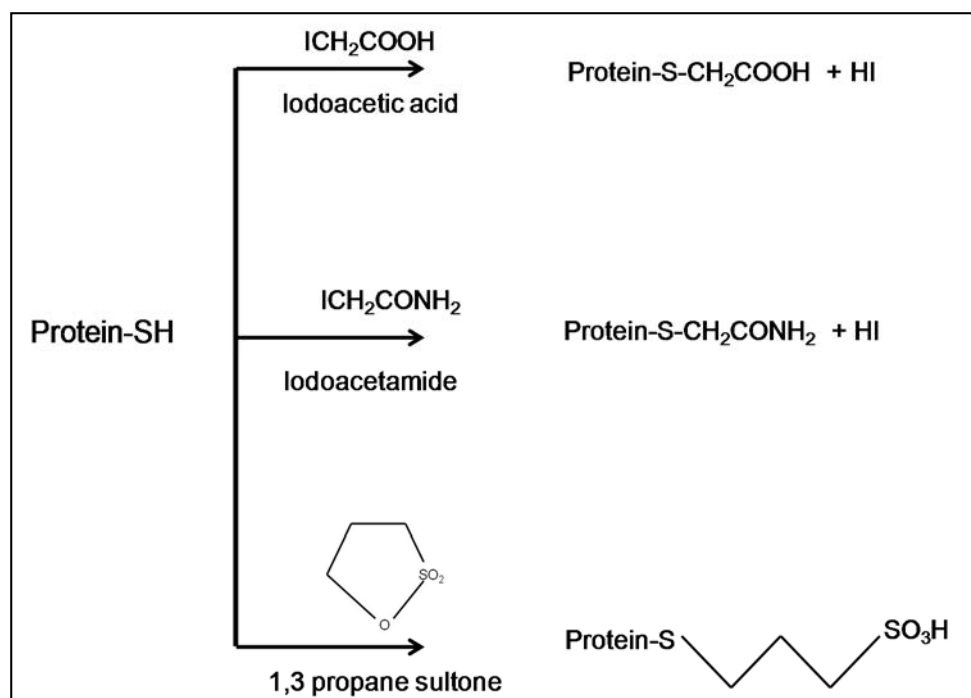


Figure 1.11: Thiol derivatizing agents that are commonly used to derivatize thiols in proteins to prevent reaction with other groups [3].

1.8.3 Protein engineering

Disulfide bond heterogeneity in therapeutic proteins can be reduced by mutating Cys residues with other non-reactive amino acids like Ser. Antibodies have a large number of disulfide bonds and they are classified by the number and type (inter/intra) of bonds. Allen et al. have shown that Cys→Ser mutations in IgG2 reduce disulfide bond heterogeneity while maintaining in vitro activity [89]. Browning et al. observed disulfide scrambling in interleukin-2 (IL-2) with one disulfide bond and a free Cys residue, under denaturing and alkaline conditions (Figure 1.12). The scrambled forms were less active than the native form [90]. A Cys125Ser mutant of IL-2 was found to be more stable to disulfide scrambling at alkaline pH.

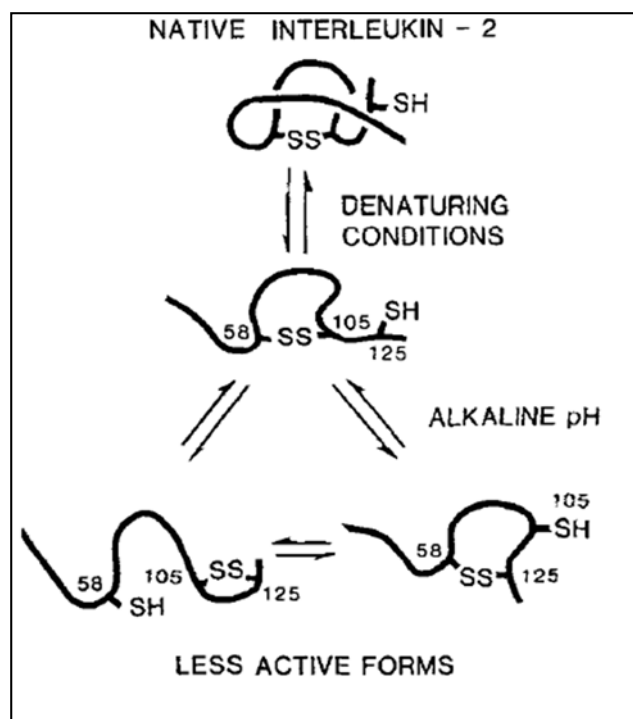


Figure 1.12: Thiol-disulfide exchange in interleukin-2. Adapted with permission from reference [90].

Junnila et al. determined the role of the C-terminal solvent exposed disulfide bond (Cys182-Cys189) in hGH by mutating the Cys residues with Ala. The hGH analogs were found to have reduced receptor binding affinity and stability compared to the wild type [91]. Although biological activity did not change drastically with this mutation, decreased stability of the mutants could lead to other degradation pathways, including aggregation. In other proteins, disulfide bonds have been introduced to improve overall stability [92]. Introducing an intermolecular disulfide bond is usually associated with increased protein stability. However, the effect of an intramolecular disulfide bond or the presence of an unpaired Cys can be unpredictable [93]. For example, Hsu et al. observed that deletion of a free Cys residue in recombinant keratinocyte growth factor affected protein stability [94]. This Cys (residue 40) was found to play an important role in maintaining protein stability

and structural integrity. Protein engineering may not always be a practical option, especially if the role of the Cys/disulfide bond is unknown. In addition to the strategies mentioned above (that cannot be applied to all therapeutic proteins), targeting specific mechanisms that contribute to and processing conditions that facilitate disulfide-mediated aggregation is instrumental in designing rational approaches to stabilize protein formulations.

1.9 Lyophilization of peptide and protein drugs

Therapeutic proteins are often lyophilized to improve storage stability. However, aggregation is known to occur even in the solid state [14, 79, 95, 96]. Proteins can undergo conformational changes during lyophilization, particularly during dehydration. Different effects of dehydration on protein conformation have been reported. Desai et al. observed freeze-drying induced partial denaturation in bovine pancreatic trypsin inhibitor [97]. In another study by Rupley et al., no difference in protein conformation was observed for lyophilized lysozyme when compared to the protein in aqueous solution [98]. Costantino et al. observed that the process of lyophilization itself induced structural changes in recombinant human albumin (rHA) [95]. During lyophilization of rHA, there was an increase in both β -sheet content and unordered structural elements resulting in partial protein unfolding. Such conformational changes can expose hydrophobic regions and reactive groups, facilitating aggregation via hydrophobic interactions and other covalent and non-covalent pathways.

Cryoprotectants and lyoprotectants such as sugars, polyols, polymers and surfactants are typically used to protect peptides and proteins from process induced degradation [99]. Solid properties of the excipients themselves must be investigated before they can be used with a protein or peptide. Mannitol, for example can crystallize into three different polymorphic forms (α , β and δ) as well as a hemi-hydrate. The type of polymorph that is generated will depend on lyophilization conditions and the presence of other excipients. The mannitol hemi-hydrate may release its crystal water during storage. Unlike mannitol, sucrose is amorphous after lyophilization. For some therapeutic proteins a combination of both amorphous and crystalline excipients may be advantageous. Prior knowledge of protein aggregation mechanisms may be beneficial to the process of excipients screening and selection to add further stability during freeze- and spray drying. This highlights the importance of understanding the effect of processing conditions and the use of excipients/stabilizers on chemical modifications in addition to determining storage stability under accelerated conditions.

1.9.1 Thiol-disulfide exchange in the solid-state

Lyophilized protein powders in the 'dry state' or 'anhydrous state' are thought to exhibit behavior and ionization states similar to pH conditions in aqueous solution before lyophilization, thus demonstrating a "pH memory" [100]. Alkaline hydrolysis of disulfide bonds and thiol-disulfide exchange are favored at neutral to alkaline pH, with the thiolate anion being the reactive species. Thus, formulating proteins with free thiols and/or disulfides in neutral to alkaline buffers prior to lyophilization would be expected to facilitate disulfide-mediated aggregation during lyophilization and storage in the solid state.

In addition, the three dimensional structure of proteins can influence disulfide-mediated degradation. Any structural rearrangement of proteins (perturbation during lyophilization) can have a profound effect on the pKa of reactive residues. Structural changes induced by process stresses can be probed using Fourier transform infrared spectroscopy (FTIR) [101]. FTIR spectra of human growth hormone lyophilized with and without excipients are shown in Figure 1.13. In addition, the presence of moisture and high storage temperatures can further influence reaction rates.

Thiol-disulfide exchange has been reported in lyophilized proteins like bovine serum albumin (BSA) when exposed to moisture at 37 °C [96]. Similarly, Constantino et al. investigated the mechanism of aggregation in recombinant human albumin (rHA) during storage in the solid state at 37 °C and 96% RH [95]. They attributed the formation of insoluble aggregates to disulfide exchange in the absence of any stabilizing excipients. Both BSA and rHA contain a free thiol in addition to disulfide bonds.

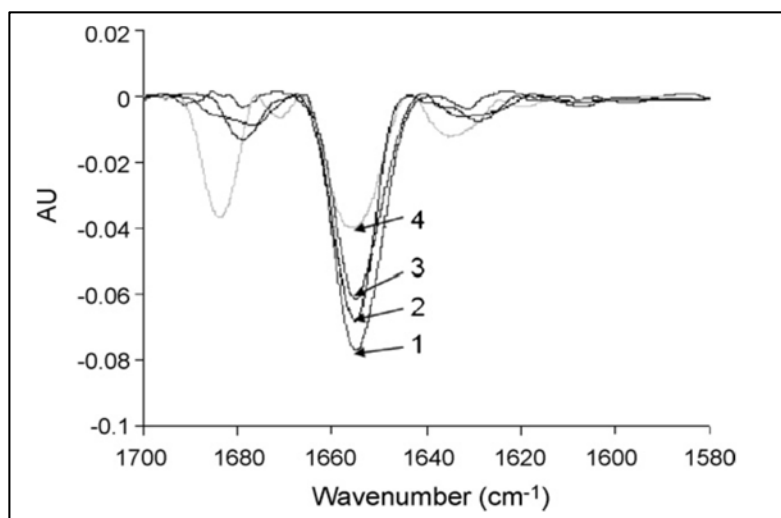


Figure 1.13: FTIR spectra of human growth hormone. 1- hGH in solution, 2- hGH lyophilized with sucrose, 3- hGH lyophilized with trehalose and 4- hGH lyophilized alone. Adapted with permission from reference [101].

Disulfide mediated aggregation can also occur in proteins with no free thiols but with disulfide bonds. One such example is insulin, in which β -elimination followed by thiol-catalyzed disulfide exchange results in the formation of insoluble aggregates during storage at 50 °C and 96% RH. These studies show how structural perturbations during lyophilization can have a profound effect on the storage stability of therapeutic proteins and disulfide bond reactivity, especially when exposed to high relative humidity and temperature.

1.10 Disulfide bond mapping

Recombinant proteins that are expressed in different systems like E.coli and CHO cells can have incorrectly folded, scrambled forms. Thus, it is important to identify the

presence and extent of scrambling in protein therapeutics to assess the quality of the final drug product, particularly for biosimilars. Conventional methods for disulfide bond determination such as NMR and Edman sequencing typically require large amounts of protein samples. Mass spectrometry coupled with ionization methods for ionizing large molecules has emerged as a novel analytical tool for characterizing protein structure and disulfide bond analysis/mapping.

The first step in disulfide bond mapping is to determine the number of disulfide bonds, by comparing MS spectra before and after protein reduction and the mass shift between the two samples. In recombinant human granulocyte-macrophage colony-stimulating factor (GM-CSF), ESI MS analysis before and after protein reduction revealed a 4Da shift in reduced protein spectra [102], suggesting that GM-CSF has two native disulfide bonds. Using an alkylating agent in addition to a reducing agent will confirm the presence of any free Cys residues when compared to the MS spectra of the native and non-reduced protein. The next step in disulfide bond mapping is to identify the location of these disulfide bonds and free Cys. This can be achieved with proteolytic and alkylating agents, comparing HPLC-UV chromatograms followed by tandem MS [103]. A combination of two or more proteolytic agents may be required for proteins where disulfide bonds are found to hinder proteolysis to form simple disulfide-linked peptides. Different ionization methods such as FAB/liquid secondary ion, plasma desorption (PD) and MALDI have been used to map disulfide bonds recombinant human interferon α -2b, human growth hormone and IL-4 [103].

Disulfide scrambling can occur even during analysis of disulfide bonding patterns in proteins and peptides. Suitable quench conditions (low pH) and thiol derivatizing agents

(described under formulation strategies for cysteine-containing proteins) can be employed to minimize these effects. Tang and Speicher describe four steps for disulfide bond mapping in proteins: i) cleaving proteins using proteases or other chemical reagents (shown in Table 1.1) under acidic and non-reducing conditions, ii) chromatographic separation of cleaved fragments, iii) use of disulfide reducing agents to confirm disulfide containing complexes and iv) characterizing disulfide-linked peptides using mass spectrometry (MS) and N-terminal Edman sequencing [104]. For large proteins (> 50 kDa) or proteins with multiple disulfide bonds and large domains that are typically resistant to denaturation and proteolysis, cyanogen bromide (CNBr) cleavage can be used. In this method, fragmentation occurs C-terminal to Met residues and large fragments are usually generated. Further, the low pH employed for CNBr cleavage prevents disulfide bond scrambling.

More recently, MS-based approaches (tandem-MS) for disulfide bond identification in proteins are becoming popular. Collision-induced dissociation (CID) in MS results in amide bond cleavage to yield b- and y- ions and is the most common tandem MS approach that is used to obtain protein structural information [105]. Disulfide bonds can either be broken or remain intact during CID. In addition to b/y ions, disulfide bonds can fragment (S-S or S-C bonds) to form free Cys residues, thioaldehydes, dehydroalanines and persulfides. Using CID as the fragmentation mode eliminates the need for sample reduction prior to MS analysis and high- end MS instruments. However, the formation of different cysteinyl peptide combinations can complicate analysis of the spectra and disulfide bond assignment, particularly for proteins for which the native disulfide linkage is unknown.

Haitao et al. have described a method for direct disulfide bond cleavage in the gas phase using electron transfer dissociation (ETD) [106]. Disulfide bond cleavage is preferred to peptide bond cleavage in ETD due to the fact that sulfur atoms capture electrons easily during the electron transfer process. This approach eliminates the need for two separate experiments, i.e., enzymatic digestion with and without reducing agents to determine the exact location of disulfide bonds. ETD and ECD are more suitable for disulfide bond identification, particularly for proteins in which the disulfide-bonding pattern is unknown. 16 disulfide bonds in an anti-HER2 mAb (Herceptin[®]) were mapped using ETD fragmentation followed by CID-MS³ on the dissociated peptides to further verify the disulfide arrangement. However, the authors report that a disadvantage of using ETD for disulfide bond identification is that for precursor ions with $m/z > 900$, in this case, the charge-reduced species is the dominant form and not the disulfide-dissociated peptide. Nevertheless, this analytical technique has been used to effectively map disulfide bonds in recombinant proteins such as human growth hormone and tissue plasminogen activator [106].

Zhang et al. used an electrolytic reduction approach coupled with desorption electrospray ionization mass spectrometry (EC/DESI-MS) to analyze disulfide linkages in insulin and somatostatin [107]. The EC/DESI-MS method could effectively map disulfide bonding patterns and determine the role of disulfide bonds in maintaining protein conformation based on charge state distributions. Use of a selenamide derivatizing agent with EC/DESI-MS facilitated the analysis of intra- and interpeptide disulfide bonds.

Table 1.1: Chemical cleavage reagents and proteases commonly used for disulfide mapping in proteins [104].

Protease	Cleavage site	Buffer conditions	Temperature	Reference
Chymotrypsin	Trp, Tyr, Phe	50 mM sodium phosphate, pH 5.5	37 °C	Schnaible et al (2002a) [108]
Endoproteinase Glu-C	Glu, Asp	100 mM sodium acetate, pH 4.0	24 °C	Lippincott and apostol (2002) [109]
Endoproteinase Lys-C	Lys	25 mM Tris-HCl, pH 6.8	37 °C	Lead et al (1999) [110]
Pepsin	non-specific	0.02N HCl, pH 2.0	37 °C	Bures et al (1998) [111]
Subtilisin	non-specific	50 mM sodium phosphate, pH 6.5	37 °C	Chong et al (2002) [112]
Thermolysin	non-specific	0.1 M triethylamine-HCl, pH 6.0	37 °C	Bures et al (1998) [111]
Trypsin	Lys, Arg	50 mM sodium phosphate, pH 6.0	37 °C	Schnaible et al (2002a) [108]
Trypsin (immobilized)	Lys, Arg	50 mM sodium phosphate, pH 6.5	23 °C	Chong and Speicher (2001) [113]

1.11 Research objectives and specific aims

The main objective of this research is to elucidate the mechanisms of thiol-disulfide exchange and identify factors that determine reaction rate in solution, during lyophilization and storage in the solid-state using model peptides derived from human growth hormone (hGH) and the intact protein. The studies test the central hypothesis that the rate of thiol-disulfide exchange differs in solution and amorphous solids and is affected by higher order structure. To test the hypothesis, the following specific aims were proposed:

Specific Aim 1: To elucidate the mechanism of thiol-disulfide exchange in aqueous solution and to determine the effect of pH, temperature, oxidation suppressants and peptide secondary structure on reaction kinetics. Thiol-disulfide exchange can result in protein aggregation via the formation of scrambled inter- and intramolecular disulfide bonds. Previous studies of thiol-disulfide exchange have been based on reactions between

proteins/peptides and low molecular weight thiols such as glutathione and DTT. However, these species are not representative of free thiol groups in larger proteins, and very little is known about the reaction mechanisms in these materials. Our hypothesis was that the reaction in solution will proceed primarily through the thiolate anion when oxidative pathways are inhibited and will be affected by secondary structure. To test this hypothesis, the effects of pH, temperature, oxidation suppressants and peptide secondary structure were explored in detail using model tryptic peptides derived from human growth hormone (hGH). The results provide mechanistic detail for thiol-disulfide exchange in aqueous solution, and are reported in Chapter 2.

Specific Aim 2: To elucidate the mechanism of thiol-disulfide exchange during lyophilization and storage in the solid state. To improve storage stability and shelf-life, many protein drugs are marketed as lyophilized powders. However, protein aggregation is known to occur even in the solid-state. Tryptic peptides derived from hGH and containing disulfide bonds were co-lyophilized with peptides containing free thiols to determine the effect of processing conditions on the thiol-disulfide exchange reaction and comparisons were drawn to aqueous solution studies. The results provide insights into the effects of lyophilization on thiol-disulfide exchange and peptide secondary structure contribution to reaction kinetics.

Specific Aim 3: To determine the effects of higher order structure on the kinetics of thiol-disulfide exchange using intact hGH. To test the applicability of studies with model peptides to a therapeutic protein, the studies of Aims 1 and 2 were extended to intact hGH. The studies in Aim 3 test the null hypothesis that the rates and mechanisms of thiol-disulfide exchange are unaffected by higher order structure and are identical in hGH and

in the model peptides. hGH has two disulfide bonds and no free cysteine residues. The results are expected to provide a qualitative measure of the effects of structure on the thiol-disulfide exchange reaction and an indication of the degradation propensity of disulfide bonds in hGH in comparison to model peptides.

1.12 Research Significance

The rate of failure of candidate drug molecules to successfully obtain regulatory approval to treat patients is significant, with only one in ten biopharmaceuticals reaching the market between 2003 and 2010 [114]. Selecting a promising molecule rather than one with inadequate developability characteristics can reduce the total cost of drug development and deliver greater value to a larger number of patients. Reducing the attrition rate of candidate drug molecules is dependent upon the selection of quality leads. Candidate drug molecules are evaluated for stability and shelf-life by assessing their potential to degrade by various physical and chemical pathways, including aggregation. Different aggregation pathways are often grouped together because of the lack of information on the mechanism of individual pathways. This can result in overlooking a relevant aggregation pathway, such as disulfide exchange, during candidate evaluation.

The aggregation of therapeutic proteins has been a major concern for the biopharmaceutical industry and regulatory agencies alike, since aggregates have been associated with adverse immune responses in patients. To make matters worse, aggregates are often difficult to detect and control. Strategies to determine aggregation propensity and to inhibit protein aggregation include molecular dynamics simulations [115], protein

engineering and process optimization [116] and formulation design [117, 118]. In addition, new analytical techniques are being developed to detect protein aggregates formed during manufacturing and storage. While these strategies are effective for some proteins, the inherent structural complexity of these large molecule drugs makes it challenging to devise a general approach that can be adapted to all classes of therapeutic proteins.

The development of protein therapeutics currently involves a trial and error paradigm, which is often the rate-limiting step in getting a drug approved and to the market. In order to effectively control aggregation in therapeutic proteins, the mechanisms of relevant degradation pathways must be understood in detail. Detailed mechanistic studies of protein aggregation pathways like thiol-disulfide exchange, in combination with computational methods will facilitate successful development of protein pharmaceuticals and minimize associated costs.

Thiol-disulfide exchange and disulfide scrambling are widely recognized as common routes to covalent aggregation in protein drugs. While there are reports of thiol-disulfide exchange reactions between low molecular weight thiols like GSH [67, 119] and CySH [120] and proteins, they are not entirely applicable to disulfide-mediated aggregation in proteins since steric effects may influence reaction rates and these low molecular weight thiols may not always be present in protein formulations. Thus, understanding the mechanisms of thiol-disulfide exchange in aqueous solution and in the solid-state will improve our ability to control aggregation in therapeutic proteins. Understanding the mechanism of chemical reactivity of a protein is strategic in that it will steer protein formulation development away from a trial and error paradigm. The results obtained will facilitate the design of rational approaches to control disulfide-mediated aggregation in

solution and lyophilized formulations and decrease the likelihood of immunogenic effects after administration.

Finally, biosimilars are proteins that are intended to be similar to the innovator drug with respect to quality, safety and efficacy. Variations in biosimilars production include manufacturing, cell culture and purification processes and the type of formulation used. These differences can have significant effects on the quality of a protein drug. There are many analytical tools that are currently being used to characterize follow-on protein products [121, 122]. A combination of these analytical methods and the knowledge of disulfide rearrangement mechanisms and kinetics are expected to provide improved screening.

CHAPTER 2. ELUCIDATING THE MECHANISM AND KINETICS OF THIOL-DISULFIDE EXCHANGE IN PEPTIDES DERIVED FROM HUMAN GROWTH HORMONE IN AQUEOUS SOLUTION

This work was published in the *Journal of Pharmaceutical Sciences* DOI 10.1002/jps.23906, content reproduced with permission from Wiley.

2.1 Abstract

Disulfide bonds stabilize proteins by crosslinking distant regions into a compact three-dimensional structure. However, disulfide bonds can participate in degradation pathways that can contribute to protein aggregation. In this chapter, experimental data for the mechanism of thiol-disulfide exchange in tryptic peptides derived from human growth hormone in aqueous solution is presented. Reaction kinetics were monitored to investigate the effect of pH (6.0-10.0), buffer concentration (10, 20 and 40 mM), temperature (4-50 °C), oxidation suppressants (EDTA and N₂ sparging) and peptide secondary structure (linear vs. cyclic). The concentrations of free thiol containing peptides, scrambled disulfides and native disulfide-linked peptides generated via thiol-disulfide exchange and oxidation reactions were determined using RP-HPLC and LC-MS. Concentration vs. time data were fitted to a mathematical model using non-linear least squares regression analysis. Excluding oxidation suppressants (EDTA and N₂ sparging) did not influence the intrinsic

rate of thiol-disulfide exchange. In addition, peptide secondary structure was found to influence the rate of thiol-disulfide exchange.

2.2 Keywords

Protein, peptide, human growth hormone, oxidation, kinetics, aggregation and thiol-disulfide exchange.

2.3 Introduction

In therapeutic proteins, correct disulfide linkages are critical to the biological activity and stability of this growing class of drugs [54]. For example, non-native disulfide bonding patterns in IgG antibodies have been associated with changes in receptor binding affinity, stability, and circulating half-life [123]. A disulfide-linked homodimer of human growth hormone (hGH) showed reduced receptor binding affinity and attenuated cell proliferative activity [124]. Human albumin or albumin fusion proteins, which contain 17 disulfides and may contain a free-thiol, also may be prone to deleterious disulfide-mediated events [125]. The fundamental mechanism of thiol-disulfide exchange has been defined in previous reports using low molecular weight thiols and proteins [45, 61, 119, 120]; however, controlling these reactions in therapeutic proteins still remains challenging. It is often difficult to predict the most labile disulfide bonds based on structure alone [126], suggesting that the structural determinants of thiol-disulfide exchange may be weaker than for other reactions such as deamidation [127, 128]. An intact IgG antibody can have more

than 20 disulfide bonds, with the potential to form more than 200 species with a single scrambled intra- or intermolecular disulfide. While “reducible” aggregates are common in protein drug formulations, the disulfide bonds involved are not often identified. There have been reports from our group [129] and others [70] that thiol-disulfide exchange is sensitive to process-induced stresses such as freezing and fluid shear, but the mechanisms of these effects and their interplay with protein structure and fluid composition have not been fully elucidated.

Different factors were critical in designing experiments relevant to achieving the overall goals of this project. First, human growth hormone (hGH) is a 4-helix bundle protein that belongs to the cytokine family with 191 amino acids and two disulfide bonds (no free cysteine residues). The C-terminal disulfide bond is known to have a functional role [91]; hence the common formulation strategies for Cys-containing proteins (discussed in Chapter 1) are not applicable for hGH. Further, hGH is known to aggregate in solution [130,131] and the solid state [132-134], facilitated by the formation of scrambled disulfides [91, 135] and/or protein unfolding [130, 136]. Thus, hGH is a tractable model system for detailed mechanistic studies. Trypsin digestion map for hGH is shown in Figure 2.1 with the disulfide linked peptides; i) T6 and T16 and ii) T20 and T21. Tryptic peptides derived from the solvent exposed disulfide bond (T20, T20-T21 and cT20-T21, Table 2.1) in hGH were used as model compounds to elucidate the mechanism of thiol-disulfide exchange (Scheme 2.1). The T20 peptide contains Cys182, which has been identified as the most reactive thiol in hGH [137].

Second, physical and chemical instabilities are interrelated, for example a chemical modification can lead to an unfolding event and vice versa, both modifications contribute

to the overall drug decomposition rate. In a review by Waterman and Adami, the authors state that drug shelf-life is determined by the rate of formation of individual products and rarely by the overall drug decomposition rate [138]. The use of peptide model compounds allows determination of mechanisms and rate constants for a specific chemical modification in the absence of higher order structure and other degradation pathways, thus facilitating better molecular and formulation design approaches.

Finally, elucidating the reaction mechanism in solution will provide a basis for better understanding reactions in solid state systems and determining the influence of other external factors like processing and storage conditions. T20 was used in its reduced form to react with linear (T20-T21) and cyclic (cT20-T21) peptide models of the native disulfide bond. The results show that for these hGH tryptic peptides, the mechanism of thiol-disulfide exchange is pH independent and the reactions follow Arrhenius behavior. However, the observed rate constant (k_{obs}) depends on the concentration of thiolate anion and hence the solution pH. Intrinsic rates of thiol-disulfide exchange are not affected by oxidation of free thiol-containing peptides even in the absence of oxidation suppressants. Additionally, cyclization of the peptide is shown to influence the kinetics of thiol-disulfide exchange, with the cyclic peptide having 10-fold lower reactivity when compared to the linear peptide.

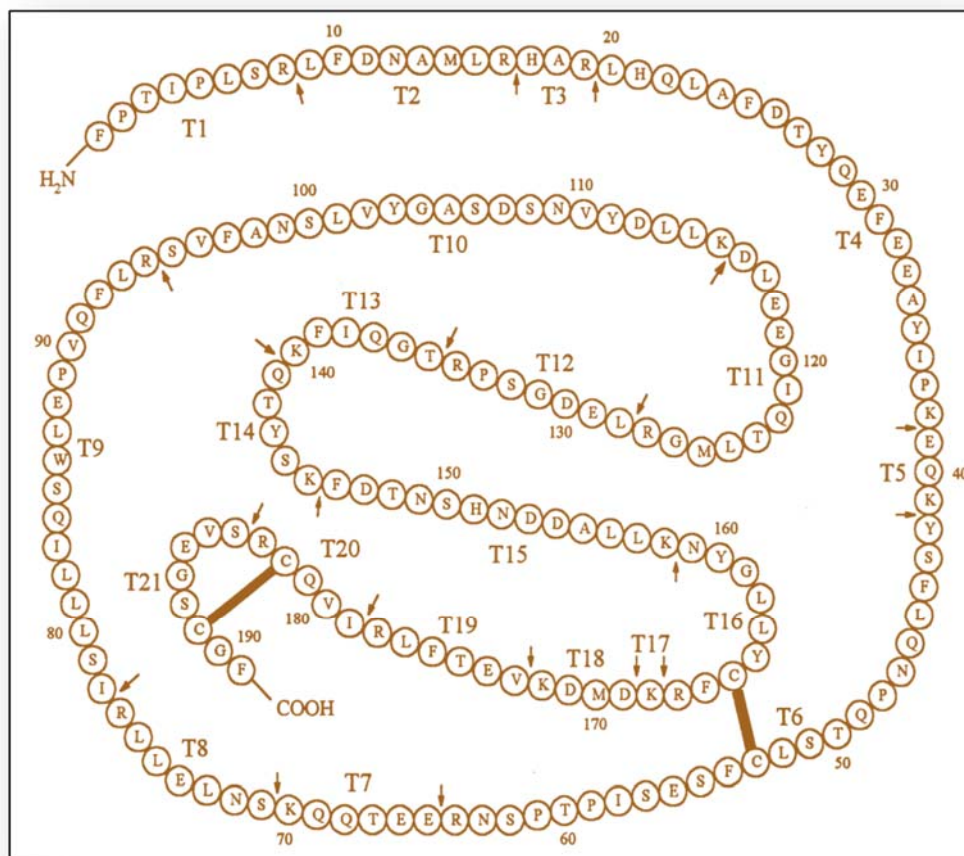


Figure 2.1: hGH-tryptic digestion map, tryptic fragments are labeled T1 to T21 starting from the N-terminus. Disulfide bonds are represented by the two solid lines between T6-T16 and T20-T21. Adapted with permission from [139].

Table 2.1: Abbreviations and amino acid sequences of hGH-derived peptides used in studies of thiol-disulfide exchange.

Abbreviation	Description	Amino acid sequence	Theoretical mass	Observed mass
T20	Monomeric peptide, free SH group	NH ₂ -IVQCR-OH	617.3319	617.3290
T21	Monomeric peptide, free SH group	NH ₂ -SVEGSCGF-OH	784.3062	784.3067
T20-T20	Homodimer, disulfide-linked	NH ₂ -IVQCR-OH ⋮ NH ₂ -IVQCR-OH	1232.6482	1232.6247
T21-T21	Homodimer, disulfide-linked	NH ₂ -SVEGSCGF-OH ⋮ NH ₂ -SVEGSCGF-OH	1566.5978	1566.5984
T20-T21	Heterodimer, disulfide-linked	NH ₂ -IVQCR-OH ⋮ NH ₂ -SVEGSCGF-OH	1399.6225	1399.6247
cT20-T21	Cyclic peptide, disulfide linked	NH ₂ -IVQCRSVEGSCGF-OH	1381.6118	1381.6201
rT20-T21	Linear peptide, free SH groups	NH ₂ -IVQCRSVEGSCGF-OH	1383.6275	1383.6344

2.4 Materials

Model peptides T20, T21, T20-T21 and cT20-T21 (see Table 2.1 for structures) were purchased from GenScript (Piscataway, NJ) with > 95% purity and supplied as a lyophilized powder. HPLC grade acetonitrile (ACN), NaCl and KCl were purchased from Fisher Scientific Co. (Pittsburgh, PA). H₂O₂ and Na₂CO₃ (anhydrous granules) were obtained from Mallinckrodt Baker Inc. (Phillipsburg, NJ). K₂HPO₄ and ethylenediaminetetraacetic acid (EDTA) were purchased from Sigma Chemical Co. (St. Louis, MO). Trifluoroacetic acid (TFA) and formic acid were obtained from Thermo

Scientific (Rockford, IL). Double-distilled water (DDI) used for buffer preparation and as HPLC mobile phase was deionized and purified using a Milli-Q water system, Millipore Ltd (Billerica, MA) and filtered with a 0.2 μm filter.

2.5 Methods

2.5.1 Preparation of peptide stock solutions and disulfide linked peptides for kinetic studies

All peptides were used as provided by the manufacturer. Stock solutions were prepared in a 0.1% formic acid solution in DDI. T20, T21, T20-T21 and cT20-T21 stock solutions were stable at 4 °C for up to 2 weeks and T20-T20, T21-T21 solutions (pH <3.0 after quenching with a 0.5% formic acid solution) were stable for 4 days at 4 °C. Far-UV (190-260 nm) CD analysis with a J-815 CD spectrometer (JASCO, Easton, MD) was used to assess peptide secondary structure.

2.5.2 Homodimer formation

T20-T20 and T21-T21 homodimers (Table 2.1) were synthesized in-house using H_2O_2 as an oxidizing agent according to a method described by Luo et al. [140]. H_2O_2 in phosphate buffer (pH 8.0, 2 mM) was added to solutions of T20 or T21 (4 mM) monomers in a 1:2 molar ratio (total reaction volume < 1 mL) and allowed to react for 1 day. The reaction was then quenched with a 0.5% formic acid solution (2x reaction volume). Conversion of monomer to homodimer was > 98% for both monomers, as determined by both RP-HPLC (Figure 2.2) and LC-MS. These homodimers were then used to construct calibration plots and synthetic standards were not purchased from GenScript. Attempts to

produce the T20-T21 heterodimer using a similar method resulted in very low yields, so synthetic T20-T21 was purchased from GenScript (Piscataway, NJ).

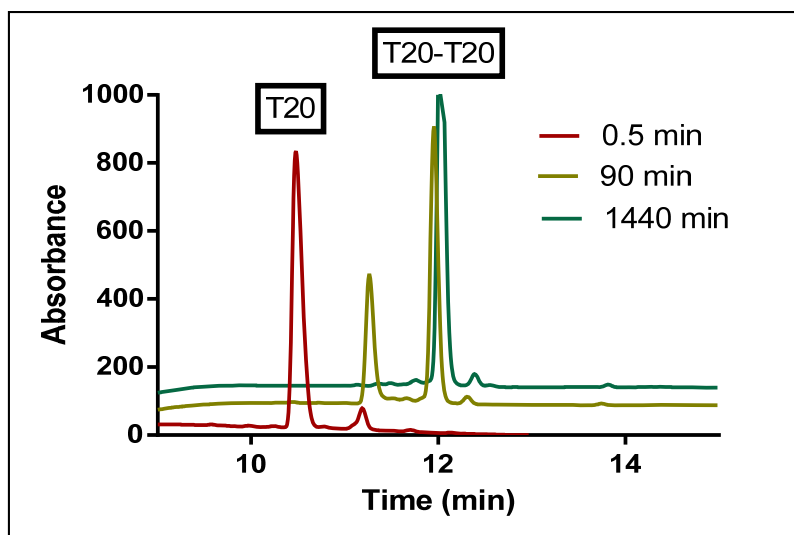


Figure 2.2: HPLC chromatograms showing T20-T20 formation over time at pH 6.0 in 50 mM phosphate buffer with H₂O₂ as the oxidizing agent.

2.5.3 Buffer preparation

Phosphate buffers (PB) for pH 6.0-8.0 and carbonate buffers (CB) for pH 9.0-10.0 were prepared at different concentrations (10, 20 and 40 mM) to enable extrapolation of rate constants to zero buffer concentration. The ionic strength of all buffers was adjusted to 0.08 M using KCl for PB and NaCl for CB. To minimize oxidation of free thiols, 0.5 mM EDTA and N₂ were used. Buffers were sparged with N₂ for 30 min and then degassed and filtered with a 0.2 μm (Millipore, MA) filter before use. For reactions without suppression of oxidation, PB (pH 7.0, 10 mM) was used without EDTA and N₂.

2.5.4 Quantification of reactants and products by HPLC

RP-HPLC assays were developed to detect and quantify each of the seven species (T20, T20-T20, T20-T21, T21, T21-T21, cT20-T21, rT20-T21) with baseline resolution (Figure 2.3). Samples were analyzed using reverse-phase high-performance liquid chromatography (RP-HPLC, Agilent 1200 series). The system was equipped with a UV detector operating at 215 nm for all studies. Agilent Chemstation software was used for data acquisition and analysis. A ZORBAX Eclipse plus C18, 5 μm (4.6 X 250 mm) analytical column (Agilent Technologies, Santa Clara, CA) was used with gradient elution (column temperature was maintained at 25 $^{\circ}\text{C}$). Solvent A was 0.1% TFA (pH~2.5) in water and Solvent B was 0.1 % TFA in acetonitrile. Elution was performed at 1 mL/min starting with 14% Solvent B, which was increased to 47% in 5.2 min, then held at 47% for 3 min and finally returned to 14% at 8.3 min. Total run time for each sample was 12 min. The retention times for T20, T20-T20, T20-T21, T21 and T21-T21 were 4.7 min, 5.2 min, 6.5 min, 7.2 min and 7.9 min respectively (Figure 2.3), as confirmed by mass spectrometry (ESI-QTOF-MS, Agilent). For studies with the cyclic peptide, a similar gradient elution was used with a total run time of 13 min. The retention times for T20, T20-T20, cT20-T21 and rT20-T21 were 4.8 min, 5.3 min, 7.3 min and 7.7 min, respectively, as confirmed by MS. Calibration curves were linear in the following concentration ranges: 20 μM -1 mM (T20), 10-500 μM (T20-T20), 5-500 μM (T20-T21), 20-180 μM (T21), 10-200 μM (T21-T21), 5-500 μM (cT20-T21), and 5-500 μM (rT20-T21). Limits of detection (S/N = 2) were 15 μM (T20), 2.5 μM (T20-T20), 1 μM (T20-T21), 5 μM (T21), 5 μM (T21-T21) and 5 μM (cT20-T21 and rT20-T21). No cleavage of disulfide bonds was observed at pH levels above the Cys thiol pKa, as has been previously reported [141].

At the end of each experiment, the total mass of the identified products was >98% for pH 6.0-9.0 and >95% for pH 10.0 of the total initial mass of the reactants. Based on the limits of detection and linear ranges of the calibration curves, initial reactant concentrations of 350 μM (T20) and 250 μM (T20-T21) were used. The amount of T20-T20 and T20-T21 formed via oxidative pathways was determined by mass balance. For example, in the absence of oxidation, the amount of T20-T20 generated will equal the amount of T20-T21 consumed. Any additional T20-T20 formed is assumed to occur via oxidation.

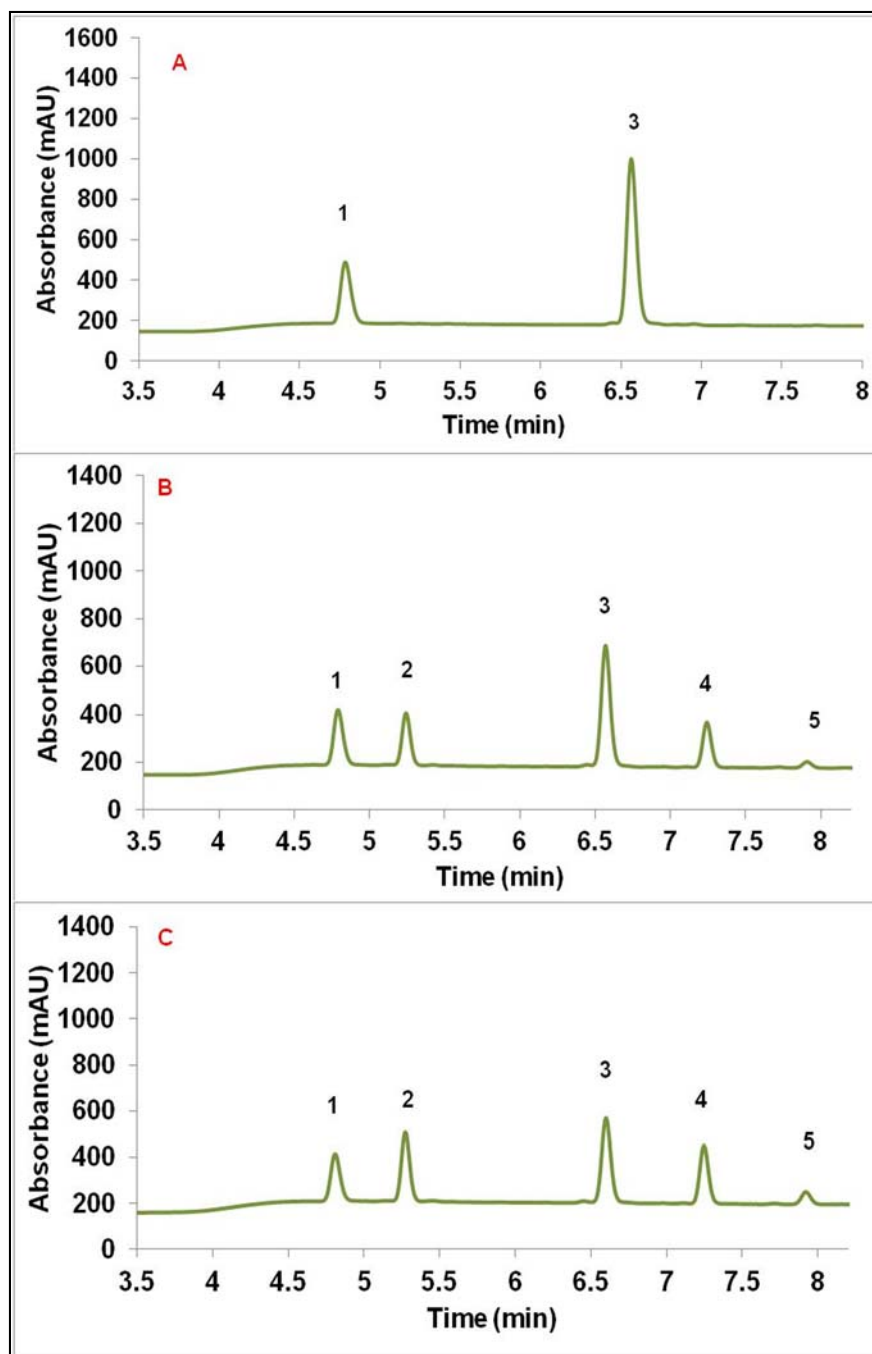


Figure 2.3: HPLC chromatograms (215nm) at various times during the reaction of T20 with T20-T21 at pH 7.0, 10 mM phosphate buffer with 0.5 mM EDTA. A) 0 mins. B) 180 mins and C) 1440 mins.

2.5.5 Determination of reaction order

The initial reaction rates were monitored at room temperature (22 °C) and pH 7.0 (10 mM PB, 0.5 mM EDTA, 0.08 M ionic strength, N₂ sparged) in a 2 mL microcentrifuge tube with a total reaction volume of 1250 μ L. Initial volumes of T20 were 500 μ L, 500 μ L and 250 μ L, respectively and initial concentrations were calculated based on final concentrations listed below. To determine the reaction order with respect to T20, a final concentration of T20-T21 of 250 μ M was used and kinetics monitored at different initial concentrations of T20 (80, 250, 370 and 630 μ M). In the same way, the reaction order with respect to T20-T21 was determined using a fixed initial concentration of T20 (350 μ M) and different initial concentrations of T20-T21 (130, 270, 410 and 600 μ M).

2.5.6 Thiol-disulfide exchange reactions

Reaction kinetics were monitored at five different pH values (6.0, 7.0, 8.0, 9.0, and 10.0). For the reaction, 500 μ L of T20 (875 μ M), 500 μ L of T20-T21 (625 μ M) and 250 μ L of buffer (50, 100 and 200 mM) were added to a 2 mL microcentrifuge tube and mixed by pipetting. The final pH of the reaction mixture was adjusted using NaOH or HCl (exact volume to be added was determined from pilot studies at each pH) after a 100 μ L aliquot was removed and quenched to verify initial concentrations ($t = 0$ min). Samples were withdrawn in triplicate at all time points and quenched with 10 μ L of 20% formic acid solution in DDI to prevent further scrambling. 30 μ L of this quenched solution was then used for RP-HPLC analysis. Dilution factors from total reaction volume, addition of NaOH/HCl for pH adjustment and quench solution were accounted for in determining final peptide concentrations. No measurable changes in concentration were observed in

quenched samples within the time scale of the experiment. The cyclic peptide cT20-T21 (see Table 2.1) was reacted with T20 in 10 mM PB and CB (0.08 M ionic strength, 0.5 mM EDTA and N₂ sparged). The reaction was monitored kinetically at 22 °C and at 40 °C at pH 7.0 and 9.0 for 6 hours. Initial reactant concentrations were [T20] = 450 μM and [cT20-T21] = 45 μM. Quench conditions were the same as in studies with T20-T21 and aliquots were withdrawn in triplicate and analyzed using RP-HPLC.

2.5.7 Determining activation parameters for the reaction of T20 with T20-T21

Reaction kinetics were also monitored at five different temperatures (in triplicate): 4, 15, 25, 40 and 50 °C at pH 7.0 (PB, 10 mM with 0.5 mM EDTA). Initial reactant concentrations, quench conditions and sample analysis were identical to those in the pH studies. Arrhenius parameters obtained from accelerated storage conditions are generally used to predict protein stability at low temperatures [142]. However, for proteins, non-Arrhenius behavior is not uncommon due to the complexity of the aggregation process itself. In simpler model compounds like peptides, we expect the reaction to follow Arrhenius behavior in a narrow temperature window. Use of high temperatures (≥ 60 °C) can lead to degradation of the peptides. Thus, for the hGH-derived peptides used in studies here, Arrhenius behavior was investigated from 4 to 50 °C using Equation 2.1 below.

$$k = A \exp [-(E_a/RT)] \quad \text{Eq. 2.1}$$

Where, k- rate constant, A- preexponential factor, R- gas constant, T-temperature and E_a is the activation energy.

The Eyring equation (Eq 2.2) provides molecular insight into how a reaction progresses with changing temperature. Activation energy, E_a and enthalpy of activation (ΔH^\ddagger) only have small differences in their values and are often used interchangeably.

$$\ln (k/T) = (-\Delta H^\ddagger/T)(1/T) + \ln (k_B/h) + (\Delta S^\ddagger/R) \quad \text{Eq. 2.2}$$

Where, k - rate constant, T -temperature, ΔH^\ddagger - enthalpy of activation, ΔS^\ddagger - entropy of activation, k_B – Boltzmann constant, h – Planck's constant and R – gas constant.

2.6 Data analysis

For the reaction of T20 with linear T20-T21, the data were consistent with a reaction scheme involving: (i) equilibrium ionization of T20 and T21, (ii) reversible thiol-disulfide exchange reactions of the ionized thiolate forms of T20 and T21 (i.e., T20-S⁻, T21-S⁻) with T20-T21 and (iii) oxidation of the ionized thiolate forms of T20 and T21 (Scheme 2.1). A system of equations corresponding to this scheme was used to describe the time-varying concentrations of each species and to estimate values of the microscopic rate constants.

$$T20S^- = T20 / \{1 + (10^{-7}) / (10^{-pK_a})\} \quad \text{Eq. 2.3}$$

$$T21S^- = T21 / \{1 + (10^{-7}) / (10^{-pK_a})\} \quad \text{Eq. 2.4}$$

$$\frac{d [T20-T21]}{dt} = -k_1 [T20S^-][T20-T21] + k_2 [T20-T20] - k_3 [T21S^-][T20-T21] + k_4 [T21-T21][T20S^-] + k_5 [T20S^-]^3 [T21S^-] \quad \text{Eq. 2.5}$$

$$\frac{d [T20-T20]}{dt} = k_1 [T20S^-][T20-T21] - k_2 [T20-T20][T21S^-] + k_5 [T20S^-]^3 [T21S^-] \quad \text{Eq. 2.6}$$

$$\frac{d [T21-T21]}{dt} = k_3 [T21S^-][T20-T21] - k_4 [T21-T21][T20S^-] + k_6 [T21S^-]^2 \quad \text{Eq. 2.7}$$

$$\frac{d [T20S^-]}{dt} = -k_1 [T20S^-][T20-T21] + k_2 [T20-T20][T21S^-] + k_3 [T21S^-][T20-T21] - k_4 [T21-T21][T20S^-] - k_5 [T20S^-]^3 [T21S^-] \quad \text{Eq. 2.8}$$

$$\frac{d [T21S^-]}{dt} = k_1 [T20S^-][T20-T21] - k_2 [T20-T20][T21S^-] - k_3 [T21S^-][T20-T21] + k_4 [T21-T21][T20S^-] - k_5 [T20S^-]^3 [T21S^-] - k_6 [T21S^-]^2 \quad \text{Eq. 2.9}$$

In the kinetic model, time is the independent variable, reactant and product concentrations are dependent variables, and the rate constants (k_1 , k_2 , k_3 , k_4 , k_5 and k_6) are treated as parameters to be determined by non-linear regression. The model returned a value of 8.3 for thiol pKa when it was defined as a parameter to be determined by regression of pH 7.0 data. Thus, the pKa values for the ionization of the T20 and T21 thiol groups (K_{a20} , K_{a21}) were fixed at 8.3 for all reaction conditions, consistent with previous reports for cysteine [143, 144]. Rate constants k_1 , k_2 , k_3 , and k_4 are second-order rate constants for thiol-disulfide exchange; k_5 is a composite rate constant for the production of T20-T21 and T20-T20 by the oxidation of T20S⁻ and T21S⁻. A composite oxidation rate constant (k_5)

was used to minimize model parameters. This composite reaction (R5, Scheme 2.1) was sufficient to describe the minor oxidation observed when oxidation was suppressed (i.e., with EDTA and N₂ sparging). Kinetic data were fitted to the model (Equations 2.3-2.9) using non-linear regression (SCIENTIST[®], Micromath Research, St. Louis, MO). SCIENTIST[®] reports Model Selection Criterion (MSC) values to determine the most appropriate models; a greater MSC value represents a better model. MSC is independent of the scaling of data points and is similar to the Akaike Information Criterion (AIC), which is considered to be a better measure of model validity than R² values for non-linear models [145]. MSC value for the model with composite k₅ was greater than the MSC value for a model with two separate oxidation rate constants. When oxidation was not suppressed, the additional parameter k₆ for the oxidation of ionized T21 to T21-T21 (R6, Scheme 2.1) was included to compare data to oxidation suppressed studies and to obtain better model fits based on MSC values.

Average values of the measured concentrations of each of the five species (i.e., T20, T21, T20-T20, T21-T21 and T20-T21), as measured by RP-HPLC in triplicate at each time point, defined the data set. In studies of the effect of pH, kinetic studies were repeated at several buffer concentrations and the values of the rate constants extrapolated to zero buffer concentration. An Arrhenius plot was constructed from reactions at various temperatures to estimate the activation energy (E_a) of the reactions. All calculated E_a values were evaluated by one-way ANOVA using SAS, a statistical analysis software (SAS Institute, Cary, NC) at 95% confidence to determine significant differences in E_a among the four thiol-disulfide exchange reactions (R3 and R4, Scheme 2.1). For the reaction of T20 with

cT20-T21, the data were fitted to the equation (Eq. 2.10) for first order irreversible reaction to give k_{obs} .

$$A/A_0 = \exp(-k_{\text{obs}} t) \quad \text{Eq. 2.10}$$

Here, $A = [\text{T20-T21}]$ or $[\text{cT20-T21}]$ and A_0 is the initial concentration of the respective disulfide. A reaction scheme was proposed for the reactions with cT20-T21 (Scheme 2.2).

2.7 Results

2.7.1 Addition of oxidation suppressants to favor the thiol-disulfide exchange reaction

Peptides derived from hGH were used to investigate thiol-disulfide exchange in aqueous solution. Initial studies of the reaction of T20 with T20-T21 in buffer without EDTA or N_2 sparging (pH 7.0) showed that the reactants and products did not appear to reach equilibrium (Figure 2.4), suggesting another reaction pathway in addition to thiol-disulfide exchange. In reactions of T20 and T20-T21, only five species (i.e., T20, T21, T20-T20, T20-T21, and T21-T21) were detected at all reaction conditions studied (Figure 2.3). Similarly, in reactions of T20 and cT20-T21, only four species were detected (i.e., T20, T20-T20, cT20-T21, rT20-T21). No additional oxidation products (e.g., sulfenic, sulfinic, or sulfonic acids) were detected with either RP-HPLC or LC-MS both in the presence and absence of oxidation suppressants, strongly suggesting that the additional reaction pathway is the formation of T20-T20, T20-T21 and T21-T21 from their respective monomers via oxidation. In order to isolate the thiol-disulfide exchange reaction for further

investigation, PB buffers (pH 7.0) were sparged with N₂ for 30 minutes, degassed, and different concentrations of EDTA (0.5 mM, 1 mM and 2 mM) were evaluated for their ability inhibit the oxidation reactions. Because the reactions were unaffected by higher EDTA concentrations (data not shown), 0.5 mM was chosen for all subsequent studies in which oxidation was suppressed. Although the rates of the oxidation reactions were significantly attenuated (see below), oxidation could not be eliminated completely using EDTA and N₂ sparging. Other methods to inhibit oxidation like using a nitrogen controlled atmosphere were not investigated as <10% of T20 and T21 participate in the oxidation pathways in the presence of EDTA and N₂ (based on mass balance from RP-HPLC data).

Oxidation of rT20-T21 to cT20-T21 is the major reaction (Figure 2.5, concentration of cT20-T21 increases while rT20-T21 decreases beyond 500 min), even in oxidation suppressed conditions, after 6 hours. As the main aim was to study thiol-disulfide exchange, we monitored the reaction for up to 6 hours, a time period within which oxidation of T20 to T20-T20 or rT20-T21 to cT20-T21 does not occur to an appreciable extent (determined from pilot studies that were monitored at later time points, Figure 2.5). Also, mass balance showed that the amount of T20-T20 formed was equivalent to the amount of cT20-T21 consumed, further supporting thiol-disulfide exchange as the major pathway for disulfide scrambling for $t < 6$ h. For studies with cT20-T21 at pH 7.0 and T20 and T20-T21 at pH 7.0 and 9.0, a similar sampling schedule was used

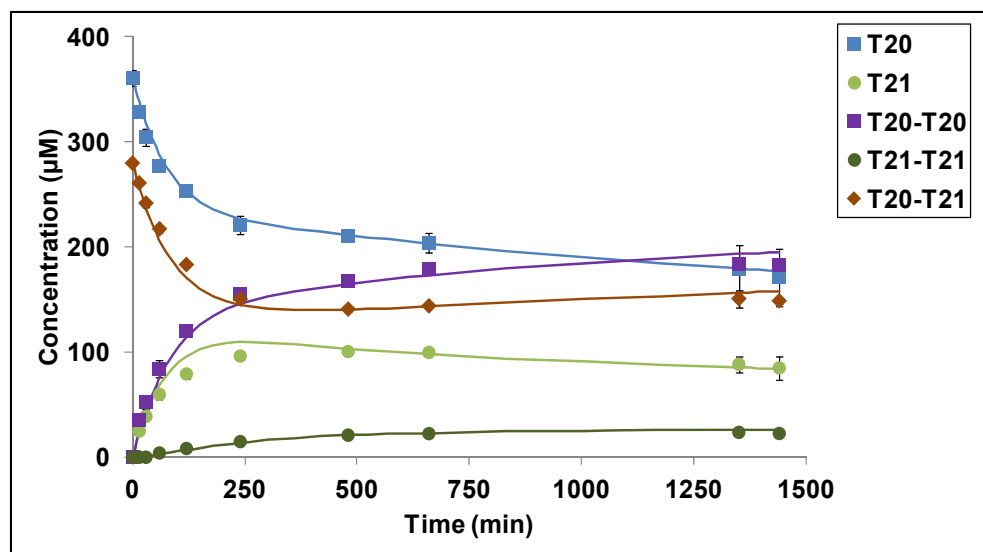


Figure 2.4: The concentration of reactants and products for a kinetic study with T20 and T20-T21 at pH 7.0, 10 mM PB and 0.08 M ionic strength (without EDTA or N₂ sparging). Initial concentrations of peptides were: [T20] = 350 µM; [T20-T21] = 250 µM. The symbols represent actual data points obtained from samples at different times (n=3, +/-SD). Solid lines are model predictions for the reactions in Scheme 2.1.

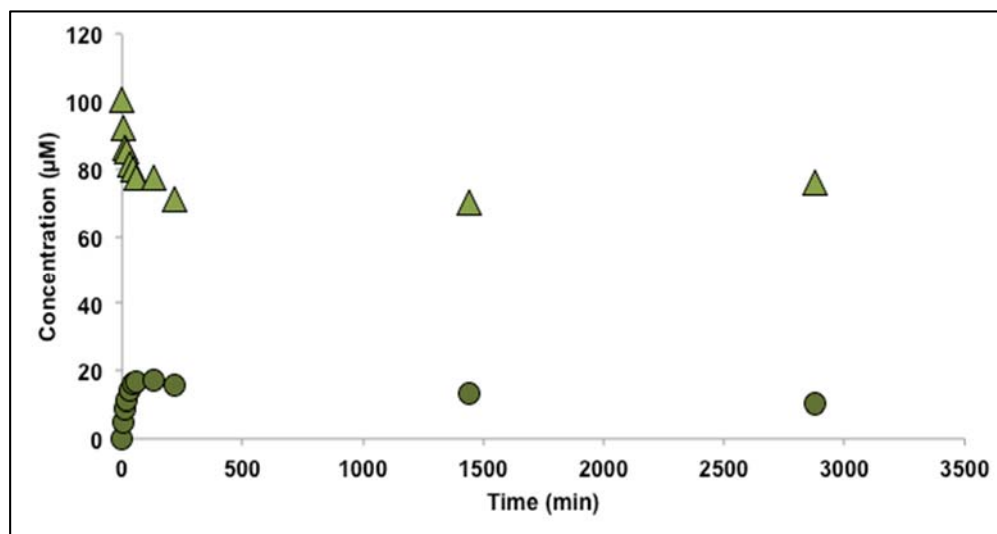


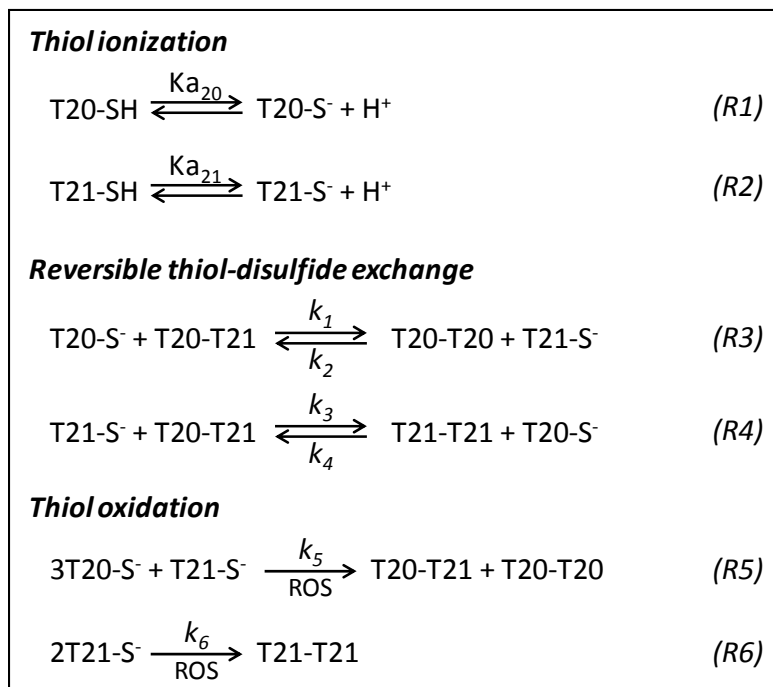
Figure 2.5: Concentrations of cT20-T21 (▲) and rT20-T21 (●) for the reaction of cT20-T21 with T20 in 10 mM carbonate buffer, pH 9.0, and 0.08 M ionic strength (with EDTA and N₂ sparged) at 22 °C.

2.7.2 Apparent order of reaction; reaction of T20 and T20-T21

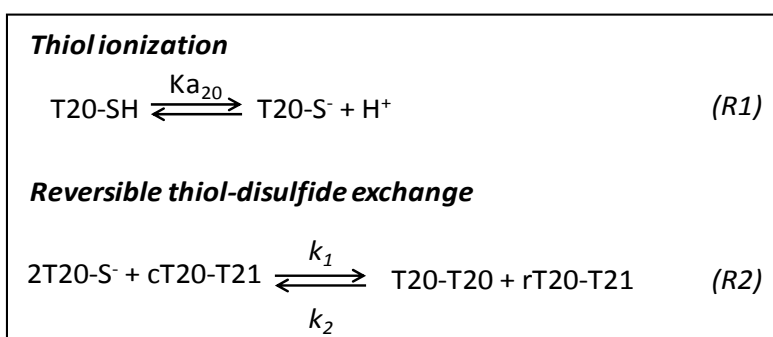
To estimate the order of the disulfide exchange reaction and guide the development of a proposed reaction scheme (Scheme 2.1), reactant and product concentrations were monitored in the early stages of the reaction (pH 7.0, 10 mM PB, 0.5 mM EDTA and N₂ sparging) where <5% change in both reactants was observed. The apparent first-order reaction rates were estimated for a range of initial concentrations. Slopes of log-log plots of the rate of reactant disappearance versus reactant concentration were 0.99 ± 0.01 for T20 and 0.93 ± 0.03 for T20-T21 (Figure 2.6), indicating that the reaction is first-order with respect to the thiol and disulfide reactants and second-order overall. Kuwajima et al. investigated disulfide bond reduction in α -lactalbumin with DTT [66]. The authors reported that the kinetics of disulfide bond reduction is rate-limited by inter-molecular disulfide exchange between α -lactalbumin and DTT and that such a reaction is second-order [66], consistent with our findings using hGH-derived peptides. This report and our observation that thiol-disulfide exchange is a second-order reaction are also consistent with other literature reports [45, 119].

Reaction schemes for thiol-disulfide exchange in hGH-derived peptides

Scheme 2.1: Reaction of T20 with T20-T21



Scheme 2.2: Reaction of T20 with cT20-T21



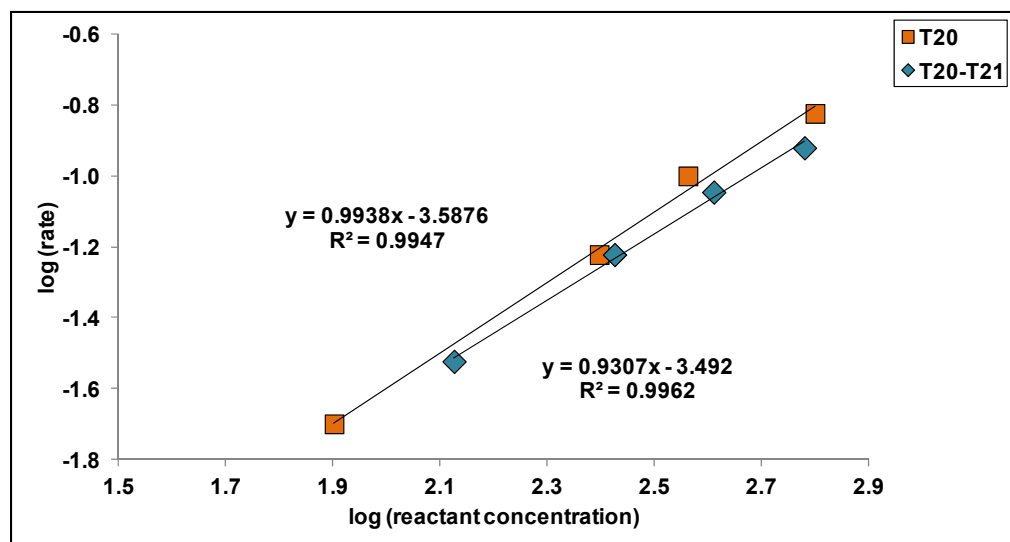


Figure 2.6: Thiol-disulfide exchange initial rate studies in which the concentration of one reactant (either T20 or T20-T21) was fixed while the concentration of the second reactant (either T20 or T20-T21) was varied (see text). Reaction kinetics was monitored at pH 7.0, 10mM PB, 0.08M ionic strength with EDTA and N₂ sparging at 22 °C. Log-log plots of rate of loss of T20 versus T20 concentration (■) and rate of loss of T20-T21 versus T20-T21 concentration (◆).

2.7.3 Effect of oxidation suppressants on thiol-disulfide exchange

To determine the effect of oxidation on the rate and mechanism of thiol-disulfide exchange at pH 7.0, the rate constants for the exchange and oxidation reactions were estimated by fitting the experimental data from reactions with and without EDTA and N₂ sparging to the model described in Scheme 2.1 (Figures 2.4 and 2.7). The oxidation suppressed thiol-disulfide exchange data of T20 with T20-T21 were well described by the model in Scheme 2.1 without R6 ($R^2 \geq 0.95$, see below), as T21-T21 was formed only via thiol-disulfide exchange in the presence of oxidation suppressants at all pH 6.0-10.0. In the absence of oxidation suppressants, including a separate reaction (Scheme 2.1, R6), described the data better than combining all oxidation reactions into a composite reaction

for all three oxidation reactions in Scheme 2.1 (R5 and R6). For the oxidation of T21 to form T21-T21 in the absence of oxidation suppressants (R6, Scheme 2.1), the estimated value of rate constant k_6 was $8.9 \pm 2.6 \text{ M}^{-1}\text{s}^{-1}$. In the presence of oxidation suppressants, oxidation of T21 was not observed ($k_6 = 0$). Rate constants for thiol-disulfide exchange were similar with and without oxidation suppressants, while k_5 increased 3.6-fold and k_6 increased from 0 to $8.9 \pm 2.6 \text{ M}^{-1}\text{s}^{-1}$ (Figure 2.8). Statistical analysis showed no significant difference in rate constants for thiol-disulfide exchange ($p > 0.05$) and a significant difference for the oxidation reaction rate constant ($p < 0.05$) in the presence and absence of EDTA and N_2 , indicating that the intrinsic rate of the disulfide exchange reactions are not affected by the presence of oxidation side-reactions.

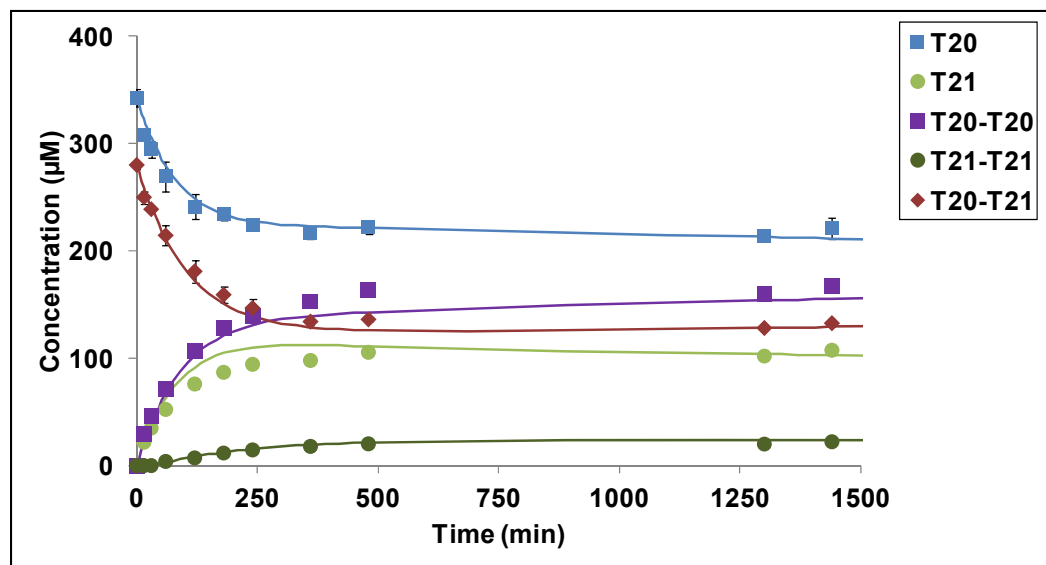


Figure 2.7: The concentration of reactants and products for a kinetic study with T20 and T20-T21 at pH 7.0, 10mM phosphate buffer with 0.5 mM EDTA and N_2 sparging. Initial concentrations of peptides were: $[\text{T20}] = 350 \text{ } \mu\text{M}$; $[\text{T20-T21}] = 250 \text{ } \mu\text{M}$. The symbols represent actual data points obtained from samples at different times ($n=3$, \pm SD). Solid lines are model predictions for the reactions in Scheme 2.1.

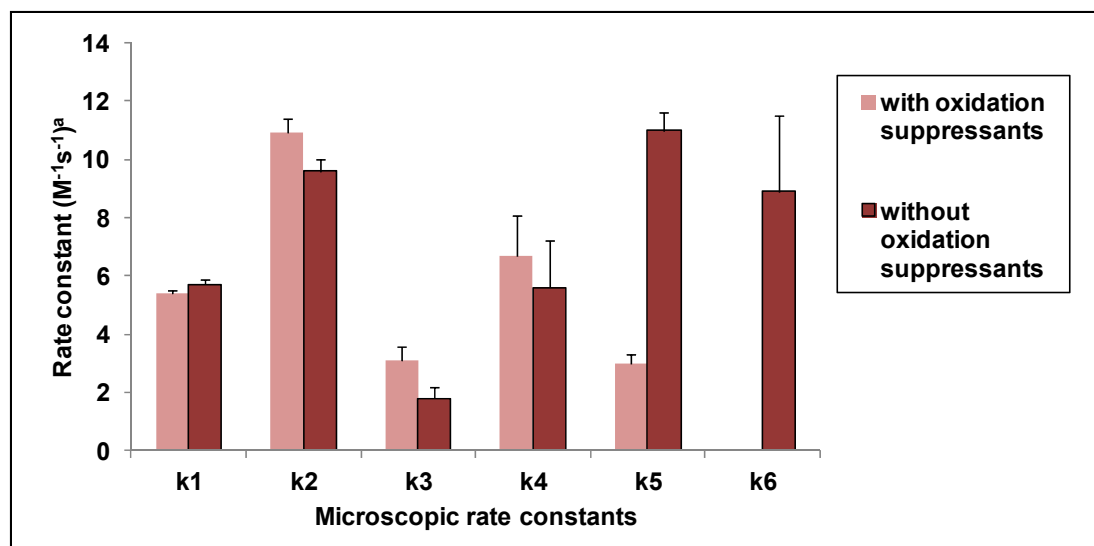
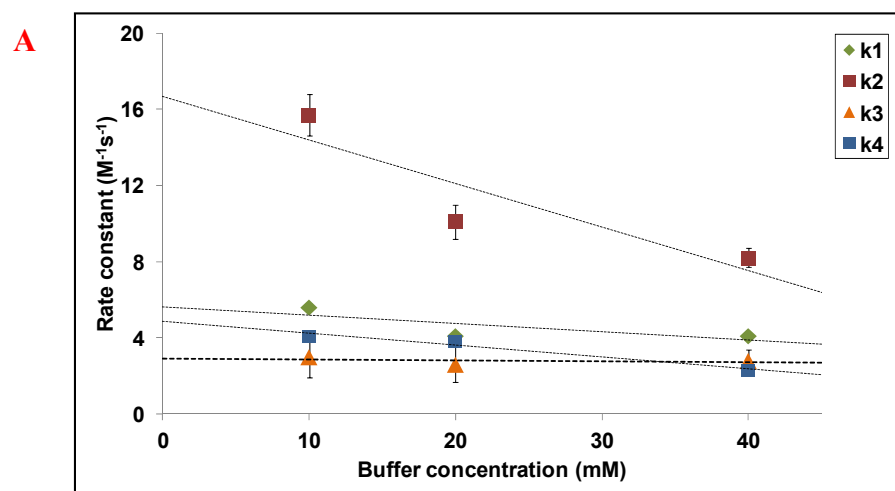


Figure 2.8: Comparison of rate constants for reactions with and without oxidation suppressants (0.5 mM EDTA and N₂ sparging) at pH 7.0, 10 mM PB and 0.08 M ionic strength at 22 °C. Initial concentrations of peptides were: [T20] = 350 μM and [T20-T21] = 250 μM (n=3, +/- SD). Unit for k₅ is M⁻³s⁻¹.

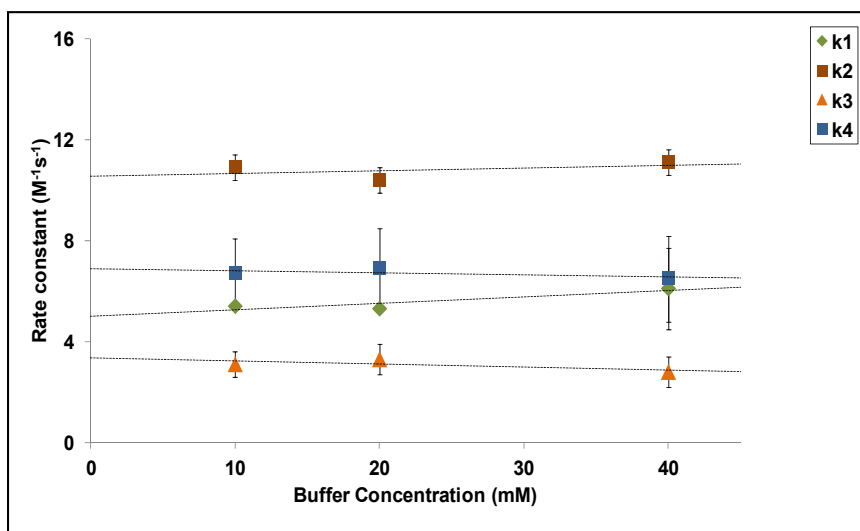
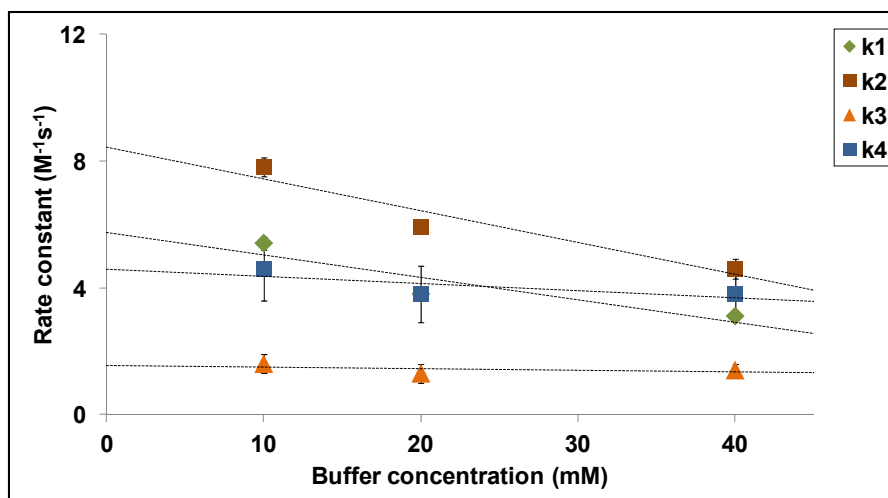
2.7.4 Effect of pH on the reaction of T20 with T20-T21

Thiol-disulfide exchange reactions were monitored as a function of buffer concentration to determine the effect of buffer catalysis. At pH 6.0, 8.0, 9.0 and 10.0, a high buffer concentration (40 mM) appears to have had a moderate stabilizing effect (Figure 2.9; A, C, D and E). Statistical analysis showed no significant difference between extrapolated rate constants and the rate constants at 10 mM buffer ($p > 0.05$). Nevertheless, at all pH values, we report rate constants extrapolated to zero buffer concentration. An example of the fit of the data to the model (Scheme 2.1) at pH 7.0 is shown in Figure 2.7; similar fits were obtained at the other pH values (Figure 2.10; A, B, C and D). At pH 7.0, the extrapolated rate constants of the reactions shown in Scheme 2.1 were: $k_1 = 5.0 \pm 0.2 \text{ M}^{-1} \text{ s}^{-1}$, $k_2 = 10.6 \pm 0.3 \text{ M}^{-1} \text{ s}^{-1}$, $k_3 = 3.4 \pm 0.1 \text{ M}^{-1} \text{ s}^{-1}$, $k_4 = 6.9 \pm 0.1 \text{ M}^{-1} \text{ s}^{-1}$. Rate constants at other pH values and buffer concentrations are in Table 2.2. A pH-rate profile for pH 6.0-10.0 is

shown in Figure 2.11 for the extrapolated rate constants. Statistical analysis showed no significant difference ($p > 0.05$) in the rate constants for this pH range. This suggests that the mechanism of thiol-disulfide exchange is independent of pH as reported by others [146, 147]. Although a change in solution pH did not affect the rate of thiol-disulfide exchange in tryptic peptides, it can influence reaction kinetics in proteins, which can undergo pH-induced conformational changes that can alter the exposure of disulfides and/or free thiols. The pseudo-first order rate constant (k_{obs}) for the loss of T20-T21 was determined by monitoring the change in concentration over time. Data at different pH values (6.0-10.0) are shown as a pH-rate profile in Figure 2.12. The slope of the pH-rate profile in the pharmaceutically relevant range of pH 6.0 to 8.0, below the thiol pKa (8.3), is ~ 1 . The change in k_{obs} with increasing pH (i.e., the slope of the pH rate profile) decreases above pH 8.0. However, there is a slight increase in k_{obs} above pH 8.0 as the population of thiolate anion still changes, albeit at decreasing proportions at $\text{pH} > \text{thiol pKa}$. The observed pH dependence of k_{obs} and the pH independence of k_1 - k_4 indicate that thiol-disulfide exchange depends on the concentration of thiolate anion.



Continued from previous page

B**C**

Continued from previous page

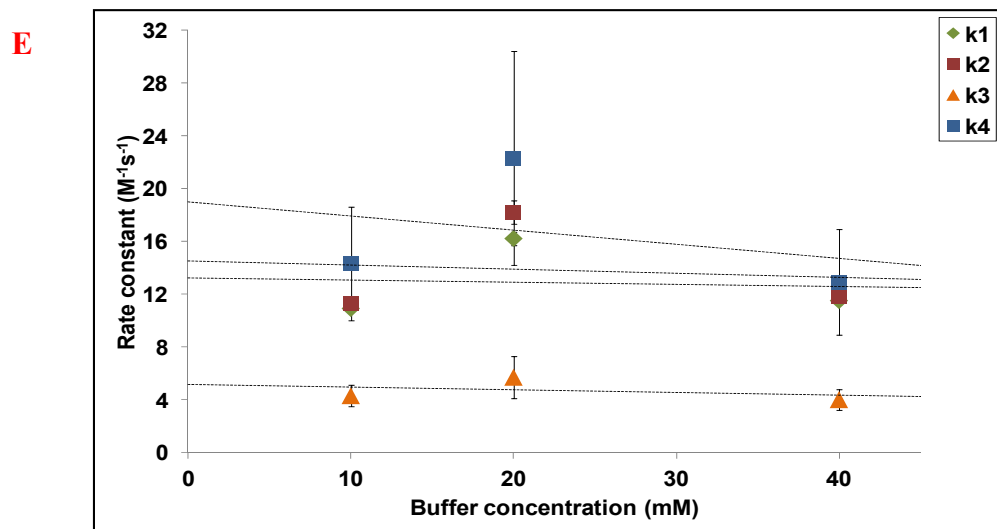
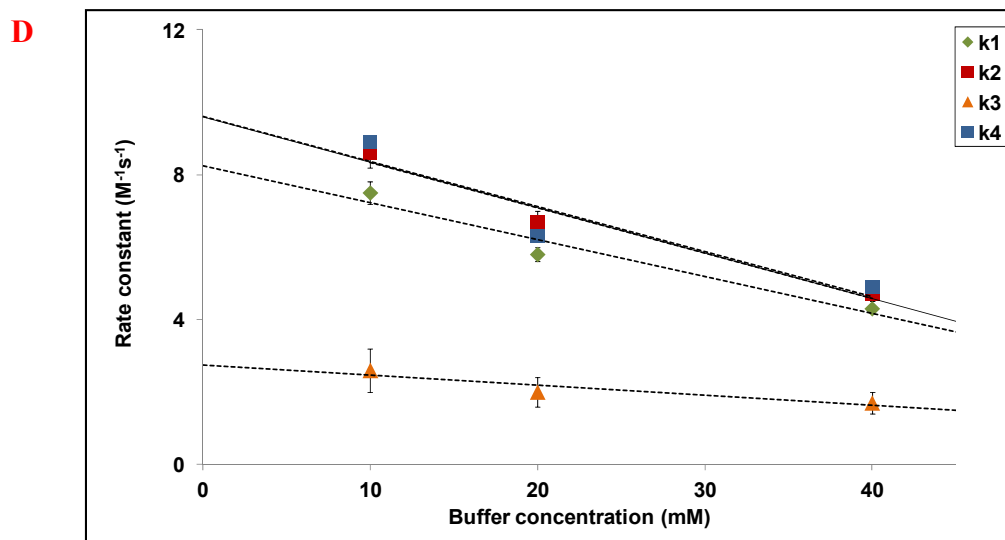
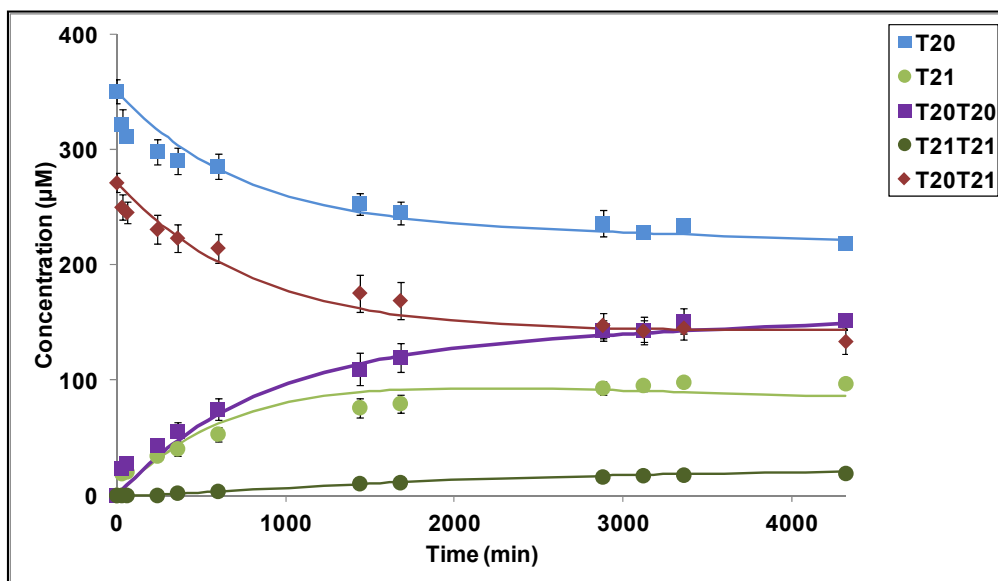
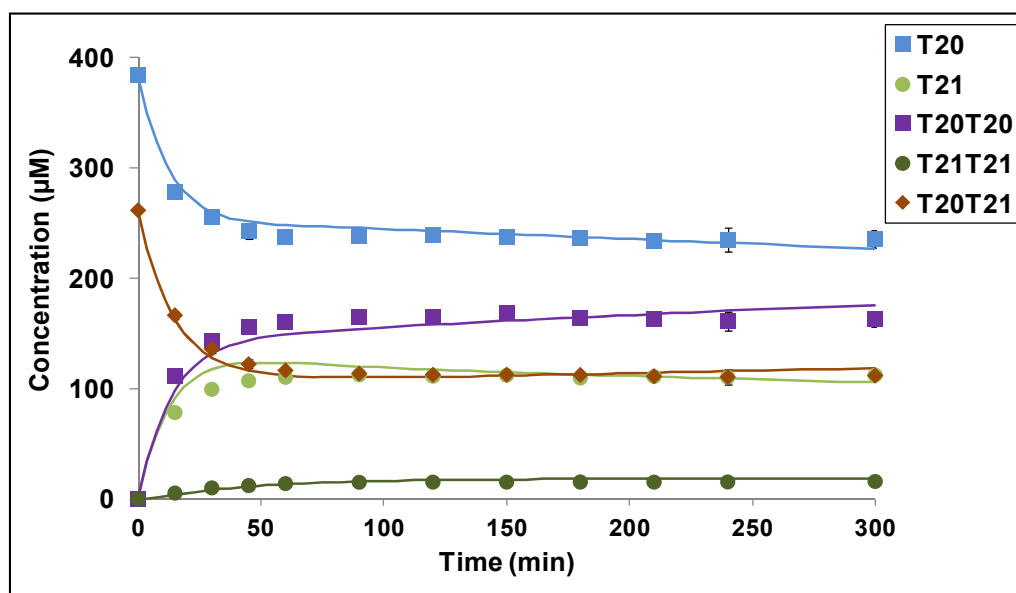


Figure 2.9: Rate constants vs. buffer concentration. Rate constants were obtained from model fits to reaction scheme 2.1 ($n=3$, \pm SD): A) pH 6.0, B) pH 7.0, C) pH 8.0, D) pH 9.0, and E) pH 10.0 at 0.08 M ionic strength, different buffer concentrations of 10, 20 and 40 mM (with EDTA and N₂ sparging) and at 22 °C. Initial concentrations of peptides were: [T20] = 350 μ M; [T20-T21] = 250 μ M. Dotted lines are trendlines.

A



B



Continued from previous page

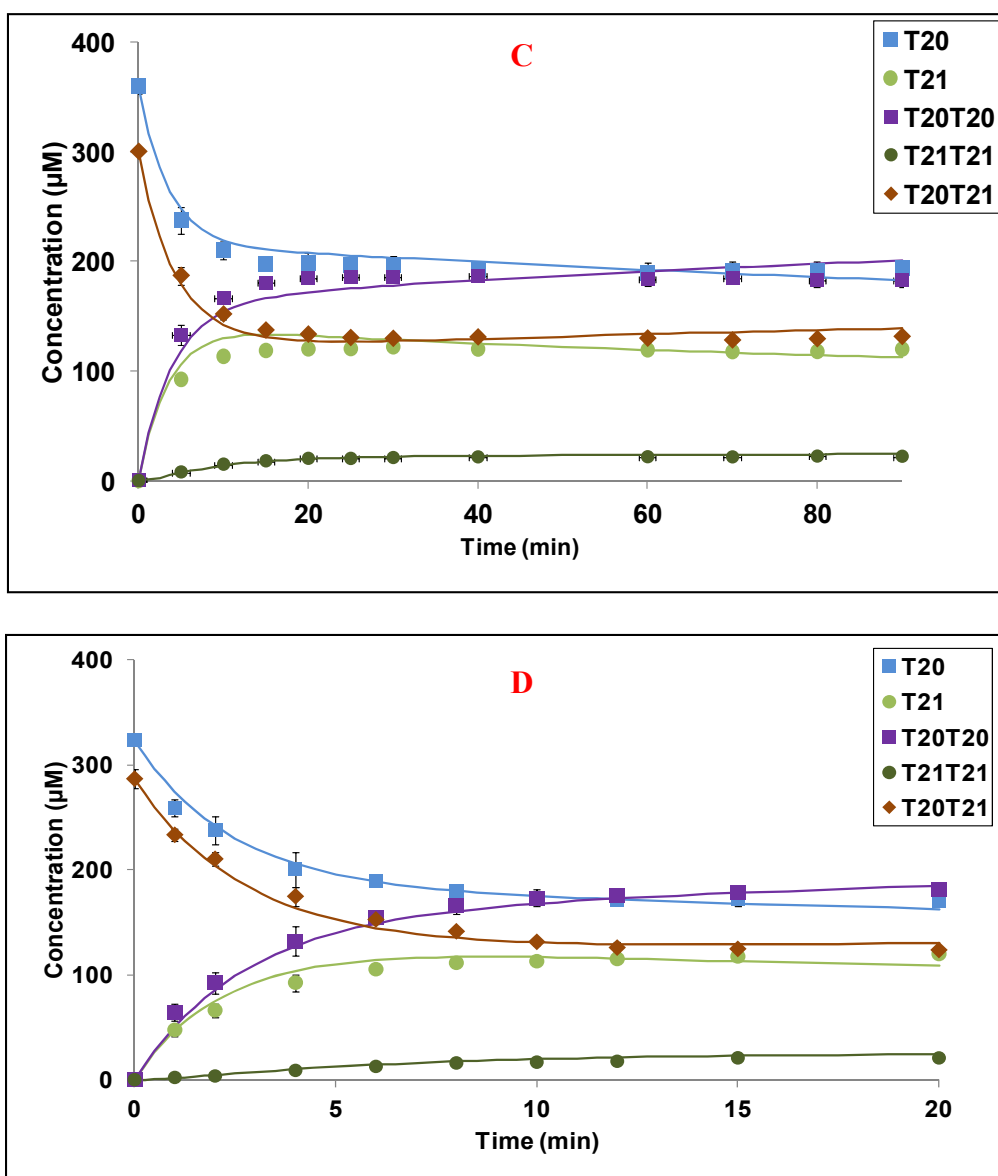


Figure 2.10: Kinetic plots at different pH for the reaction of T20 with T20-T21 at 22 °C. Symbols represent actual data points ($n=3$, \pm SD) and solid lines represent model fits. $[\text{T20}] = 350 \mu\text{M}$; $[\text{T20-T21}] = 250 \mu\text{M}$. Buffer conditions: pH 6.0-8.0 is with 10 mM phosphate buffer and pH 9.0-10.0 is with 10 mM carbonate buffer. Ionic strength (0.08 M) and EDTA (0.5 mM) were the same at all pH values. A) pH 6.0, B) pH 8.0, C) pH 9.0, and D) pH 10.0.

Table 2.2: Measured rate constants for all buffer concentrations for the reaction of T20 with T20-T21, 0.08 M ionic strength (with EDTA and N₂ sparged) at 22 °C.

pH	Buffer concentration (mM)	$k_1(\text{M}^{-1}\text{s}^{-1})$	$k_2(\text{M}^{-1}\text{s}^{-1})$	$k_3(\text{M}^{-1}\text{s}^{-1})$	$k_4(\text{M}^{-1}\text{s}^{-1})$	$k_5(\text{M}^{-3}\text{s}^{-1}) \cdot 10^6$
6.0	40	4.1±0.1	8.2±0.5	2.8±0.6	4.2±2.3	(163±11)·10 ⁶
	20	4.1±0.2	10.1±0.9	2.6±0.9	4.4±3.8	(143±15)·10 ⁶
	10	5.6±0.2	15.7±1.1	3.0±1.1	5.6±4.1	(147±14)·10 ⁶
7.0	40	6.1±1.6	11.1±0.5	2.8±0.6	6.5±1.7	(223±17)·10 ²
	20	5.3±0.1	10.4±0.5	3.3±0.6	6.9±1.6	(350±33)·10 ²
	10	5.4±0.1	10.9±0.5	3.1±0.5	6.7±1.4	(333±28)·10 ²
8.0	40	3.1±0.1	4.6±0.3	1.4±0.2	3.8±0.6	123±6
	20	3.8±0.1	5.9±0.2	1.3±0.3	3.8±0.9	80±4
	10	5.4±0.2	7.8±0.3	1.6±0.3	4.6±1.0	82±4
9.0	40	4.3±0.1	4.7±0.2	1.7±0.3	4.9±1.1	12±1
	20	5.8±0.2	6.7±0.3	2.0±0.4	6.3±1.5	13±1
	10	7.5±0.3	8.6±0.4	2.6±0.6	8.9±2.2	13±1
10.0	40	11.5±0.3	11.8±0.5	4.0±0.8	12.9±4.0	35±2
	20	16.2±0.5	18.2±0.9	5.7±1.6	22.3±8.1	37±2
	10	10.9±0.2	11.3±0.5	4.3±0.8	14.3±4.3	36±2

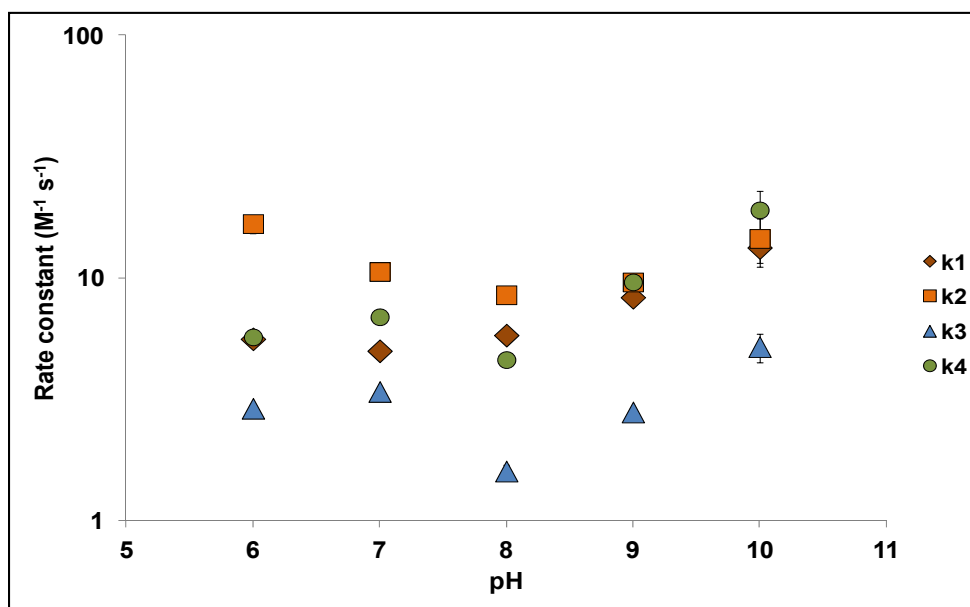


Figure 2.11: pH-rate profile for second order microscopic rate constants (see Scheme 2.1 and text for details) obtained for kinetic studies with T20 and T20-T21 at 22 °C. All rate constants are values extrapolated to zero buffer concentration (n=3, +/- SD).

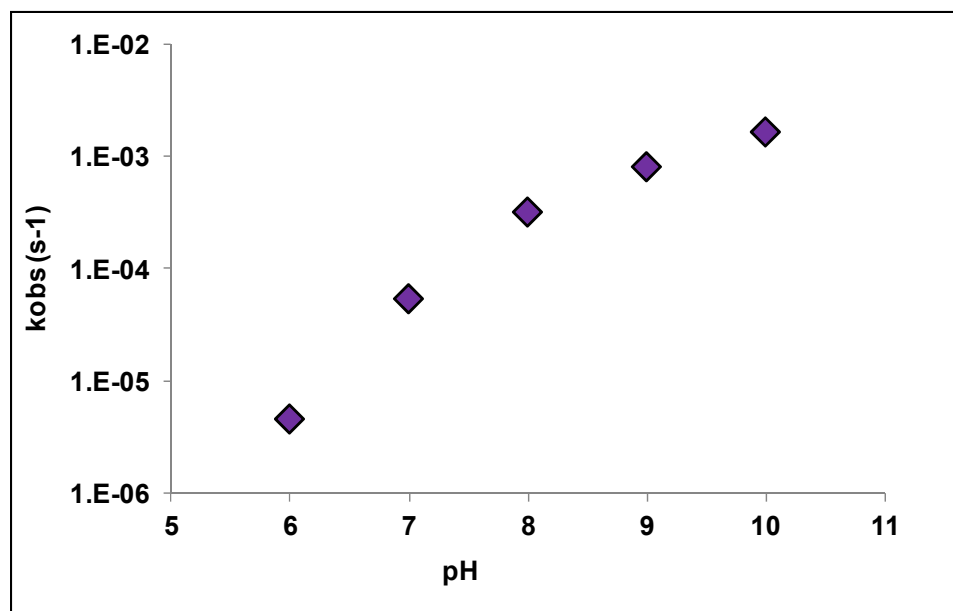


Figure 2.12: Pseudo-first order rate constant for the loss of T20-T21 (◆) at different pH (10 mM buffer, 0.08 M ionic strength with oxidation suppressants) and at 22 °C. Rate constants were determined by non-linear regression. Uncertainties are within the size of the symbol (n=3, +/-SD).

2.7.5 Activation parameters for the reaction of T20 with T20-T21

Microscopic rate constants for thiol-disulfide exchange (k_1 , k_2 , k_3 , and k_4) obtained from model fits to data at 4, 15, 35, 40 and 50 °C were used to construct an Arrhenius plot (Figure 2.13, see Figure 2.14 for Arrhenius plot of k_5). The resulting Arrhenius parameters can be used to predict the extent to which temperature changes during storage and processing conditions can affect thiol-disulfide exchange. The thiol-disulfide exchange reaction was found to follow linear Arrhenius behavior in the temperature range 4-50 °C. Linear Arrhenius plots suggest that a change in temperature within this range does not result in a change in the proposed reaction mechanism or the rate-limiting step (Scheme 2.1). There is no significant difference ($p > 0.05$) in the activation energy values for the any of the thiol-disulfide exchange reactions in Scheme 2.1 (R3 and R4) based on a one-way

ANOVA. R3 and R4 represent two mechanistically equivalent reversible reactions and thus would be expected to have similar activation energies. We estimated Arrhenius activation energies for the reaction of T20 and T20-T21 to be in the range of 41-53 kJ/mol (Table 2.3). An Eyring plot (Figure 2.15) was used to estimate values for enthalpy (ΔH^\ddagger), entropy (ΔS^\ddagger) and free energy of activation (ΔG^\ddagger) at 25 °C (Table 2.3).

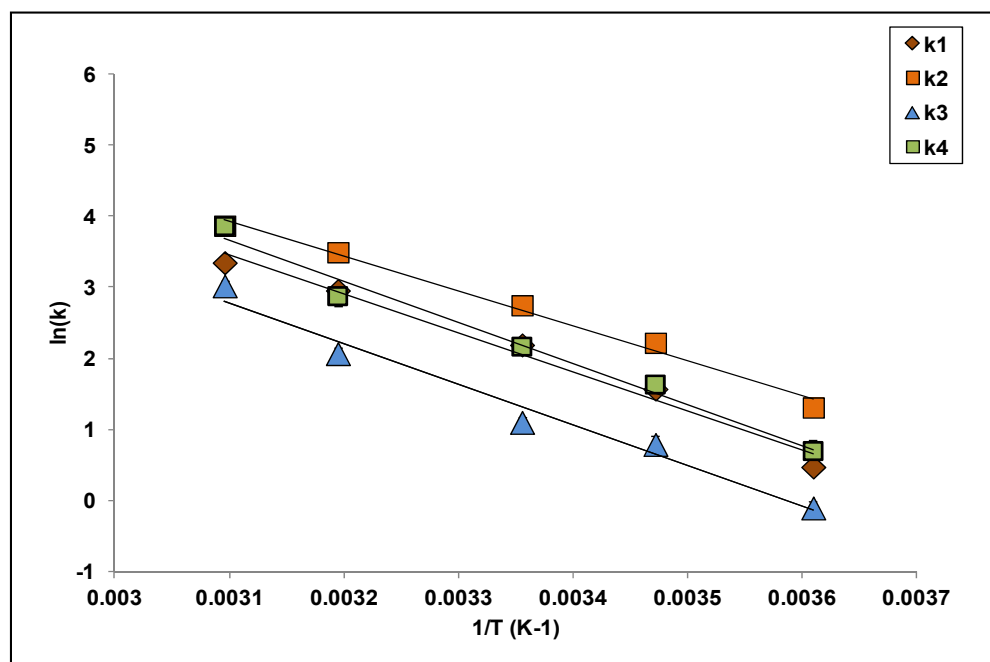


Figure 2.13: Arrhenius plots for microscopic rate constants for the reaction of T20 and T20-T21 (Scheme 2.1) at pH 7.0, 10 mM phosphate buffer and 0.08 M ionic strength with 0.5 M EDTA and N_2 sparging ($n=3$, \pm SD). Solid lines represent trendlines.

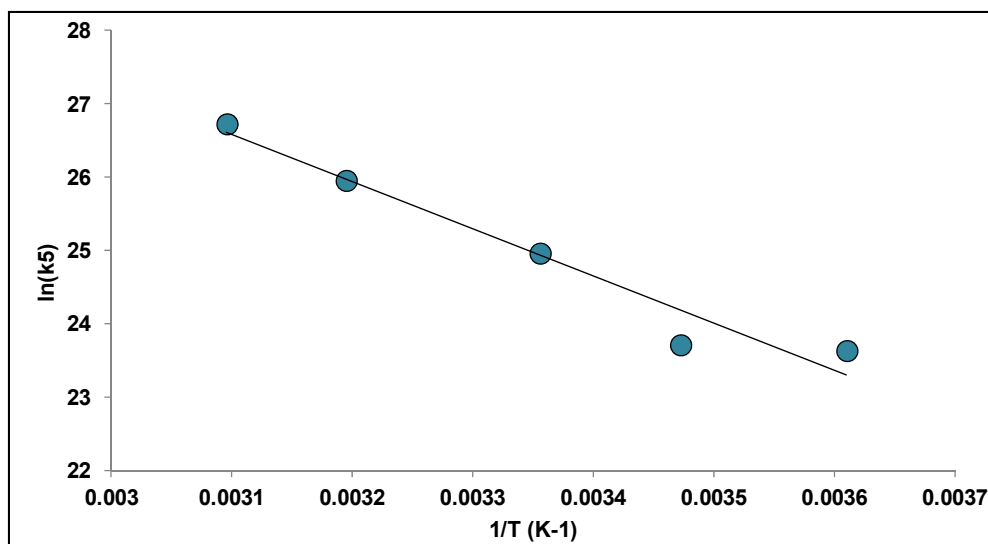


Figure 2.14: Arrhenius plot for microscopic rate constant k_5 (●) for the reaction of T20 and T20-T21 (see 2.1). The reaction was monitored at pH 7.0, 10 mM buffer and 0.08 M ionic strength (with EDTA and N₂ sparging) (n=3, +/- SD). Solid lines represent trendlines.

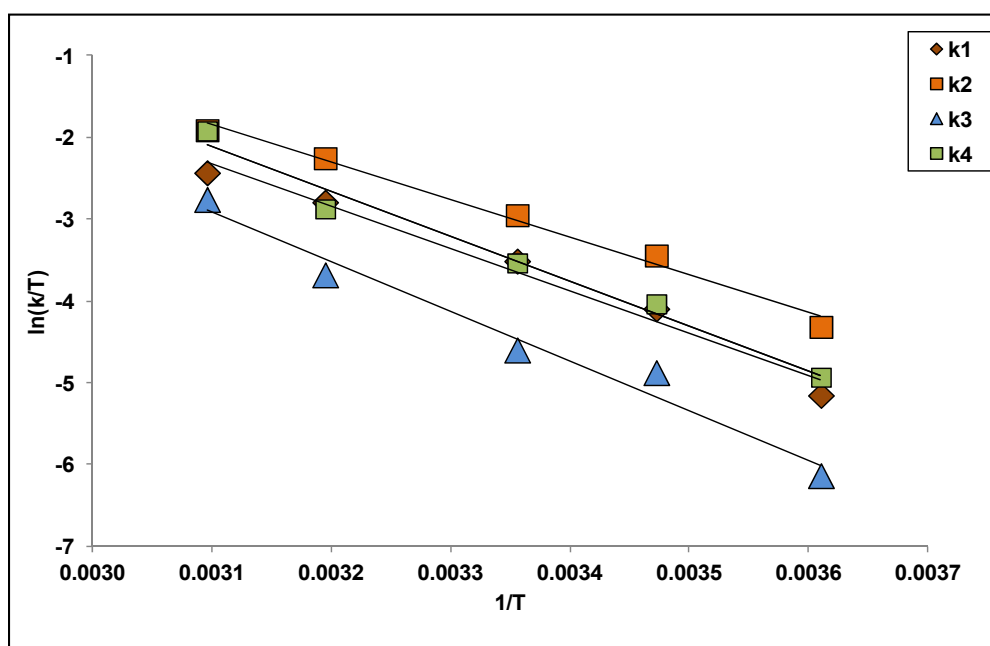


Figure 2.15: Eyring plot for microscopic rate constants for the reaction of T20 with T20-T21 at pH 7.0, 10 mM buffer and 0.08 M ionic strength (with EDTA and N₂ sparging) (n=3, +/- SD). Solid lines represent trendlines.

2.7.6 Effect of peptide cyclization on thiol-disulfide exchange

The non-cyclic model peptides (T20, T21, T20-T20, T21-T21 and T20-T21) do not have any secondary structure, as confirmed by far-UV CD analysis. However, the CD spectrum for cT20-T21 shows internal hydrogen bonding, possibly due to the presence of a beta-turn-like structure (Figure 2.16). Initial studies carried out with T20 and cT20-T21 with the same molar ratios as the heterodimer study (thiol: disulfide = 1.4:1) showed no reaction at 22, 40, or 60 °C. Thus, a higher thiol: disulfide ratio of 10:1 was used for kinetic studies using cT20-T21. We compared the rate of reaction of T20 with cT20-T21 at two different pH values and temperatures with that of T20-T21 under similar reaction conditions (Table 2.4) to determine the effect of peptide secondary structure on reaction kinetics. For scrambling reactions involving cT20-T21 and T20, rates were considerably slower than for the linear form (Figure 2.17). Even with a 10:1 molar ratio of thiol: disulfide, only a 26% decrease in disulfide content was observed after 6 hours at pH 9.0 and 22 °C, as compared to an 86% decrease for the linear T20-T21. Our results suggest that secondary structure has a marked effect on the reaction rate, and that secondary structural constraints may attenuate thiol-disulfide exchange in intact hGH relative to the intrinsic exchange rate of the peptides.

Table 2.3: Activation parameters for thiol-disulfide exchange reactions and oxidation reaction (k_5). Values for ΔH^\ddagger , ΔS^\ddagger and ΔG^\ddagger were obtained from the Eyring plot shown in Figure 2.15.

Rate constant	Ea (kJ/mol)	A	ΔH^\ddagger (kJ/mol)	ΔS^\ddagger (J/mol.K)	ΔG^\ddagger 25 °C (kJ/mol)
k_1	46±4	$7.5 \cdot 10^8 \pm 4.2^a$	43±6	-83±20	68±9
k_2	41±2	$2.0 \cdot 10^8 \pm 2.6^a$	38±4	-96±15	66±6
k_3	48±4	$8.9 \cdot 10^8 \pm 5.9^a$	50±6	-66±21	70±9
k_4	48±4	$2.3 \cdot 10^9 \pm 4.4^a$	45±5	-75±16	67±7
k_5	53±7	$1.5 \cdot 10^{12} \pm 16.0^b$	51±6	134±19	11±8

^aunits in $M^{-1} s^{-1}$

^bunits in $M^{-3} s^{-1}$

Table 2.4: The change in cT20-T21 and T20-T21 concentrations obtained after 6 hours for thiol-disulfide exchange reactions with T20 at different pH and temperature at thiol: disulfide of 10:1.

Peptide	pH	Temp (°C)	% decrease after 6 hours
cT20-T21	7.0	22	17.3±3.3
	7.0	40	18.6±2.4
	9.0	22	26.0±3.6
	9.0	40	23.6±3.2
T20-T21	7.0	22	79.9±9.8
	9.0	22	86.4±2.9

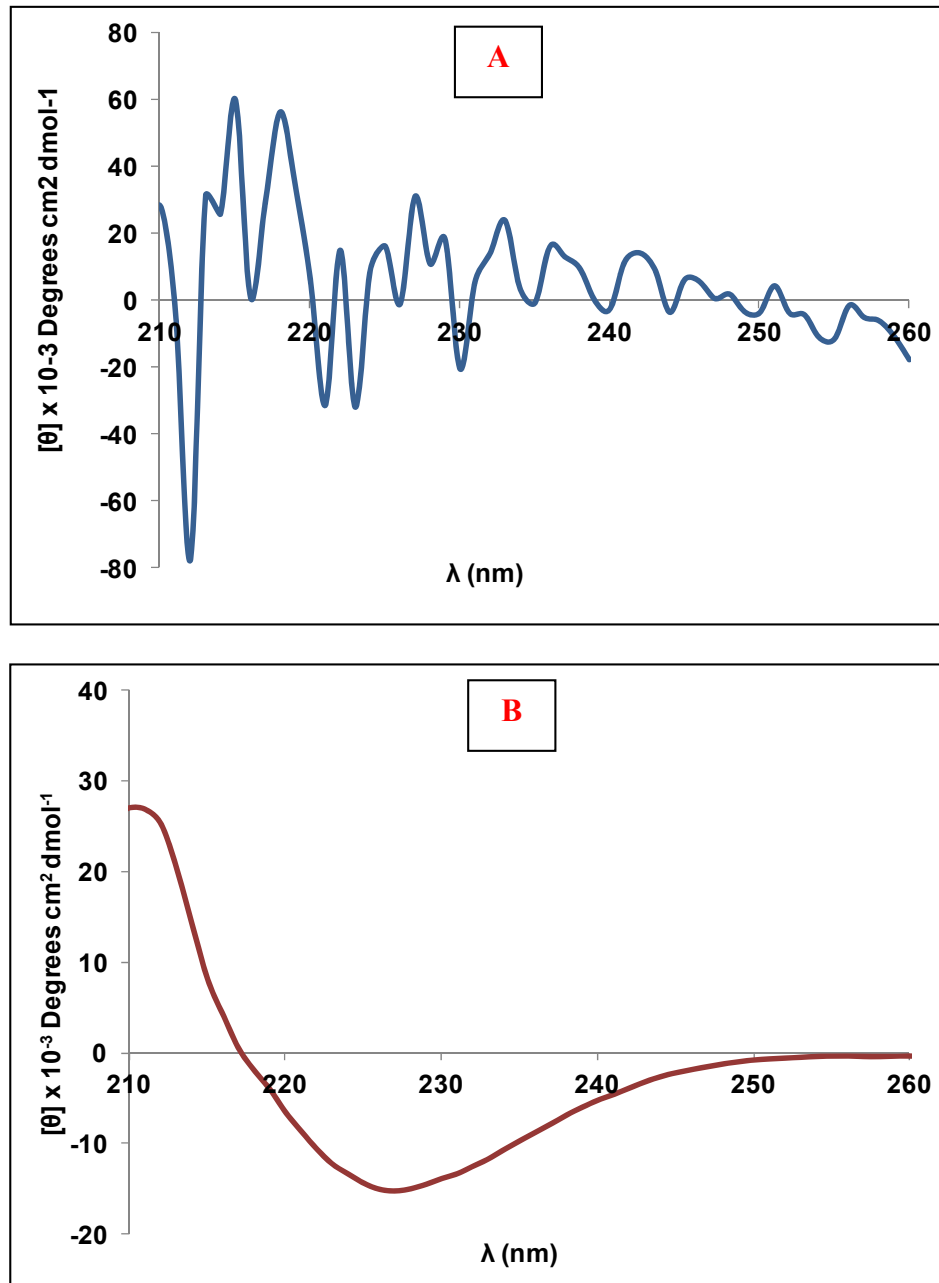


Figure 2.16: Far-UV CD spectra for A) T20-T21 and B) cT20-T21. The far-UV CD spectrum for T20-T21 is representative of peptides T20, T21, T20-T20 and T20-T21.

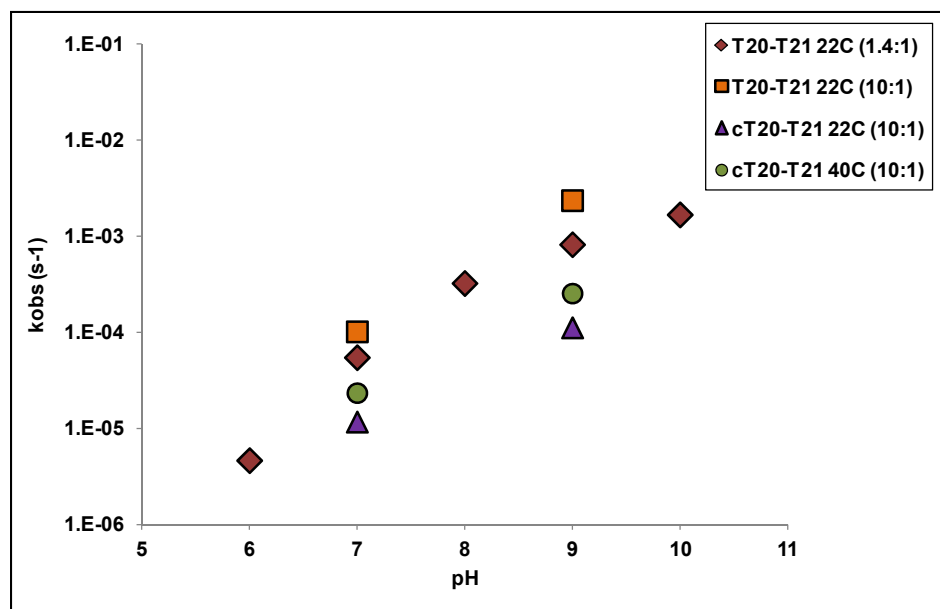


Figure 2.17: Observed pseudo-first order rate constants for the loss of cT20-T21 and T20-T21 at different concentration ratios and temperatures. Ratios in figure legend represents thiol:disulfide ratio (T20:T20-T21/cT20-T21). Initial concentrations of peptides were: [T20] = 450 μ M; [T20-T21] = 45 μ M for 10:1 studies and [T20] = 350 μ M; [T20-T21] = 250 μ M for the 1.4:1 study. Uncertainties are within the size of the symbol (n=3).

2.8 Discussion

The mechanism of thiol-disulfide exchange involves reaction of the thiolate anion (RS⁻) with a disulfide bond (R'SSR'') at neutral to alkaline pH [45, 46, 71]. The thiol group undergoes deprotonation to form the reactive nucleophile (RS⁻), this step is followed by the exchange of redox equivalents leading to oxidation of the attacking thiol and reduction of R'SSR'' [45]. In our studies with model peptides derived from hGH, products consistent with this mechanism were detected, including T20-T20, T21, T21-T21 and rT20-T21. No additional oxidation products such as cysteine sulfenic acid, cysteine sulfinic acid, cysteine sulfonic acid or thiosulfonates were detected, either in the presence or absence of EDTA and N₂, as confirmed by MS analysis and mass balance upon completion of the kinetic

studies. Here we report thiol-disulfide exchange using model peptides (T20-T21, cT20-T21, T20) representative of proteins containing an unpaired Cys and disulfide bonds. Although native hGH and most mAbs generally do not have unpaired Cys, these may be generated by β -elimination, incomplete folding or disulfide bond reduction during expression, folding, purification and/or fill-finish operations, and during storage in solution or solid formulations.

The reaction between thiols and disulfides has been studied in detail by other groups [50, 119, 120]. Previously Luo et al. used a data modeling approach to determine oxidation reaction kinetics for the reaction of Cys-SH and H_2O_2 [140] and we have used a similar approach to study thiol-disulfide exchange. To our knowledge, however, this is the first report of a detailed kinetic model allowing the determination of both observed and microscopic rate constants for thiol-disulfide exchange in peptide model compounds. In the kinetic model, reactions R1-R5 (Scheme 2.1) were sufficient to describe both thiol-disulfide exchange and thiol oxidation in studies with oxidation suppressants. Thiol oxidation reactions R5 and R6 represent composite reactions that involve oxidation of T20 or T21 via a RSOH intermediate [140]. RSOH is a reactive species that is completely consumed, was not detected analytically and as a result was excluded from the reaction scheme. Excellent fits of the model to our data suggest that the reactions represented by Scheme 2.1 effectively describe the mechanism for thiol-disulfide exchange between T20 and T20-T21 and oxidation of free thiols (T20, T21) to form homodimers (T20-T20, T21-T21) and heterodimer (T20-T21). In the reaction of T20 with T20-T21, omitting oxidation suppressants (EDTA and N_2 sparging) resulted in an increase in the oxidation rate constant k_5 by 366% and k_6 to $8.9 \pm 2.6 M^{-1} s^{-1}$ from ~ 0 , while the other rate constants remained

unchanged (Figure 2.8). The k_{obs} value for the loss of T20 decreased by 130% in the presence of oxidation suppressants while k_{obs} for the loss of T20-T21 remained unchanged. The results show that excluding oxidation suppressants accelerates the formation of scrambled disulfides (T20-T20 and T21-T21) via oxidative pathways. Hydroxyl ion mediated disulfide exchange and aggregation has been reported for atrial natriuretic peptide (ANP), a cyclic peptide with 25 amino acids and a disulfide bond (C4-C28) in the solid state [141]. However, alkaline hydrolysis of peptide bonds in T20-T21 and cT20-T21 was not observed up to pH 10.0.

Rate constants obtained here for the reaction of T20 with T20-T21 are comparable to previous reports. For example, Holmgren et al. studied disulfide bond reduction in insulin with dithiothreitol (DTT) at neutral pH and determined a second-order rate constant for the reaction of $5 \text{ M}^{-1}\text{s}^{-1}$ [47]. In another study with DTT, Wiita et al. studied force-dependent chemical kinetics of disulfide bond reduction [70]. In the absence of an external force and at pH 7.2, a second-order rate constant of $6.45 \text{ M}^{-1}\text{s}^{-1}$ was obtained. These values for thiol mediated disulfide exchange are similar to our model predictions for the reactions of both T20 and T21 with T20-T21 (Scheme 2.1, R3 and R4) at pH 7.0 ($3\text{-}11 \text{ M}^{-1}\text{s}^{-1}$).

Arrhenius activation energy values reported here (Table 2.3) are similar to those obtained by Fernandes et al., who reported E_a values for thiol-disulfide exchange in solution in the range 60-66 kJ/mol [148]. Wiita et al. assumed values for the Arrhenius parameter (A) of $10^5\text{-}10^{12} \text{ M}^{-1}\text{s}^{-1}$, and obtained activation energies between 30-65 kJ/mol for thiol-disulfide exchange [70]. Whitesides et al. determined activation parameters for the reaction of Ellman's reagent and glutathione with three different thiols in water at 30

$^{\circ}\text{C}$ [71]; $\Delta G^{\ddagger} = 44.4 - 65.7 \text{ kJ/mol}$, $\Delta H^{\ddagger} = 37.7 - 66.9 \text{ kJ/mol}$ and $\Delta S^{\ddagger} = -19.7 - +13.4 \text{ J/mol.K}$.

The activation parameters reported here, with the exception of more negative values of ΔS^{\ddagger} , are similar to values cited above. Thiol-disulfide exchange proceeds via a linear $\text{S}_{\text{N}}2$ mechanism [149, 150], with greater translational and vibrational constraint of the transition state than the reactants, resulting in a negative ΔS^{\ddagger} and a positive ΔG^{\ddagger} . The values of the activation parameters reported here are consistent with expected values of $-85 - -125 \text{ J/mol.K}$ for this mechanism [71] and suggest that translational and vibrational constraints play a more significant role for thiol-disulfide exchange reactions involving peptides than in small molecules. Youngman et al. have shown that carbamidomethylation of all four Cys residues in hGH decreases stability by $\sim 37.7 \text{ kJ/mol}$ [151]. Protein destabilization by disulfide bond reduction increased the population of self-associated forms. This is similar to the activation energies reported here, suggesting that the activation energy for thiol-disulfide exchange in model peptides is of the same order as the decrease in stability that results from the reduction of disulfide bonds in native hGH.

The results also show that the reaction is ten-fold slower in the cyclic peptide (cT20-T21) than in the linear form (T20-T21), suggesting that secondary structural constraints in hGH slow thiol-disulfide exchange. Interestingly, this observation is contrary to previous reports. Rabenstein et al. determined observed rate constants for thiol-disulfide exchange with Cys and Arg-vasopressin (AVP) at pH 7.0 and $25 \text{ }^{\circ}\text{C}$ [120]. AVP is a cyclic peptide with 9 amino acid residues. The reaction of AVP with Cys (CysSH) was 100 times faster than the reaction between glutathione disulfide (GSSG) and CysSH. The authors attributed this to several factors including a more accessible disulfide bond formed

between two terminal Cys residues in AVP. The disulfide bond in cT20-T21 (C4-C11) is somewhat removed from the N- and C-termini, and may be less solvent exposed than in T20-T21, perhaps contributing to the reduction in rate observed here. Internal hydrogen bonding in the cT20-T21 peptide (CD spectrum, Figure 2.16) could impose a structural constraint which translates to reduced reactivity of the disulfide bond with T20. Additionally, in peptides with 1-3 residues between the Cys, cyclization is unfavorable due to geometric strain, while a stable disulfide bond is formed in peptides with 4-5 intervening amino acids [50]. The differences in structural effects between the studies reported here and previous reports indicate that the relationship between peptide secondary structure and reactivity in thiol-disulfide exchange is not completely understood, and that further studies are warranted, particularly given the relevance to therapeutic proteins such as hGH, monoclonal antibodies (mAbs) and human serum albumin. The results can be extended to therapeutic proteins and biosimilars to determine the influence of sequence, structure and processing conditions on reaction mechanisms and disulfide-mediated aggregation propensity and to improve candidate selection during development.

2.9 Conclusion

The studies reported here define the mechanistic details of thiol-disulfide exchange and oxidation in hGH model peptides in solution. Microscopic and apparent rate constants obtained from model predictions provide an insight into the effects of pH, temperature and secondary structure on thiol-disulfide exchange. Detailed kinetic analysis of degradation pathways like thiol-disulfide exchange is valuable for the development of protein drug

formulations, both in solution and in the solid state. Further, the information can be used to improve our understanding of the contributions of thiol-disulfide exchange to aggregation in other therapeutic proteins with disulfide bonds and/or Cys residues.

CHAPTER 3. INVESTIGATING THE EFFECT OF LYOPHILIZATION AND SUBSEQUENT STORAGE IN THE SOLID STATE ON THIOL- DISULFIDE EXCHANGE IN PEPTIDES DERIVED FROM HUMAN GROWTH HORMONE

This work was published in the *Journal of Pharmaceutical Sciences*
DOI: 10.1002/jps.24370, content reproduced with permission from Wiley.

3.1 Abstract

Lyophilization (freeze-drying) is frequently used to stabilize protein therapeutics. However, covalent modifications such as thiol-disulfide exchange and disulfide scrambling can occur even in the solid-state. The effects of lyophilization and storage of lyophilized powders on the mechanism and kinetics of thiol-disulfide exchange have not been elucidated and were investigated in the studies presented here. Reaction kinetics were monitored during different stages of lyophilization (freezing, primary drying and secondary drying) and during storage of the lyophilized powders at 22 °C and ambient RH. The concentrations of reactants and products were determined using RP-HPLC and product identity confirmed using LC-MS. Loss of native disulfide was observed for both linear and cyclic peptide during the primary drying step, however, the native disulfides were regenerated during secondary drying with no further change till the end of lyophilization. Deviations from Arrhenius parameters predicted from solution studies and the absence of

buffer effects during lyophilization suggest that factors such as temperature, initial peptide concentration, buffer type and concentration do not influence thiol-disulfide exchange during lyophilization. Results from a ‘cold finger’ method used to study peptide adsorption to ice indicate that there is no preferential peptide adsorption to the ice surface and the presence of an ice surface may not influence disulfide reactivity during primary drying. Overall, reaction rates and product distribution are different for the reaction of T20 with T20-T21 or cT20-T21 in the solid-state and aqueous solution while the mechanism of thiol-disulfide remains unchanged. Increased reactivity of the cyclic peptide in the solid-state suggests that peptide cyclization does not offer protection against lyophilization and that damage induced by a process stress further affects storage stability at 22 °C and ambient RH.

3.2 Keywords

Lyophilization, freezing, cold finger, peptide, human growth hormone, kinetics and thiol-disulfide exchange.

3.3 Introduction

Protein therapeutics continue to grow in commercial and therapeutic importance, providing new treatments for cancer, cardiovascular and autoimmune diseases. The biologics sector in the US grew by 18.2% between 2012-2013, with sales of \$63.6 billion in 2012 [1]. Nevertheless, the development of therapeutic proteins can be compromised by

the inherent complexity and instability of these macromolecules [152, 153]. To improve stability and retain potency, protein pharmaceuticals are often lyophilized [154-156]. Lyophilization (freeze-drying) produces solid powders with high surface area and is used for storage of the protein following expression and for final marketed drug product [157]. Though lyophilization often reduces the rates of chemical and physical degradation, chemical and physical degradation can still occur during processing and subsequent storage in the solid state [132, 158, 159].

Lyophilization cycles typically consist of freezing, primary drying and secondary drying steps [160]. The process can expose proteins to undesirable stresses such as cold denaturation, increased concentration of solutes and protein (“freeze concentration”), pH changes and dehydration, all of which can induce protein unfolding and/or structural perturbations [161, 162]. Costantino et al. observed secondary structure changes, a decrease in α -helicity and an increase in β -sheet and unordered structure, upon lyophilization of human growth hormone (hGH) [163]. Lyophilization induced structural changes have also been reported for recombinant human albumin (rHA) [95]. Such structural and/or conformational changes can further lead to aggregation during storage [14] and rehydration [164, 78]. Solid-phase aggregation of proteins can occur via different mechanisms in the presence of moisture; namely, thiol-disulfide exchange, disulfide scrambling, non-disulfide covalent aggregation and non-covalent aggregation [165].

While there are reports of disulfide-mediated aggregation in the solid state for proteins that contain cysteines and/or disulfides [79, 166], the lack of a complete understanding of factors that influence reactivity reduces formulation to trial-and-error, informed by experience, in selecting composition and stabilizing excipients. Thus, an

improved mechanistic understanding of aggregation-inducing processes such as thiol-disulfide exchange will be beneficial for the rational design of formulations that stabilize proteins during lyophilization and storage.

Native disulfide bonds scramble via oxidative and hydrolytic pathways to form non-native bonds that can affect protein stability and activity. Two predominant pathways lead to disulfide-mediated covalent aggregation: (i) thiol-disulfide exchange ($\text{RSH} + \text{R}^1\text{SSR}^2 \leftrightarrow \text{R}^1\text{SSR} + \text{R}^2\text{SH}$) and (ii) disulfide scrambling ($\text{RSSR} + \text{R}^1\text{SSR}^1 \leftrightarrow 2\text{R}^1\text{SSR}$) [2, 3, 141]. In solution at neutral to alkaline pH, the thiolate anion (RS^-) is the reactive species that initiates thiol-disulfide exchange. Nucleophilic attack of RS^- on a native disulfide (R^1SSR^2) generates a non-native disulfide (R^1SSR) and a new thiol (R^2S^-) in an $\text{S}_{\text{N}}2$ nucleophilic displacement reaction [45, 71]. Disulfide scrambling, a related reaction, is initiated by disulfide bond cleavage to generate a thiolate that then initiates thiol-disulfide or thiol-catalyzed exchange [165].

Disulfide-mediated aggregation has been reported in lyophilized bovine serum albumin (BSA) [79] and β -galactosidase [166]. In rHA, lyophilization produced an increase in both β -sheet content and unordered structural elements resulting in partial protein unfolding, which further facilitated moisture-induced aggregation via thiol-disulfide exchange upon storage [95]. Andya et al. observed disulfide linked dimers and trimers in recombinant humanized monoclonal antibody (rhuMAb) formulations following lyophilization and storage at 30 °C [167]. In the absence of excipients, reversible structural alterations during lyophilization promoted covalent aggregate formation upon storage. Degradation reactions can also occur in the solid state in the absence of process-induced structural changes. For example, in the absence of a stabilizing excipient, a rhuMAb (IgG)

aggregated in the solid state though native secondary structure was retained after spray drying [163]. Reports of disulfide-linked aggregates in lyophilized protein samples [79, 166, 168] demonstrate the importance of designing processes and formulations that can inhibit disulfide bond degradation.

Disulfide bonds can be cleaved under neutral to alkaline conditions via the attack of a hydroxyl ion. Alkaline hydrolysis of disulfide bonds can be classified into three pathways: i) direct attack-this results in the formation of sulfenic acid and a free thiol, ii) α -elimination- where the β proton of Cys is attacked to produce thiolate and thioaldehyde and iii) β -elimination- where the α proton of Cys is abstracted to produce dehydroalanine and persulfide.

Human growth hormone (hGH) is a therapeutic protein used to treat growth hormone deficiency and other growth disorders. It has two disulfide bonds and no free thiols; with 191 amino acids the monomeric form has a molecular weight of 22 kDa. Structural perturbations in hGH have been reported in the solid state [101] and could further result in the formation of disulfide-linked aggregates during storage. A disulfide-linked dimer of hGH (45 kDa) was found to have diminished receptor binding affinity and cell-proliferative activity [124]. Thus, given its relatively small size, therapeutic value and tendency to aggregate [135, 136], hGH was chosen as a suitable model to study thiol-disulfide exchange kinetics in the solid state.

The mechanistic information obtained from aqueous solution studies in Chapter 2 provided a basis for understanding the effects of lyophilization process stresses and the solid environment on thiol-disulfide exchange. In this Chapter, studies pertaining to thiol-disulfide exchange and disulfide scrambling in hGH-derived peptides during lyophilization

and subsequent room temperature storage of the lyophilized powders are reported. The hGH-derived peptides were lyophilized without excipients to determine process effects on disulfide exchange and scrambling kinetics. The results demonstrate that the rate of thiol-disulfide exchange is accelerated during primary drying, and that peptide secondary structure does not influence reactivity during lyophilization. Factors such as temperature, initial peptide concentration, buffer type and concentration and peptide adsorption to ice did not influence thiol-disulfide exchange during primary drying. During storage in lyophilized solids, both the rates and the distribution of products differed for linear and cyclic disulfide-containing peptides when compared to those observed in aqueous solution. Peptide cyclization does not offer protection against thiol-disulfide exchange in the solid state, the observed rate constant (k_{obs}) for the loss of cT20-T21 was 10-fold greater than that in aqueous solution.

3.4 Materials

Model peptides T20, T21, T20-T21, rT20-T21 and cT20-T21 (see Table 3.1 for structures) were purchased from GenScript (Piscataway, NJ) with >90% purity as a lyophilized powder. HPLC grade acetonitrile (ACN), NaCl and KCl were purchased from Fisher Scientific Co. (Pittsburgh, PA). K_2HPO_4 , 5,5-dimethyl-1,3-cyclohexanedione (dimedone), ethylenediaminetetraacetic acid (EDTA) and sodium citrate tribasic dihydrate were purchased from Sigma Chemical Co. (St. Louis, MO). Trifluoroacetic acid (TFA) and formic acid (FA) were obtained from Thermo Scientific (Rockford, IL). Double-distilled water (DDI) used for buffer preparation and as HPLC mobile phase was deionized and

purified using a Milli-Q water system, (Millipore Ltd., Billerica, MA) and filtered with a 0.2 μm filter. Glass vials (2 mL) and stoppers (13 mm gray butyl) for lyophilization were purchased from Wheaton (Millville, NJ). Methods

3.4.1 Quantification of reactants and products by HPLC


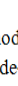

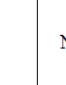

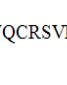
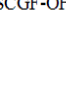

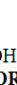

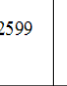
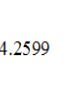
Samples were analyzed using reverse-phase high-performance liquid chromatography (RP-HPLC, Agilent 1200 series) with UV detection at 215 nm. Agilent Chemstation software was used for data acquisition and analysis. A ZORBAX Eclipse plus C18, 5 μm (4.6 X 250 mm) analytical column (Agilent Technologies, Santa Clara, CA) was used with gradient elution and the column temperature maintained at 25 °C. The gradient elution method and associated calibration plots were as described in our previous work [169]. ***Identification of reactants and products on LC-MS:*** Samples were analyzed using an ESI-LC/MS system (1200 series LC, 6520 qTOF; Agilent Technologies, Santa Clara, CA) with a ZORBAX 300SB-C18 column (1.0 X 50 mm, 3.5 μm) with gradient elution similar to that used in HPLC quantitation. Mobile phase A was 0.1% formic acid in water and mobile phase B was 0.1% formic acid in acetonitrile. A gradient run was initiated with 5% B, which was increased to 50% in 6.10 min, then held at 50% for 1 min followed by an increase to 100% in 0.6 min, decreased to 0% in 0.6 min, increased again to 100% in 0.6 min and finally returned to 5% in 0.6 min. The flow rate was maintained at 50 $\mu\text{L}/\text{min}$ and the column temperature was not controlled. Data were analyzed using MassHunter software. Reactants and products were identified using mass filters with peptide masses corresponding to the different reaction mechanisms for thiol-disulfide exchange and oxidation reactions.

3.4.2 Thiol-disulfide exchange reactions

All peptides were used as provided by the manufacturer without further purification. Stock solutions were prepared in a 0.1% formic acid solution in DDI. Reaction kinetics were monitored during lyophilization and storage of lyophilized powders at 22 °C. For the reaction, 1500 µL of T20 (1125 µM), 1500 µL of T20-T21/cT20-T21 (112.5 µM) and 750 µL of 50 mM phosphate buffer (PB) were added to a 15 mL BD falcon tube and mixed by pipetting. The final pH of the reaction mixture was adjusted using NaOH or HCl (exact volume to be added was determined from pilot studies) after a 100 µL aliquot was removed and quenched with 10 µL 20% formic acid in DDI (FA) to verify initial concentrations ($t = 0$ min before lyophilization). 200 µL aliquots of the reaction mixture were transferred into vials (on ice) and placed inside the freeze-dryer; shelves were pre-cooled to -40 °C. Frozen samples, collected during the freezing step, were thawed and quenched with 20 µL of 20% FA to prevent disulfide exchange prior to analysis. Lyophilization samples at the end of primary drying and during secondary drying were reconstituted with 200 µL of 0.1% FA; 150 µL of the reconstituted sample was quenched with 15 µL of 20% FA. For storage stability studies, reaction mixtures, solution and lyo samples were prepared as described above. At the end of the lyophilization cycle, vials were capped under a vacuum (not sealed) and stored at 22 °C. Samples were withdrawn in triplicate at each time point during lyophilization and storage. 30 µL and 10 µL of the quenched solution were then used for RP-HPLC and LC-MS analysis, respectively. Dilution factors from total reaction volume, addition of NaOH/HCl for pH adjustment and quench solution were accounted for in determining final peptide concentrations. No measurable changes in concentration were observed in quenched samples within the time scale of the experiment.

Buffer effect: T20 and T20-T21 were also lyophilized with 2.5 mM potassium phosphate and 10 mM sodium citrate buffer at pH 7.0 to investigate the effect of buffer type and concentration on thiol-disulfide exchange. Initial peptide concentrations and total reaction volume were as described above. For 2.5 mM PB, 750 μ L of 10 mM buffer stock was used and for 10 mM sodium citrate, 750 μ L of 50 mM buffer stock was used. Samples were withdrawn in triplicate, quenched and analyzed as described above.

Table 3.1: Abbreviations and amino acid sequences of peptides detected in solid-state studies with hGH-derived peptides.

Abbreviation	Description	Designation in general reaction scheme	Amino acid sequence	Theoretical mass	Observed mass
T20	Monomeric peptide, free SH group	R_1 and R_2	NH_2 -IVQCR-OH	617.3319	617.3290
T21	Monomeric peptide, free SH group	R_3	NH_2 -SVEGSCGF-OH	784.3062	784.3067
T20-T20	Homodimer, disulfide-linked	R_1SSR_2 and R_1SSR_1	NH_2 -IVQCR-OH  NH_2 -IVQCR-OH	1232.6482	1232.6247
T21-T21	Homodimer, disulfide-linked	R_3SSR_3	NH_2 -SVEGSCGF-OH  NH_2 -SVEGSCGF-OH	1566.5978	1566.5984
T20-T21	Heterodimer, disulfide-linked	R_2SSR_3	NH_2 -IVQCR-OH  NH_2 -SVEGSCGF-OH	1399.6225	1399.6247
cT20-T21	Cyclic peptide, disulfide linked		NH_2 -IVQCRSVEGSCGF-OH 	1381.6118	1381.6201
rT20-T21	Linear peptide, free SH groups		NH_2 -IVQCRSVEGSCGF-OH	1383.6275	1383.6344
Single mixed disulfide (SMD)	linear peptide, disulfide linked to T20	 OR 	NH_2 -IVQCRSVEGSCGF-OH  NH_2 -IVQCR-OH OR NH_2 -IVQCRSVEGSCGF-OH  NH_2 -IVQCR-OH	1998.9437	1998.9347
Double mixed disulfide (DMD)	linear peptide, disulfide linked to two T20 peptides		NH_2 -IVQCRSVEGSCGF-OH  NH_2 -IVQCR-OH	2614.2599	2614.2488

3.4.3 Lyophilization of peptide samples

Solid samples were prepared by lyophilization in a programmable benchtop VirTris freeze-dryer (SP scientific, Gardiner, NY), using methods routine in our labs [129] (Table 3.2). Briefly, the lyophilization cycle consisted of the following steps; freezing at -40 °C, then drying at -35 °C under vacuum (70 mTorr) for 2 h, -5 °C for 8 h, 5 °C for 8 h, 15 °C for 6 h (100 mTorr) and 25 °C for 10 h (100 mTorr). The same lyophilization cycle was used for all solid-state studies to eliminate processing conditions as a variable and was not optimized. The instrument was operated in manual mode to monitor disulfide exchange during lyophilization so that samples could be removed at the end of each step. Lyophilized samples at the end of the cycle appeared as dried powders and did not form elegant cakes due to the absence of any bulking agents. The glass transition temperature (T_g) of the lyophilized samples was measured using a DSC Q2000 (TA instruments, New Castle, DE) and moisture content was measured using TGA Q5000 (TA instruments, New Castle, DE) and SGA-100 (VTI Corporation, Hialeah, FL).

Table 3.2: Lyophilization cycle used for solid-state studies with hGH-derived peptides

Step	1	2	3	4	5	6
Temperature (°C)	-40	-35	-5	5	15	25
Duration (h)	2	2	8	8	6	10
Total time (h)	2	4	12	20	26	36
Vacuum (mTorr)	N/A	70	70	70	100	100

N/A, not applicable

Step 1: Freezing, Step 2: primary drying and Steps 3-6: secondary drying

3.4.4 Peptide adsorption to ice

The rates of thiol-disulfide exchange in hGH model peptides were affected by lyophilization. The role of adsorption to ice in these effects was assessed using a cold finger. A cold finger condenser (24/40 inner joints from Fisher Scientific) was connected with insulated tubing to a circulating water bath (Thermo Scientific) containing an ethylene glycol/water (1:1) mixture and the temperature set to $-10\text{ }^{\circ}\text{C}$. This method was used previously by Kuiper et. al for purification of antifreeze proteins by adsorption to ice [170]. The cold finger was first placed in DDI seeded with ice crystals for 10 minutes to form an ice surface (Figure 3.1). Ice surface area and ice crystal morphology on the cold finger were not controlled using this method. The cold finger was then placed in a solution of peptides inside a Styrofoam box and the ice surface allowed to grow for 1 hour. A peptide solution was prepared by adding 32 mL of T20 ($1250\text{ }\mu\text{M}$), 32 mL of T20-T21 ($125\text{ }\mu\text{M}$) and 16 mL PB buffer (10 mM, pH 7.0, 0.08 M ionic strength, 0.5 mM EDTA and N_2 sparged). After adsorption for 1 hour, the cold finger was removed from the solution and placed inside an empty beaker (Figure 3.1). The coolant temperature was maintained at $-10\text{ }^{\circ}\text{C}$ for another 6 hours. 100 μL of the solution remaining in the beaker (not frozen) and thawed ice surface on the cold finger were quenched with 10 μL of 20% FA and 30 μL of the quenched samples were injected onto the RP-HPLC column and analyzed for free thiols, native and scrambled disulfides using the method described above.

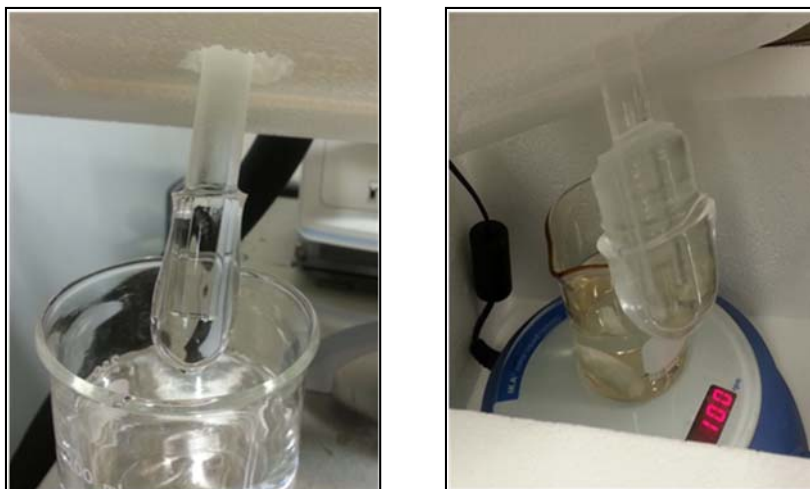


Figure 3.1: Picture of an ice surface formed on the cold finger after 10 mins (left). Picture of cold finger after adsorption of the peptide solution to the ice surface for one hour (right).

3.4.5 Method for detecting reaction intermediates

Sulfenic acid determination (reaction with dimedone): Dimedone was used as a trapping reagent to detect the presence of sulfenic acids, potential intermediates in oxidation-mediated thiol-disulfide exchange [52]. To detect sulfenic acids in lyophilized samples, dimedone was co-lyophilized with model peptides. To 10 mM PB (0.08 M ionic strength, 0.5 mM EDTA), 1.72 g of dimedone was added (total buffer volume = 200 mL) and the buffer sparged with N_2 . 1500 μ L of T20-T21 (625 μ M) was then added to 1500 μ L of 0.1% formic acid in DDI and 750 μ L of buffer with dimedone. The pH of the reaction mixture was adjusted to 8.0 using NaOH/HCl and the final concentration of dimedone before lyophilization was 12.5 mM (dimedone: T20-T21 = 50:1). 200 μ L aliquots of the reaction mixture were transferred into glass vials and the samples were lyophilized using the cycle shown in Table 3.2. To compare with solution samples, 200 μ L aliquots of the same reaction mixture were transferred to glass vials, capped and stored at 22 $^{\circ}$ C. At different time points during storage, samples were reconstituted with 200 μ L 0.1% FA and

analyzed using RP-HPLC and LC-MS. Dehydroalanine detection: To detect dehydroalanine, an intermediate in the degradation of disulfide bonds via β -elimination [3], LC-MS spectra were scanned for a characteristic mass loss of 34 Da as reported previously [171].

3.4.6 Data analysis

For the reaction of T20 with linear T20-T21 in the solid state during storage, the data were consistent with a reaction scheme involving: (i) equilibrium ionization of T20 and T21, (ii) irreversible thiol-disulfide exchange reaction of the ionized thiolate form of T20 ($T20-S^-$) with T20-T21 and (iii) oxidation of the ionized thiolate forms of T20 and T21 (Scheme 3.1). The scheme is similar to that reported earlier for the reaction in solution [169], but with an irreversible thiol-disulfide exchange reaction rather than a reversible one. The following equations were used to estimate microscopic rate constants:

$$T20S^- = T20 / \{1 + (10^{-7}) / (10^{-pK_a})\} \quad \text{Eq.3.1}$$

$$T21S^- = T21 / \{1 + (10^{-7}) / (10^{-pK_a})\} \quad \text{Eq.3.2}$$

$$d[T20-T21]/dt = -k_1' [T20S^-][T20-T21] + k_2' [T20S^-][T21S^-] \quad \text{Eq.3.3}$$

$$d[T20-T20]/dt = k_1' [T20S^-][T20-T21] \quad \text{Eq.3.4}$$

$$d[T20S^-]/dt = -k_1' [T20S^-][T20-T21] - k_2' [T20S^-][T21S^-] \quad \text{Eq.3.5}$$

$$d[\text{T21S}^-]/dt = k_1' [\text{T20S}^-][\text{T20-T21}] - k_2' [\text{T20S}^-][\text{T21S}^-] \quad \text{Eq.3.6}$$

In the kinetic model, time is the independent variable, reactant and product concentrations are dependent variables, and the rate constants (k_1' and k_2') are treated as parameters to be determined by non-linear regression. The model returned a value of 8.3 for thiol pKa when it was defined as a parameter to be determined by regression of pH 7.0 data. Thus, the pKa values for the ionization of T20 and T21 (K_{a20} , K_{a21}) were fixed at 8.3, consistent with previous reports for cysteine [143, 144] and with our previous model for the solution-state reaction [169]. Rate constants k_1' and k_2' are second-order rate constants for thiol-disulfide exchange and thiol oxidation, respectively (Scheme 3.1). Kinetic data were fitted to the model (eqns. 4.1-4.6) using non-linear regression (SCIENTIST®, Micromath Research, St. Louis, MO). Pertinent models in SCIENTIST® were selected based on reported Model Selection Criterion (MSC) values; a greater MSC value represents a better model. MSC is independent of the scaling of data points and is similar to the Akaike Information Criterion (AIC), which is considered to be a better measure of model validity than R^2 values for non-linear regression [145]. For the reaction of T20 with T20-T21 or cT20-T21 in lyophilized powders during storage at 22 °C, the data were fitted to an equation (Eq.3.7) for first-order irreversible reaction to determine the observed rate constant (k_{obs})

$$A/A_0 = \exp(-k_{\text{obs}} t) \quad \text{Eq.3.7}$$

Here, $A = [T20-T21]$ or $[cT20-T21]$, A_0 is the initial concentration of the respective disulfide and t is time.

3.5 Results

The mechanisms of thiol-disulfide exchange reactions between T20 and T20-T21 or cT20-T21 have been elucidated in aqueous solution [169] and provide a basis for the quantitative analysis of thiol-disulfide exchange in the solid state. Here, thiol-disulfide exchange reactions were investigated in tryptic peptides derived from hGH during lyophilization and storage of lyophilized powders. Native disulfides are T20-T21 and cT20-T21 and scrambled disulfides formed as products of thiol-disulfide exchange are T20-T20, T21-T21, SMDs and DMD (amino acid sequence of all peptides are shown in Table 3.1).

3.5.1 Effect of lyophilization on thiol-disulfide exchange

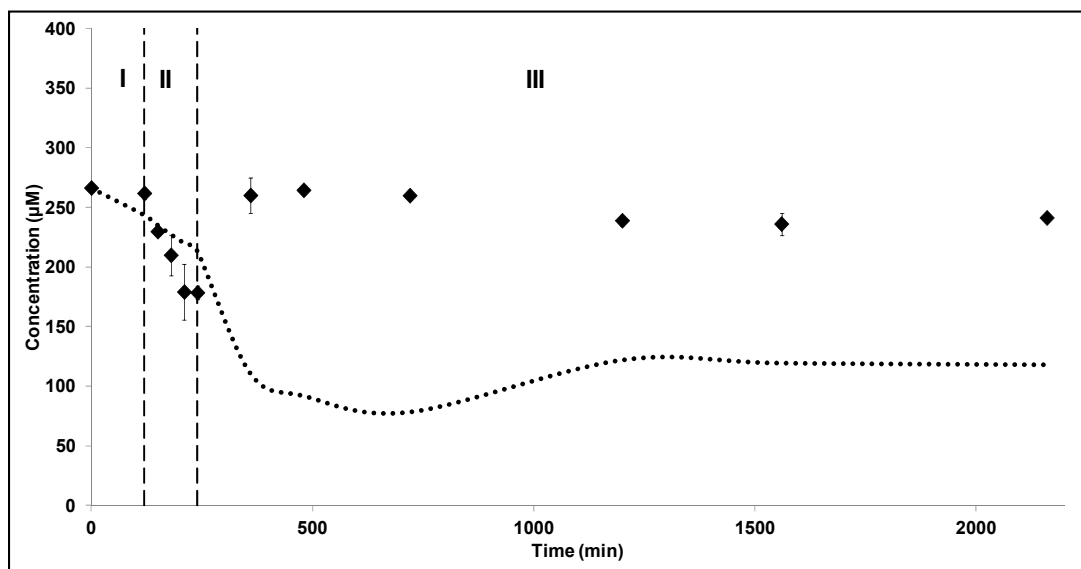
For the reaction of T20 with T20-T21 (thiol: disulfide = 1.4: 1(molar ratio)), primary drying resulted in a 33% loss of native disulfide (Figure 3.2a). The subsequent increase in T20-T21 levels during secondary drying (Figure 3.2a) can be attributed in part to the reversibility of the thiol-disulfide exchange reaction. Despite this increase, a net 9% loss remained at the end of secondary drying (Figure 3.2a). At a greater initial thiol: disulfide ratio of 10:1 (molar ratio), a 24% decrease in T20-T21 was observed after primary drying (Figure 3.2b). During secondary drying, T20-T21 was regenerated from the monomers and scrambled disulfides, resulting in an overall decrease in native disulfide of

10% at the end of the lyophilization cycle (Figure 3.2b). Black dotted lines in Figures 3.2a and 3.2b are the predicted concentrations of T20-T21 based on solution-state model predictions, adjusted for the changing temperature profile during lyophilization using Arrhenius parameters (see below). The solution-state model provides reasonable predictions during freezing and primary drying, but does not describe concentrations during secondary drying. A mass balance from RP-HPLC and LC-MS data shows that products other than T20-T20 and T21 were not generated in detectable quantities and that $\geq 96\%$ of the initial peptide mass was accounted for at all time points during lyophilization. The distribution of free thiols (T20 and T21), native disulfide (T20-T21) and scrambled disulfide (T20-T20) for the reaction of T20 with T20-T21 at 10:1 is shown in Figure 3.3.

For the cyclic peptide, a 29% decrease in native disulfide was observed after primary drying (Figure 3.2b). Like the linear peptide, cT20-T21 was partially regenerated during secondary drying, resulting in a 17% decrease overall in native disulfide content at the end of lyophilization (Figure 3.2b). The distribution of free thiols (T20 and rT20-T21), native disulfide (cT20-T21) and scrambled disulfide (T20-T20) is shown in Figure 3.3. In addition to these species, small amounts of single mixed disulfides (SMD1, SMD2) and double mixed disulfide (DMD) (structures in Table 3.1) were also detected on LC-MS and RP-HPLC (data not shown), though these could not be analyzed quantitatively due to the lack of synthetic standards. Mass balance from RP-HPLC data obtained during freezing, primary and secondary drying accounts for $\geq 90\%$ of the initial mass of cT20-T21 (determined from concentrations of cT20-T21 and rT20-T21). The distribution of free thiols (T20 and rT20-T21), native disulfide (cT20-T21) and scrambled disulfide (T20-T20) for the reaction of T20 with cT20-T21 at 10:1 is shown in Figure 3.4. The factors that may

influence thiol-disulfide exchange during freeze-drying and the results of studies designed to elucidate their effects are described in greater detail below.

a)



b)

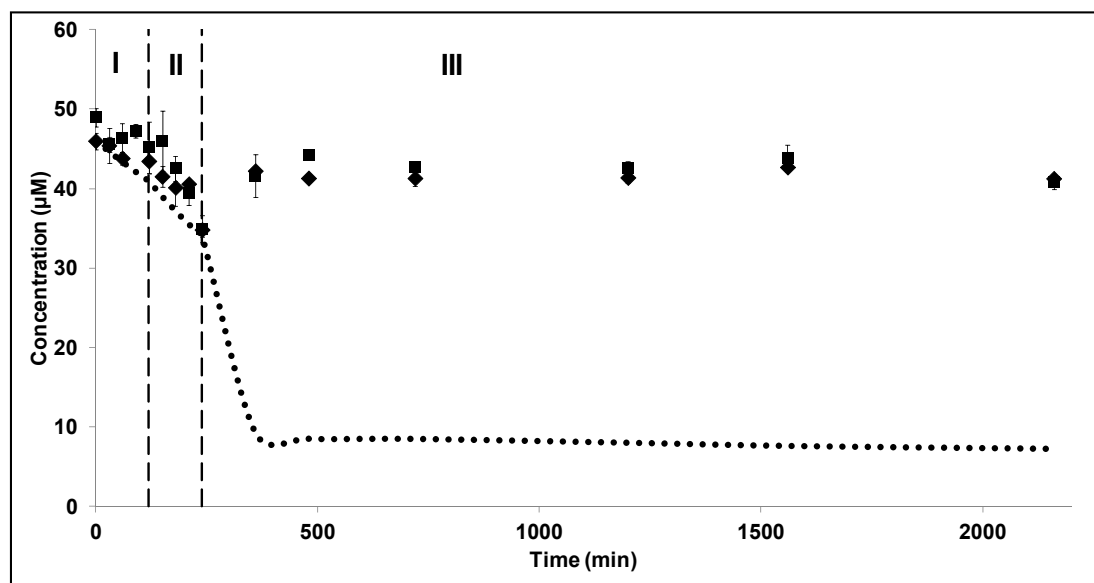


Figure 3.2: Change in native disulfide content during lyophilization ($n=3$, \pm SD) at pH 7.0 (10 mM PB, 0.08 M ionic strength, 0.5 mM EDTA and N_2 sparged); I-freezing, II-primary drying and III-secondary drying. Reaction of T20 with a) T20-T21 (thiol: disulfide = 1.4:1), b) T20-T21 (◆) and cT20-T21 (■) at thiol: disulfide = 10:1. Black dashed lines indicate the end of each stage during lyophilization and the black dotted lines represent predicted values from solution Arrhenius parameters (see text).

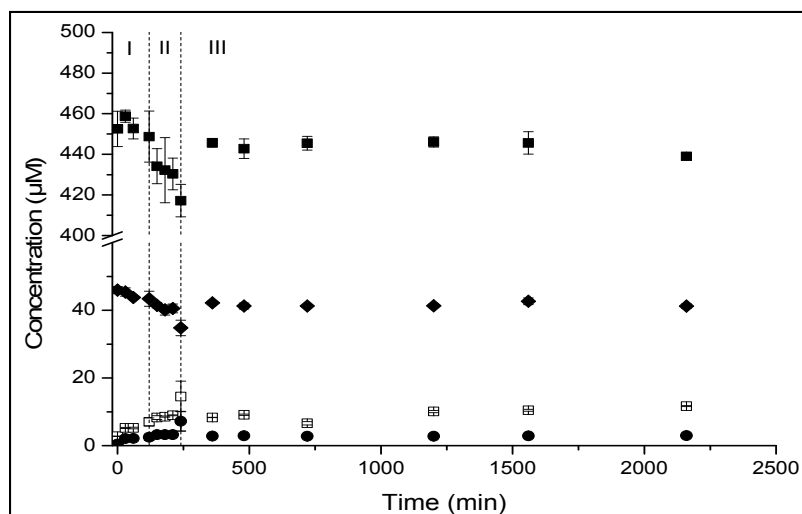


Figure 3.3: Change in concentrations of reactants and products during lyophilization (n=3, +/- SD) for the reaction of T20 with T20-T21 (thiol: disulfide = 10:1, pH 7.0, 10 mM PB, 0.08 M ionic strength, 0.5 mM EDTA and N₂ sparged); I-freezing, II-primary drying and III-secondary drying. Symbols represent actual data points: T20 (■), T21 (●), T20-T20 (□), T21-T21 (○) and T20-T21 (◆). Initial concentrations of reactants in solution (before lyophilization): [T20] = 450 µM; [T20-T21] = 45 µM. On the plot, t=0 (min) represents solution concentrations before lyophilization.

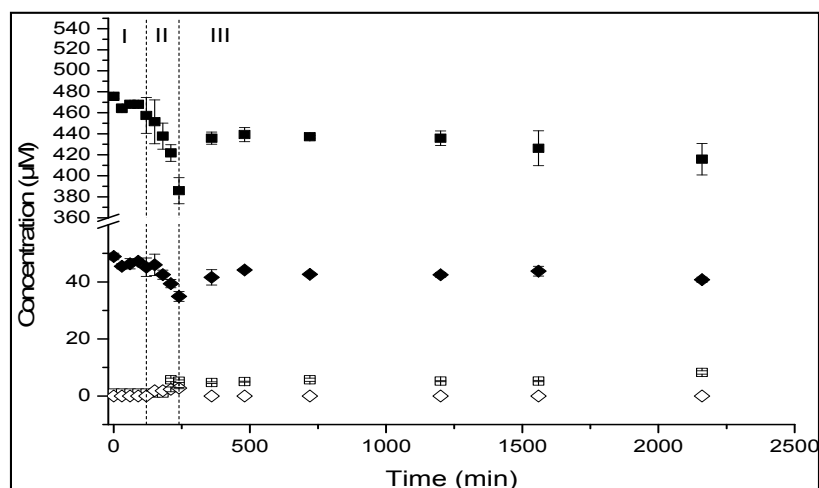


Figure 3.4: Change in concentrations of reactants and products during lyophilization (n=3, +/- SD) for the reaction of T20 with cT20-T21 (thiol: disulfide = 10:1, pH 7.0, 10 mM PB, 0.08 M ionic strength, 0.5 mM EDTA and N₂ sparged); I-freezing, II-primary drying and III-secondary drying. Symbols represent actual data points: T20 (■), T20-T20 (□), cT20-T21 (◆) and rT20-T21 (◇). Initial concentrations of reactants in solution (before lyophilization): [T20] = 450 µM; [T20-T21] = 45 µM. On the plot, t=0 (min) represents solution concentrations before lyophilization.

3.5.2 Disulfide bond stability during lyophilization

Lyophilization of hGH derived peptides showed a difference in the distribution of scrambled disulfides when compared to solution studies. Native disulfides (T20-T21 and cT20-T21) were regenerated during secondary drying. For the cyclic peptide, non-native disulfides (SMDs and DMD, Table 3.1) were detected in the solid state in addition to T20-T20. While previous studies have shown that lyophilization alters thiol-disulfide product distribution [129], the factors contributing to these differences were not identified. Here, we investigated the effects of temperature, peptide concentration, buffer and peptide adsorption to ice on disulfide bond stability during lyophilization.

Effect of temperature and concentration: Arrhenius parameters determined from thermal stress studies in aqueous solution (thiol: disulfide = 1.4:1) were used to predict reaction kinetics at reactant concentrations and temperatures used in lyophilization (black dotted line in Figures 3.2a and 3.2b). At a higher thiol: disulfide ratio (Figure 3.2b), Arrhenius predictions agree well with data obtained during freezing and primary drying. However, the solution-state model overestimates the extent of thiol-disulfide exchange during secondary drying and does not account for the increase in native disulfide during the transition from primary drying to secondary drying. Deviations from Arrhenius behavior suggest that factors other than temperature and initial peptide concentrations (e.g., phase change, peptide adsorption to ice, peptide structural changes, changes in reaction mechanism and/or freeze concentration) influence thiol-disulfide exchange during the freeze-drying process, since the model predictions are based on both the concentrations of the reactants and temperature.

Effect of buffer type and buffer concentration: T20 was lyophilized with T20-T21 at pH 7.0 and 4-fold lower buffer concentration (2.5 mM PB, 0.04 M ionic strength, 0.5 mM EDTA and N₂ sparged). The rate of loss of T20-T21 was similar to that observed during lyophilization with 10 mM PB (Figure 3.5). Similarly, when T20 was co-lyophilized with T20-T21 in sodium citrate buffer (10 mM, 0.5 mM EDTA and N₂ sparged), the native disulfide concentration decreased during primary drying and then increased during secondary drying (Figure 3.5). While there are some differences in T20-T21 concentration during primary drying, particularly at a low buffer concentration (2.5 mM PB), the T20-T21 concentration is similar at the end of primary drying and after two hours of secondary drying (-5 °C, 70 mTorr) in all three buffers (Figure 3.5). These results suggest that buffer concentration and type (phosphate vs. citrate) do not contribute to the observed loss of native disulfide during primary drying.

Lyophilization induced damage to disulfide bonds: To investigate the effect of peptide adsorption to an ice surface on thiol-disulfide exchange, a “cold finger” was used (see methods, Figure 3.1). The ice surface on the cold finger and the solution after adsorption were analyzed using RP-HPLC (data not shown). Peptide concentrations on the ice after adsorption for 1 hr were; [T20] = 326 μM and [cT20-T21] = 33 μM. The results showed that the ratio of T20 to cT20-T21 on the ice (10:1) after adsorption for 1 hr is similar to the molar ratio (10:1) in the initial reaction mixture before adsorption. Although cT20-T21 does not adsorb preferentially to the ice surface, thiol-disulfide exchange between T20 and cT20-T21 still occurs on ice (6 hr sample thawed and analyzed on the HPLC, data not shown).

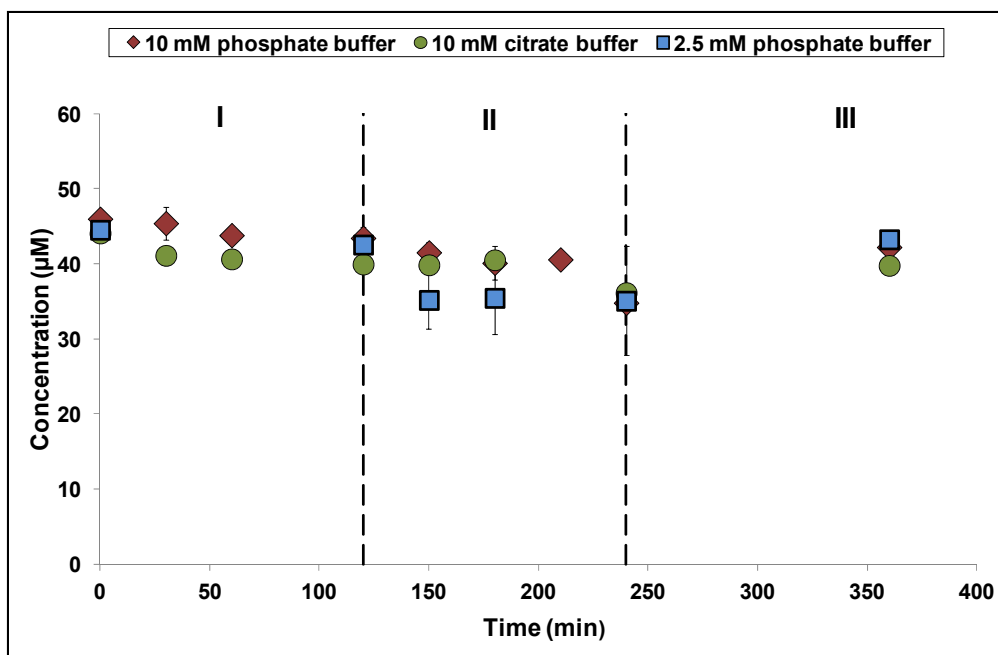


Figure 3.5: Effect of buffer type and buffer concentration on thiol-disulfide exchange during lyophilization; freezing (I), primary drying (II) and secondary drying (III). Plot shows change in T20-T21 concentration ($n=3$, \pm SD), co-lyophilized with T20. All buffers contain 0.5 mM EDTA and were sparged with N_2 , pH of reaction mixture was adjusted to 7.0 before lyophilization. Initial concentrations of reactants in solution (before lyophilization): $[T20] = 450 \mu\text{M}$; $[T20-T21] = 45 \mu\text{M}$. On the plot, $t=0$ (min) represents solution concentrations before lyophilization.

Primary drying duration: The duration of the primary drying step ($-35 \text{ }^\circ\text{C}$, 70 mTorr) was increased from 2 to 6 hours to determine the effect of drying time on thiol-disulfide exchange (Figure 3.6). The concentration of native disulfide decreases in the initial 2 hours of primary drying. After this initial loss, the native disulfide is regenerated with continued drying for another 2 hours. Between 4 and 6 hours, there is no further change in T20-T21. While a longer primary drying step can preserve the native disulfide to some extent, lyophilization induced damage to the disulfide bond still occurs and may influence the storage stability of the resulting solids.

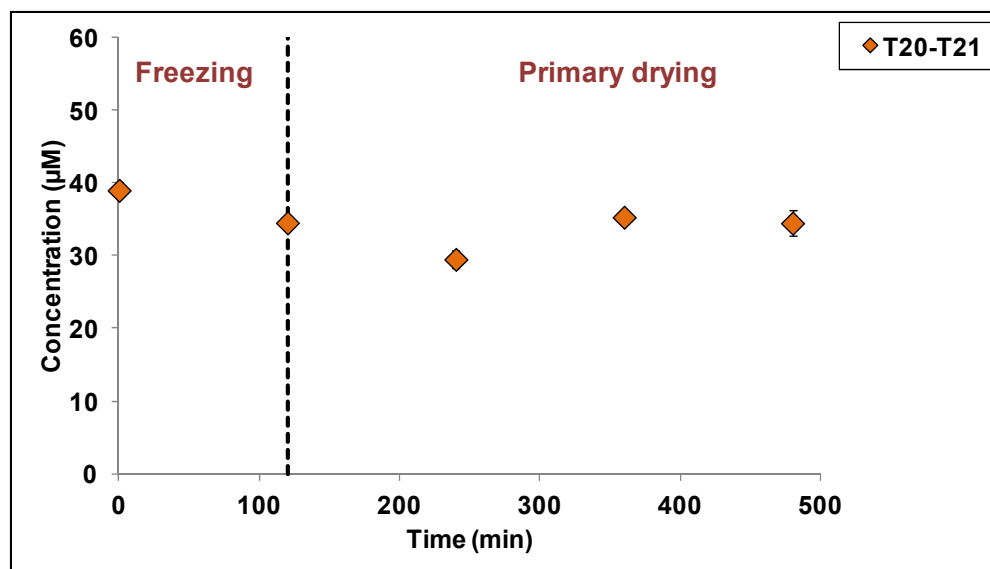


Figure 3.6: Change in concentration of T20-T21 lyophilized with T20 (thiol: disulfide = 6:1, pH 7.0, 10 mM PB, 0.08 M ionic strength, 0.5 mM EDTA and N₂ sparged) during freezing and primary drying (n=3) (♦). Primary drying time was increased from 2 to 6 hours. On the plot, t=0 (min) represents solution concentrations before lyophilization.

3.5.3 Thiol-disulfide exchange in lyophilized powders during storage

The thiol-disulfide exchange reaction between T20 and T20-T21 or cT20-T21 at pH 7.0 (pre-lyophilization) in lyophilized powders stored at 22 °C was monitored over 0-7 and 0-12 days for T20-T21 and cT20-T21, respectively. Storage stability studies were truncated after 7 days for T20-T21, since oxidative pathways began to dominate (Figure 3.7). T_g measured for the lyophilized powder at the end of secondary drying was 20.6 °C, and the moisture content at the end of secondary drying and after storage for 14 days at 22 °C was 1-1.5%.

Reaction of T20 with T20-T21: The change in the concentration of T20-T21 during storage is shown in Figure 3.8. Rate constants for the exchange (k_1') and oxidation reaction (k_2') were estimated by fitting the data to the model of Scheme 3.1. Excellent model fits to the data were obtained and these model fits are represented by solid lines in Figure 3.9.

The rate constants for the reaction of T20 with T20-T21 in the solid state are shown in (Table 3.3). Mass balance from RP-HPLC data at the end of 7 days accounts for 95% of initial mass of peptides. The observed pseudo-first order rate constant (k_{obs}) for the loss of T20-T21 during storage in aqueous solution is of the same order as k_{obs} in the solid state, indicating that the reaction is not slowed appreciably in the lyophilized form.

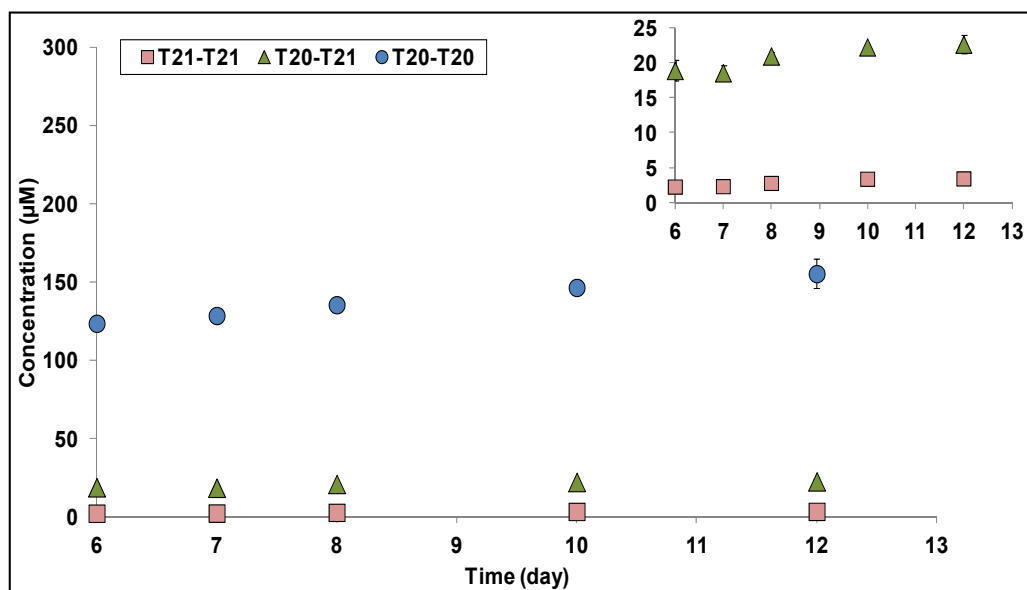
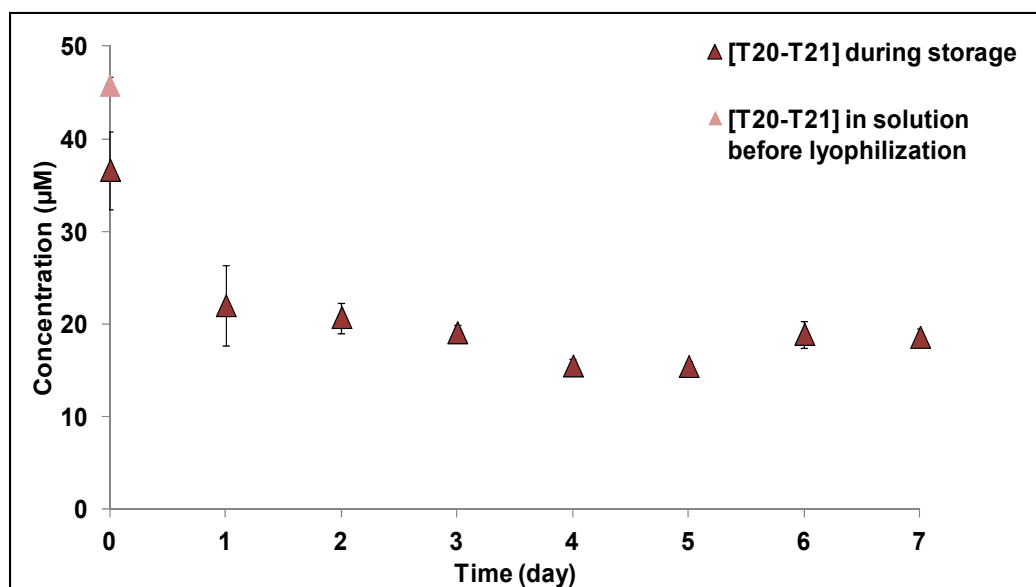
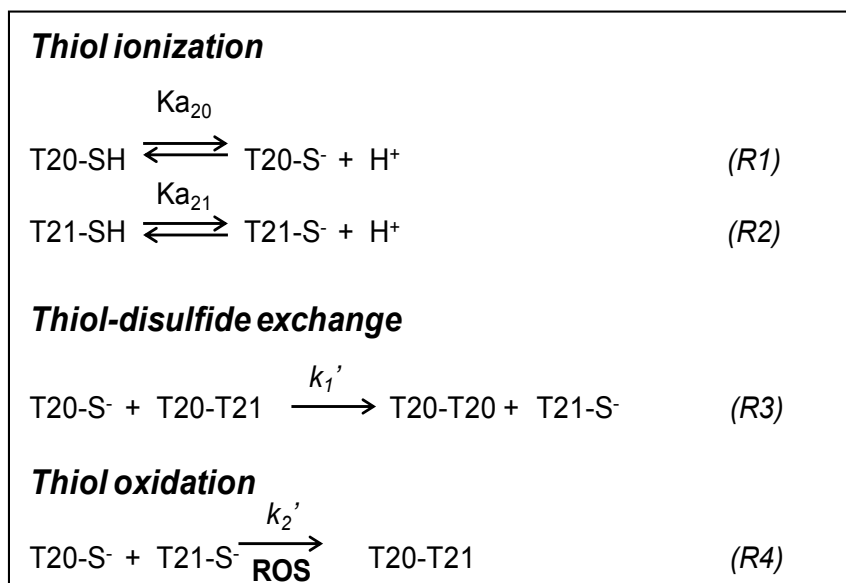


Figure 3.7: Concentration of scrambled and native disulfides formed via oxidative pathways during storage of lyophilized powders ($n=3$, \pm SD). Inset zooms in to show change in concentrations of T20-T21 and T21-T21. T20-T21 was co-lyophilized with T20 (thiol: disulfide = 10:1, pH 7.0, 10 mM PB, 0.08 M ionic strength, 0.5 mM EDTA and N_2 sparged) (see text for details).

Scheme 3.1. Thiol-disulfide exchange in T20-T21 during storage in the solid state.**Figure 3.8:** Reaction of T20 with T20-T21 in lyophilized powders stored at 22 °C (n=3, +/- SD). Initial concentrations of reactants in solution (before lyophilization): [T20] = 450 μM; [T20-T21] = 45 μM. Buffer conditions: pH 7.0 , 10 mM phosphate buffer, 0.08 M ionic strength, 0.5 mM EDTA and N₂ sparged.

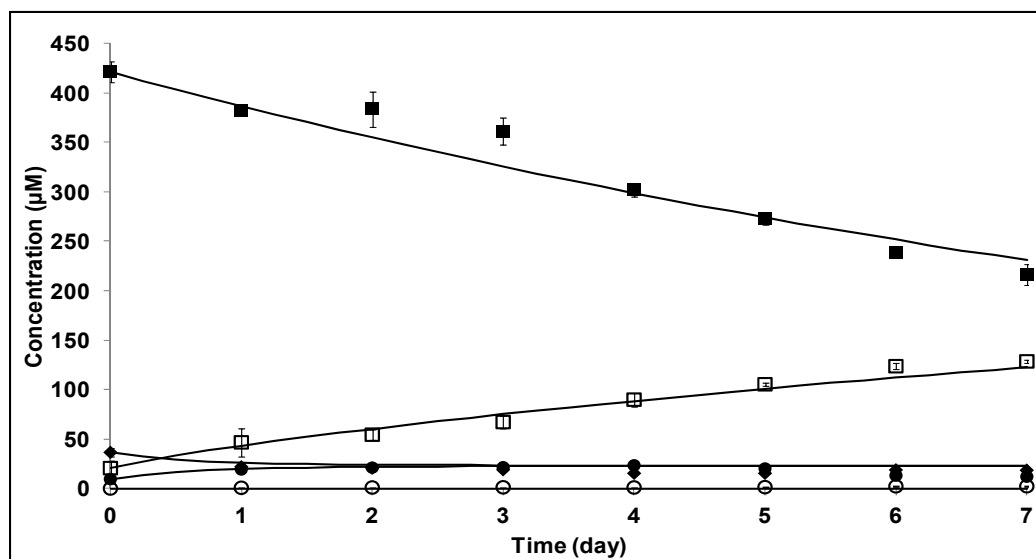


Figure 3.9: Reaction of T20 with T20-T21 in lyophilized powders stored at 22 °C (n=3, +/- SD). Initial concentrations of reactants in solution (before lyophilization): [T20] = 450 μM ; [T20-T21] = 45 μM . Buffer conditions: pH 7.0, 10 mM phosphate buffer, 0.08 M ionic strength, 0.5 mM EDTA and N_2 sparged. Plot shows concentrations of T20 (\blacksquare), T21 (\bullet), T20-T20 (\square), T21-T21 (\circ) and T20-T21 (\blacklozenge). Solid lines are non-linear regressions based on the model in Scheme 3.1. Initial time point (t = 0 days) corresponds to a sample reconstituted immediately after lyophilization.

Table 3.3: Microscopic and observed rate constants for thiol-disulfide exchange between T20 and T20-T21 in lyophilized solids and aqueous solution.

Parameter	Aqueous solution (22 °C), pH 7.0	Lyophilized solids (22 °C), pH 7.0
k_1' (T20-T21)	n/a	$0.45 \pm 0.04 \text{ M}^{-1} \text{ s}^{-1}$
k_2' (T20-T21)	n/a	$9.57 \pm 1.00 \text{ M}^{-1} \text{ s}^{-1}$
k_{obs} (T20-T21)	$1.00 \cdot 10^{-4} \pm 4.00 \cdot 10^{-6} \text{ s}^{-1}$ ^a	$1.78 \cdot 10^{-4} \pm 1.84 \cdot 10^{-5} \text{ s}^{-1}$
k_{obs} (cT20-T21)	$1.15 \cdot 10^{-5} \pm 1.00 \cdot 10^{-6} \text{ s}^{-1}$ ^a	$1.56 \cdot 10^{-4} \pm 1.14 \cdot 10^{-5} \text{ s}^{-1}$

n/a -not applicable, different model was used to determine k_1' and k_2'

^a values obtained from Chapter 2, [169]

Reaction of T20 with cT20-T21: During storage of the cyclic peptide cT20-T21 in lyophilized powders containing T20, the loss of the disulfide bond was faster in the solid state than in aqueous solutions stored at the same conditions (Figure 3.10). The concentration of cT20-T21 in solution increases over time due to oxidation as rT20-T21 is oxidized to cT20-T21, behavior similar to that observed for cT20-T21 in aqueous solution studies [169]. Mixed disulfides (SMDs and DMD; structures in Table 3.1) were detected on both RP-HPLC (Figure 3.11) and LC-MS (data not shown), consistent with the reaction mechanism in Scheme 3.3b. No other oxidation products such as sulfenic, sulfinic or sulfonic acid were detected. A mass balance from RP-HPLC data at the end of 12 days accounts for 80% of all peptides present in the storage samples. This suggests that the remaining 20% of the initial mass is present as SMDs or DMD, which are not quantitated but detected on LC-MS and RP-HPLC, or as other undetected species. Figure 3.12 shows a concentration vs. time plot for T20, rT20-T21, native (cT20-T21) and scrambled disulfide (T20-T20) obtained during storage of cyclic peptide. Unlike T20-T21, the concentration of cT20-T21 does not increase during storage after 7 days (Figure 3.10). This suggests that lyophilization induced stresses favor thiol-disulfide exchange between T20 and cT20-T21, as temperature and pH did not influence reactivity to as great an extent in solution [169]. Observed rate constants (k_{obs}) for the loss of cT20-T21 during storage in lyophilized powders are shown in Table 3.3. At a pH 7.0, the k_{obs} value for cT20-T21 in the solid state is ~10-fold greater than its k_{obs} value in aqueous solution, and is comparable to k_{obs} for T20-T21 in lyophilized solids at pH 7.0. This suggests that structural constraints imposed by cyclization slow the thiol-disulfide exchange reaction in solution but not in lyophilized solids.

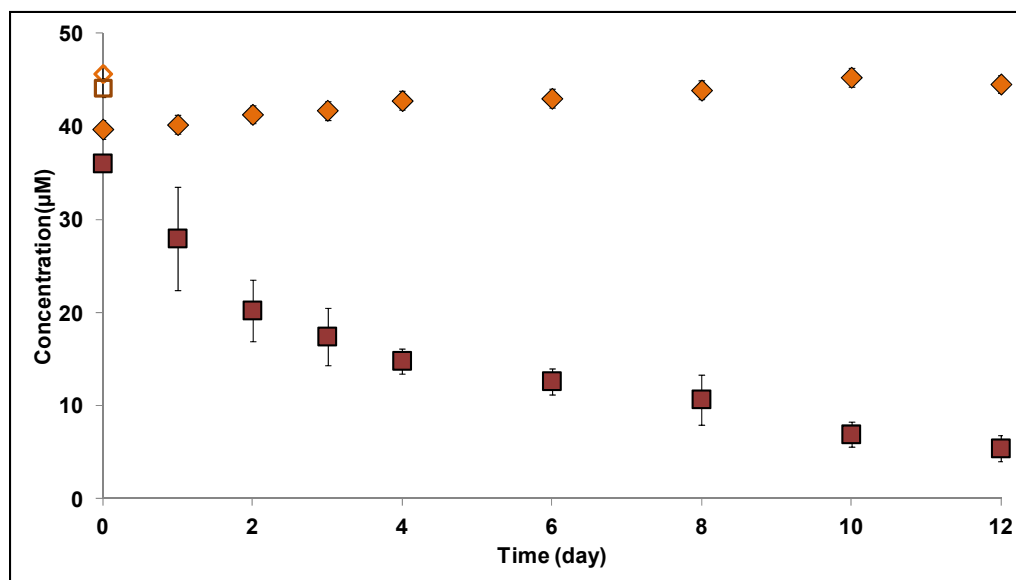


Figure 3.10: Change in concentration of cT20-T21 lyophilized with T20 (thiol: disulfide = 10:1, pH 7.0, 10 mM PB, 0.08 M ionic strength, 0.5 mM EDTA and N_2 sparged) during storage ($n=3$, \pm SD) at 22 °C (■), and in solution (◆) (thiol: disulfide = 10:1, pH 7.0, 10 mM PB, 0.08 M ionic strength, 0.5 mM EDTA and N_2 sparged). Both solid and solution samples were stored at 22 °C in lyo vials, $n = 3$. Open symbols show the initial concentration of cT20-T21 in solution before lyophilization (□) and before storage as solution at 22 °C (◇). Initial data points ($t = 0$ days, filled symbols) represent solution sample and lyophilized sample reconstituted immediately after lyophilization.

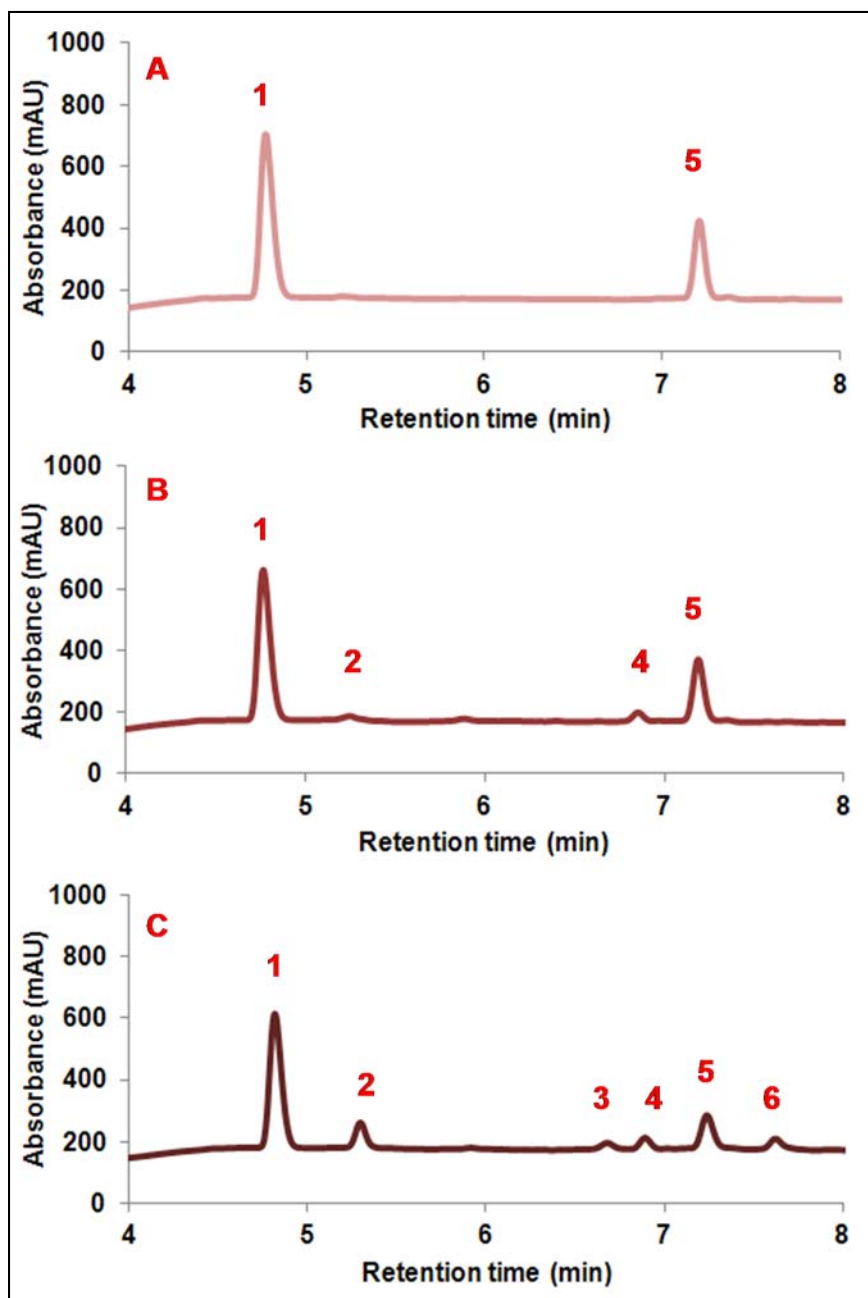


Figure 3.11: HPLC chromatograms (215 nm) obtained at various times during storage of lyophilized T20 and cT20-T21 at 22 °C (pH before lyophilization was 7.0). Solution sample before lyophilization (A), solid sample immediately after lyophilization (B) and solid sample after 3 days (C). Peak labels: 1) T20; 2) T20-T20; 3) DMD; 4) SMD 1&2; 5) cT20-T21 and 6) rT20-T21.

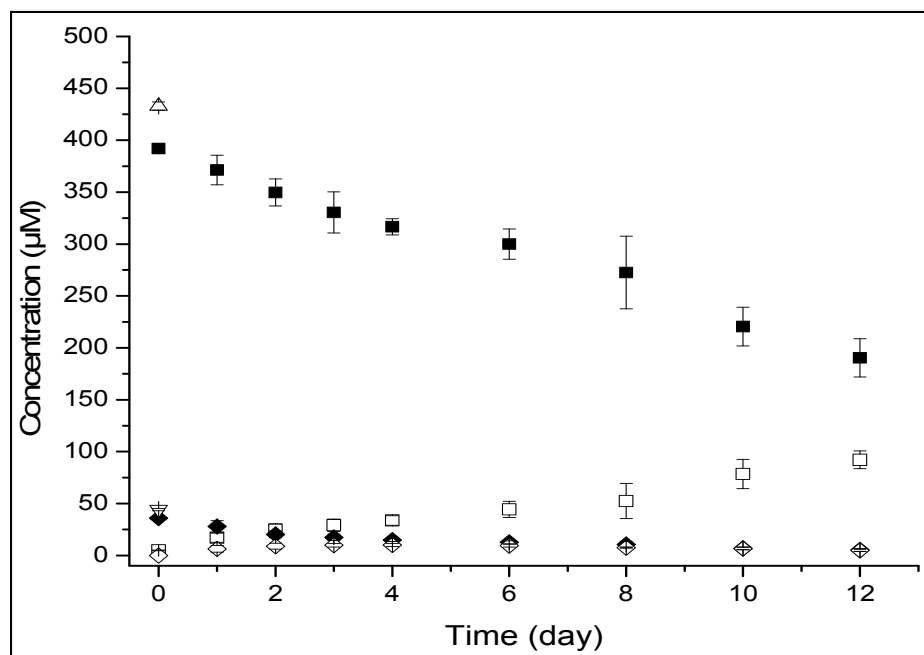


Figure 3.12: The concentration of reactants and products for a kinetic study with T20 and cT20-T21 during storage at 22 °C. Buffer conditions before lyophilization: pH 7.0, 10mM phosphate buffer with 0.5 mM EDTA and N₂ sparging. Initial concentrations of peptides were: [T20] = 450 µM (Δ); [cT20-T21] = 45 µM (○). The symbols represent actual data points obtained from samples at different times (n=3, +/- SD): T20 (■), cT20-T21 (◆), T20-T20 (□) and rT20-T21 (◇).

To determine disulfide bond stability without a free thiol in the solid state, T20-T21/cT20-T21 was lyophilized without T20. When T20-T21 was lyophilized without T20 at pH 7.0, only the two homodimers; T20-T20 and T21-T21 were detected as products of disulfide bond scission on RP-HPLC. While cT20-T21 lyophilized without T20 at pH 7.0 was very stable even after a few weeks at 22 °C. To further elucidate the mechanism of disulfide bond degradation in the solid state, T20-T21/cT20-T21 was co-lyophilized with dimedone at pH 8.0 (see methods). Change in T20-T21 and cT20-T21 concentrations with time at pH 8.0 (pH in solution before lyophilization) are shown in Figures 3.13 and 3.14.

T20 sulfenic acid (T20-SOH) and dimedone adduct ($m/z = 378.7059$) was detected in solid samples stored at 22 °C for 2 weeks using LC-MS after reconstitution and in solution samples stored at the same conditions (Figure 3.15). In addition, T20-SO₂H (T20 sulfonic acid) was detected in solution samples; this is formed by further reaction of T20-SOH with a hydroxyl ion [172, 173]. These products of alkaline hydrolysis are consistent with a direct attack of OH⁻ on the disulfide bond in T20-T21 (Scheme 3.2). Damage to the disulfide bond in the cyclic peptide at pH 8.0 by alkaline hydrolysis was lower than that of the linear form. No dimedone adducts were detected on the LC-MS. However, small amounts of cysteine dehydroalanine (Scheme 3.2) were observed. This is consistent with disulfide bond degradation via β -elimination mechanism.

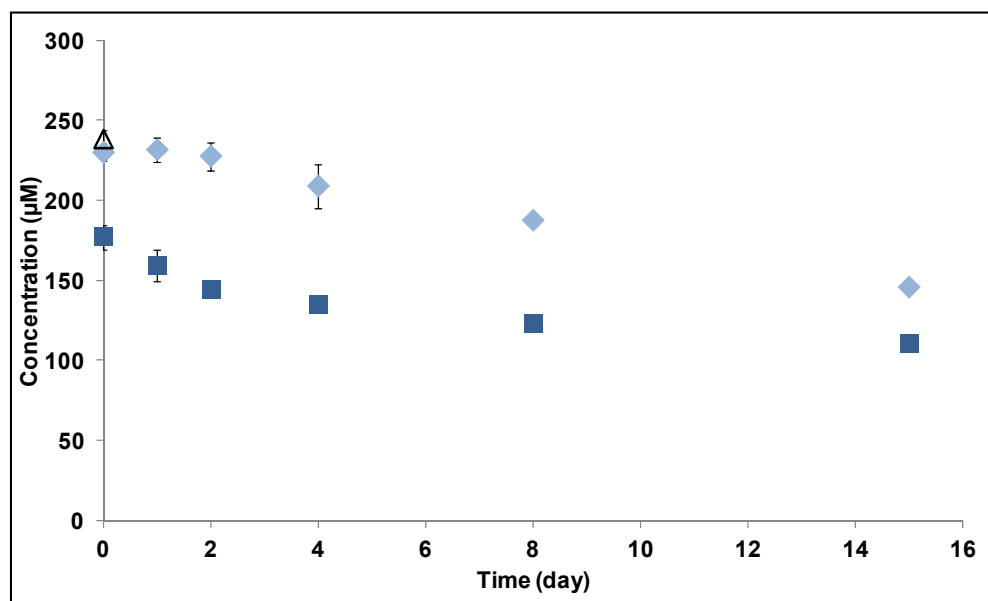


Figure 3.13: Change in T20-T21 (pH 8.0, 10 mM PB, 0.08 M ionic strength, 0.5 mM EDTA and N₂ sparged) concentration during storage (n=3, +/- SD) without T20, as a lyophilized powder (♦) and in solution (■). T = 0 (day) on plot represents solution sample analyzed at the same time as samples reconstituted immediately after lyophilization. Initial concentration of T20-T21 in solution before lyophilization is represented by Δ.

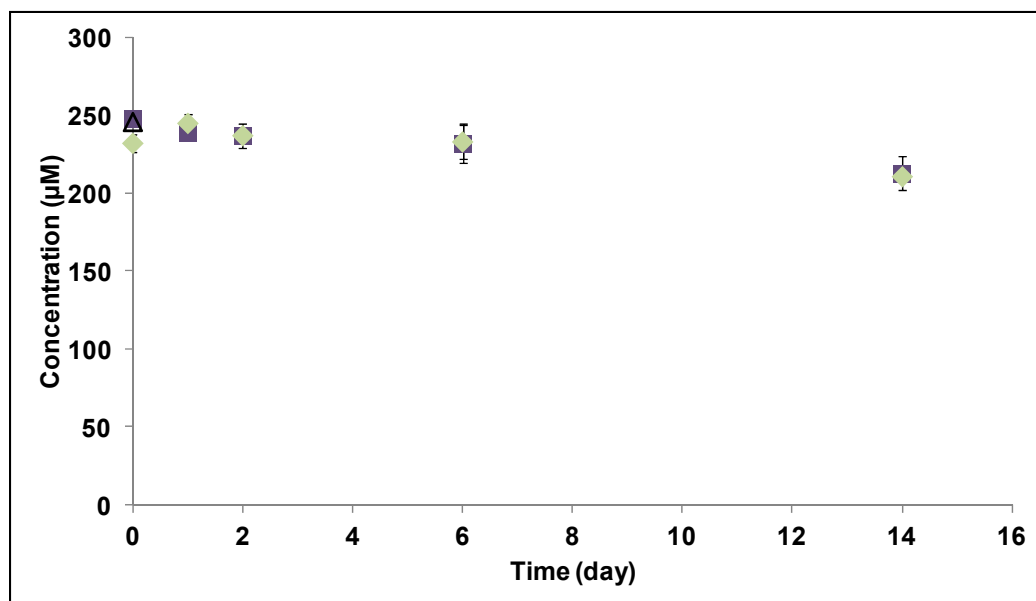


Figure 3.14: Change in cT20-T21 (pH 8.0, 10 mM PB, 0.08 M ionic strength, 0.5 mM EDTA and N₂ sparged) concentration during storage (n=3, +/- SD) without T20, as a lyophilized powder (◆) and in solution (■). T = 0 (day) on plot represents solution sample analyzed at the same time as samples reconstituted immediately after lyophilization. Initial concentration of cT20-T21 in solution before lyophilization is represented by Δ.

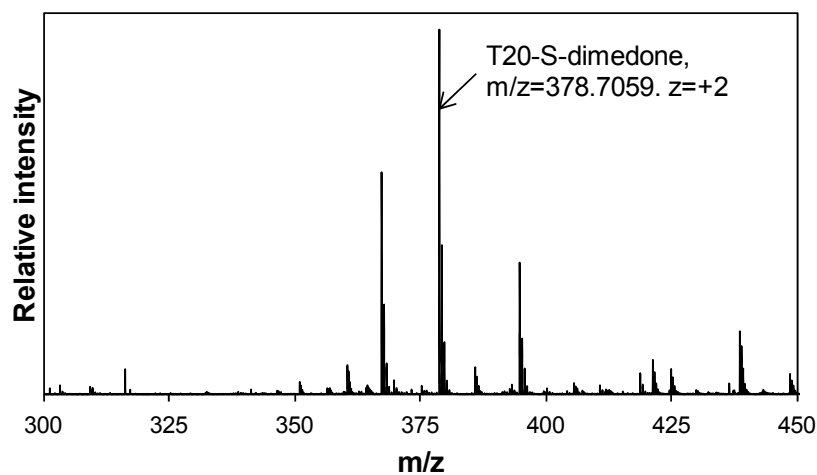
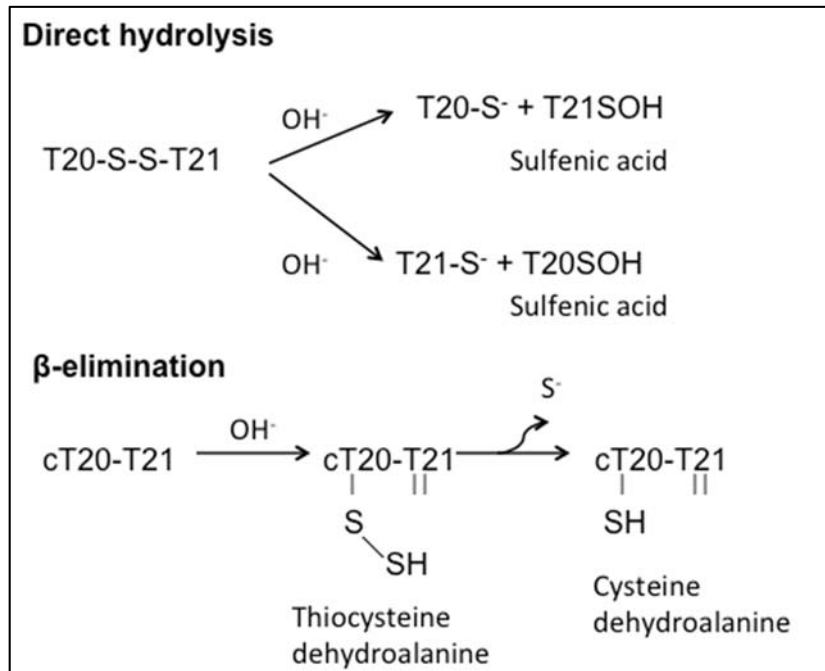


Figure 3.15: Mass spectrum (extracted ion chromatogram) showing the T20-S-dimedone adduct. Lyophilized T20-T21 (initial concentration = 250 µM, PB pH 8.0, 0.5 mM EDTA, 0.08 M ionic strength and N₂ sparged) was analyzed on the LC-MS upon reconstitution after storage at 22 °C for 2 weeks.

Scheme 3.2. Alkaline hydrolysis of disulfide bonds in the linear and cyclic peptide.

3.6 Discussion

The mechanism of thiol-disulfide exchange is well established in aqueous solution. In neutral to basic solution, the thiolate anion is the reactive nucleophile, attacking a disulfide bond via an $\text{S}_{\text{N}}2$ mechanism [45, 71]. Thiol-disulfide exchange is known to occur in the solid state as well [14, 79, 95], though the reaction mechanisms have not been fully elucidated. In the studies reported here, hGH-derived model peptides were lyophilized without excipients to investigate the effect of lyophilization on thiol-disulfide exchange kinetics and mechanisms. The amino acid sequences of the model and their masses are shown in Table 3.1. In studies of the solution-state reaction of the linear peptide (T20-T21) with T20, the T20-T20 homodimer and T21 were detected as the initial products, as we

have reported previously [169]. At longer time points, the T21-T21 homodimer was also observed. These products are consistent with two thiol-disulfide exchange reactions, in which: (i) T20-T21 initially reacts with T20 to produce the T20-T20 homodimer and T21, and (ii) T20-T21 reacts with T21 produced in the first reaction to produce the T21-T21 homodimer and regenerate T20 (Scheme 3.3a). Solution-state reaction kinetics were not adequately described by a kinetic scheme based only on these two reactions, however, and oxidative pathways were included. This suggests that even in the presence of oxidation suppressants (EDTA and N₂ sparging), T20 and T21 also undergo oxidation to form T20-T20, T21-T21 and T20-T21 via a sulfenic acid intermediate. Kinetic models including both thiol-disulfide exchange and oxidation steps provided excellent fits to data, both in the presence and in the absence of oxidation suppressants [169].

When the reaction of T20-T21 with T20 was monitored during lyophilization and storage in the solid state, T20-T20 and T21 were again detected as initial products, consistent with reaction 1 in Scheme 3.3a. Reaction 2 in scheme 3.3a was not observed in the solid state during storage (in the timeframe that the reaction was monitored) based on model fits to the data in SCIENTIST[®]. As in solution [169], kinetic profiles suggested that T20 and T21 were oxidized to T20-T20, T21-T21 and T20-T21 on extended storage in the solid state (> 7days at 22 °C; Figure 3.7). Oxidation products such as cysteine sulfenic, sulfinic and sulfonic acid and thiosulfinates were not detected for samples containing T20-T21 co-lyophilized with T20. However, when T20-T21 was lyophilized without T20 (see methods), sulfenic acid and a dimedone adduct were detected (Figure 3.15). The presence of sulfenic acid as an intermediate suggests that disulfide linked peptides can undergo alkaline hydrolysis when a free thiol (T20) is not present, as reported previously [172, 174].

Kinetic analysis further suggests that, during lyophilization, T20-T20 and T21 are generated ($k_1 > k_{-1}$) during primary drying and then partly consumed ($k_1 < k_{-1}$) during the first step of secondary drying (Table 3.2), after which there is no appreciable change in product distribution. During storage in the lyophilized solid, the product distribution is altered and kinetic analysis suggests that thiol-disulfide exchange is essentially irreversible. Possible physicochemical contributions to these kinetic effects are discussed below.

In solution-state reactions of the cyclic peptide (cT20-T21) with T20, only T20-T20 and rT20-T21 were detected as products [169]. Mixed disulfides (SMDs and DMD; Table 3.1) were not observed under any conditions in aqueous solution. After 6 hours, oxidation of rT20-T21 to cT20-T21 was the dominant pathway even under oxidation-suppressed conditions. In contrast, SMDs, DMD, rT20-T21 and T20-T20 were identified as products of the reaction of cT20-T21 with T20 in the solid state. Oxidation of rT20-T21 to cT20-T21 was not the dominant reaction even after 12 days of storage in lyophilized solids at 22 °C, and the concentration of cT20-T21 did not increase with time (Figures 3.10 and 3.12). As with the linear peptide, oxidation products such as cysteine sulfenic, sulfinic and sulfonic acid and thiosulfinates were not detected. While sulfenic acid and dimer adducts were not detected for cT20-T21 lyophilized without T20, trace amounts of cysteine dehydroalanine were detected (data not shown), again suggestive of alkaline hydrolysis in the absence of a free thiol.

In the reaction of the cyclic peptide cT20-T21 with T20 in the solid state, mixed disulfides (SMDs and DMD) were detected in addition to T20-T20 and rT20-T21 during lyophilization and storage (Figure 3.11, Scheme 3.3b). Mixed disulfides were not detected in solution studies [169], suggesting that rates of loss from this pool (k_{-3} , k_4) are rapid

relative to rates of formation (k_3 , k_4) so that these species do not accumulate in solution (Scheme 3.3b). The absence of the double mixed disulfide (DMD) in solution can be attributed to the decreased reactivity of cT20-T21 and hence lower concentrations of T20-T20, which in solution did not accumulate to levels sufficient to drive the reaction towards DMD. In contrast, both SMDs and DMD were detected during the primary drying stage of lyophilization, and the native disulfide was regenerated during secondary drying (Table 3.2).

The observed mechanism of thiol-disulfide exchange between T20 and cT20-T21 is similar to that reported previously for tocinoic acid (TA (ox)) and glutathione (GSH) during lyophilization, where both SMDs and the DMD were detected [129]. TA (ox) is a cyclic peptide with 6 amino acids and terminal Cys residues linked by a disulfide bond (Scheme 3.3b, Table 3.4). Though the mechanism remains unchanged here, the relative rates of some thiol-disulfide exchange reactions (scheme 3.3b) are different for cT20-T21 and TA (ox). TA (ox) was consumed in an irreversible thiol-disulfide exchange reaction at the end of lyophilization [129], while for cT20-T21 most of the native disulfide was regenerated at the end of step 3 (Table 3.2). The results suggest that although the type of disulfide and thiol containing peptides may play a role in reaction kinetics during lyophilization, the overall mechanism for thiol-disulfide exchange in cyclic peptides can be represented by Scheme 3.3b.

The loss of native disulfide for both T20-T21 and cT20-T21 during the freezing step may be initiated by freeze-concentration, leading to high local concentrations of the peptide reactants (T20 and T20-T21 or cT20-T21). The loss of disulfide bonds during freezing is consistent with previous studies of tumor growth factor- β 1, in which increased

intra- and intermolecular disulfide bond exchange was observed during freezing and long-term storage at -70 °C [175]. Here, deviations from solution Arrhenius parameters (Figure 3.2) and the absence of a buffer effect (Figure 3.5) suggest that factors such as temperature, peptide concentration, buffer type and concentration have no effect on thiol-disulfide exchange observed during primary drying. Further, the absence of preferential peptide adsorption to ice using the 'cold finger' method suggests that the ice surface itself does not play a role in thiol-disulfide exchange. Instead, loss of the disulfide bond during primary drying may be due to a reduced activation barrier for thiol-disulfide exchange as the environment becomes less polar, as observed at the active site of ribonucleotide reductase [148].

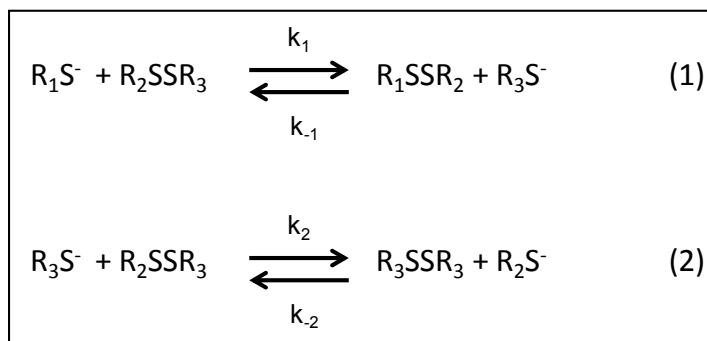
In the simple peptides studied here, most of the native disulfide in T20-T21 and cT20-T21 is regenerated during secondary drying (Figure 3.2). In larger proteins with multiple disulfide bonds, such reverse reactions may not regenerate the original disulfide bond, but may instead result in intramolecular disulfide scrambling and/or covalent aggregation, depending on the proximity of the groups involved. The role of thiol group proximity to a disulfide bond was investigated previously for small heat shock protein and glutathione [67]. The distance between thiols and disulfides, and their relative mobility, can be affected by freeze-drying induced unfolding, particularly for hGH, which is known to undergo structural perturbations during lyophilization [101]. The formation of intermolecular disulfide bonds can further lead to aggregation during storage and/or rehydration. Here, the reactivity of the native disulfide bonds in T20-T21 and cT20-T21 appears to decrease as drying proceeds (Figure 3.2 and Steps 4, 5 and 6, Table 3.2), perhaps the result of reduced mobility of the reactive species in the solid state.

The results suggest that, at neutral to slightly alkaline pH, proteins with free thiols and disulfides can undergo thiol-disulfide exchange during lyophilization and storage in the solid state, which can further lead to the formation of disulfide-linked aggregates. Though peptide cyclization retards disulfide exchange in solution, in the solid state the observed disulfide bond degradation for cT20-T21 is greater than in solution and similar to that of the linear peptide, T20-T21. Thus, increased stability of a disulfide bond conferred by secondary structure in solution may not necessarily translate to increased stability in the solid state. Further, structural constraints may not influence disulfide degradation kinetics during lyophilization and storage in the solid state, especially when free thiols are present on the surface of proteins and are in close proximity to a disulfide bond. Thus, the use of lyophilization alone as a stabilizing strategy may not be sufficient to retard thiol-disulfide exchange and offer protection against chemical degradation during storage. Reasonable formulation strategies include restricting free thiol content before lyophilization, using suitable excipients to stabilize protein structure when free thiols are not present on the surface, excluding O₂ from formulations (if products of oxidative pathways are detected) and formulating proteins at low pH followed by reconstitution at near neutral pH (these strategies are discussed in detail in Chapter 5).

Scheme 3.3. Reaction schemes for thiol-disulfide exchange in a) T20-T21 and b) cT20-

T21

a)

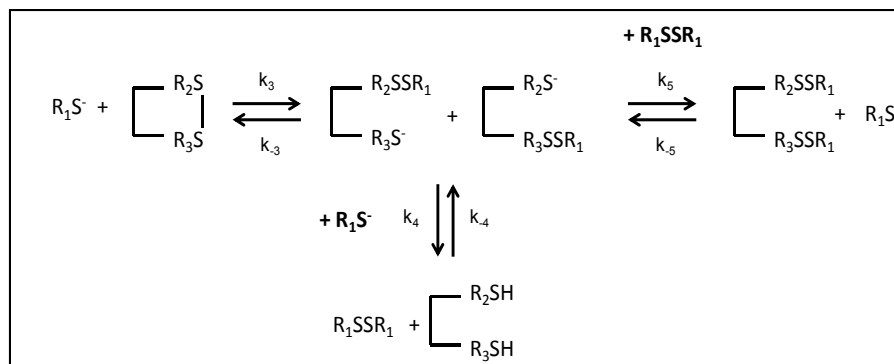


Reaction scheme	Rate constant ($\text{M}^{-1}\text{s}^{-1}$)			
	k_1	k_{-1}	k_2	k_{-2}
linear peptide, aqueous solution	+ (fast)	+ (fast)	+ (fast)	+ (fast)
linear peptide, lyophilization	+ (slow)	+ (slow)	nd	nd
linear peptide, storage in the solid-state	+ (slow)	nd	nd	nd

+ : reaction observed

nd- not detected, based on products observed

b)

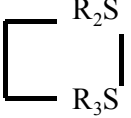

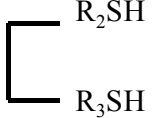
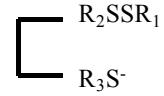
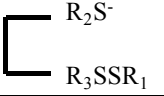
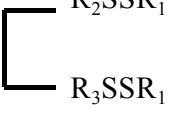


Reaction scheme	Rate constant ($\text{M}^{-1}\text{s}^{-1}$)					
	k_3	k_{-3}	k_4	k_{-4}	k_5	k_{-5}
cyclic peptide, aqueous solution	+ (fast)	+ (fast)	+ (fast)	+ (fast)	nd	nd
cyclic peptide, lyophilization	+ (slow)	+ (slow)	+ (slow)	+ (slow)	+ (slow)	+ (slow)
cyclic peptide, storage in the solid-state	+ (slow)	+ (very slow)	+ (slow)	+ (very slow)	+ (slow)	+ (very slow)

+ : reaction observed

nd- not detected, based on products observed

Table 3.4: Abbreviations and amino acid sequences of tocinoic acid, glutathione and their mixed disulfides.

Abbreviation	Description	Designation in general reaction scheme	Amino acid sequence
GSH	Monomeric peptide, free SH group	R_1	NH_2 -ECG-OH
GSSG	Homodimer, disulfide-linked	R_1SSR_1	NH_2 -ECG-OH \vdots NH_2 -ECG-OH
TA(ox)	Cyclic peptide, disulfide linked		NH_2 -CNQIYC-OH 
TA(red)	Linear peptide, free SH groups		NH_2 -CNQIYC-OH
Single mixed disulfide (SMD)	linear peptide, disulfide linked to GSH	 OR 	NH_2 -CNQIYC-OH \vdots NH_2 -ECG-OH OR NH_2 -CNQIYC-OH \vdots NH_2 -ECG-OH
Double mixed disulfide (DMD)	linear peptide, disulfide linked to two GSH peptides		NH_2 -CNQIYC-OH \vdots NH_2 -ECG-OH \vdots NH_2 -ECG-OH

3.7 Conclusion

The studies reported here detail the effects of lyophilization and storage of lyophilized powders on the mechanisms and rates of thiol-disulfide exchange. Peptide secondary structure does not influence disulfide (T20-T21 or cT20-T21) reactivity in the solid state when co-lyophilized with a free thiol (T20). Further, lyophilization does not retard thiol-disulfide exchange during storage in the solid state. The results obtained provide an insight into the effect of process stresses on disulfide exchange and are valuable to the design of robust lyophilization processes for the development of stable peptide and protein drug products that contain free thiols and/or disulfide bonds.

CHAPTER 4. THIOL-DISULFIDE EXCHANGE IN HUMAN GROWTH HORMONE

This work has been submitted to the *FEBS Journal*.

4.1 Abstract

Protein therapeutics such as hormones and monoclonal antibodies contain thiols and/or disulfides that can participate in thiol-disulfide exchange reactions at neutral to alkaline pH. This can result in the formation of mixed/scrambled disulfides that affect protein therapeutic efficacy and elicit undesirable immunogenic responses upon administration. Thiol-disulfide exchange reactions were monitored in recombinant human growth hormone (rhGH) and model tryptic peptides derived from hGH (cT20-T21 and T20-T21_{pep}) to investigate higher-order structure effects on reaction kinetics. Different free thiol-containing peptides (varying length and amino acid sequence) were used to initiate thiol-disulfide exchange in intact hGH and in model peptides at pH 7.0 and 37 °C. Protein samples were digested with trypsin and analyzed for native disulfides, scrambled disulfides and free thiols on the LC-MS. For peptide-level studies, concentration of disulfide-linked peptides were determined using RP-HPLC and product identity was confirmed on the LC-MS. Loss of native disulfide in cT20-T21 and T20-T21_{pep} within 60 min of reaction was greater than loss of the C-terminal disulfide in hGH, consistent with higher-order structural

effects. Of all the peptides tested, GSH was the most reactive, forming the highest percentage of mixed disulfides in intact hGH and in the model peptides. At longer time-points (>240 min) during the reaction, native disulfides in both hGH and cT20-T21 were regenerated and the fastest rates of regeneration were observed for cysteine © and the dipeptide CR. Tripeptides, RCR and QCR, had lower reactivity towards native disulfides but facilitated faster regeneration of native disulfides compared to GSH.

4.2 Keywords

Human growth hormone, protein, peptide, kinetics, thiol-disulfide exchange, glutathione

4.3 Introduction

In the biopharmaceutical industry, formation of correct disulfide links in recombinant proteins is central to the development of safe and efficacious protein therapeutics. While perturbation of native disulfide bonds is advantageous for regulating the biological activity of enzymes such as thioredoxin reductase, disulfide bond disruption is undesirable in protein drugs; mismatched disulfides can result in misfolding, aggregation, loss of biological activity and stability [54]. To ensure drug quality and product homogeneity, particularly with an increase in the development of biosimilars globally, the presence of these scrambled disulfides and the extent of scrambling need to be determined in protein therapeutics. A detailed mechanistic understanding of degradation pathways like

thiol-disulfide exchange is expected to reduce attrition rates during drug development and decrease the time to market protein drug products.

Formation of protein mixed disulfides (P-S-S-R) is not uncommon and occurs in all biological environments, typically by two mechanisms; a) thiol-disulfide exchange; $P-S-S-P + R-SH \leftrightarrow P-S-S-R + P-SH$ and b) via sulfenic acid formation; $P-SOH + R-SH \rightarrow P-S-S-R + H_2O$ [61], where R-SH is any low-molecular weight thiol (reduced), P-S-S-P is the native disulfide bond in a protein, P-SH is the protein with a free thiol, P-SOH is protein sulfenic acid and P-S-S-R is the mixed disulfide. Thiol-disulfide exchange reactions are favored at neutral to alkaline pH and the reaction proceeds via an S_N2 nucleophilic displacement. The oxidized form of low-molecular weight thiols (R-S-S-R) are used to form protein disulfide bonds via oxidation while the reduced forms (R-SH) are used to rearrange scrambled disulfide bonds *in vivo*. The leaving group typically has a lower pKa compared to the central sulfur atom that is attacked by a thiolate anion [61]. For example, small molecule catalysts that facilitate folding of proteins contain thiol groups with a low pKa [176], which enhances the leaving group ability of the corresponding thiolate anion (RS-) and increases the redox potential.

Intrinsic factors other than thiol pKa are also known to affect thiol-disulfide exchange; these include ionic strength of the medium [63], geometric strain imposed on the disulfide bond by higher-order structure [66] and stability of the native disulfide bond relative to a non-native bond [65].

Proteins can form mixed/scrambled disulfides with other thiols, that are either present as an impurity or in the protein as a free Cys [177,178]. The sulfur group that has better exposure to the attacking nucleophile is more prone to undergo thiol-disulfide

exchange reactions in comparison to more buried residues, even if it exists as a free Cys [179]. These protein mixed disulfides can then initiate other thiol-disulfide exchange reactions resulting in the formation of disulfide-linked aggregates. Disulfide bond degradation in therapeutic proteins can also occur via β -elimination [3] and thiol-catalyzed exchange [78] during processing and storage or after administration in vivo in the presence of low-molecular weight thiols in serum [49]. In some proteins like monoclonal antibodies, incomplete disulfide bond formation also results in free Cys [123] that can then initiate disulfide-mediated degradation events.

Rearrangement of native disulfide bonds to form mixed disulfides via thiol-disulfide exchange has been reported in a number of therapeutic proteins [14, 72, 78]. Disulfide-linked isomers of interleukin-2 (IL-2) were observed in the presence of a chaotrope under alkaline conditions. IL-2 has one free Cys and one disulfide bond in its native form, alkaline and denaturing conditions deprotonate the free thiol thus mediating thiol-disulfide exchange reactions that generate less active disulfide-linked isomers [90]. Thiol-disulfide exchange reactions have also been observed in monoclonal antibodies, the C_H1 domain of IgG2 contains a free Cys that is involved in the formation of disulfide-linked oligomers (intermolecular disulfides) upon agitation stress [178]. While thiol-disulfide exchange is known to occur in proteins and peptides, the effects of protein higher-order structure and peptide primary structure on reaction kinetics are not as well understood and are the focus of studies reported here.

Human growth hormone is a therapeutic protein that is used for the treatment of a number of growth related disorders; these include Turner's syndrome, Prader-Will

syndrome, chronic kidney insufficiency and hGH deficiencies. In 2012, hGH was one of the top 200 pharmaceutical products by retail sales in the US [180]. Amino acid sequences of the two native disulfide-containing tryptic peptides are shown in Table 4.1. There are no free Cys residues in hGH, however, a free thiol group maybe generated via β -elimination [3, 141] and can facilitate disulfide exchange and lead to loss of therapeutic efficacy. With access to cDNA for hGH expression in-house, relatively small size of the protein and results obtained previously for model tryptic peptides derived from hGH, hGH was the model protein of choice for investigating thiol-disulfide exchange.

In our previous studies (Chapters 2 and 3), we investigated the mechanism and kinetics of thiol-disulfide exchange in tryptic peptides derived from human growth hormone in aqueous solution and in the solid state at a thiol: disulfide = 10: 1 (molar ratio) [69, 181]. Results showed that peptide secondary structure (peptide cyclized by a disulfide bond) offers protection against thiol-disulfide exchange in solution [69]. However, in the solid state, no protection was observed and reaction kinetics were similar for both linear and cyclic peptides while the mechanism remained unchanged [181]. Here, we report experimental data for the effect of higher order structure and peptide primary structure on thiol-disulfide exchange using model peptides and recombinant human growth hormone (rhGH). Thiol-disulfide exchange reactions were monitored at a thiol: disulfide molar ratio of 100: 1 at pH 7.0 and 37 °C. Results show that loss of native disulfide via thiol-disulfide exchange in cT20-T21 and T20-T21_{pep} (peptides mimicking native C-terminal disulfide in hGH) is greater than loss of native disulfide in hGH in the presence of T20a, GSH, RCR, CR and C, indicating the role of higher-order structure. GSH was the most reactive of all free-thiol containing peptides used to initiate thiol-disulfide exchange, resulting in 84.7%

and 57.7% loss of native disulfide in cT20-T21 and hGH respectively. Tripeptides, RCR and QCR had lower reactivities towards the native disulfide when compared to GSH but favored faster (>GSH) regeneration of native disulfides in hGH. In the presence of RCR, native disulfide was faster than with QCR. Loss of native disulfide was the lowest and regeneration of the native disulfide was the fastest with free thiols CR and C.

4.4 Materials

HPLC grade acetonitrile (ACN), NaCl and KCl were purchased from Fisher Scientific Co. (Pittsburgh, PA). H₂O₂ and Na₂CO₃ (anhydrous granules) were obtained from Mallinckrodt Baker Inc. (Phillipsburg, NJ). K₂HPO₄, ethylenediaminetetraacetic acid (EDTA), Trizma® hydrochloride (Tris.HCl), urea, sucrose, glutathione (oxidized-GSSG), glutathione (reduced-GSH), L-Cysteine (Cys/C) and glycerol were purchased from Sigma Chemical Co. (St. Louis, MO). Trifluoroacetic acid (TFA) and formic acid (FA) were obtained from Thermo Scientific (Rockford, IL). Double-distilled water (DDI) used for buffer preparation and as HPLC mobile phase was deionized and purified using a Milli-Q water system, Millipore Ltd (Billerica, MA) and filtered with a 0.2 µm filter. Flash digest kit (trypsin) for protein digestion was obtained from Perfinity Biosciences (West Lafayette, IN). Human growth hormone (1 mg/mL) was purchased as a lyophilized powder (0.34 mg phosphate buffer and 8 mg mannitol) from ProSpec-Tany TechnoGene Ltd., Ness Ziona, Israel. Synthetic peptides were obtained from GenScript (Piscataway, NJ).

4.5 Method

4.5.1 hGH expression and purification

The plasmid containing the recombinant human growth hormone (r-hGH) expression gene was obtained from Dr. J. Laurence (Kansas University). This plasmid codes for hGH with an additional 28 amino acids at the N-terminus with a molecular weight of 25 kDa (Figure 4.1). The plasmid was transformed into the BL21 (DE3) *E.coli* cells for protein expression, using the protocol provided by New England BioLabs. Cells carrying the plasmid for hGH were grown in terrific broth media containing 100 µg/ mL ampicillin in an incubator shaker at 37° C. The cells were induced at OD₆₀₀ = 0.8 with 1 mM IPTG. Post-induction was carried out in incubator shaker at 20° C for 16 hours. Expression of r-hGH in the induced cells was checked with 12% SDS-PAGE and was found to be over-expressed as inclusion bodies (Figure 4.2a).

Purification of rhGH: rhGH was purified using the method as described previously [182]. Induced *E.coli* cells were harvested by centrifugation at 6500 rpm for 15 min. The cell pellet was resuspended in 50 mM Tris-HCl, 100 mM NaCl, 5 mM EDTA at pH 8.0 and sonicated to lyse the cells. r-hGH inclusion bodies were separated from the soluble cell lysate by centrifugation at 13, 000 rpm for 30 mins. The pellet with cell debris was resuspended in buffer, 50 mM Tris-HCl, 5 mM EDTA, 1% deoxycholate (DOC) at pH 8.0, sonicated and centrifuged to further clarify the inclusion bodies. The pellet was washed with buffer, 50 mM Tris-HCl at pH 8.0 and centrifuged to remove any DOC from the previous step. Pure inclusion bodies were solubilized in buffer containing 100 mM Tris-HCl and 2 M Urea at pH 12.5. The solution were further diluted 10 times in a buffer

containing, 50 mM Tris-HCl, 2 M Urea, 0.5 mM EDTA, 3 mM GSH, 0.6 mM GSSG, 10% Glycerol and 2% sucrose at pH 8.0. Refolding of r-hGH was carried out by the step-wise dialysis of the protein solution against buffer 50 mM Tris-HCl, 0.5 mM EDTA, 10% Glycerol, 2% sucrose at pH 8.0 by descending the concentration of urea from 2-0 M at each step (1.5, 0.5 and 0 M). The refolded r-hGH was filtered and purified further using a HiPrep 26/60 Sephacryl S-100 high resolution column (Amersham Biosciences) equilibrated with 50 mM Tris-HCl, 2% sucrose at pH 8.0 and the fraction containing the monomeric r-hGH were checked with 12% SDS-PAGE for the purity (Figure 4.2b). Concentration of purified hGH was determined using a UV-Vis spectrophotometer (Agilent Technologies, Santa Clara, CA). MS analysis of the purified protein confirms the presence of two native disulfide bonds as found in the commercially available recombinant hGH (Figure 4.3 and Table 4.1). Near-UV CD analysis with a J-815 CD spectrometer (JASCO, Easton, MD) was used to assess protein tertiary structure.

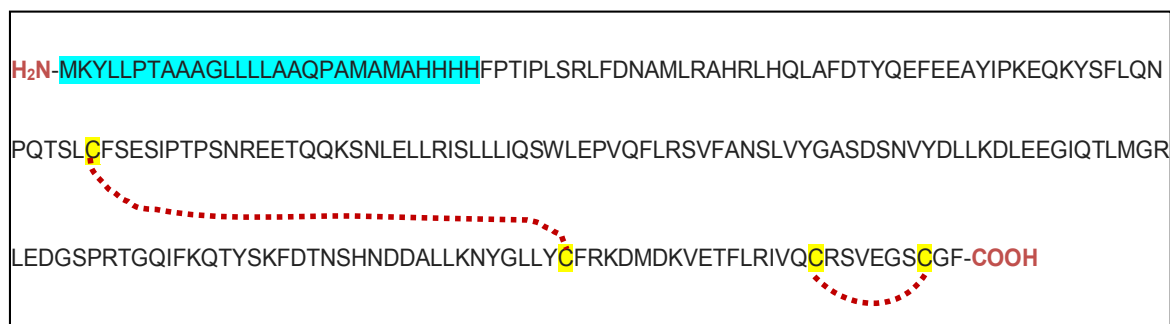


Figure 4.1: Amino acid sequence of hGH expressed and purified in our lab (MW = 25 kDa). Sequence highlighted in blue shows the additional 28 amino acids at the N-terminus. Highlighted in yellow are the four Cys residues and the native disulfide bonds are represented by the red dotted lines.

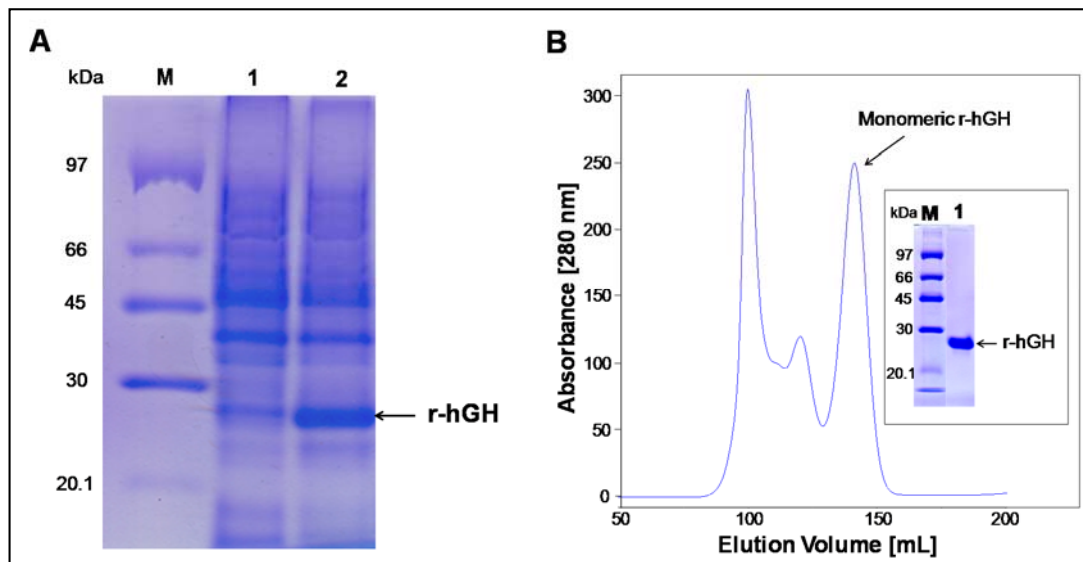


Figure 4.2: *Expression and purification of rhGH:* (A) Expression of r-hGH in uninduced (lane 1) and induced (lane 2) culture was checked with 12% SDS-PAGE. (B) Purification of refolded r-hGH in HiPrep 26/60 Sephacryl S-100 high resolution column (Amersham Biosciences, Piscataway, NJ). Gel filtration chromatogram showing the resolved monomeric r-hGH. Inset, 12% SDS-PAGE shows the purified r-hGH (lane 1). (M: Molecular weight marker).

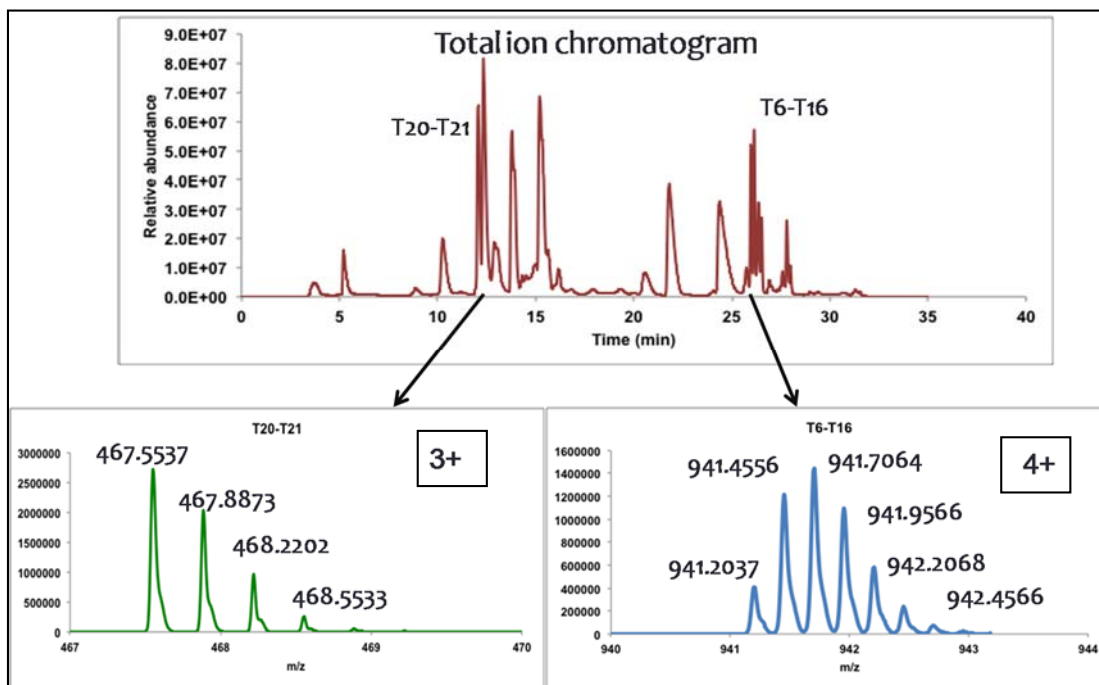


Figure 4.3: Total ion chromatogram for the tryptic digest of r-hGH. The two native disulfide bonds are in peptides T6-T16 and T20-T21 with retention times 26.1 and 12.17 min respectively. The figure insets show the isotope pattern and charge states of the two disulfide-containing peptides.

4.5.2 Thiol-disulfide exchange in model peptides

RP-HPLC analysis: peptide samples were analyzed using an Agilent 1200 series HPLC system equipped with a UV-detector operated at 215 nm. Analytical column and gradient elution were the same as described previously [69]. Calibration plots were linear in the following concentration ranges; 5-500 μM (T20-T21_{pep}), 20-200 μM (T20), 20-200 μM (T21), 5-500 μM (cT20-T21), and 5-500 μM (rT20-T21).

Sample preparation: Peptides T20a (GIVQCR), T20 (IVQCR), CR, RCR, QCR, cT20-T21, T20-T21_{pep} and rT20-T21 (Table 4.2) were obtained from GenScript (Piscataway, NJ) with >90% purity as lyophilized powders. Stock solutions were made in 0.1% formic acid in DDI (pH \sim 2.5) to minimize oxidation of free thiols. Peptide T20a was synthesized to study thiol-disulfide exchange in intact hGH and draw comparisons to previous studies with model peptides, where T20 was used as the reactive thiol [69, 181]. Using T20 to initiate disulfide exchange in hGH would make differentiation of scrambled and native disulfides difficult, for example, T20-T21 could be the native disulfide, product of disulfide exchange with T20 or an intermolecular disulfide (between two protein molecules). T20a is similar in sequence to T20 with the addition of a Gly at the N-terminal, this difference allows easy identification of scrambled disulfides with T20a. To determine reactivity of T20a and to investigate buffer effect, reaction of T20a with T20-T21 peptide (thiol: disulfide = 10: 1) was monitored kinetically in 10 mM phosphate buffer (PB) and 50 mM Tris.Hcl with 2% sucrose at 22 °C. Final pH of the reaction mixture was 7.0, samples were analyzed as described previously [69]. k_{obs} (Pseudo-first order) for the loss of T20-T21 is similar in PB and Tris.HCl with 2% sucrose (Figure 4.4). Thus all peptide-

level studies were monitored kinetically in 10 mM PB to quantitate thiol-disulfide exchange.

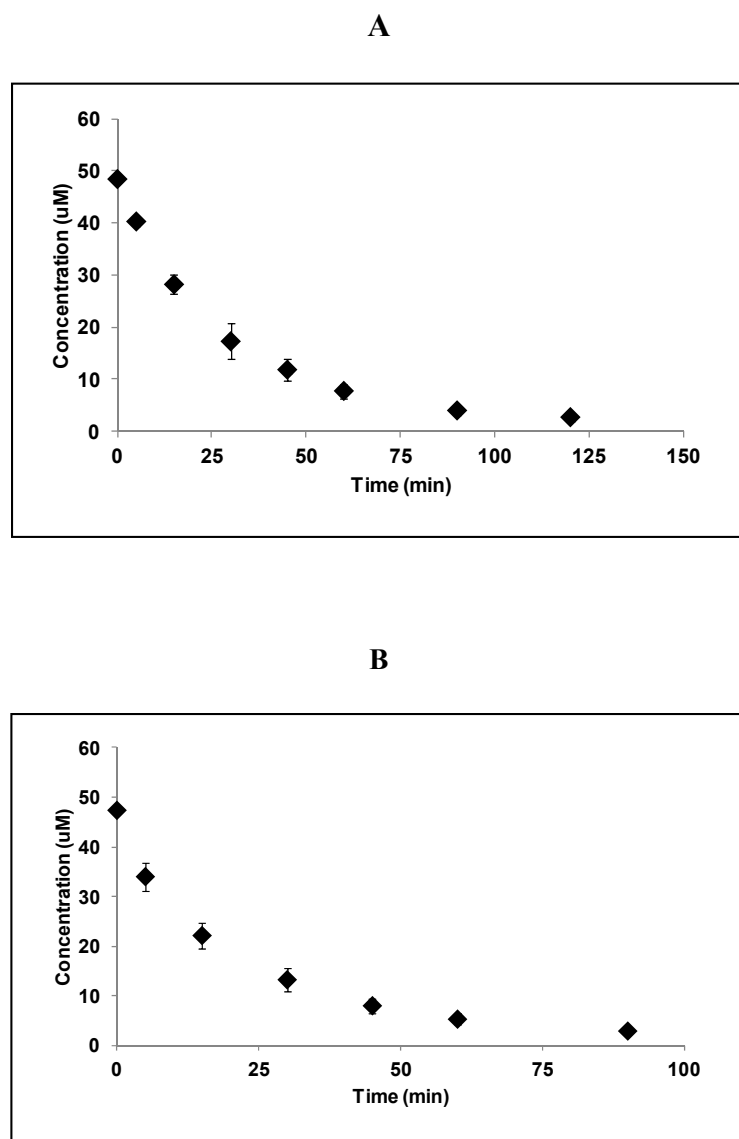


Figure 4.4: Change in concentration of T20-T21 (\blacklozenge) for the reaction with A) T20a (10 mM PB, pH 7.0, 0.08 M ionic strength, 0.5 mM EDTA and N_2 sparged) and with B) T20a (50 mM Tris.HCl and 2% sucrose, pH 7.0) at 22 $^\circ\text{C}$ ($n=3$, \pm SD). Initial concentration of peptides were; $[\text{T20a}] = 500 \mu\text{M}$ and $[\text{T20-T21}] = 50 \mu\text{M}$.

Investigating the effect of amino acid sequence and peptide length on thiol-disulfide exchange: reaction kinetics were monitored at pH 7.0 and 37 °C in aqueous solution. For the reaction, 1500 µL of T20a/T20/GSH/RCR/QCR/CR/C (12500 µM), 1500 µL of T20-T21_{pep}/cT20-T21 (125 µM) and 750 µL of 50 mM phosphate buffer (0.08 M ionic strength and 0.5 mM EDTA) were added to a 15 mL BD falcon tube and mixed by pipetting. The final pH of the reaction mixture was adjusted to 7.0 using NaOH or HCl (exact volume to be added was determined from pilot studies) after a 100 µL aliquot was removed and quenched with 10 µL 20% formic acid in DDI (FA) to verify initial concentrations (t=0 min). Samples were withdrawn in triplicate at different time points, quenched with 20% FA, analyzed and quantitated using RP-HPLC as described in Chapters 2 and 3.

4.5.3 Enzymatic digestion using the Perfinity flash digest protocol

hGH samples were added to the Perfinity flash digest kit tubes with digestion buffer (ratio of sample to buffer was 1:2.4). Digestion was performed at 60 °C and 1400 rpm using a ThermoMixer C (Eppendorf, Hauppauge, NY) for 15-17 mins. Digested samples were then transferred to microcentrifuge tubes and centrifuged at 14000 rpm for 2 mins. After centrifugation, the supernatant was removed, quenched with 10 µL of 20% FA in DDI and analyzed on the LC-MS (~20 µL).

4.5.4 Removal of unreacted peptides using a desalting column

To minimize scrambling during digestion, Zeba™ spin desalting columns with 7K MWCO (Pierce Biotechnology, Rockland, IL) were used to remove any unreacted

peptides from the reaction mixture with hGH. The spin columns were first placed in an empty collection tube (1.5-2 mL) and centrifuged at 4700 rpm using an Eppendorf centrifuge (Eppendorf, Hauppauge, NY) equipped with a F45-11-12 rotor for 1 min to remove the storage buffer. Reacted samples (80-85 μ L) were then added carefully to the center of the resin bed. After the sample had adsorbed onto the resin bed, the spin columns were then placed inside new collection tubes and centrifuged at 4700 rpm for 2 mins. Desalted sample was collected and digested using the Perfinity flash digest kit as described above and analyzed on the LC-MS.

4.5.5 LC-MS analysis and disulfide bond identification using MassHunter software

Mass analyses were carried out on an LC-MS system (1200 series LC, 6520 qTOF, Agilent Technologies, Santa Clara, CA). Peptides in the digested samples were separated prior to MS analysis using a Zorbax 300SB-C18 column from Agilent Technologies. Solvent A was 0.1% FA in water and solvent B was 0.1% FA in ACN. A gradient run was initiated with 5% B then held at 5% for 5 min and increased to 20% in 8 min, in the next step gradient was increased to 25% in 10 min and to 60% in 5 min. followed by an increase to 100% in 0.6 min, decreased to 0% in 0.6 min and finally returned to 5% in 2.4 min. The flow rate was maintained at 50 μ L/min and the column temperature was not controlled. To determine native and scrambled disulfide species, a library of all peptides containing a disulfide bond and/or free Cys was generated. Briefly, amino acid sequence of hGH was entered into the software and after selecting the digestion enzyme and missed cleavages, an *in silico* digest was performed. We used trypsin as the enzyme and the number of missed cleavages was set to four to generate a list of all possible tryptic fragments. The same

process was then repeated by switching out native disulfides to scrambled disulfides and free thiols. From these lists, all peptides with disulfide bonds and/or free cysteines were selected and combined to create a mass filter list. Mass spectra of all digested hGH samples were then scanned against the mass filter list to determine the presence of scrambled disulfides and the extent of disulfide scrambling. Loss of native disulfide (T20-T21) was monitored at different reaction times using peak areas from extracted ion chromatograms (XIC); concentration was calculated using the calibration plot (Figure 4.5) constructed with a peptide standard from GenScript (Piscataway, NJ). Similar calibration plots were constructed for T20 and T21 using peptide standards.

4.5.6 Thiol-disulfide exchange in hGH

For the reaction of hGH with thiol-containing peptides (T20a, GSH RCR or CR) and C, 280 μL of hGH purified in-house (0.56 mg/mL or 22.4 μM) in 50 mM Tris.HCl buffer and 2% sucrose (pH 8.0) was mixed with 70 μL T20a/GSH/RCR/CR/C (8950 μM in 0.1% FA in DDI). The pH of the final reaction mixture was 7.0 and the final molar ratio of peptide to protein was 100:1 (1790 μM : 17.9 μM). 90 μL aliquots of the reaction mixture were then transferred to microfuge tubes (n=3 for each time point) and placed in an incubator at 37 °C. Samples were withdrawn in triplicate at various times, desalted, digested and analyzed using LC/MS as described above. Control samples (hGH alone or model disulfide peptides alone) were diluted, desalted and digested as for the reaction samples at other time points. To determine contributions from the additional 28 amino acids in the modified hGH expressed in-house, the reaction of Prospec hGH with GSH was also monitored. Prospec hGH was first buffer exchanged (overnight at 4 °C) into 50 mM

Tris.HCl and 2% sucrose before reaction with GSH. Sample dilution and analysis were carried out as above.

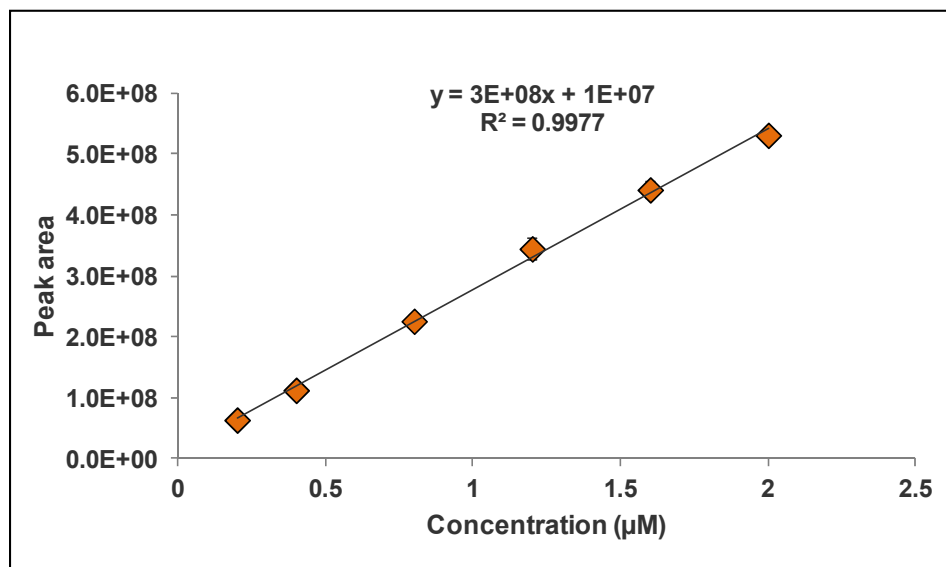


Figure 4.5: Calibration plot for T20-T21 (synthetic standard from GenScript); constructed using peak areas ($n=3$, \pm SD) from XIC at different peptide concentrations.

Table 4.1: Amino acid sequence of disulfide-linked peptides in hGH: native and scrambled disulfides




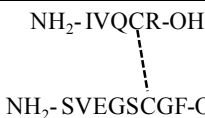
Tryptic peptide	Description	Amino acid sequence	Theoretical mass (Da)	Observed mass (Da)
T6-T16	Native disulfide-linked peptide	NH ₂ -YSFLQNPQTSLCFSES IPTPSNR-OH  NH ₂ -NYGLLYCFR-OH	3760.766	3760.7903
T20-T21	Native disulfide-linked peptide	NH ₂ -IVQCR-OH  NH ₂ -SVEGSCGF-OH	1399.6225	1399.6243
T6	Monomer, free thiol group	NH ₂ -YSFLQNPQTSLCFSES IPTPSNR-OH	2615.233	2615.2284
T16	Monomer, free thiol group	NH ₂ -NYGLLYCFR-OH	1147.549	1147.5412
T20	Monomer, free thiol group	NH ₂ -IVQCR-OH	617.3319	617.33
T21	Monomer, free thiol group	NH ₂ -SVEGSCGF-OH	784.3061	784.3017

Table 4.2: Amino acid sequence of model peptides used to investigate thiol-disulfide exchange reactions

Peptide	Description	Amino acid sequence
<i>Disulfide-linked peptides</i>		
cT20-T21	Cyclic peptide	NH ₂ -IVQCRSVEGSCGF -OH 
T20-T21 _{pep}	Heterodimer, disulfide-linked peptide	NH ₂ -IVQCR-OH NH ₂ -SVEGSCGF-OH 
<i>Free thiol-containing peptides</i>		
rT20-T21	Monomer, free thiol group	NH ₂ -IVQCRSVEGSCGF-OH
T20a	Monomer, free thiol group	NH ₂ -GIVQCR-OH
T20	Monomer, free thiol group	NH ₂ -IVQCR-OH
GSH	Monomer, free thiol group	NH ₂ -ECG-OH
RCR	Monomer, free thiol group	NH ₂ -RCR-OH
QCR	Monomer, free thiol group	NH ₂ -QCR-OH
CR	Monomer, free thiol group	NH ₂ -CR-OH

4.5.7 Near-UV CD measurement

Near-UV CD spectroscopy was used to assess the effects of disulfide reduction on the tertiary structure of hGH. Samples with and without 5 mM β -mercaptoethanol were diluted to 2 μ M final hGH concentration. Molar ellipticity was measured on a JASCO J-815 spectrometer (JASCO Analytical Instruments, Easton, MD) in a 10 mm path length

quartz cuvette. Spectra were acquired for wavelengths of 250 nm to 350 nm at a scanning speed of 50 nm/min.

4.5.8 Amide hydrogen-deuterium exchange mass spectrometry (HDX-MS)

HDX-MS was conducted to determine the solvent accessibility of hGH under native and reduced conditions. A 2 mg/mL solution of hGH was prepared in buffer containing 10 mM sodium phosphate, 1.6 % mannitol, pH 7.0 (buffer A). To obtain reduced hGH, a 2 mg/mL solution was prepared in buffer containing 10 mM sodium phosphate, 1.6 % mannitol, 10 mM DTT, pH 7.0 (buffer B) and incubated on ice for 1 h. HDX was initiated by mixing 3 μ L of the sample with 27 μ L of deuterated buffer A and buffer B for native and reduced hGH, respectively. Exchange was carried out at 23 °C for 10 s to 10 min. Reactions were quenched by adding 30 μ L of ice cold buffer containing 0.2 M sodium phosphate, 0.5 M Tris(2-carboxyethyl)phosphine hydrochloride, 6 M guanidine hydrochloride to a final pH of 2.5. Deuterium uptake was measured using the LC/MS system described above and equipped with a custom-built column refrigeration unit (0 °C) to minimize back exchange. Approximately 50 pmol of protein was injected onto to an immobilized pepsin column. The digests were desalted and trapped in a peptide microtrap (Michrom Bioresources, Auburn, CA) with 10% ACN, 90% water, and 0.1% FA for 4 min. Peptides were eluted onto a reverse phase analytical column (Zorbax 300SB-C18; Agilent Technologies, Santa Clara, CA) for 4.3 min using a gradient to 60% ACN, 40% water, and 0.1% FA. Mass spectra were acquired in the m/z range 200-1700. Peptic digests of undeuterated hGH were analyzed and their mass identified using the MassHunter software (Agilent). Peptides identified from undeuterated hGH were mapped onto data from

deuterated samples using HDExaminer software (Sierra Analytics, Modesto, CA) to determine the level of deuterium uptake. The analysis times for all HDX samples were very similar, so that the observed deuterium uptake values were not subjected to back-exchange corrections. Data from 5 min HDX were mapped onto the crystal structure of hGH (PDB ID: 1 HGU) using PyMOL software (PyMOL Molecular Graphics System, Version 1.3, Schrodinger, LLC).

4.6 Results

4.6.1 Thiol-disulfide exchange in hGH: product identification

Thiol-disulfide exchange in hGH was investigated using T20a, GSH, cysteine (C) and several small Cys-containing peptides such as CR and RCR (Table 4.2), to explore the effects of different thiol containing molecules on reaction kinetics. Control samples containing hGH alone incubated at 37 °C and analyzed after 60 mins and 1 day did not show scrambled species (data not shown), indicating that disulfide exchange does not occur under the conditions investigated here in the absence of a free thiol group. LC/MS analysis of intact protein samples during the reaction of hGH with T20a showed peaks corresponding to protein mixed disulfides with T20a (data not shown), confirming that thiol-disulfide exchange does not occur during digestion. The list of scrambled species observed for hGH in reaction with various thiol-containing peptides, the amino acid sequences of the scrambled products, their molecular weights and their chromatographic retention times are listed in Table 4.3, 4.4 and 4.5, respectively.

For the reaction of hGH with T20a (at thiol: disulfide = 100:1), four scrambled disulfides; T20a-T20, T20a-T21, T20a-T6 and T20a-T16 (Table 4.3) and free thiols; T6, T16, T20 and T21 (Table 4.1) were identified. No inter- or intra-molecular disulfides were detected at any time point during the reaction. GSH is commonly used in protein refolding and is also known to form mixed disulfides with proteins [61, 67]. In the reaction of hGH with GSH, the loss of both native disulfides (T20-T21, T6-T16) was observed within a few minutes resulting in the detection of mixed disulfides (Table 4.3) and free thiols (Table 4.1). The data are consistent with a reaction mechanism identical to that proposed for T20a (Scheme 4.1), since no other degradation products were detected.

Interestingly, for the reaction with CR, the mixed disulfide (T20-CR) and free thiols (T6, T16 and T21) were not detected in any of the samples. All the other mixed disulfides, T21-CR, T6-CR and T16-CR and T20 were detected (Table 4.4). Mixed disulfides (T6-RCR, T16-RCR and T21-RCR) and free thiols (T20 and T6) were detected for the reaction of hGH with RCR (Table 4.5). With C as the thiol reagent, the loss of the native disulfide was slower than for T20a, GSH or CR. Only T21-C and T20 were detected (Table 4.5); mixed disulfides (T20-C, T6-C and T16-C) and free thiols (T6, T16 and T21) were not detected. The detection of scrambled disulfides at all four Cys residues in hGH suggests that both native disulfides are prone to attack by a reactive thiolate anion in aqueous solution at pH 7.0. It is interesting that in the presence of C, scrambling was detected only at the C-terminal disulfide bond. This may be due to rapid regeneration of the native disulfides, so that the mixed disulfides go undetected at the reaction times monitored here.

Table 4.3: Amino acid sequence of mixed disulfide-linked peptides from hGH: for the reaction of hGH with T20a.

Tryptic peptide	Description	Amino acid sequence	Theoretical mass (Da)	Observed mass (Da)	Retention time (min)
T20a-T20	Scrambled disulfide-linked peptide	NH ₂ -GIVQCR-OH NH ₂ -IVQCR-OH	1289.670	1289.6604	10.89
T20a-T21	Scrambled disulfide-linked peptide	NH ₂ -GIVQCR-OH NH ₂ -SVEGSCGF-OH	1456.644	1456.6329	13.99
T20a-T6	Scrambled disulfide-linked peptide	NH ₂ -GIVQCR-OH NH ₂ -YSFLQNPQTSLCLFSESIPSNR-OH	3287.570	3287.5724	20.32
T20a-T16	Scrambled disulfide-linked peptide	NH ₂ -GIVQCR-OH NH ₂ -NYGLLYCFR-OH	1819.886	1819.8764	17.92

Table 4.4: Amino acid sequence of mixed disulfide-linked peptides from hGH: for the reaction of hGH with GSH.

Tryptic peptide	Description	Amino acid sequence	Theoretical mass (Da)	Observed mass (Da)	Retention time (min)
T20-S-S-G	Linear peptide, disulfide linked to GSH	NH ₂ -IVQCR-OH NH ₂ -ECG-OH	922.4001	922.3976	5.26
T21-S-S-G	Linear peptide, disulfide linked to GSH	NH ₂ -SVEGSCGF-OH NH ₂ -ECG-OH	1089.374	1089.367	11.99
T6-S-S-G	Linear peptide, disulfide linked to GSH	NH ₂ -YSFLQNPQTSLCLFSESIPSNR-OH NH ₂ -ECG-OH	2920.301	2920.3053	21.09
T16-S-S-G	Linear peptide, disulfide linked to GSH	NH ₂ -NYGLLYCFR-OH NH ₂ -ECG-OH	1452.617	1452.6066	19.02

Table 4.5: Amino acid sequence of mixed disulfide-linked peptides from hGH: for the reaction of hGH with CR, C and RCR.

Tryptic peptide	Description	Amino acid sequence	Theoretical mass (Da)	Observed mass (Da)	Retention time (min)
T21-CR	Scrambled, disulfide-linked peptide	NH ₂ -IVQCR-OH NH ₂ -CR-OH	1059.411	1059.4051	9.84
T6-CR	Scrambled disulfide-linked peptide	NH ₂ -YSFLQNPQTSLCFSEIPTPSNR-OH NH ₂ -CR-OH	2890.338	2890.33	19.21
T16-CR	Scrambled disulfide-linked peptide	NH ₂ -NYGLLYCFR-OH NH ₂ -CR-OH	1422.654	1422.7074	15.65
T21-C	Scrambled disulfide-linked peptide	NH ₂ -SVEGSCGF-OH NH ₂ -C-OH	903.3103	903.3135	11.10
T21-RCR	Scrambled disulfide-linked peptide	NH ₂ -SVEGSCGF-OH NH ₂ -RCR-OH	1215.512	1215.5114	9.30
T6-RCR	Scrambled disulfide-linked peptide	NH ₂ -YSFLQNPQTSLCFSEIPTPSNR-OH NH ₂ -RCR-OH	3046.439	3046.4527	17.76
T16-RCR	Scrambled disulfide-linked peptide	NH ₂ -NYGLLYCFR-OH NH ₂ -RCR-OH	1578.755	1578.7556	14.94

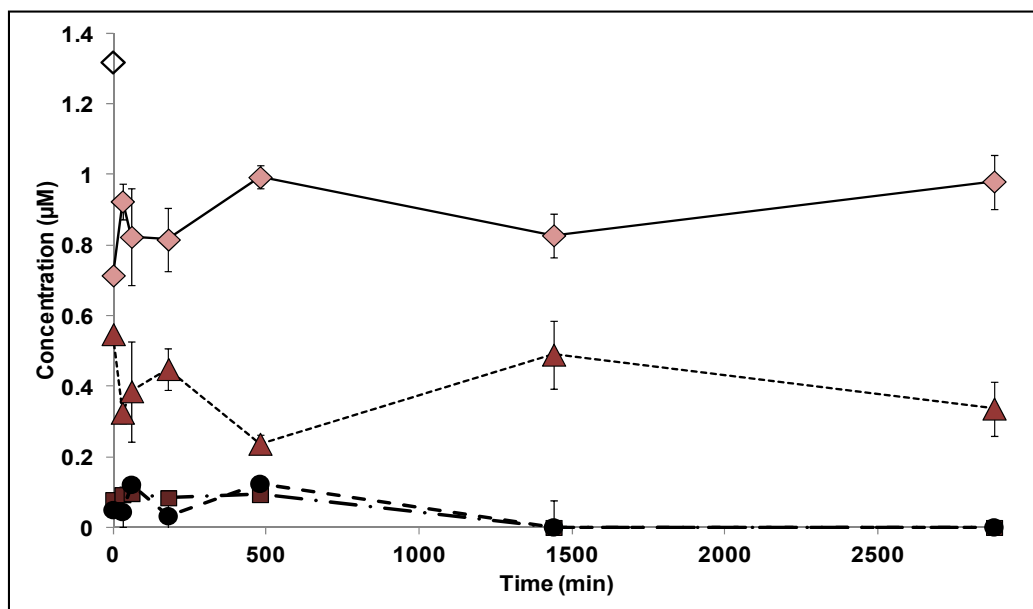
4.6.2 Thiol-disulfide exchange in hGH: product quantitation

Thiol-disulfide exchange in hGH was quantified for the C-terminal disulfide bond, which links the tryptic peptides T20 and T21. Quantitative analysis of disulfide scrambling in T6-T16 was not performed due to the lack of peptide standards (i.e., for T6-T16, T6 and T16) and the low aqueous solubility of T6. At the C-terminal disulfide bond (T20-T21), the concentrations of T20-T21, T20 and T21 were determined using XIC peak areas and calibration curves prepared using synthetic peptide standards. The concentrations of

protein-thiol mixed disulfides were determined from mass balance: [Mixed disulfides] = $[T20-T21]_{total} - ([T20-T21]_t + ([T20] + [T21])/2)$. Intra- and intermolecular disulfides and products of thiol oxidation such as sulfenic, sulfinic and sulfonic acid were not detected. Thus, it was assumed that disulfide bond cleavage of 1 mol of T20-T21 releases 1 mol of T20 and 1 mol of T21 that are present either in their free thiol form or in mixed disulfides. The percent loss of native disulfide at different times during the reaction was determined from $[T20-T21]$ in the control sample (i.e., at $t = 0$) and $[T20-T21]$ at time, t .

The distributions of mixed disulfides, free thiols and the native disulfide (T20-T21) over time for the reaction of hGH with different thiols are shown in Figures 4.6 and 4.7. Loss of native disulfide (%) in the presence of free thiol-containing peptides and C is reported in Table 4.6. After 60 min, T20-T21 showed the greatest loss with with GSH and the least with C. After 1 day, the native disulfide was regenerated to a greater extent with C followed by CR and RCR (Table 4.6). The presence of an Arg residue adjacent to Cys was found to favor regeneration of the native disulfide over GSH. A similar product profile was obtained for Prospec hGH (22kDa) for the reaction with GSH (Figure 4.8), suggesting that the leader sequence at the N-terminus in the hGH expressed in-house (25 kDa) does not influence thiol-disulfide exchange appreciably.

A



B

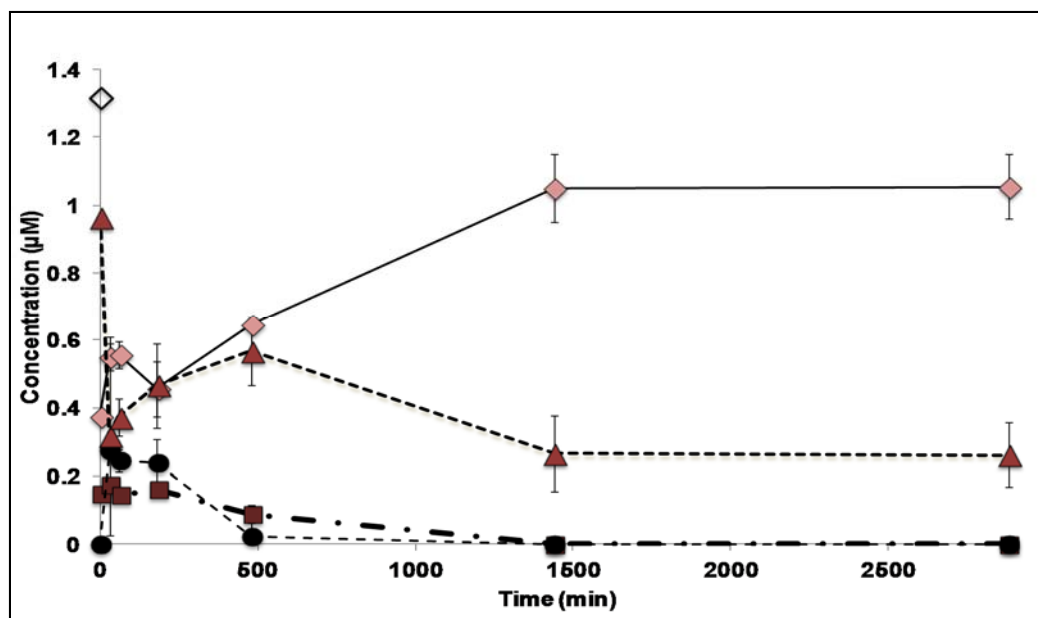


Figure 4.6: Concentrations of T20-T21 (\blacklozenge), T20 (\blacksquare), T21 (\bullet) and T20a-T20+T20a-T21 or T20-S-S-G+T21-S-S-G (\blacktriangle) for the reaction of hGH with T20a (A) and GSH (B) at pH 7.0 (40 mM Tris.HCl and 1.6% sucrose) and 37 °C (n=3, +/- SD). Initial molar ratio of thiol: hGH was 100:1. Concentration of hGH alone before reaction with T20a is represented by \diamond . Lines on plot are to improve readability and do not represent regression analysis.

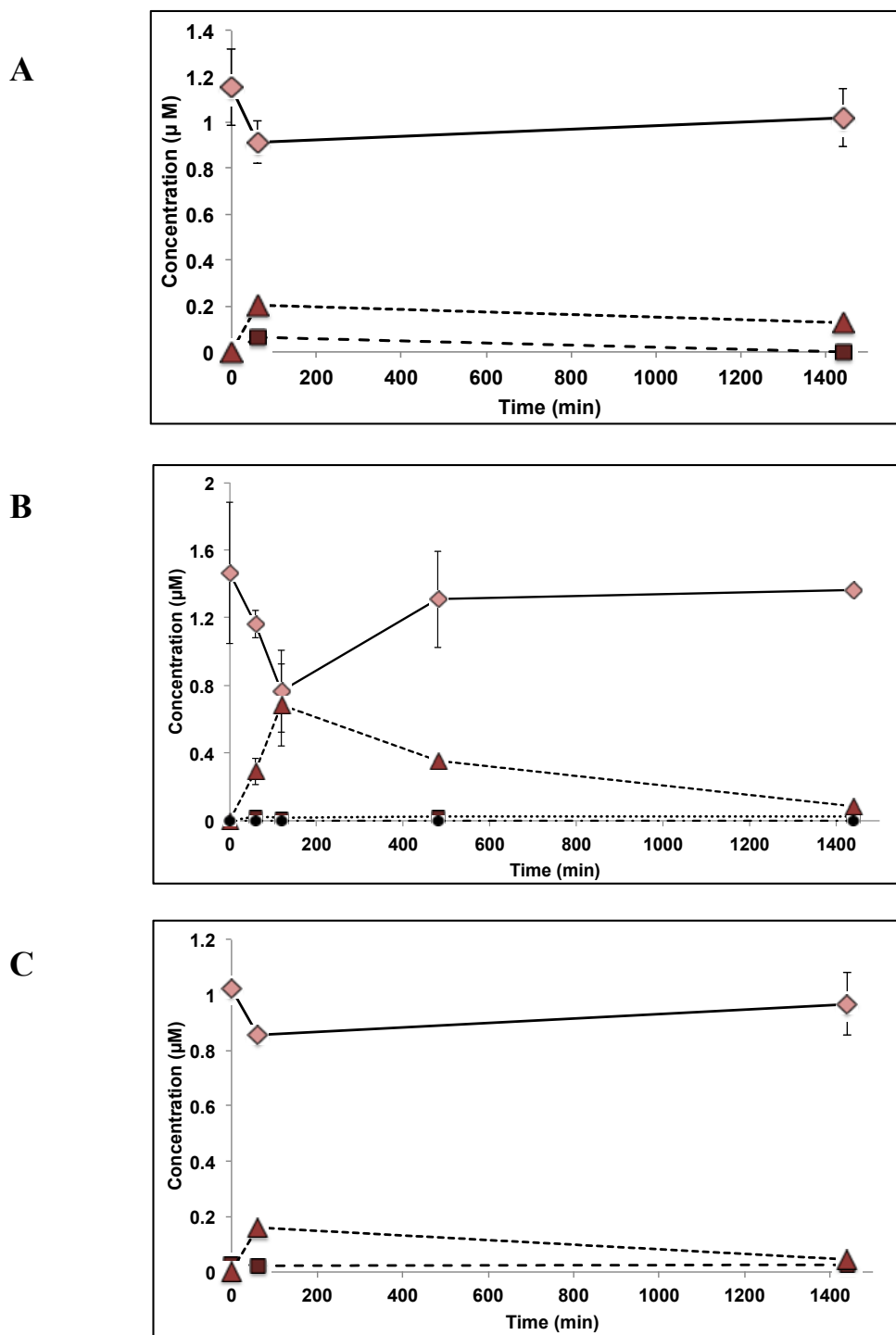


Figure 4.7: Concentrations of T20-T21 (\blacklozenge), T20 (\blacksquare), T21 (\bullet) and mixed disulfides (\blacktriangle) for the reaction of hGH with (A) RCR, (B) CR and (C) C at pH 7.0 (40 mM Tris.HCl and 1.6% sucrose) and 37 °C (n=3, +/- SD). Initial molar ratio of thiol: hGH was 100:1. Control sample represents hGH alone before reaction with CR. Lines on plot are to improve readability and do not represent regression analysis.

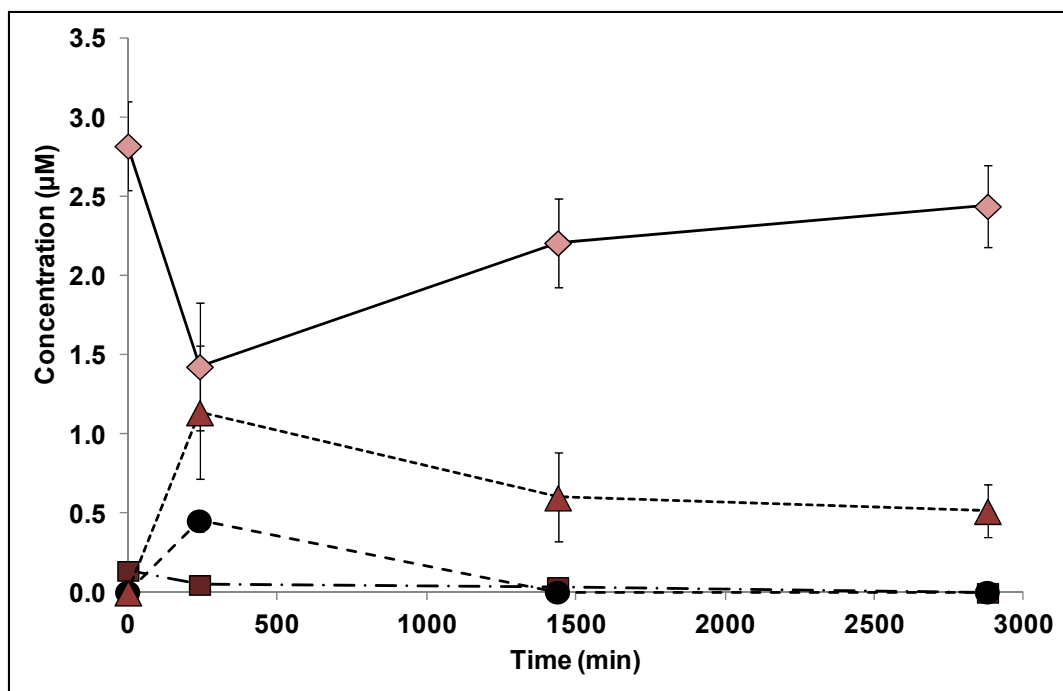


Figure 4.8: Concentrations of T20-T21 (◆), T20 (■), T21 (●) and T20-S-S-G+T21-S-S-G (▲) for the reaction of Prospeck hGH with GSH at pH 7.0 (40 mM Tris.HCl and 1.6% sucrose) and 37 °C (n=3, +/- SD). Initial molar ratio of thiol: hGH was 100:1. T=0 min sample represents hGH alone before reaction with GSH. Lines on plot are to improve readability and do not represent regression analysis.

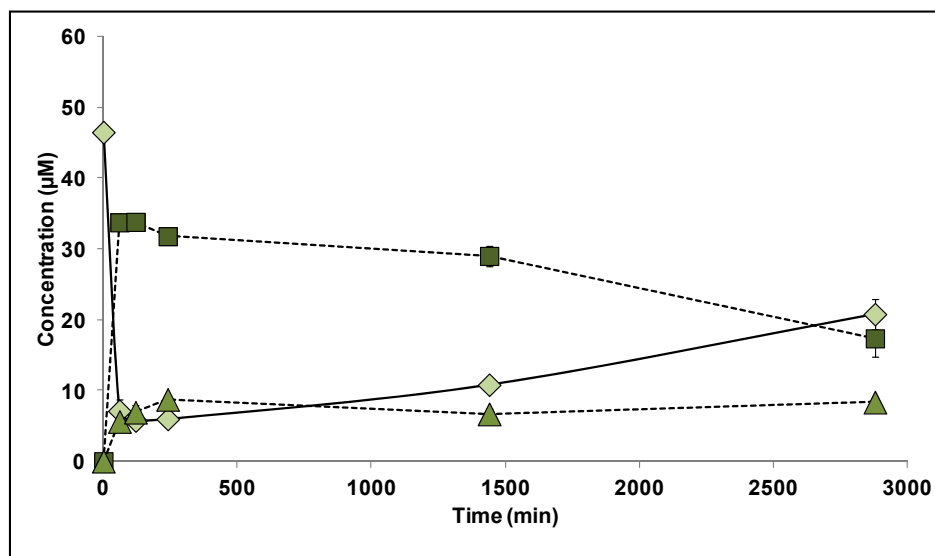
4.6.3 Effect of higher order structure on thiol-disulfide exchange

To investigate the effects of higher order structure on thiol-disulfide exchange and to show that close proximity of a free thiol group to a disulfide bond is a prerequisite for regeneration of native disulfide bonds, model disulfide-linked peptides were used. Thiol-disulfide exchange was monitored in cT20-T21 and T20-T21_{pep} at pH 7.0 and 37 °C. For cT20-T21, the concentrations of the single mixed disulfides (SMDs) and the double mixed disulfide (DMD) (Scheme 4.1) were determined from mass balance; $[SMDs + DMD] = [cT20-T21]_o - ([cT20-T21]_t + [rT20-T21]_t)$ as synthetic peptide standards for SMDs and DMD were not available. For T20-T21_{pep}, the same mass balance equation described above

was used for quantitation. In the presence of GSH (Table 4.2), SMDs and DMD and rT20-T21 were formed via thiol-disulfide exchange of the native bond in cT20-T21 (Scheme 4.1; Figure 4.9a). Though similar products (SMDs, DMD and rT20-T21) were observed for the reaction of cT20-T21 with all free thiols (Figure 4.10), the time courses of product distribution differed. As in hGH, the native disulfide was regenerated in cT20-T21 after 1 day (Table 4.6).

Thiol-disulfide exchange in T20-T21_{pep}: Disulfide bond cleavage in T20-T21_{pep} via thiol-disulfide exchange resulted in the formation of mixed disulfides with GSH (T20-S-S-G & T21-S-S-G), free thiols (T20 & T21) and trace amounts of homodimers (T20-T20 & T21-T21) (Figure 4.9b). At the end of 2 days, T20-T21_{pep} was consumed completely, unlike thiol-disulfide exchange studies with cT20-T21 and hGH in which the native disulfides were regenerated. These results obtained with disulfide-linked peptides suggest that the higher order structure influences reactivity, making the native disulfides less accessible to attack by a thiolate anion in hGH (determined by % loss of native disulfide shown in Table 4.6) but does not inhibit the reaction completely. Thus, proximity of thiol groups to a disulfide bond (dictated by peptide/protein structure) determines the type of disulfide bond (intra vs. inter) that can be re-formed. The presence of an Arg residue adjacent to Cys in the thiol influences the rate and extent of regeneration.

A



B

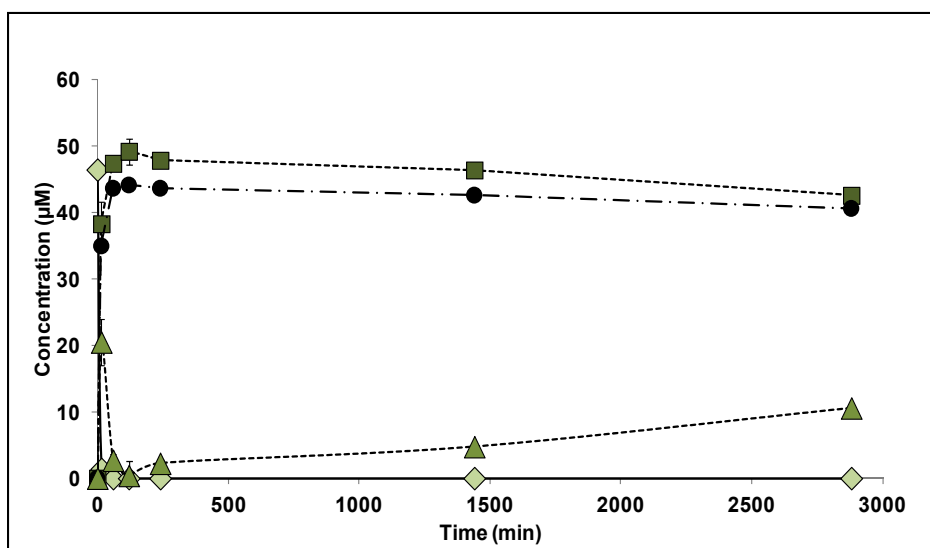


Figure 4.9: Concentrations of species for the reaction of cT20-T21/T20-T21_{peg} with GSH at pH 7.0 (10 mM phosphate buffer) and 37 °C (n=3, +/- SD), initial molar ratio of GSH: cT20-T21/T20-T21_{peg} was 100:1. A) Concentrations of cT20-T21 (♦), rT20-T21 (■) and SMDs + DMD (▲). B) Concentrations of T20-T21_{peg} (♦), T20 (■), T21 (●) and mixed disulfides (▲). T=0 min represents concentration of native disulfide (cT20-T21/T20-T21_{peg}) before initiation of reaction by adjusting the pH to 7.0. Lines on plot are to improve readability and do not represent regression analysis.

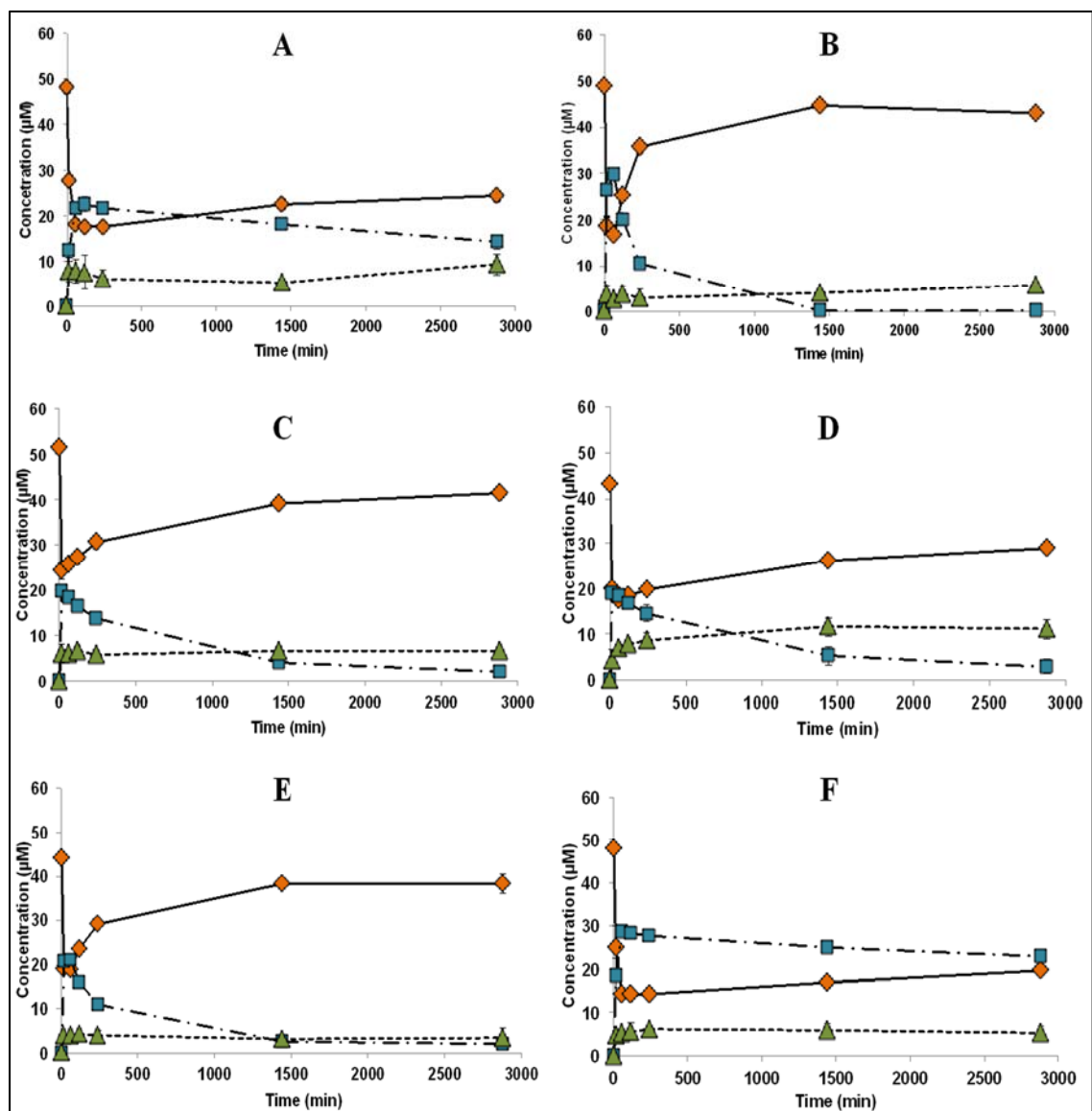


Figure 4.10: Distribution of cT20-T21 (♦), rT20-T21 (■) and SMDs+DMD (▲) for the reaction of cT20-21 with A) T20a, B) CR, C) RCR, D) QCR and E) C and F) T20 at pH 7.0 and 37 °C in 10 mM PB (0.08 M ionic strength, 0.5 mM EDTA and N₂ sparged). T=0 min represents sample collected before reaction was initiated by adjusting pH to 7.0, thiol: disulfide ratio was 100: 1 (molar ratio).

Table 4.6: The change in native disulfide concentration in peptides and hGH obtained after 1 hour and 1 day for thiol-disulfide exchange reactions with different free thiols at pH 7.0 and 37 °C.

Disulfide	Thiol	pH	Temp (°C)	% decrease of native disulfide after 60 mins	% decrease of native disulfide after 1 day
cT20-T21	GIVQCR (T20a)	7	37	61.9±4.8	53.7±1.7
	MQCR (T20)			70.5±1.1	64.5±1.2
	GSH			84.7±3.5	76.8±1.2
	RCR			49.9±0.1	23.9±0.1
	QCR			59.2±1.3	39.3±0.5
	CR			66.2±0.9	8.3±0.5
	C			57.3±0.4	13.7±0.2
T20-T21 in hGH (intact)	GIVQCR (T20a)	7	37	37.5±6.8	37.1±5.8
	GSH			57.7±6.1	23.9±4.4
	RCR			35.8±7.9	11.4±1.4
	CR			20.7±5.5	6.8±1.8
	C			16.7±0.5	3.8±2.6

4.6.4 Effect of hGH structure on regeneration of native disulfide

To measure the extent of loss of hGH native structure upon disulfide bond cleavage breakage, and to correlate the regeneration of native disulfides following thiol-disulfide exchange, near-UV CD spectroscopy and amide HDX-MS were conducted for hGH in both oxidized and reduced states. Near-UV CD showed no appreciable differences in tertiary structure between the native and reduced forms (Figure 4.11).

HDX-MS has been widely used to study protein structure and conformation at peptide level resolution [183]. Here, a total of 31 peptic peptides covering 100% of hGH sequence were identified and analyzed. Comparison of the level of deuterium uptake between the native and reduced state showed no appreciable differences (Figure 4.12), suggesting that hGH retains its native structure after disulfide bond cleavage. The C-terminal peptide fragment, 182-191 containing the two cysteine residues (C¹⁸² and C¹⁸⁹) are involved in disulfide formation is ~ 50% deuterated in both the native and reduced

states. Similarly, peptide fragment 47-53 containing C⁵³ and fragment 160-172 containing C¹⁶⁵ showed 53% and 38% deuterium uptake, respectively. Subtractive analysis of peptide fragments 160-172 and 166-175 shows that residues 160-165 are more than 60% deuterated. Overall, the near-UV CD and HDX-MS results suggest that the disulfide containing regions in hGH are highly solvent accessible and that the structure of fully reduced hGH is close to the native state. This suggests that the regeneration of native disulfide bonds following disulfide exchange may be favored by the orientations of the native Cys partners in close proximity to one another.

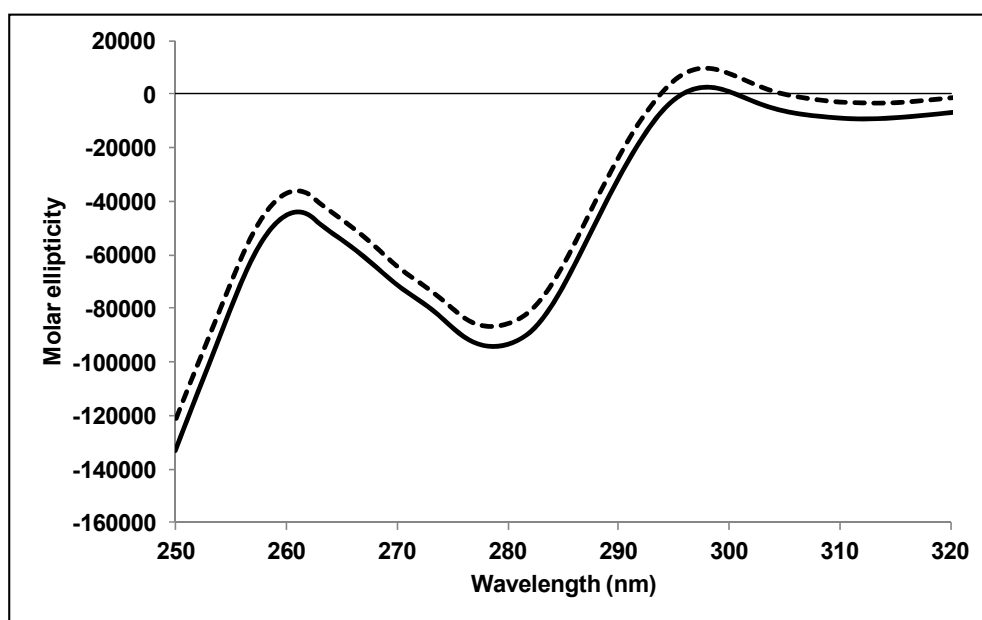


Figure 4.11: Near-UV CD spectra for hGH native (solid line) and reduced (dotted line).

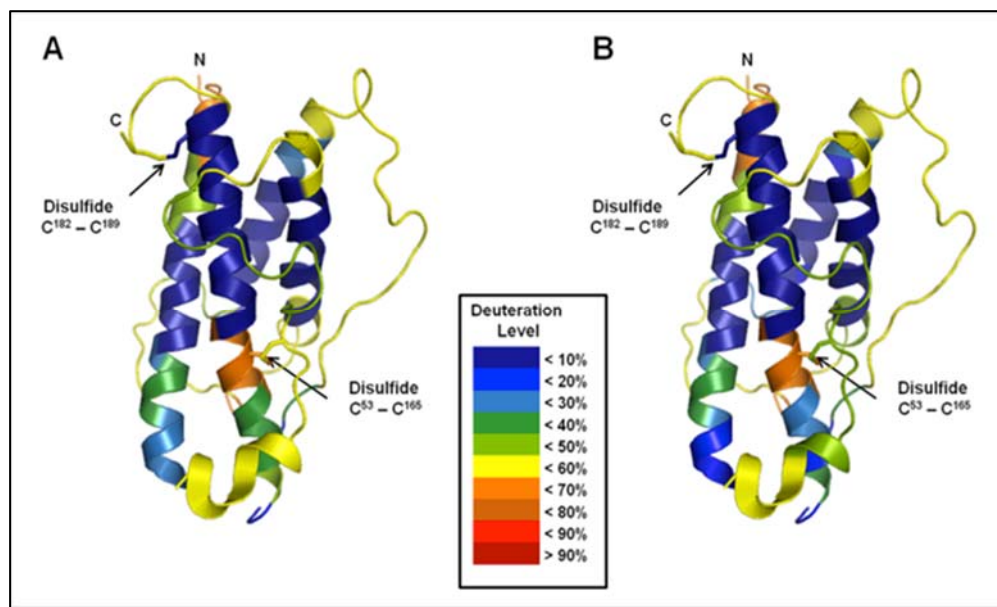
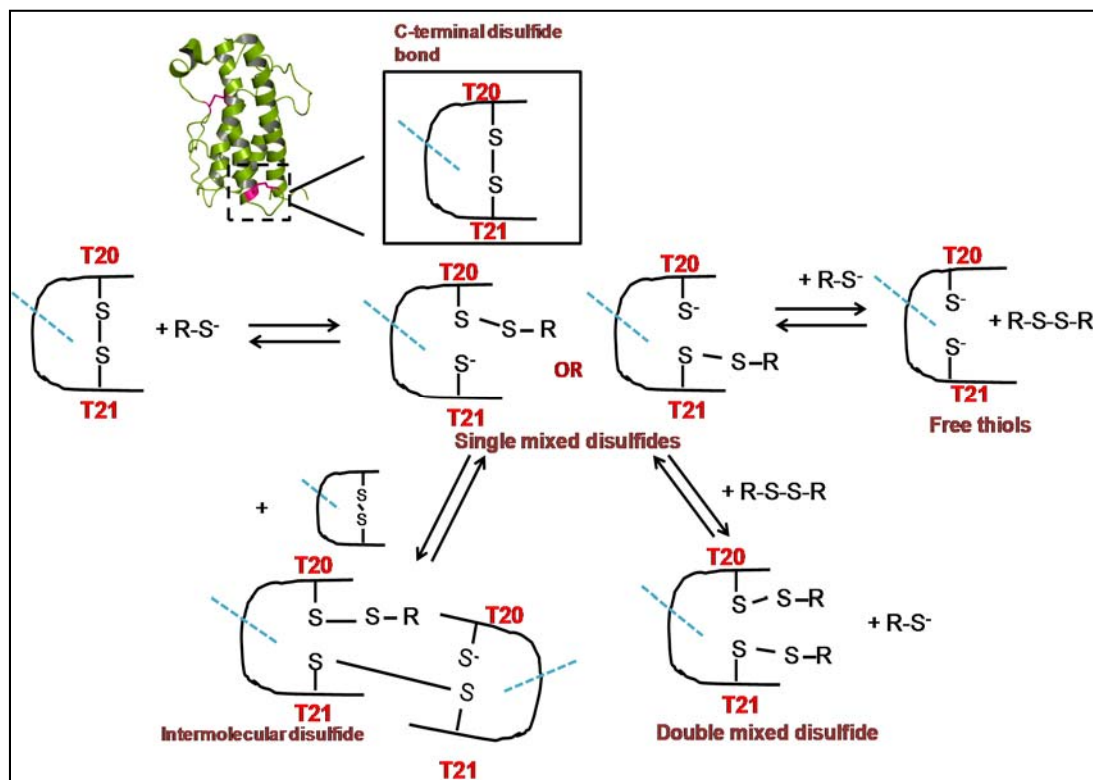


Figure 4.12: Crystal structure of hGH (PDB ID: 1 HGU) representing the percent deuterium uptake in native (A) and reduced (B) state following 5 min of HDX. Data from 31 overlapping peptic fragments were mapped onto the structure.

Scheme 4.1: Thiol-disulfide exchange at the C-terminal disulfide bond (T20-T21) in hGH/disulfide bond in cT20-T21; R-S⁻ is the thiolate form of the free thiol-containing peptide (Table 4.2) and R-S-S-R is the oxidized form. The blue dashed lines represent a trypsin cleavage site in hGH.



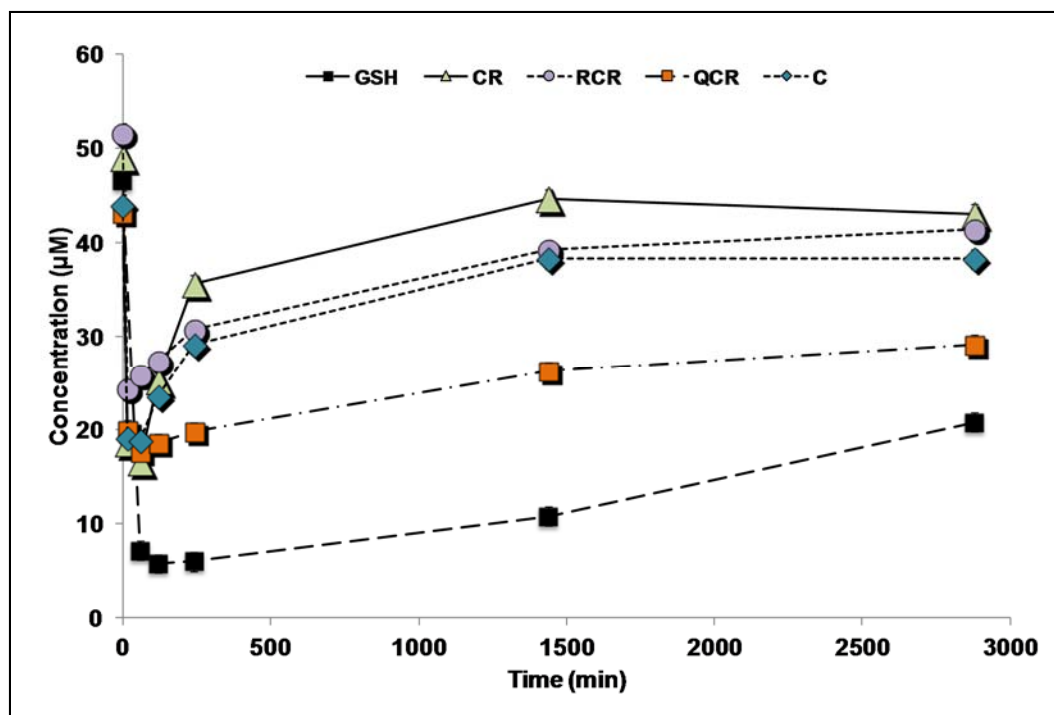


Figure 4.13: Concentration vs time plot for the loss of cT20-T21 ($n=3$, \pm SD) during the reaction with GSH, CR, RCR, QCR and C at pH 7.0 and 37 °C in 10 mM PB (0.08 M ionic strength, 0.5 mM EDTA and N_2 sparged). Initial thiol: disulfide was 100:1 (molar ratio). Lines on plot are to improve readability and do not represent regression analysis.

4.7 Discussion

In the studies reported here, thiol-disulfide exchange reactions between intact hGH/cT20-T21/T20-T21_{pep} and free thiol-containing peptides (Table 4.2) were investigated in aqueous solution at pH 7.0 and 37 °C. The amino acid sequences of native, scrambled and free thiol containing peptides and their masses are shown in Tables 4.1, 4.2, 4.3, 4.4, 4.5 and C.2. From our previous studies with hGH-derived peptides [69, 181] and other reports [45, 71], it is well known that thiol-disulfide exchange is favored at neutral to alkaline conditions. Although thiol-disulfide exchange was observed at both the native disulfides in hGH (T20-T21 and T6-T16), quantitative analysis of disulfide scrambling was performed only for the C-terminal disulfide.

After purification, hGH was digested using the Perfinity flash digest kit and analyzed using LC/MS for the presence of native, scrambled disulfides and free thiols. Perfinity digestion was compared with overnight digestion with trypsin in solution and with digestion with trypsin immobilized on magnetic and agarose beads to determine digestion efficiency (Table C.1, Appendix C). For all digestion protocols except the flash digest kit, scrambled disulfides were detected and digestion was incomplete after 60 min (Table C.1). In contrast, digestion with the flash digest kit was complete in 17 min and no scrambled disulfides were detected.

For the reaction of hGH with different thiol-containing peptides, products generally conforming to Scheme 4.1 were detected (except intermolecular disulfides), and the distribution of these species varied with reaction time. Mixed disulfides were detected at both the disulfide bonds (T20-T21 and T6-T16) and fully reduced forms of the native

disulfides (Table 4.1) were also observed. The reactivity of the C-terminal native disulfide (T20-T21) in hGH decreased in the order $\text{GSH} > \text{T20a} > \text{RCR} > \text{CR} \approx \text{C}$ and regeneration of native disulfides was favored over the formation of mixed disulfides in the order $\text{C} \approx \text{CR} > \text{RCR} > \text{GSH} > \text{T20a}$ (Table 4.6). Though most of the native disulfides were regenerated in the presence of GSH (75-80%), RCR (85-90%), CR (92-95%) and C (94-99%), the presence of even low levels of mixed disulfides may be detrimental to the therapeutic efficacy and stability of hGH, given the functional roles of the two native disulfide bonds. The C-terminal disulfide bond (T20-T21) is required for binding to the growth hormone receptor and to maintain normal stability, while the disulfide bond in T6-T16 is necessary for biological activity [91].

The concentration of hGH can also influence thiol-disulfide exchange and/or disulfide scrambling, though these effects were not investigated here. For example, in studies of porcine somatotropin (porcine hGH), disulfide exchange led to the formation of irreversible thixotropic gels (disulfide-linked aggregates) at concentrations > 25 mg/mL during storage at 39 °C for 14 days [184]. Initial concentrations used in our studies range from 0.3 to 0.45 mg/mL, concentrations ~ 100 -fold lower than those used by Buckwalter et al. High hGH concentrations within the secretory granules (50-100 mg/mL) also favor intermolecular exchange and result in the formation of disulfide-linked dimers and oligomers [137, 185]. Due to the low yield of hGH purified in-house (< 0.6 mg/mL) and the cost of commercially available hGH, studies at higher concentrations were not practical here, and the absence of any intermolecular disulfides (Table C.2 in Appendix C) may reflect low hGH concentrations.

SMDs, DMD and rT20-T21 were identified as products of the reaction of cT20-T21 with all the free thiol-containing peptides (Table 4.2). Oxidation products such as cysteine sulfenic, sulfinic and sulfonic acid and thiosulfinates were not detected, and Scheme 4.1 effectively describes the products observed. Overall, the loss of native disulfide in cT20-T21 after 60 min decreases in the order GSH>T20>CR>T20a>QCR>C>RCR and regeneration of native disulfide is favored after 1 day in the order CR>C>RCR>QCR>T20a>T20>GSH. The amino acid length of all peptides used here ranges from 1-5. The results suggest that thiol size in this range has no effect on reactivity. In contrast primary sequence, particularly the presence of Arg adjacent to a Cys, promotes the reformation of the native disulfide. The loss of native disulfide (% loss in 60 min) in cT20-T21 is greater than the loss of native disulfide (T20-T21) in hGH with GSH, T20a, RCR, CR and C (Table 4.6).

Native disulfides in hGH were re-formed in the presence of GSH, RCR, CR, C and to a lesser extent with T20a. Rabenstein et al. made a similar observation with somatostatin and GSH. At concentrations of GSH less than 4 mM, Rabenstein et al observed that the rate of thiol-disulfide exchange to re-form the native disulfide was faster than the rate of thiol-disulfide exchange to form the fully reduced form [119]. The authors also concluded that the conformational properties of the mixed disulfides may place the mixed disulfide in close proximity to the thiol group that then regenerates the native disulfide. Similar results have been reported for the reaction of small heat shock protein 25 (Hsp25) with GSH, where the formation of an intersubunit protein disulfide (native disulfide) is preferred over the mixed disulfides [67]. Here, near-UV CD and HDX-MS of both reduced (with BME) and non-reduced hGH (Figures 4.11 and 4.12) showed no differences in higher order

structure, thus favoring regeneration of native disulfides. Youngman et al. have shown that folding of hGH is similar in the presence and absence of disulfide bonds [151], further suggesting that disulfide bond reduction does not affect protein structure.

Regeneration of native disulfides was fastest in the presence of RCR, CR and C. For the reaction of hGH with C, formation of mixed disulfides was minimal and most of the native disulfide remained intact (no thiol-disulfide exchange at T6-T16) after 60 mins and 1 day. Previously, Raman et al. have shown that the Cysteine/Cystine redox system is more efficient in the oxidative folding of high concentrations (0.05 mg/mL) of lysozyme when compared to GSH/GSSG [186]. Though only Cysteine was added to the studies here, oxidation of Cys over time can result in the formation of Cystine thus providing a Cystine/Cystine redox system. This observation with lysozyme and our results suggest that Cys favors the formation of native disulfides over mixed disulfides such that the rate of formation of mixed disulfides \ll the rate of regeneration of native disulfides, attributing to the detection of only one of the mixed disulfides (T21-C). Also, the thiol group in Cys itself has a low pKa (8.3) that would make it a better leaving group.

With RCR and CR, the presence of a positively charged group adjacent to the Cys would be expected to increase reactivity of the thiol group by lowering thiol pKa. A thiol group with low pKa makes a better leaving group [61] as the charge stabilizes the thiolate form over the mixed disulfide [62] thus favoring reformation of native disulfides in both cT20-21 and hGH. The presence of an Arg adjacent to Cys182 in growth hormone is highly conserved among different species; the positively charged residue lowers pKa of the thiol group making it the most reactive of the four Cys residues [137]. Having two Arg residues flanking the reactive Cys not increase reactivity over having just one, however; similar

reactivities of CR and RCR were observed for cT20-T21 (Figure 4.13). However, with QCR, the regeneration is not as fast as it is with RCR and CR (Figure 4.13). In agreement with the results obtained here, Okumura et al. observed that with a glutathione derivative, RCG (oxidized and reduced), prouroguanylin folded into its native conformation more efficiently than with GSH [187]. The increase in folding efficiency was attributed to the presence of a positive charge (from Arg) adjacent to the Cys residue. T20a is similar in sequence to the tryptic fragment, T20, in hGH and this could explain why the native disulfide in cT20-T21 and hGH (Table 4.6) is not regenerated faster than with GSH as observed for other peptides with a neighboring Arg.

The unified software package DiANNA was used to determine the Cys state in all the free thiol-containing peptides to gain a better understanding of the observed differences in reactivities. The algorithm predicts the susceptibility of Cys residues to either participate in a disulfide bond or to be in the reduced state with 76-81 % accuracy [188]. Scores obtained for the different peptides used to initiate thiol-disulfide exchange are shown in Table 4.7. A higher score corresponds to an increased susceptibility to be in that state. The lowest scores for half Cys were obtained for C and CR, suggesting that in the presence of these thiols, regeneration of the native disulfide will be favored over mixed disulfides, in accordance with the results obtained here (Figure 4.13). However, similar half Cys scores were obtained for RCR, QCR and GSH and no correlations could be made to the results reported here. rT20-T21, reduced form of cT20-T21 had the highest half Cys score, suggesting that the disulfide bond in cT20-T21 would be favored over its reduced form or a mixed disulfide with another free thiol-containing peptide. The differences in peptide reactivity between DiANNA scores and the reactivities reported here suggest that, in

addition to the influence of primary structure on thiol pKa, higher order structure also plays a role and can determine the type of disulfide bond that can be regenerated.

Table 4.7: Oxidation state prediction for thiol-containing peptides using DiANNA

Peptide	Free Cys	Half Cys
C	0.869	0.131
CR	0.835	0.165
RCR	0.711	0.289
QCR	0.799	0.201
GSH	0.798	0.202
T20	0.608	0.392
T20a	0.692	0.308
rT20-T21	0.546	0.454

values represented as scores obtained using DiANNA

4.8 Conclusion

The studies reported in this chapter using intact hGH, disulfide-linked and free thiol-containing peptides as model compounds, demonstrate that higher-order structure, proximity of thiols to a disulfide and primary structure influence thiol-disulfide exchange. Higher-order structure was found to protect the native disulfides to some extent, however, thiol-disulfide exchange still occurs at both the native disulfides in intact hGH. Loss of the native disulfides in hGH did not result in structural changes as observed using CD and HDX. Regeneration of the native disulfide was favored in the presence of peptides that contain an Arg residue adjacent to the reactive Cys for both hGH and a cyclic peptide

(cT20-T21). These results provide an improved understanding of thiol-disulfide exchange reactions in hGH and are valuable to the development of protein drugs that contain disulfide bonds.

CHAPTER 5. CONCLUSIONS AND SUGGESTIONS FOR FUTURE WORK

In order to improve stability of therapeutic proteins during the manufacturing process and storage, it is important to understand the mechanisms of degradation pathways both in aqueous solution and in the solid state. These deleterious degradation reactions can significantly affect the therapeutic value of proteins. The studies reported in this dissertation have elucidated the mechanism of one such pathway, thiol-disulfide exchange, in human growth hormone. Model tryptic peptides derived from hGH were used to investigate reaction mechanisms and kinetics in Chapters 2 and 3, providing mechanistic details on the reaction in the absence of higher order structure and other degradation pathways. Chapter 4 provided insight into the effects of higher-order structure on thiol-disulfide exchange using intact hGH as a model protein.

5.1 Thiol-disulfide exchange in aqueous solution (Chapter 2)

The results presented in chapter 2 demonstrated that in aqueous solution, microscopic rate constants for thiol-disulfide exchange are pH independent while the observed rate constants for the loss of native disulfide are pH dependent. Further, thiol-disulfide exchange follows Arrhenius behavior and the calculated activation parameters are similar to previous reports in the literature for low-molecular weight thiols and proteins [71]. The activation energy values for all four reversible thiol-disulfide exchange reactions

(R3 and R4, Scheme 2.1) were similar suggesting that they are all essentially the same reaction. The negative entropy of activation values that were obtained (Table 2.3) for thiol-disulfide exchange reactions (R3 and R4, Scheme 2.1) are representative of S_N2 nucleophilic displacement reactions. Though the presence of oxidation suppressants (EDTA and N_2 sparging) did not completely inhibit oxidation reactions (R5 and R6, Scheme 2.1), the oxidation reactions did not affect the intrinsic rates of thiol-disulfide exchange. Finally, peptide secondary structure was shown to influence reactivity of the disulfide bond; loss of native disulfide in the linear peptide was ~ 10 -fold greater than in the cyclic peptide.

5.2 Thiol-disulfide exchange during lyophilization and storage in the solid state

(Chapter 3)

These studies explored the effects of a process stress (lyophilization) and subsequent storage in the solid state on thiol-disulfide exchange in hGH-derived peptides. The results from Chapter 3 demonstrate that the mechanism of thiol-disulfide exchange is similar in aqueous solution and in the solid state. However, differences in reaction rates and distribution of products were observed. Further, peptide cyclization offered little or no protection from thiol-disulfide exchange during lyophilization and storage. Increased reactivity of the cyclic peptide in the solid state shows that lyophilization may not always be a suitable approach to improve the stability of peptide and protein formulations. This information is valuable to the pharmaceutical industry, especially when protein formulations are switched from solution to the solid state with the assumption that they are

more stable during storage in the solid state. The ‘cold finger’ was used to study adsorption of peptides and proteins to ice surfaces and evaluate the role of surfactants in protein formulations where ice-induced degradation is suspected. A general reaction scheme for the reaction of linear or cyclic peptides that contain disulfide bonds with a free thiol (Scheme 3.3, Chapter 3) was also proposed. This reaction scheme can be used as a guide to identify scrambled species when the reactive thiol group and disulfide-containing moiety (linear or cyclic) are known. The relative rates of these reactions may vary between solution and the solid state and will be influenced by the type of thiol/disulfide, pH and temperature.

5.3 Thiol-disulfide exchange in human growth hormone (Chapter 4)

The results presented in Chapter 4 show that thiol-disulfide exchange also occurs in intact hGH in the presence of reactive thiolate anions. By using the Perfinity flash digest protocol, scrambled disulfides were not produced during digestion, allowing analysis of hGH samples. However, scrambling may occur during digestion for proteins that have a free Cys in their native form (not tested here) and suitable alkylating agents need to be evaluated for their ability to minimize disulfide exchange in parallel with their effect on digestion efficiency and digestion times.

For the protein concentrations tested here, no intermolecular or intramolecular disulfides were detected. Protein mixed-disulfides were detected with GSH, free thiol-containing peptides and cysteine. However, most of the native disulfide was regenerated at the end of one day. A similar trend was observed with the cyclic peptide, suggesting that the proximity of free Cys residues in hGH and cT20-T21 favors reformation of the native

disulfide. Overall, loss of native disulfide in cT20-T21 and T20-T21_{pep} was greater than loss of native disulfide in hGH. Further, the presence of an Arg residue neighboring the reactive Cys was found to favor regeneration of the native disulfide over GSH. Together, the results suggest that protein higher order structure and peptide secondary structure influence thiol-disulfide exchange.

5.4 Recommendations for future work

The stabilizing effects of excipients on thiol-disulfide exchange are not well known; this is an area for future investigation. A previous report of thiol-disulfide exchange examined the effect of sucrose on the reaction during lyophilization [129]. Though some protection was observed during the freezing and primary drying steps, loss of native disulfide during secondary drying in the presence of sucrose was similar to vials lyophilized without sucrose [129]. It would also be interesting to study thiol-disulfide exchange in intact hGH in the solid state both in the presence and absence of excipients, since hGH is known to undergo structural changes upon lyophilization. Though an excipient may have a stabilizing effect on thiol/disulfide mediated degradation, it may facilitate degradation via a different mechanism. Thus, the compatibilities of excipients with different proteins and potential degradation pathways (both physical and chemical) have to be carefully assessed in aqueous solution and in solid-state formulations.

The effects of glass transition temperature (T_g) and moisture content on thiol-disulfide exchange were not investigated here. Incorporation of some excipients in formulations will increase T_g, thus improving storage stability while others may have a

negative effect (e.g., low T_g , change in pH and/or loss of structure). The moisture content of lyophilized peptide samples in Chapter 2 was 1-1.5% immediately after lyophilization and after storage for 14 days. Even with such low moisture content, the cyclic peptide degraded more rapidly in the solid state than in solution samples. It is possible that as the moisture content increases, sample dilution with water molecules protects the native disulfide bond from thiol-disulfide exchange as reported previously for recombinant human albumin [95]. Thus, studies relating the kinetics of thiol-disulfide exchange and the kinetics of water sorption are needed, in order to identify the particular moisture content that can lead to protein instability.

The results obtained in Chapter 4 with intact hGH showed that no structural changes were observed upon disulfide bond cleavage thus favoring regeneration of the native disulfide over inter-/intramolecular scrambled disulfides. Even though lyophilization is known to induce structural changes in hGH [101], denaturants (e.g., GdnHCl, urea), mechanical force and agitation may have different effects on higher-order structure that can result in an altered distribution of scrambled disulfides in the presence of reactive thiols. It would be interesting to monitor thiol-disulfide exchange in hGH with different denaturing agents/stresses and to identify conditions in which disulfide degradation is favored.

The results reported in this dissertation can also be extended to understand the effects of primary structure and length of the attacking thiol groups on thiol-disulfide exchange. Though steric effects related to the size of the reactive nucleophile are known to influence reaction kinetics to a greater extent than the size of disulfide-containing moiety and/or the pH [179], this is still an area that has not been explored extensively as it has

been for deamidation in peptides and proteins [189, 190]. For example, the effects of amino acids flanking the Cys residue are not well understood except for the presence of an arginine, which was shown to favor regeneration of the native disulfides, as reported here and by Okumura et al [187]. Other positively charged amino acids such as His and Lys may have similar effects and are yet to be investigated. Another area for future work is to use the information presented here to study therapeutic proteins with similar and distinct higher order structures, e.g., using model peptides from a protein that is rich in β -sheets instead of α -helices.

Finally, since serum is known to contain low molecular weight thiols such as Cys and GSH [72], the mechanistic details of thiol-disulfide exchange reported here can be extended to understand the reaction in therapeutic proteins *in vivo* after administration. Jiang et al. have used a continuous flow dialysis system to evaluate protein disulfide conversion [191]; a similar system can be used for other therapeutic proteins to evaluate the potential for loss of native protein disulfides. This can provide an insight into the formation of modified forms of the protein drug that may have altered properties. It is already known that monoclonal antibodies of the IgG4 class undergo Fab-arm exchange, a disulfide rearrangement phenomena, in serum and these modified molecules have been shown to have therapeutic effects that differ from those of the native protein.

5.5 Implications for protein formulation

The results obtained in Chapter 3 with both the linear and cyclic peptides suggest that lyophilization at near neutral pH does not inhibit thiol-disulfide exchange. A common

approach to inhibiting thiol-disulfide exchange and β -elimination is to formulate proteins and peptides that contain thiols and disulfides at low pH prior to lyophilization, followed by reconstitution in near neutral buffer before administration. Low pH prior to lyophilization has been shown to arrest β -elimination in insulin during storage in the solid state [79]. This approach may work well for some proteins when compared to others depending on inherent protein stability at low pH. Thermal stability of proteins varies with pH [192] and may further facilitate disulfide-mediated degradation events during and after lyophilization. Overall, the effect of pH on the conformational stability of a protein and excipients must be well understood before this approach can be employed.

Another stabilization strategy is to use excipients in peptide and protein formulations before lyophilization. In the absence of excipients, proteins can undergo structural changes during processing that may favor thiol and/or disulfide-mediated degradation. For example, upon structural changes, a buried Cys residue may be exposed to oxidative agents or be brought in close proximity to a native disulfide bond resulting in the formation of intermolecular bonds, high molecular weight aggregated and/or non-native intramolecular disulfides. Increasing the buffer concentration is another strategy that can be used to control thiol-disulfide exchange. The buffer concentrations tested in the studies reported here (10 – 40 mM) did not have a significant effect on thiol-disulfide exchange in the linear peptide (Chapter 2). However, in a study with bovine serum albumin, disulfide-mediated aggregation was reduced when 1 M sodium phosphate was added to the initiating buffer (5 mM phosphate, 150 mM NaCl, pH = 7.3). A possible explanation for the observed reduction is that phosphate anions prevent the attack of thiolate anions on the disulfide bond [96].

For proteins that contain free thiols such as human serum albumin, protein tyrosine phosphatases and recombinant human α 1-antitrypsin, thiol derivatizing agents and protein engineering approaches can be employed to retain biological activity and improve stability [3]. These approaches are discussed in detail in Chapter 1 and can be used when the free Cys residues are known to have no functional role. Thiol derivatization, however, is not a suitable strategy for proteins where the role of Cys is unknown. Derivatization restricts free thiol content and will minimize thiol-catalyzed and thiol-disulfide exchange reactions during lyophilization and storage. Protein concentration may also influence the formation of disulfide-linked aggregates. For example, at high concentrations of porcine somatotropin (>25 mg/mL), disulfide-linked aggregates were detected at 39 °C after 14 days during storage [184]. Optimizing protein concentrations to a range that delivers an effective dose and provides stability during storage is essential to developing safe and effective protein therapeutics.

The presence of oxygen, metal ions (Cu^{II} and Fe^{III}) and reactive oxygen species (ROS) such as peroxides, superoxide and hydroxyl radical can result in the formation of sulfenic, sulfinic and sulfonic acids and thiolsulfinate or a new non-native disulfide bond [140, 193, 194]. Although oxidative pathways were found to have no effect on the intrinsic rates of thiol-disulfide exchange (Chapter 2), these products of oxidative pathways can diminish the therapeutic efficacy of protein and peptide drugs that contain free thiols. Nitrogen sparging and storage of protein formulations in a nitrogen atmosphere will inhibit O_2 -mediated oxidative pathways. Some common excipients like polyvinyl pyrrolidone and polyethylene glycol contain peroxides as impurities. These excipients should be excluded from protein formulations and suitable antioxidants can be employed as stabilizers when

peroxides are detected. If metal-catalyzed thiol oxidation is suspected, EDTA can be used as a metal ion chelator to stabilize thiol containing peptides and proteins. In some cases however, the presence of transition metal cations (Cu^{2+}) can be beneficial when used as an oxidizing agent to minimize free thiol groups prior to lyophilization [78]. The addition of divalent metal ions (Cu^{2+}) catalyzed thiol oxidation at a rapid rate relative to thiol-disulfide exchange and stabilized insulin from aggregation [78].

REFERENCES

REFERENCES

1. Aggarwal RS 2014. What's fueling the biotech engine-2012 to 2013. *Nat Biotechnol* 32(1):32-39.
2. Wang W, Roberts CJ. 2010. Aggregation of therapeutic proteins. ed., Hoboken, N.J.: Wiley. p xxii, 486 p.
3. Trivedi MV, Laurence JS, Siahaan TJ 2009. The role of thiols and disulfides on protein stability. *Curr Protein Pept Sci* 10(6):614-625.
4. Chen BL, Arakawa T, Morris CF, Kenney WC, Wells CM, Pitt CG 1994. Aggregation pathway of recombinant human keratinocyte growth factor and its stabilization. *Pharm Res* 11(11):1581-1587.
5. DiMasi JA, Hansen RW, Grabowski HG 2003. The price of innovation: new estimates of drug development costs. *J Health Econ* 22(2):151-185.
6. Manning MC, Chou DK, Murphy BM, Payne RW, Katayama DS 2010. Stability of protein pharmaceuticals: an update. *Pharm Res* 27(4):544-575.
7. Bhopale GM, Nanda RK 2005. Recombinant DNA expression products for human therapeutic use. *Current Science* 89(4):614-622.
8. Rathore AS 2009. Follow-on protein products: scientific issues, developments and challenges. *Trends Biotechnol* 27(12):698-705.
9. Walsh G, Jefferis R 2006. Post-translational modifications in the context of therapeutic proteins. *Nat Biotechnol* 24(10):1241-1252.
10. Jiskoot W, Randolph TW, Volkin DB, Middaugh CR, Schoneich C, Winter G, Friess W, Crommelin DJ, Carpenter JF 2012. Protein instability and immunogenicity: roadblocks to clinical application of injectable protein delivery systems for sustained release. *J Pharm Sci* 101(3):946-954.
11. Schellekens H 2010. The immunogenicity of therapeutic proteins. *Discov Med* 9(49):560-564.

12. Wang W, Singh SK, Li N, Toler MR, King KR, Nema S 2012. Immunogenicity of protein aggregates--concerns and realities. *Int J Pharm* 431(1-2):1-11.
13. Chi EY, Krishnan S, Randolph TW, Carpenter JF 2003. Physical stability of proteins in aqueous solution: mechanism and driving forces in nonnative protein aggregation. *Pharm Res* 20(9):1325-1336.
14. Costantino HR, Schwendeman SP, Langer R, Klibanov AM 1998. Deterioration of lyophilized pharmaceutical proteins. *Biochemistry (Mosc)* 63(3):357-363.
15. Lai MC, Topp EM 1999. Solid-state chemical stability of proteins and peptides. *J Pharm Sci* 88(5):489-500.
16. Flores-Fernandez GM, Pagan M, Almenas M, Sola RJ, Griebenow K 2010. Moisture-induced solid state instabilities in alpha-chymotrypsin and their reduction through chemical glycosylation. *BMC Biotechnol* 10:57.
17. Webb JN, Webb SD, Cleland JL, Carpenter JF, Randolph TW 2001. Partial molar volume, surface area, and hydration changes for equilibrium unfolding and formation of aggregation transition state: high-pressure and cosolute studies on recombinant human IFN-gamma. *Proc Natl Acad Sci U S A* 98(13):7259-7264.
18. Philo JS, Arakawa T 2009. Mechanisms of protein aggregation. *Curr Pharm Biotechnol* 10(4):348-351.
19. Kendrick BS, Carpenter JF, Cleland JL, Randolph TW 1998. A transient expansion of the native state precedes aggregation of recombinant human interferon-gamma. *Proc Natl Acad Sci U S A* 95(24):14142-14146.
20. Bam NB, Cleland JL, Yang J, Manning MC, Carpenter JF, Kelley RF, Randolph TW 1998. Tween protects recombinant human growth hormone against agitation-induced damage via hydrophobic interactions. *J Pharm Sci* 87(12):1554-1559.
21. Chang BS, Kendrick BS, Carpenter JF 1996. Surface-induced denaturation of proteins during freezing and its inhibition by surfactants. *J Pharm Sci* 85(12):1325-1330.
22. Katakam M, Bell LN, Banga AK 1995. Effect of surfactants on the physical stability of recombinant human growth hormone. *J Pharm Sci* 84(6):713-716.
23. Randolph TW, Jones LS 2002. Surfactant-protein interactions. *Pharm Biotechnol* 13:159-175.

24. Vidanovic D, Milic Askrabic J, Stankovic M, Poprzen V 2003. Effects of nonionic surfactants on the physical stability of immunoglobulin G in aqueous solution during mechanical agitation. *Pharmazie* 58(6):399-404.
25. Colombie S, Gaunand A, Lindet B 2001. Lysozyme inactivation under mechanical stirring: effect of physical and molecular interfaces. *Enzyme Microb Technol* 28(9-10):820-826.
26. Maa YF, Hsu CC 1997. Protein denaturation by combined effect of shear and air-liquid interface. *Biotechnol Bioeng* 54(6):503-512.
27. Matheus S, Friess W, Schwartz D, Mahler HC 2009. Liquid high concentration IgG1 antibody formulations by precipitation. *J Pharm Sci* 98(9):3043-3057.
28. Rosenberg AS 2006. Effects of protein aggregates: an immunologic perspective. *AAPS J* 8(3):E501-507.
29. Davies MJ 2005. The oxidative environment and protein damage. *Biochim Biophys Acta* 1703(2):93-109.
30. Liu D, Ren D, Huang H, Dankberg J, Rosenfeld R, Cocco MJ, Li L, Brems DN, Remmele RL, Jr. 2008. Structure and stability changes of human IgG1 Fc as a consequence of methionine oxidation. *Biochemistry* 47(18):5088-5100.
31. Yang J, Wang S, Liu J, Raghani A 2007. Determination of tryptophan oxidation of monoclonal antibody by reversed phase high performance liquid chromatography. *J Chromatogr A* 1156(1-2):174-182.
32. Hepner F, Csaszar E, Roitinger E, Pollak A, Lubec G 2006. Massspectrometrical analysis of recombinant human growth hormone Norditropin reveals amino acid exchange at M14_V14 rhGH. *Proteomics* 6(3):775-784.
33. Joshi AB, Sawai M, Kearney WR, Kirsch LE 2005. Studies on the mechanism of aspartic acid cleavage and glutamine deamidation in the acidic degradation of glucagon. *J Pharm Sci* 94(9):1912-1927.
34. Liu H, Gaza-Bulsecu G, Sun J 2006. Characterization of the stability of a fully human monoclonal IgG after prolonged incubation at elevated temperature. *J Chromatogr B Analyt Technol Biomed Life Sci* 837(1-2):35-43.
35. Hageman MJ, Bauer JM, Possert PL, Darrington RT 1992. PREFORMULATION STUDIES ORIENTED TOWARD SUSTAINED DELIVERY OF RECOMBINANT SOMATOTROPINS. *Journal of Agricultural and Food Chemistry* 40(2):348-355.

36. Schwendeman SP, Costantino HR, Gupta RK, Siber GR, Klivanov AM, Langer R 1995. Stabilization of tetanus and diphtheria toxoids against moisture-induced aggregation. *Proc Natl Acad Sci U S A* 92(24):11234-11238.
37. Malencik DA, Anderson SR 2003. Dityrosine as a product of oxidative stress and fluorescent probe. *Amino Acids* 25(3-4):233-247.
38. Dillon TM, Ricci MS, Vezina C, Flynn GC, Liu YD, Rehder DS, Plant M, Henkle B, Li Y, Deechongkit S, Varnum B, Wypych J, Balland A, Bondarenko PV 2008. Structural and functional characterization of disulfide isoforms of the human IgG2 subclass. *J Biol Chem* 283(23):16206-16215.
39. Jiang C, Chang JY 2005. Unfolding and breakdown of insulin in the presence of endogenous thiols. *FEBS Lett* 579(18):3927-3931.
40. Grigorian AL, Bustamante JJ, Hernandez P, Martinez AO, Haro LS 2005. Extraordinarily stable disulfide-linked homodimer of human growth hormone. *Protein Sci* 14(4):902-913.
41. Fasman GD. 1989. Prediction of protein structure and the principles of protein conformation. ed., New York: Plenum Press. p xiii, 798 p.
42. Wolfenden R, Andersson L, Cullis PM, Southgate CC 1981. Affinities of amino acid side chains for solvent water. *Biochemistry* 20(4):849-855.
43. Frand AR, Cuozzo JW, Kaiser CA 2000. Pathways for protein disulphide bond formation. *Trends Cell Biol* 10(5):203-210.
44. Lu BY, Beck PJ, Chang JY 2001. Oxidative folding of murine prion mPrP(23-231). *Eur J Biochem* 268(13):3767-3773.
45. Gilbert HF 1995. Thiol/disulfide exchange equilibria and disulfide bond stability. *Methods Enzymol* 251:8-28.
46. Hogg PJ 2003. Disulfide bonds as switches for protein function. *Trends Biochem Sci* 28(4):210-214.
47. Holmgren A 1985. Thioredoxin. *Annu Rev Biochem* 54:237-271.
48. Klink TA, Woycechowsky KJ, Taylor KM, Raines RT 2000. Contribution of disulfide bonds to the conformational stability and catalytic activity of ribonuclease A. *Eur J Biochem* 267(2):566-572.
49. Correia IR 2010. Stability of IgG isotypes in serum. *MAbs* 2(3):221-232.

50. Szajewski RP, Whitesides GM 1980. Rate Constants and Equilibrium-Constants for Thiol-Disulfide Interchange Reactions Involving Oxidized Glutathione. *Journal of the American Chemical Society* 102(6):2011-2026.
51. Jensen KS, Hansen RE, Winther JR 2009. Kinetic and thermodynamic aspects of cellular thiol-disulfide redox regulation. *Antioxid Redox Signal* 11(5):1047-1058.
52. Carballal S, Alvarez B, Turell L, Botti H, Freeman BA, Radi R 2007. Sulfenic acid in human serum albumin. *Amino Acids* 32(4):543-551.
53. Carballal S, Radi R, Kirk MC, Barnes S, Freeman BA, Alvarez B 2003. Sulfenic acid formation in human serum albumin by hydrogen peroxide and peroxyntirite. *Biochemistry* 42(33):9906-9914.
54. Zhang L, Chou CP, Moo-Young M 2011. Disulfide bond formation and its impact on the biological activity and stability of recombinant therapeutic proteins produced by *Escherichia coli* expression system. *Biotechnol Adv* 29(6):923-929.
55. Tous GI, Wei Z, Feng J, Bilbulian S, Bowen S, Smith J, Strouse R, McGeehan P, Casas-Finet J, Schenerman MA 2005. Characterization of a novel modification to monoclonal antibodies: thioether cross-link of heavy and light chains. *Anal Chem* 77(9):2675-2682.
56. Zhang Q, Schenauer MR, McCarter JD, Flynn GC 2013. IgG1 thioether bond formation in vivo. *J Biol Chem* 288(23):16371-16382.
57. Briggs RG, Fee JA 1978. Sulfhydryl reactivity of human erythrocyte superoxide dismutase. On the origin of the unusual spectral properties of the protein when prepared by a procedure utilizing chloroform and ethanol for the precipitation of hemoglobin. *Biochim Biophys Acta* 537(1):100-109.
58. Breton J, Avanzi N, Valsasina B, Sgarella L, La Fiura A, Breme U, Orsini G, Wenisch E, Righetti PG 1995. Detection of traces of a trisulfide derivative in the preparation of a recombinant truncated interleukin-6 mutein. *J Chromatogr A* 709(1):135-146.
59. Gu S, Wen D, Weinreb PH, Sun Y, Zhang L, Foley SF, Kshirsagar R, Evans D, Mi S, Meier W, Pepinsky RB 2010. Characterization of trisulfide modification in antibodies. *Anal Biochem* 400(1):89-98.
60. Andersson C, Edlund PO, Gellerfors P, Hansson Y, Holmberg E, Hult C, Johansson S, Kordel J, Lundin R, Mendel-Hartvig IB, Noren B, Wehler T, Widmalm G, Ohman J 1996. Isolation and characterization of a trisulfide variant of recombinant human growth hormone formed during expression in *Escherichia coli*. *Int J Pept Protein Res* 47(4):311-321.

61. Summa D, Spiga O, Bernini A, Venditti V, Priora R, Frosali S, Margaritis A, Di Giuseppe D, Niccolai N, Di Simplicio P 2007. Protein-thiol substitution or protein dethiolation by thiol/disulfide exchange reactions: the albumin model. *Proteins* 69(2):369-378.
62. Hansen RE, Ostergaard H, Winther JR 2005. Increasing the reactivity of an artificial dithiol-disulfide pair through modification of the electrostatic milieu. *Biochemistry* 44(15):5899-5906.
63. Snyder GH, Cennerazzo MJ, Karalis AJ, Field D 1981. Electrostatic Influence of Local Cysteine Environments on Disulfide Exchange Kinetics. *Biochemistry* 20(23):6509-6519.
64. Parente A, Merrifield B, Geraci G, D'Alessio G 1985. Molecular basis of superreactivity of cysteine residues 31 and 32 of seminal ribonuclease. *Biochemistry* 24(5):1098-1104.
65. Zhang RM, Snyder GH 1989. Dependence of formation of small disulfide loops in two-cysteine peptides on the number and types of intervening amino acids. *J Biol Chem* 264(31):18472-18479.
66. Kuwajima K, Ikeguchi M, Sugawara T, Hiraoka Y, Sugai S 1990. Kinetics of disulfide bond reduction in alpha-lactalbumin by dithiothreitol and molecular basis of superreactivity of the Cys6-Cys120 disulfide bond. *Biochemistry* 29(36):8240-8249.
67. Zavialov AV, Gaestel M, Korpela T, Zav'yalov VP 1998. Thiol/disulfide exchange between small heat shock protein 25 and glutathione. *Biochim Biophys Acta* 1388(1):123-132.
68. Benesch RE, Benesch R 1958. The Mechanism of Disulfide Interchange in Acid Solution - Role of Sulfenium Ions. *Journal of the American Chemical Society* 80(7):1666-1669.
69. Ryle AP, Sanger F 1955. Disulphide interchange reactions. *Biochem J* 60(4):535-540.
70. Wiita AP, Ainaravapu SR, Huang HH, Fernandez JM 2006. Force-dependent chemical kinetics of disulfide bond reduction observed with single-molecule techniques. *Proc Natl Acad Sci U S A* 103(19):7222-7227.
71. Whitesides GM, Houk J, Patterson MAK 1983. Activation Parameters for Thiolate Disulfide Interchange Reactions in Aqueous-Solution. *Journal of Organic Chemistry* 48(1):112-115.

72. Liu YD, Chen X, Enk JZ, Plant M, Dillon TM, Flynn GC 2008. Human IgG2 antibody disulfide rearrangement in vivo. *J Biol Chem* 283(43):29266-29272.
73. Yoo EM, Wims LA, Chan LA, Morrison SL 2003. Human IgG2 can form covalent dimers. *J Immunol* 170(6):3134-3138.
74. van der Neut Kofschoten M, Schuurman J, Losen M, Bleeker WK, Martinez-Martinez P, Vermeulen E, den Bleker TH, Wiegman L, Vink T, Aarden LA, De Baets MH, van de Winkel JG, Aalberse RC, Parren PW 2007. Anti-inflammatory activity of human IgG4 antibodies by dynamic Fab arm exchange. *Science* 317(5844):1554-1557.
75. Takagi H, Takahashi T, Momose H, Inouye M, Maeda Y, Matsuzawa H, Ohta T 1990. Enhancement of the thermostability of subtilisin E by introduction of a disulfide bond engineered on the basis of structural comparison with a thermophilic serine protease. *J Biol Chem* 265(12):6874-6878.
76. Livney YD, Verespej E, Dalglish DG 2003. Steric effects governing disulfide bond interchange during thermal aggregation in solutions of beta-lactoglobulin B and alpha-lactalbumin. *J Agric Food Chem* 51(27):8098-8106.
77. Cabra V, Vazquez-Contreras E, Moreno A, Arreguin-Espinosa R 2008. The effect of sulfhydryl groups and disulphide linkage in the thermal aggregation of Z19 alpha-zein. *Biochim Biophys Acta* 1784(7-8):1028-1036.
78. Costantino HR, Langer R, Klibanov AM 1994. Moisture-induced aggregation of lyophilized insulin. *Pharm Res* 11(1):21-29.
79. Jordan GM, Yoshioka S, Terao T 1994. The aggregation of bovine serum albumin in solution and in the solid state. *J Pharm Pharmacol* 46(3):182-185.
80. Kibria FM, Lees WJ 2008. Balancing conformational and oxidative kinetic traps during the folding of bovine pancreatic trypsin inhibitor (BPTI) with glutathione and glutathione disulfide. *J Am Chem Soc* 130(3):796-797.
81. Scheraga HA, Wedemeyer WJ, Welker E 2001. Bovine pancreatic ribonuclease A: oxidative and conformational folding studies. *Methods Enzymol* 341:189-221.
82. Qiao ZS, Min CY, Hua QX, Weiss MA, Feng YM 2003. In vitro refolding of human proinsulin. Kinetic intermediates, putative disulfide-forming pathway folding initiation site, and potential role of C-peptide in folding process. *J Biol Chem* 278(20):17800-17809.

83. Labrecque J, Mc Nicoll N, Marquis M, De Lean A 1999. A disulfide-bridged mutant of natriuretic peptide receptor-A displays constitutive activity. Role of receptor dimerization in signal transduction. *J Biol Chem* 274(14):9752-9759.
84. Liu W, Onda M, Kim C, Xiang L, Weldon JE, Lee B, Pastan I 2012. A recombinant immunotoxin engineered for increased stability by adding a disulfide bond has decreased immunogenicity. *Protein Eng Des Sel* 25(1):1-6.
85. Franey H, Brych SR, Kolvenbach CG, Rajan RS 2010. Increased aggregation propensity of IgG2 subclass over IgG1: role of conformational changes and covalent character in isolated aggregates. *Protein Sci* 19(9):1601-1615.
86. Trivedi M, Davis RA, Shabaik Y, Roy A, Verkhivker G, Laurence JS, Middaugh CR, Siahaan TJ 2009. The role of covalent dimerization on the physical and chemical stability of the EC1 domain of human E-cadherin. *J Pharm Sci* 98(10):3562-3574.
87. Ruegg UT, Rudinger J 1977. Alkylation of cysteine thiols with 1,3-propane sultone. *Methods Enzymol* 47:116-122.
88. Brocchini S, Balan S, Godwin A, Choi JW, Zloh M, Shaunak S 2006. PEGylation of native disulfide bonds in proteins. *Nat Protoc* 1(5):2241-2252.
89. Allen MJ, Guo A, Martinez T, Han M, Flynn GC, Wypych J, Liu YD, Shen WD, Dillon TM, Vezina C, Balland A 2009. Interchain disulfide bonding in human IgG2 antibodies probed by site-directed mutagenesis. *Biochemistry* 48(17):3755-3766.
90. Browning JL, Mattaliano RJ, Chow EP, Liang SM, Allet B, Rosa J, Smart JE 1986. Disulfide scrambling of interleukin-2: HPLC resolution of the three possible isomers. *Anal Biochem* 155(1):123-128.
91. Junnila RK, Wu Z, Strasburger CJ 2013. The role of human growth hormone's C-terminal disulfide bridge. *Growth Hormone & IGF Research* 23(3):62-67.
92. Bulaj G 2005. Formation of disulfide bonds in proteins and peptides. *Biotechnol Adv* 23(1):87-92.
93. Chakraborty K, Thakurela S, Prajapati RS, Indu S, Ali PS, Ramakrishnan C, Varadarajan R 2005. Protein stabilization by introduction of cross-strand disulfides. *Biochemistry* 44(44):14638-14646.
94. Hsu E, Osslund T, Nybo R, Chen BL, Kenney WC, Morris CF, Arakawa T, Narhi LO 2006. Enhanced stability of recombinant keratinocyte growth factor by mutagenesis. *Protein Eng Des Sel* 19(4):147-153.

95. Costantino HR, Langer R, Klibanov AM 1995. Aggregation of a lyophilized pharmaceutical protein, recombinant human albumin: effect of moisture and stabilization by excipients. *Biotechnology (N Y)* 13(5):493-496.
96. Liu WR, Langer R, Klibanov AM 1991. Moisture-induced aggregation of lyophilized proteins in the solid state. *Biotechnol Bioeng* 37(2):177-184.
97. Desai UR, Klibanov AM 1995. Assessing the Structural Integrity of a Lyophilized Protein in Organic-Solvents. *Journal of the American Chemical Society* 117(14):3940-3945.
98. Rupley JA, Careri G 1991. Protein hydration and function. *Adv Protein Chem* 41:37-172.
99. Jorgensen L, Hostrup S, Moeller EH, Grohganz H 2009. Recent trends in stabilising peptides and proteins in pharmaceutical formulation - considerations in the choice of excipients. *Expert Opin Drug Deliv* 6(11):1219-1230.
100. Klibanov AM 1989. Enzymatic Catalysis in Organic-Solvents. *Biochemistry* 28(4):1932-1933.
101. Salnikova MS, Middaugh CR, Rytting JH 2008. Stability of lyophilized human growth hormone. *Int J Pharm* 358(1-2):108-113.
102. Tsarbopoulos A, Pramanik BN, Labdon JE, Reichert P, Gitlin G, Patel S, Sardana V, Nagabhushan TL, Trotta PP 1993. Isolation and characterization of a resistant core peptide of recombinant human granulocyte-macrophage colony-stimulating factor (GM-CSF); confirmation of the GM-CSF amino acid sequence by mass spectrometry. *Protein Sci* 2(11):1948-1958.
103. Chen G, SpringerLink (Online service). 2013. *Characterization of Protein Therapeutics using Mass Spectrometry*. ed., Boston, MA: Springer US : Imprint: Springer.
104. Tang HY, Speicher DW 2004. Determination of disulfide-bond linkages in proteins. *Curr Protoc Protein Sci* Chapter 11:Unit 11 11.
105. Tsai PL, Chen SF, Huang SY 2013. Mass spectrometry-based strategies for protein disulfide bond identification. *Rev Anal Chem* 32(4):257-268.
106. Jiang H, Wu SL, Karger BL, Hancock WS 2009. Mass spectrometric analysis of innovator, counterfeit, and follow-on recombinant human growth hormone. *Biotechnol Prog* 25(1):207-218.

107. Zhang Y, Dewald HD, Chen H 2011. Online mass spectrometric analysis of proteins/peptides following electrolytic cleavage of disulfide bonds. *J Proteome Res* 10(3):1293-1304.
108. Schnaible V, Wefing S, Bucker A, Wolf-Kummeth S, Hoffmann D 2002. Partial reduction and two-step modification of proteins for identification of disulfide bonds. *Analytical Chemistry* 74(10):2386-2393.
109. Lippincott J, Apostol I 1999. Carbamylation of cysteine: A potential artifact in peptide mapping of hemoglobins in the presence of urea. *Analytical Biochemistry* 267(1):57-64.
110. Leal WS, Nikonova L, Peng GH 1999. Disulfide structure of the pheromone binding protein from the silkworm moth, *Bombyx mori*. *Febs Letters* 464(1-2):85-90.
111. Bures EJ, Hui JO, Young Y, Chow DT, Katta V, Rohde MF, Zeni L, Rosenfeld RD, Stark KL, Haniu M 1998. Determination of disulfide structure in agouti-related protein (AGRP) by stepwise reduction and alkylation. *Biochemistry* 37(35):12172-12177.
112. Chong JM, Uren A, Rubin JS, Speicher DW 2002. Disulfide bond assignments of secreted frizzled-related protein-1 provide insights about frizzled homology and netrin modules. *Journal of Biological Chemistry* 277(7):5134-5144.
113. Chong JM, Speicher DW 2001. Determination of disulfide bond assignments and N-glycosylation sites of the human gastrointestinal carcinoma antigen GA733-2 (CO17-1A, EGP, KS1-4, KSA, and Ep-CAM). *Journal of Biological Chemistry* 276(8):5804-5813.
114. Knablein Jr. 2013. *Modern biopharmaceuticals : recent success stories*. ed., Weinheim: Wiley-Blackwell.
115. Godwin A, Choi JW, Pedone E, Balan S, Jumnah R, Shaunak S, Brocchini S, Zloh M 2007. Molecular dynamics simulations of proteins with chemically modified disulfide bonds. *Theor Chem Acc* 117(2):259-265.
116. Conley GP, Viswanathan M, Hou Y, Rank DL, Lindberg AP, Cramer SM, Ladner RC, Nixon AE, Chen J 2011. Evaluation of protein engineering and process optimization approaches to enhance antibody drug manufacturability. *Biotechnol Bioeng* 108(11):2634-2644.
117. Carpenter JF, Chang BS, Garzon-Rodriguez W, Randolph TW 2002. Rational design of stable lyophilized protein formulations: theory and practice. *Pharm Biotechnol* 13:109-133.

118. Carpenter JF, Pikal MJ, Chang BS, Randolph TW 1997. Rational design of stable lyophilized protein formulations: some practical advice. *Pharm Res* 14(8):969-975.
119. Rabenstein DL, Weaver KH 1996. Kinetics and Equilibria of the Thiol/Disulfide Exchange Reactions of Somatostatin with Glutathione. *J Org Chem* 61(21):7391-7397.
120. Rabenstein DL, Yeo PL 1994. Kinetics and Equilibria of the Formation and Reduction of the Disulfide Bonds in Arginine-Vasopressin and Oxytocin by Thiol/Disulfide Interchange with Glutathione and Cysteine. *Journal of Organic Chemistry* 59(15):4223-4229.
121. Dillon TM, Bondarenko PV, Rehder DS, Pipes GD, Kleemann GR, Ricci MS 2006. Optimization of a reversed-phase high-performance liquid chromatography/mass spectrometry method for characterizing recombinant antibody heterogeneity and stability. *J Chromatogr A* 1120(1-2):112-120.
122. Forrer K, Hammer S, Helk B 2004. Chip-based gel electrophoresis method for the quantification of half-antibody species in IgG4 and their by- and degradation products. *Anal Biochem* 334(1):81-88.
123. Liu H, May K 2012. Disulfide bond structures of IgG molecules: structural variations, chemical modifications and possible impacts to stability and biological function. *MAbs* 4(1):17-23.
124. Bustamante JJ, Grigorian AL, Munoz J, Aguilar RM, Trevino LR, Martinez AO, Haro LS 2010. Human growth hormone: 45-kDa isoform with extraordinarily stable interchain disulfide links has attenuated receptor-binding and cell-proliferative activities. *Growth Horm IGF Res* 20(4):298-304.
125. Kratz F 2008. Albumin as a drug carrier: design of prodrugs, drug conjugates and nanoparticles. *J Control Release* 132(3):171-183.
126. Shaked Z, Szajewski RP, Whitesides GM 1980. Rates of thiol-disulfide interchange reactions involving proteins and kinetic measurements of thiol pKa values. *Biochemistry* 19(18):4156-4166.
127. Robinson NE, Robinson AB 2001. Molecular clocks. *Proc Natl Acad Sci U S A* 98(3):944-949.
128. Xie M, Schowen RL 1999. Secondary structure and protein deamidation. *J Pharm Sci* 88(1):8-13.

129. Thing M, Zhang J, Laurence J, Topp EM 2010. Thiol-disulfide interchange in the tocinoic acid/glutathione system during freezing and drying. *J Pharm Sci* 99(12):4849-4856.
130. Otzen DE, Knudsen BR, Achmann F, Larsen KL, Wimmer R 2002. Structural basis for cyclodextrins' suppression of human growth hormone aggregation. *Protein Sci* 11(7):1779-1787.
131. St John RJ, Carpenter JF, Randolph TW 1999. High pressure fosters protein refolding from aggregates at high concentrations. *Proc Natl Acad Sci U S A* 96(23):13029-13033.
132. Pikal MJ, Dellerman KM, Roy ML, Riggin RM 1991. The effects of formulation variables on the stability of freeze-dried human growth hormone. *Pharm Res* 8(4):427-436.
133. Pikal MJ, Rigsbee D, Roy ML, Galreath D, Kovach KJ, Wang B, Carpenter JF, Cicerone MT 2008. Solid state chemistry of proteins: II. The correlation of storage stability of freeze-dried human growth hormone (hGH) with structure and dynamics in the glassy solid. *J Pharm Sci* 97(12):5106-5121.
134. Pikal MJ, Rigsbee DR, Roy ML 2007. Solid state chemistry of proteins: I. glass transition behavior in freeze dried disaccharide formulations of human growth hormone (hGH). *J Pharm Sci* 96(10):2765-2776.
135. Lewis UJ, Peterson SM, Bonewald LF, Seavey BK, VanderLaan WP 1977. An interchain disulfide dimer of human growth hormone. *J Biol Chem* 252(11):3697-3702.
136. St John RJ, Carpenter JF, Balny C, Randolph TW 2001. High pressure refolding of recombinant human growth hormone from insoluble aggregates. Structural transformations, kinetic barriers, and energetics. *J Biol Chem* 276(50):46856-46863.
137. Wang YJ, Pearlman R. 1993. *Stability and characterization of protein and peptide drugs : case histories.* ed., New York: Plenum Press. p xxi, 353 p.
138. Waterman KC, Adami RC 2005. Accelerated aging: prediction of chemical stability of pharmaceuticals. *Int J Pharm* 293(1-2):101-125.
139. Lei J, Chen DA, Regnier FE 1998. Rapid verification of disulfide linkages in recombinant human growth hormone by tandem column tryptic mapping. *J Chromatogr A* 808(1-2):121-131.

140. Luo D, Smith SW, Anderson BD 2005. Kinetics and mechanism of the reaction of cysteine and hydrogen peroxide in aqueous solution. *J Pharm Sci* 94(2):304-316.
141. Wu SL, Leung D, Tretyakov L, Hu J, Guzzetta A, Wang YJ 2000. The formation and mechanism of multimerization in a freeze-dried peptide. *Int J Pharm* 200(1):1-16.
142. Wang W, Roberts CJ 2013. Non-Arrhenius protein aggregation. *AAPS J* 15(3):840-851.
143. Krekel F, Samland AK, Macheroux P, Amrhein N, Evans JN 2000. Determination of the pKa value of C115 in MurA (UDP-N-acetylglucosamine enolpyruvyltransferase) from *Enterobacter cloacae*. *Biochemistry* 39(41):12671-12677.
144. Tajc SG, Tolbert BS, Basavappa R, Miller BL 2004. Direct determination of thiol pKa by isothermal titration microcalorimetry. *J Am Chem Soc* 126(34):10508-10509.
145. Spiess AN, Neumeyer N 2010. An evaluation of R2 as an inadequate measure for nonlinear models in pharmacological and biochemical research: a Monte Carlo approach. *BMC Pharmacol* 10:6.
146. Patai S, Rappoport Z. 1993. *The Chemistry of sulphur-containing functional groups*. ed., Chichester England ; New York: Wiley. p xiv, 1122 p.
147. Nagy P 2013. Kinetics and mechanisms of thiol-disulfide exchange covering direct substitution and thiol oxidation-mediated pathways. *Antioxid Redox Signal* 18(13):1623-1641.
148. Fernandes PA, Ramos MJ 2004. Theoretical insights into the mechanism for thiol/disulfide exchange. *Chemistry* 10(1):257-266.
149. Keire DA, Strauss E, Guo W, Noszal B, Rabenstein DL 1992. Kinetics and Equilibria of Thiol Disulfide Interchange Reactions of Selected Biological Thiols and Related Molecules with Oxidized Glutathione. *Journal of Organic Chemistry* 57(1):123-127.
150. Pappas JA 1977. Theoretical Studies of Reactions of Sulfur-Sulfur Bond .1. General Heterolytic Mechanisms. *Journal of the American Chemical Society* 99(9):2926-2930.
151. Youngman KM, Spencer DB, Brems DN, DeFelippis MR 1995. Kinetic analysis of the folding of human growth hormone. Influence of disulfide bonds. *J Biol Chem* 270(34):19816-19822.

152. Cleland JL, Powell MF, Shire SJ 1993. The development of stable protein formulations: a close look at protein aggregation, deamidation, and oxidation. *Crit Rev Ther Drug Carrier Syst* 10(4):307-377.
153. Manning MC, Patel K, Borchardt RT 1989. Stability of protein pharmaceuticals. *Pharm Res* 6(11):903-918.
154. Franks F 1994. Long-term stabilization of biologicals. *Biotechnology (N Y)* 12(3):253-256.
155. Tang X, Pikal MJ 2004. Design of freeze-drying processes for pharmaceuticals: practical advice. *Pharm Res* 21(2):191-200.
156. Costantino HR, Pikal MJ. 2004. *Lyophilization of biopharmaceuticals*. ed., Arlington, VA: AAPS Press. p xxx, 686 p.
157. Banga AK. 2006. *Therapeutic peptides and proteins : formulation, processing, and delivery systems*. 2nd ed., Boca Raton, FL: CRC/Taylor & Francis. p 354 p.
158. Pikal MJ, Dellerman K, Roy ML 1992. Formulation and stability of freeze-dried proteins: effects of moisture and oxygen on the stability of freeze-dried formulations of human growth hormone. *Dev Biol Stand* 74:21-37; discussion 37-28.
159. Roy I, Gupta MN 2004. Freeze-drying of proteins: some emerging concerns. *Biotechnol Appl Biochem* 39(Pt 2):165-177.
160. Nail SL, Jiang S, Chongprasert S, Knopp SA 2002. Fundamentals of freeze-drying. *Pharm Biotechnol* 14:281-360.
161. Bhatnagar BS, Bogner RH, Pikal MJ 2007. Protein stability during freezing: separation of stresses and mechanisms of protein stabilization. *Pharm Dev Technol* 12(5):505-523.
162. Tang XC, Pikal MJ 2005. Measurement of the kinetics of protein unfolding in viscous systems and implications for protein stability in freeze-drying. *Pharm Res* 22(7):1176-1185.
163. Costantino HR, Nguyen TH, Hsu CC 1996. Fourier-transform Infrared Spectroscopy Demonstrates that Lyophilization Alters the Secondary Structure of Recombinant Human Growth Hormone. *Pharmacy and Pharmacology Communications* 2(5):229-232.
164. Liu WR, Langer R, Klibanov AM 1991. Moisture-induced aggregation of lyophilized proteins in the solid state. *Biotechnol Bioeng* 37(2):177-184.

165. Costantino HR, Langer R, Klibanov AM 1994. Solid-phase aggregation of proteins under pharmaceutically relevant conditions. *J Pharm Sci* 83(12):1662-1669.
166. Yoshioka S, Aso Y, Izutsu K, Terao T 1993. Aggregates formed during storage of beta-galactosidase in solution and in the freeze-dried state. *Pharm Res* 10(5):687-691.
167. Andya JD, Hsu CC, Shire SJ 2003. Mechanisms of aggregate formation and carbohydrate excipient stabilization of lyophilized humanized monoclonal antibody formulations. *AAPS PharmSci* 5(2):E10.
168. Wang W 2005. Protein aggregation and its inhibition in biopharmaceutics. *Int J Pharm* 289(1-2):1-30.
169. Chandrasekhar S, Epling DE, Sophocleous AM, Topp EM 2014. Thiol-disulfide exchange in peptides derived from human growth hormone. *J Pharm Sci* 103(4):1032-1042.
170. Kuiper MJ, Lankin C, Gauthier SY, Walker VK, Davies PL 2003. Purification of antifreeze proteins by adsorption to ice. *Biochem Biophys Res Commun* 300(3):645-648.
171. Nakanishi T, Sato T, Sakoda S, Yoshioka M, Shimizu A 2004. Modification of cysteine residue in transthyretin and a synthetic peptide: analyses by electrospray ionization mass spectrometry. *Biochim Biophys Acta* 1698(1):45-53.
172. Donovan JW, White TM 1971. Alkaline hydrolysis of the disulfide bonds of ovomucoid and of low molecular weight aliphatic and aromatic disulfides. *Biochemistry* 10(1):32-38.
173. Helmerhorst E, Stokes GB 1983. Generation of an acid-stable and protein-bound persulfide-like residue in alkali- or sulfhydryl-treated insulin by a mechanism consonant with the beta-elimination hypothesis of disulfide bond lysis. *Biochemistry* 22(1):69-75.
174. Andersson LO 1970. Hydrolysis of disulfide bonds in weakly alkaline media. II. Bovine serum albumin dimer. *Biochim Biophys Acta* 200(2):363-369.
175. Pearlman R, Wang YJ. 1996. Formulation, characterization, and stability of protein drugs : case histories. ed., New York: Plenum Press. p xxviii, 432 p.
176. Hawkins HC, Freedman RB 1991. The reactivities and ionization properties of the active-site dithiol groups of mammalian protein disulphide-isomerase. *Biochem J* 275 (Pt 2):335-339.

177. Zhang T, Zhang J, Hewitt D, Tran B, Gao X, Qiu ZJ, Tejada M, Gazzano-Santoro H, Kao YH 2012. Identification and characterization of buried unpaired cysteines in a recombinant monoclonal IgG1 antibody. *Anal Chem* 84(16):7112-7123.
178. Huh JH, White AJ, Brych SR, Franey H, Matsumura M 2013. The identification of free cysteine residues within antibodies and a potential role for free cysteine residues in covalent aggregation because of agitation stress. *J Pharm Sci* 102(6):1701-1711.
179. Kerr J, Schlosser JL, Griffin DR, Wong DY, Kasko AM 2013. Steric effects in peptide and protein exchange with activated disulfides. *Biomacromolecules* 14(8):2822-2829.
180. <http://cbc.arizona.edu/njardarson>. ed.
181. Chandrasekhar S, Topp EM 2015. Thiol-disulfide exchange in peptides derived from human growth hormone during lyophilization and storage in the solid state. *J Pharm Sci* 104(4):1291-1302.
182. Patra AK, Mukhopadhyay R, Mukhija R, Krishnan A, Garg LC, Panda AK 2000. Optimization of inclusion body solubilization and renaturation of recombinant human growth hormone from *Escherichia coli*. *Protein Expr Purif* 18(2):182-192.
183. Konermann L, Pan J, Liu YH 2011. Hydrogen exchange mass spectrometry for studying protein structure and dynamics. *Chem Soc Rev* 40(3):1224-1234.
184. Buckwalter BL, Cady SM, Shieh HM, Chaudhuri AK, Johnson DF 1992. Improvement in the Solution Stability of Porcine Somatotropin by Chemical Modification of Cysteine Residues. *J Agr Food Chem* 40(2):356-362.
185. Cunningham BC, Mulkerrin MG, Wells JA 1991. Dimerization of human growth hormone by zinc. *Science* 253(5019):545-548.
186. Raman B, Ramakrishna T, Rao CM 1996. Refolding of denatured and denatured/reduced lysozyme at high concentrations. *J Biol Chem* 271(29):17067-17072.
187. Okumura M, Saiki M, Yamaguchi H, Hidaka Y 2011. Acceleration of disulfide-coupled protein folding using glutathione derivatives. *FEBS J* 278(7):1137-1144.
188. Ferre F, Clote P 2005. Disulfide connectivity prediction using secondary structure information and diresidue frequencies. *Bioinformatics* 21(10):2336-2346.
189. Johnson BA, Shirokawa JM, Hancock WS, Spellman MW, Basa LJ, Aswad DW 1989. Formation of isoaspartate at two distinct sites during in vitro aging of human growth hormone. *J Biol Chem* 264(24):14262-14271.

190. Robinson AB, Rudd CJ 1974. Deamidation of glutaminy and asparaginy residues in peptides and proteins. *Curr Top Cell Regul* 8(0):247-295.
191. Jiang XG, Wang T, Kaltenbrunner O, Chen K, Flynn GC, Huang G 2013. Evaluation of protein disulfide conversion in vitro using a continuous flow dialysis system. *Anal Biochem* 432(2):142-154.
192. Mulinacci F, Capelle MA, Gurny R, Drake AF, Arvinte T 2011. Stability of human growth hormone: influence of methionine oxidation on thermal folding. *J Pharm Sci* 100(2):451-463.
193. Hanaki A, Kamide H 1975. Autoxidation of cysteine catalyzed by copper in glycyglycine buffer. *Chem Pharm Bull (Tokyo)* 23(8):1671-1676.
194. Ehrenberg L, Harmsringdahl M, Fedorcsak I, Granath F 1989. Kinetics of the Copper-Catalyzed and Iron-Catalyzed Oxidation of Cysteine by Dioxygen. *Acta Chem Scand* 43(2):177-187.

APPENDICES

Appendix A: Data modeling with SCIENTIST®

// Micromath Scientist Model File for the reaction of T20 with T20-T21 at pH 7.0 in aqueous solution

IndVars: T

DepVars: T20,T21,T20T20,T21T21,T20T21,T20S,T21S

Params: K1,K2,K3,K4,K5,pKa,pKb

$T20T20' = K1 * T20S * T20T21 - K2 * T20T20 * T21S + K5 * T20S * T20S * T20S * T21S$

$T21T21' = K3 * T21S * T20T21 - K4 * T21T21 * T20S$

$T20T21' = - K1 * T20S * T20T21 + K2 * T20T20 * T21S - K3 * T21S * T20T21 +$

$K4 * T21T21 * T20S + K5 * T20S * T20S * T20S * T21S$

$T20' = -K1 * T20S * T20T21 + K2 * T20T20 * T21S + K3 * T21S * T20T21 - K4 * T20S * T21T21 -$
 $K5 * T20S * T20S * T20S * T21S$

$T21' = K1 * T20S * T20T21 - K2 * T20T20 * T21S - K3 * T21S * T20T21 + K4 * T20S * T21T21 -$
 $K5 * T20S * T20S * T20S * T21S$

//Parameter values:

K1 = 0.0004

K2 = 0.0006

K3 = 0.0002

K4 = 0.0006

pKa = 8.3

pKb = 8.3

// Initial conditions:

T = 0.0

T20 = 350.00

T20T21 = 250.00

T21 = 0.0

T20T20 = 0.0

T21T21 = 0.0

$T20S = T20 / (1 + ((10^{-7}) / (10^{-pKa})))$

$T21S = T21 / (1 + ((10^{-7}) / (10^{-pKb})))$

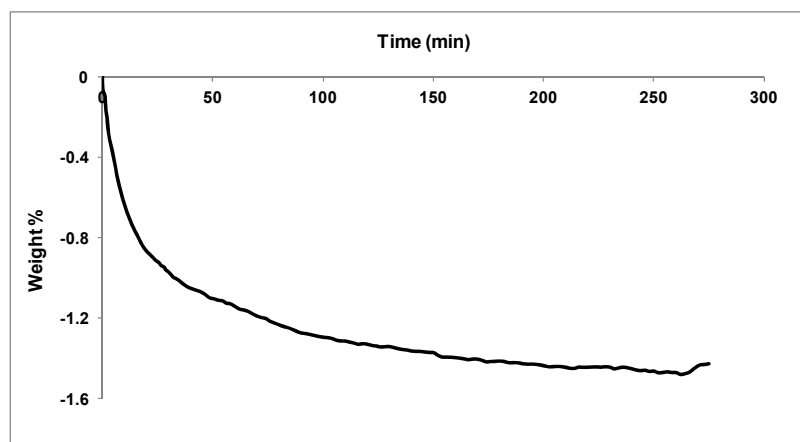
Appendix B: SGA and DSC measurements for lyophilized samples

Figure B.1: VTI data for lyo sample (T20 and cT20-T21, pH 7.0, 10 mM PB, 0.08 M ionic strength and 0.5 mM EDTA) collected on SGA-100 (VTI Corporation, Hialeah, FL). Data was measured at 0% RH and at 25 °C at the end of secondary drying.

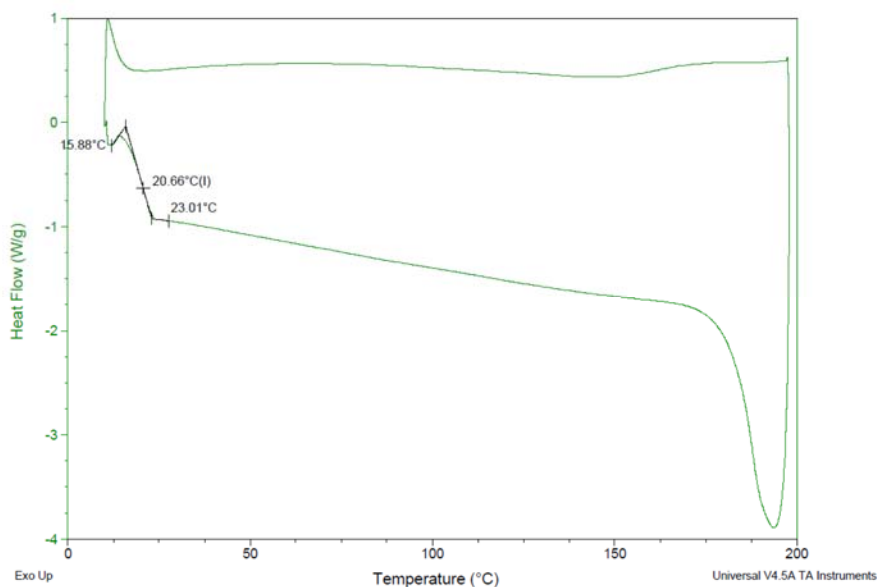


Figure B.2: DSC data for lyo sample (T20 and cT20-T21, pH 7.0, 10 mM PB, 0.08 M ionic strength and 0.5 mM EDTA) collected on DSC Q-2000 (TA instruments, New Castle, DE).

Appendix C: Purification and digestion optimization of hGH

rhGH was purified from *E. coli* after cell harvesting using the protocol shown in the flow chart below.

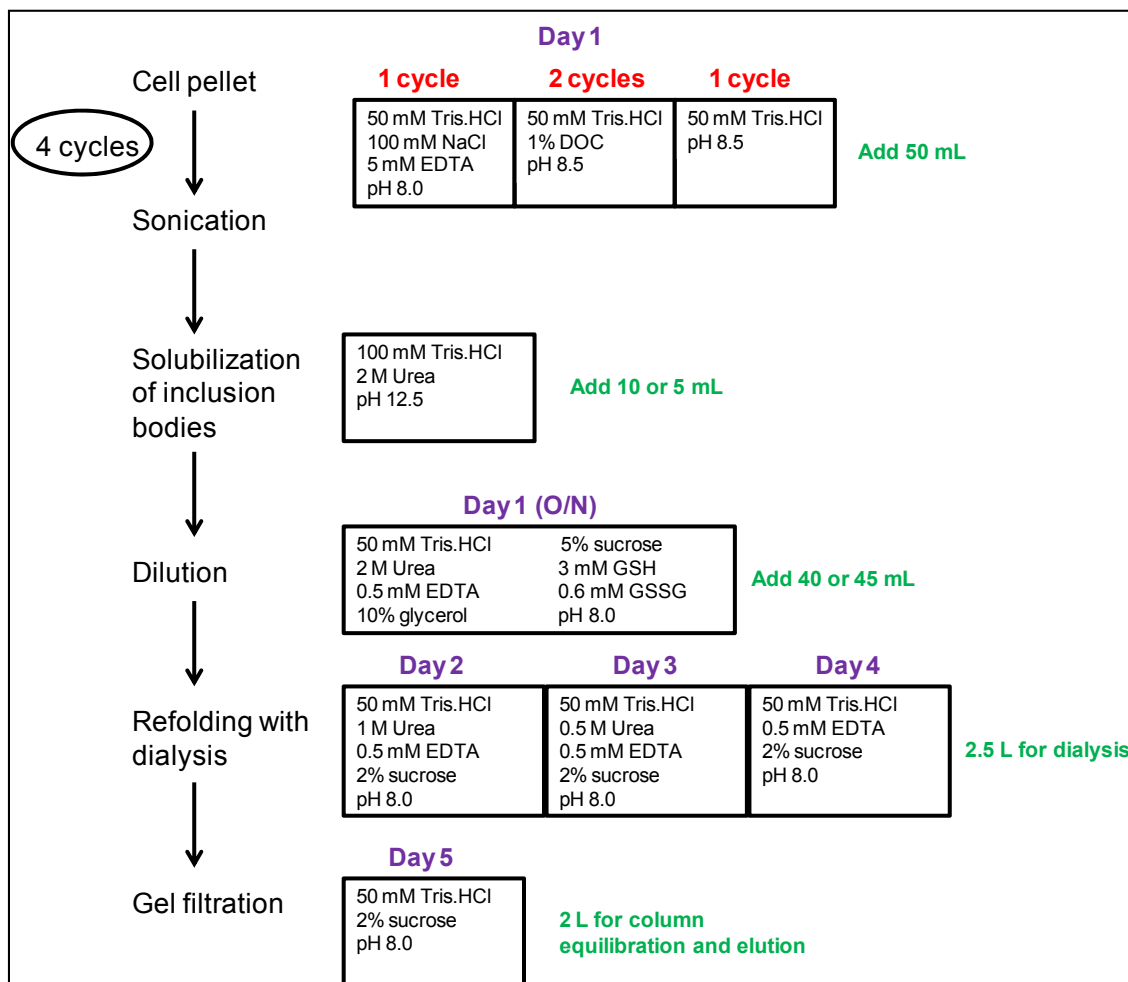










Figure C.1: Flow chart showing purification steps for hGH from the cell pellet. Buffers used for each step are shown in boxes and amount of each buffer added are in green next to the boxes.

Table C.1: Comparing different digestion protocols for hGH

Digestion protocol	Disulfide scrambling	Digestion complete in less than 60 mins
Trypsin digestion in solution	Y	N
Trypsin immobilized on magnetic beads	Y	N
Trypsin immobilized on agarose beads	Y	N
Perfinity flash digest protocol	N	Y

Table C.2: Amino acid sequence of all possible scrambled intra-and intermolecular disulfide-linked peptides from hGH.

Tryptic peptide	Description	Amino acid sequence	Theoretical mass (Da)	Observed mass (Da)
T6-T20	Scrambled disulfide-linked peptide	NH ₂ -YSFLQNPQTSLCFSES IPTPSNR-OH  NH ₂ -IVQCR-OH	3230.549	nd
T6-T21	Scrambled disulfide-linked peptide	NH ₂ -YSFLQNPQTSLCFSES IPTPSNR-OH  NH ₂ -SVEGSCGF-OH	3397.523	nd
T16-T20	Scrambled disulfide-linked peptide	NH ₂ -NYGLLYCFR-OH  NH ₂ -IVQCR-OH	1762.865	nd
T16-T21	Scrambled disulfide-linked peptide	NH ₂ -NYGLLYCFR-OH  NH ₂ -SVEGSCGF-OH	1929.839	nd
T6-T6	Homodimer, Scrambled disulfide-linked peptide	NH ₂ -YSFLQNPQTSLCFSES IPTPSNR-OH  NH ₂ -YSFLQNPQTSLCFSES IPTPSNR-OH	5228.45	nd
T16-T16	Homodimer, Scrambled disulfide-linked peptide	NH ₂ -NYGLLYCFR-OH  NH ₂ -NYGLLYCFR-OH	2293.081	nd
T20-T20	Homodimer, Scrambled disulfide-linked peptide	NH ₂ -IVQCR-OH  NH ₂ -IVQCR-OH	1232.648	nd
T21-T21	Homodimer, Scrambled disulfide-linked peptide	NH ₂ -SVEGSCGF-OH  NH ₂ -SVEGSCGF-OH	1566.597	nd

nd- not detected

VITA

VITA

Saradha ChandrasekharEducation

B.Tech., Biotechnology, 2007, Anna University, Chennai, India.

MS., Biotechnology, 2009, Northeastern University, Boston, MA.

Ph.D., Pharmaceutics, 2015, Purdue University, West Lafayette, IN.

Certificate in Applied Management Principles, 2014, Purdue University, West Lafayette, IN.

Work Experience

Intern- EMD Serono, Billerica, MA

January 2009- June 2009

Research Associate- Novartis Vaccines and Diagnostics, Cambridge, MA

October 2009-July 2010